

Regulation of protein transport into the ER by phosphorylation of Sbh1/Sec61 β

Dissertation

zur Erlangung des Grades

des Doktors der Naturwissenschaften

der naturwissenschaftlich-Technischen Fakultät

der **Universität des Saarlandes**

von

Guido Barbieri

Saarland University
Saarbrücken, Germany
2022

Tag des Kolloquiums: 15. November 2022

Dekan: Prof. Dr. Ludger Santen

Berichterstatter: Prof. Dr. Karin Römisch

Prof. Dr. Martin van der Laan

Vorsitz: Dr. Ruth Kiefer

Akad. Mitarbeiter: Prof. Dr. Volkhard Helms

Contents

List of figures	6
List of tables	9
List of Abbreviation	10
Abstract	13
Zusammenfassung	14
Introduction	15
1.1 Secretory pathway in eukaryotes	16
1.2 Protein translocation	21
1.2.1 The endoplasmic reticulum	21
1.2.2 Targeting	22
1.2.3 Translocation	25
1.3 Sec61 channel	30
1.3.1 Sbh1	34
1.4 Translocational regulation	38
1.4.1 Potential mechanisms	38
1.4.2 Physiological implications	41
1.4.3 Selective regulation of ER translocation	42
1.4.4 Mitochondrial example	43
1.5 Phosphorylation of the Sec61 translocon	44
1.5.1 Protein phosphorylation	44
1.5.2 Phosphorylation of ER translocation-relevant components	45
1.5.3 Phosphorylation β -subunit of the Sec61 complex	46
1.5.3 Phosphorylation-dependent prolyl cis-trans isomerization of Sbh1	48
Material and Methods	50
2.1 Material	51
2.1.1 Laboratory equipment and their Suppliers	51
2.1.2 Reagents, consumables and Chemicals	52
2.1.3 Software	58
2.1.4 <i>Saccharomyces cerevisiae</i> strains	59
2.1.5 <i>Escherichia coli</i> strains and Plasmids	65
2.1.6 Primers	67
2.1.7 Antibodies	69
2.1.8 Enzymes	70
2.1.9 Media and Buffers	70
2.2 Methods	72

2.2.1 Sterilization	72
2.2.2 Growth cultures	72
2.2.3 DNA Extraction.....	73
2.2.4 DNA manipulation.....	75
2.2.5 Transformation of <i>E. coli</i> Cells with plasmidic DNA.....	81
2.2.6 Isolation of <i>S.cerevisiae</i> RNA	83
2.2.7 HAC1 mRNA Splice Assay	83
2.2.8 Protein Gel Electrophoresis and Western Blot Analysis.....	84
2.2.9 Isolation of Membrane and Cytosolic Fractions	87
2.2.10 Alkaline Phosphatase Treatment and TCA Precipitation.....	87
2.2.11 Preparation of Rough Microsomal Membranes	88
2.2.12 Radioactive labelling	90
2.2.13 Mutant construction	92
2.2.14 Automated microscopic screen	96
Results	98
3.1 Characterization of <i>sbh1</i> mutants	99
3.1.1 Temperature sensitivity test for <i>Sbh1</i> mutant strains.....	99
3.1.2 Translocation of different substrates in $\Delta sbh1/\Delta sbh2$ mutant strain.....	100
3.1.3 Translocation of different substrates in <i>sbh1S3A/T5A</i> mutant strain.....	106
3.1.4 Tunicamycin sensitivity test in <i>Sbh1</i> mutant strains	109
3.1.5 UPR induction assay in <i>sbh1</i> mutant strains.....	110
3.2 <i>Sbh1</i> antibodies.....	111
3.3 Automated microscopic screen	113
3.3.1 Identification of <i>Sbh1</i> -dependent, <i>Sbh1</i> phosphorylation-dependent and <i>Ess1</i> -dependent ER translocation substrates.....	115
3.3.2 Identification of potential S3/T5 <i>Sbh1</i> Kinases and Phosphatases	131
3.4 Functional characterization of <i>sbh1</i> mutant strains.....	134
3.4.1 Sorbitol growth rescue assay for <i>sbh1</i> mutant strains	134
3.4.2 <i>Sbh1</i> phosphorylation pattern in plasma membrane stabilized cells	135
3.4.3 <i>Sbh1</i> expression and <i>Sbh1</i> phosphorylation pattern in different growth phases.....	136
3.4.4 <i>Gas1</i> maturation in $\Delta sbh1/\Delta sbh2$ mutant strain.....	137
3.4.5 Amino acids transport integrity in $\Delta sbh1/\Delta sbh2$ mutant strain	139
3.5 Identification of potential S3/T5 <i>Sbh1</i> Kinases.....	140
3.5.1 High concentrated Urea SDS gels for the Kinase screen	140
3.5.2 Identification of potential S3/T5 <i>Sbh1</i> Kinase by screening through proline-directed kinases	142
3.6 Kinases mutants potentially involved in <i>Sbh1</i> N-terminal phosphorylation.....	152
3.6.1 <i>Kar2</i> ER translocation in kinases mutants potentially involved in <i>Sbh1</i> N-terminal phosphorylation.....	152
3.6.2 General protein translocation defect check in kinases mutants potentially involved in <i>Sbh1</i> N-terminal phosphorylation.....	154
3.6.3 Tunicamycin sensitivity in kinases mutants potentially involved in <i>Sbh1</i> N-terminal phosphorylation.....	156

3.6.4 Gls1 ER import in kinases mutants potentially involved in Sbh1 N-terminal phosphorylation.....	157
3.6.5 GST-Gls1 ER import in kinases mutants potentially involved in Sbh1 N-terminal phosphorylation.....	158
3.7 Phosphorylation-dependent proline isomerase Ess1 contributes to Sbh1 regulation	161
3.7.1 Previous data on Ess1 contribution to Sbh1 regulation	161
3.7.2 Kar2 translocation in <i>ess1H164R</i> mutant strain	162
3.7.3 Sorbitol growth rescue assay for <i>ess1H164R</i> mutant strain.....	163
3.7.4 Sbh1 phosphorylation pattern in <i>ess1H164R</i> mutant strain	163
3.7.5 Epistasis assay for <i>ess1H164R</i> and $\Delta sbh1/\Delta sbh2$ mutations	164
Discussion	166
4.1 Characterization of <i>Sbh1</i> mutants	169
4.2 Sbh1 antibodies.....	175
4.3 Secretome automated microscopic screen	177
4.4 Screening for the kinase responsible for Sbh1 S3/T5 phosphorylation	182
4.5 Phosphorylation-dependent proline isomerase Ess1 contributes to Sbh1 regulation	187
4.6 Model for Sbh1 function during ER protein translocation and its regulation by S3/T5 phosphorylation.....	189
References	194
Acknowledgements	219

List of figures

Figure 1.1: Schematic representation of protein secretion in eukaryotes.....	16
Figure 1.2: SNARE mediated vesicle fusion	19
Figure 1.3: Anterograde and retrograde transport pathways.....	21
Figure 1.4: Schematic representation of a typical signal peptide	23
Figure 1.5: Schematic representation of translocation of a secretory protein	27
Figure 1.6: Schematic representation of membrane insertion of a protein	28
Figure 1.7: Schematic representation of post-translational translocation in eukaryotes	29
Figure 1.8: Sec61 complex in yeast.....	31
Figure 1.9: Sec61 structure	32
Figure 1.10: Heptameric Sec complex	33
Figure 1.11: Sequence alignments of Sbh1 with Sbh2 and mammalian Sec61 β	35
Figure 1.12: Signal sequence-Sec61 complex dynamic interaction.....	39
Figure 1.13: Translocational regulation mechanisms.....	41
Figure 1.14: Ess1 isomerization scheme	48
Figure 3.1: Temperature sensitivity of sbh1 phosphorylation site mutant strains	100
Figure 3.2: Analysis of pp α F ER import in Δ sbh1/ Δ sbh2 strain.....	101
Figure 3.3: Analysis of the DPAPB ER translocation in Δ sbh1/ Δ sbh2 strain.....	102
Figure 3.4: Analysis of the Gls1 ER translocation in Δ sbh1/ Δ sbh2 strain.....	103
Figure 3.5: Analysis of the Kar2 ER translocation in Δ sbh1/ Δ sbh2 strain	104
Figure 3.6: Bacillus amyloliquefaciens α -amylase integration Scheme	105
Figure 3.7: Analysis of the bacterial α -amylase ER translocation in Δ sbh1/ Δ sbh2 strain.....	106
Figure 3.8: Analysis of the Kar2 ER translocation in sbh1S3A/T5A strain	107
Figure 3.9: Analysis of Kar2 at steady state in Δ sbh1/ Δ sbh2 and sbh1S3A/T5A strains.....	108
Figure 3.10: Analysis of the Gls1 ER translocation in sbh1S3A/T5A, sbh1S3A and sbh1T5A strains.....	109
Figure 3.11: Tunicamycin sensitivity of sbh1 mutant strains	110
Figure 3.12: UPR activation in sbh1 mutants.....	111
Figure 3.13: Sbh1 antibodies recognition scheme	111
Figure 3.14: Sbh1 ₍₁₋₁₈₎ and Sbh1 ₍₁₀₋₂₃₎ antibodies recognition test	112
Figure 3.15: Sbh1 ₍₁₀₋₂₃₎ and Sbh1 _(PI) antibodies recognition test.....	113
Figure 3.16: Automated microscopic screen in yeast Scheme	115
Figure 3.17: SBH2 and SBH2 deletion Scheme	117
Figure 3.18: Analysis of Sbh1 expression and temperature sensitivity in KRY1156 and KRY1160 strains.....	118
Figure 3.19: sbh1S3A/T5A subcloning Scheme.....	120
Figure 3.20: ess1H164R mutant construction Scheme.....	121
Figure 3.21: Image analysis from automated microscopic screen of secretome-GFP library in wildtype cells and the indicated mutants.....	123
Figure 3.22: Analysis of the Erp1, Gpi8 and Irc22 ER translocation in Δ sbh1/ Δ sbh2 and sbh1S3A/T5A strains	125
Figure 3.23: Analysis of the Irc22 ER translocation in Δ sbh1/ Δ sbh2 and sbh1S3A/T5A strains	126

Figure 3.24: Signal peptide scheme	127
Figure 3.25: Statistical analysis of the signal peptides	128
Figure 3.26: Statistical analysis of the transmembrane targeting sequences.....	128
Figure 3.27: Examples of signal peptides or first transmembrane domain from the microscopic screen	130
Figure 3.28: Mns1 GFP tagging Scheme	132
Figure 3.29: Image analysis from automated microscopic screen of Mns1-GFP cells in Wildtype, knockout and overexpression kinase mutant libraries	133
Figure 3.30: Sorbitol growth rescue assay for $\Delta sbh1/\Delta sbh2$ mutant strains.....	135
Figure 3.31: Sorbitol growth rescue assay for <i>sbh1S3A/T5A</i> mutant strains.....	135
Figure 3.32: Analysis of the Sbh1 phosphorylation pattern in wildtype cells with and without stabilization of the plasma membrane	136
Figure 3.33: Analysis of Sbh1 phosphorylation pattern of and Sbh1 expression in different growth phases.....	137
Figure 3.34: Analysis of Gas1 maturation in wildtype, $\Delta sbh1/\Delta sbh2$ and <i>sec23-1</i> strains ...	138
Figure 3.35: Metsulfuron-methyl (MM) sensitivity of $\Delta sbh1/\Delta sbh2$ mutant strains.....	139
Figure 3.36: Analysis of Sbh1 migration in high concentrated Urea SDS gels for different <i>sbh1</i> mutant strains.....	141
Figure 3.37: Analysis of Sbh1 migration in high concentrated Urea SDS gels for the <i>ess1H164R</i> mutant strain.....	142
Figure 3.38: Analysis of the Sbh1 phosphorylation pattern in proline-directed kinases overexpression mutants	144
Figure 3.39: Analysis of the Sbh1 phosphorylation pattern in <i>cka1/cka2</i> mutant strain.....	146
Figure 3.40: Analysis of Sbh1 phosphorylation pattern in <i>sbh1S3A/T5A</i> mutant strain.....	147
Figure 3.41: Reporter construct scheme	147
Figure 3.42: Mns1 Δ gp α F reporter construct construction scheme.....	149
Figure 3.43: Characterization of Mns1 Δ gp α F reporter construct in <i>sbh1</i> mutant strains....	150
Figure 3.45: Analysis of Mns1 Δ gp α F ER import in <i>cka1/cka2</i> mutant strain.....	152
Figure 3.46: Analysis of the Kar2 ER translocation in proline-directed kinase deficient mutants potentially involved in Sbh1 N-terminal phosphorylation	153
Figure 3.47: Analysis of pp α F ER import in proline-directed kinase deficient mutants potentially involved in Sbh1 N-terminal phosphorylation	155
Figure 3.48: Analysis of the DPAPB ER translocation import in proline-directed kinase deficient mutants potentially involved in Sbh1 N-terminal phosphorylation.....	156
Figure 3.49: Tunicamycin (TM) sensitivity of proline-directed kinase deficient mutants potentially involved in Sbh1 N-terminal phosphorylation	157
Figure 3.50: Analysis of the Gls1 ER translocation in proline-directed kinase deficient mutants potentially involved in Sbh1 N-terminal phosphorylation	158
Figure 3.51: pYEX4T-1-GLS1 Scheme	159
Figure 3.52: Analysis of the GST-Gls1 ER translocation in wildtype, $\Delta sbh1/\Delta sbh2$ and <i>sbh1S3A/T5A</i> mutant strains	160
Figure 3.53: Analysis of the GST-Gls1 ER translocation in proline-directed kinase deficient mutants potentially involved in Sbh1 N-terminal phosphorylation	161
Figure 3.54: Analysis of the Kar2 ER translocation in <i>ess1H164R</i> mutant strain	162
Figure 3.55: Sorbitol growth rescue assay for <i>ess1H164R</i> mutant strains.....	163
Figure 3.56: Analysis of the phosphorylation pattern of Sbh1 in <i>ess1H164R</i> mutant strain	164

Figure 3.57: Analysis of the Glc1 ER translocation in <i>ess1H164R</i> , $\Delta sbh1/\Delta sbh2$, and $\Delta sbh1/\Delta sbh2/ess1H164R$ mutant strains.....	165
Figure 4.1: Signal sequences of Sec61 β /Sbh1-dependent ER translocation substrates demonstrated so far	173
Figure 4.2: Sbh1 phosphorylation/dephosphorylation and potential change in conformation scheme	176
Figure 4.3: Model for Sbh1 function during ER protein translocation and its regulation by S3/T5 phosphorylation.....	191

List of tables

Table 2.1: Laboratory equipment	52
Table 2.2: Reagents, chemicals and consumables.....	58
Table 2.3: Software used in this study	59
Table 2.4: <i>E. coli</i> strains used in this study	64
Table 2.5: <i>S. cerevisiae</i> strains used in this study	67
Table 2.6: Primers used in this study	69
Table 2.7: Antibodies used in this study	69
Table 2.8: Enzymes used in this study	70
Table 2.9: <i>S.cerevisiae</i> growth media used in this study	71
Table 2.10: Composition of synthetic complete amino acid drop-out mixture for <i>S. cerevisiae</i> used in this study	72
Table 2.11: <i>E. coli</i> growth media used in this study	72
Table 2.12: Standard reaction mixture for PCR used in this study	76
Table 2.13: Standard thermal cycle program for PCR used in this study	76
Table 2.14: Standard colony PCR reaction mixture used in this study	77
Table 2.15: Standard thermal cycle program for colony PCR used in this study.....	77
Table 2.16: Standard reaction mixture for the restriction digestion of DNA used in this study	79
Table 2.17: Standard reaction mixture for the dephosphorylation of digested vector DNA used in this study	80
Table 2.18: Standard reaction mixture for the phosphorylation of digested vector DNA used in this.....	80
Table 2.19: Standard reaction mixture for the ligation of the vector and insert DNA used in this.....	81
Table 2.20: Reverse transcription reaction mixture used in this.....	84
Table 3.1: The Sbh1-dependent, Sbh1 phosphorylation-dependent and Ess1-dependent ER translocation substrates from the automated microscopic screen	124
Table 3.2: Results from Kinase identification Screen	133
Table 3.3: Proline-directed Kinases and other kinases of interest	143

List of abbreviations

A: Alanine
Ade: Adenine
ATP: Adenosine triphosphate
BiP: Immunoglobulin binding protein
C: Cysteine
C-terminal: Carboxy terminal
CaCl₂: Calcium chloride
Cdc28: Cell division control protein 28
ConA: Concanavalin A
COPI/II: Coat protein complex I/II
CPY: Carboxypeptidase Y
D: Aspartic acid
DEPC: Diethyl pyrocarbonate
DMSO: Dimethyl sulfoxide
DNA: Deoxyribonucleic acid
DPAPB: Diaminopeptidase B
DTT: Dithiothreitol
E: Glutamic acid
E. coli: Escherichia coli
EDTA: Ethylene diamine tetraacetic acid
Eq: Equivalent
ER: Endoplasmic reticulum
ERAD: ER-associated degradation
ERES: ER exit sites
ERGIC: ER-Golgi intermediate compartment
Ess1: Peptidylprolyl-cis/trans-isomerase
F: Phenylalanine
G: Glycine
Gas1: Beta-1,3-glucanosyltransferase
GFP: Green Fluorescent Protein
Gls1: Glucosidase 1
GPI-anchor: glycosylphosphatidylinositol anchors
GST: glutathione-S-transferase
GTP: Guanosine triphosphate
h: Hour(s)
H: Histidine
Hac1: Homolog to Atf/Creb1
HCl: Hydrochloric acid
HEPES: 4-(2-hydroxyethyl)-1-piperazineethanesulfonic acid
His: Histidine
Hsp70: 70 kilodalton heat shock protein
I: Isoleucine
IP: Immunoprecipitation

IPTG: Isopropyl- β -D-thio-galactopyranoside
Ire1: Inositol-requiring protein 1
K: Lysine
KAc: Potassium acetate
Kar2: Karyogamy protein 2
KCl: Potassium chloride
kD: Kilodalton
KOAc: Potassium acetate
L: Leucine
LB: Lysogeny broth
Leu: Leucine
LiAc: Lithium acetate
Lys: Lysine
M: Methionine
MES: 2-(N-morpholino)ethanesulfonic acid
Mg(OAc)₂: Magnesium acetate
MgSO₄: Magnesium sulphate
Min: Minutes
MM: Metsulfuron-Methyl
MnCl₂: Manganese chloride
Mns1: Mannosidase 1
MOPS: 3-(N-morpholino)propanesulfonic acid
MQ: H₂O ultrapure water
mRNA: Messenger RNA
N: Asparagine
N-terminal: Amino terminal
Na₂CO₃: Sodium carbonate
NaAc: Sodium acetate
NaCl: Sodium chloride
OD: Optical density
PCR: Polymerase chain reaction
Pdi1: Protein disulfide isomerase
PEG: Polyethylene glycol
PMSF: Phenylmethylsulfonyl fluoride
Pmt 1-7: Protein O-mannosyltransferase
pp α F: Pre pro alpha factor
Q: Glutamine
QC: Quality control
RNC: Ribosome-nascent chain complex
RP: Regulatory particle
Rpn12: Subunit of the 19S regulatory particle of the 26S proteasome lid
RT: Room temperature
S: Serine
S. cerevisiae: *Saccharomyces cerevisiae*
SA: Signal anchor
Sbh1: Sec61 beta homolog 1
SDS: Sodium dodecyl sulfate

SDS-PAGE: SDS-polyacrylamide gel electrophoresis
Sec61/62/63/71/72: Protein transport protein Sec61/62/63/71/72
Sec: Seconds
Ser: Serine
Shr3: Endoplasmic reticulum packaging chaperone
SNARE: Soluble NSF Attachment Protein Receptor
SP: Signal peptide
SR: SRP receptor
SRP: Signal recognition particle
SS: Signal sequence
Ssh1: Sec sixty-one homolog 1
Sss1: Sec sixty-one suppressor 1
T: Threonine
TAE: Tris, acetate, EDTA
TBS: Tris-buffered saline
TBST: 0.1% Tween 20 TBS
TCA: Trichloroacetic acid
TE: Tris-EDTA
tER: Transitional ER
TGN: Trans-Golgi network
Thr: Threonine
TM: Tunicamycin
TMD: Transmembrane domain
Tm: Melting temperature
tRNA: Transfer RNA
Trp: Tryptophan
Ts: Temperature sensitivity
UPR: Unfolded Protein Response
Ura: Uracyl
V: Valine
Y: Tyrosine
YP: Yeast peptone
YPD: Yeast peptone dextrose
YPDS: Yeast peptone dextrose sorbitol
YPD+MM: Yeast peptone dextrose sorbitol+Metsulfuron-Methyl
 α -amy: α -amylase
 Δ gp α F: mutant alpha factor precursor without glycosylation sites

Regulation of protein transport into the ER by phosphorylation of *Sbh1/Sec61 β*

Abstract

The ER protein translocation channel subunit *Sbh1* is non-essential, but contains multiple phosphorylation sites suggesting a regulatory role in ER protein import. It has been already shown that mutating two N-terminal, proline-flanked, phosphorylation sites in the *Sbh1* cytosolic domain phenocopies the temperature-sensitivity of a yeast strain lacking *SBH1/SBH2*, and results in reduced translocation into the ER of an *Sbh1*-dependent substrate, *Gls1*. In the present work I characterized the *sbh1* mutant strains. I also identified targeting signals that are *Sbh1*-dependent, Phospho-*Sbh1* dependent, or *Ess1*-dependent. In a high content microscopic screen, I identified about 12% of secretory proteins assayed as *Sbh1*-dependent and I found that *Sbh1*-dependent proteins have suboptimal ER targeting sequences, with lower hydrophobicity and frequently without or with an inverse charge bias. A smaller fraction of proteins was dependent on N-terminal phosphorylation of *Sbh1*. I also developed and optimized different screens for finding the kinase responsible for S3/T5-*Sbh1* phosphorylation, with no conclusive result. I conclude that *Sbh1* promotes ER import of substrates with suboptimal targeting sequences and its activity can be regulated by a conformational change induced by N-terminal phosphorylation and I suggested a model for ER protein translocation regulation.

Regulation of protein transport into the ER by phosphorylation of Sbh1/Sec61 β

Abstract

Die ER-Protein-Translokationskanal-Untereinheit Sbh1 ist nicht essentiell, enthält aber mehrere Phosphorylierungsstellen, was auf eine regulatorische Rolle beim ER-Proteinimport hindeutet. Es wurde bereits gezeigt, dass die Mutation von zwei N-terminalen, Prolin-flankierten Phosphorylierungsstellen in der zytosolischen Sbh1-Domäne die Temperaturempfindlichkeit eines Hefestamms, dem SBH1/SBH2 fehlt, phänokopiert und zu einer verringerten Translokation in das ER eines Sbh1-Abhängigen führt Substrat, Glc1. In der vorliegenden Arbeit habe ich die sbh1-Mutantenstämme charakterisiert. Ich habe auch Targeting-Signale identifiziert, die Sbh1-abhängig, Phospho-Sbh1-abhängig oder Ess1-abhängig sind. In einem mikroskopischen High-Content-Screen identifizierte ich etwa 12 % der sekretorischen Proteine, die als Sbh1-abhängig getestet wurden, und ich fand heraus, dass Sbh1-abhängige Proteine suboptimale ER-Targeting-Sequenzen mit geringerer Hydrophobizität und häufig ohne oder mit einer inversen Ladungsverzerrung aufweisen. Ein kleinerer Teil der Proteine war von der N-terminalen Phosphorylierung von Sbh1 abhängig. Ich habe auch verschiedene Screens entwickelt und optimiert, um die für die S3/T5-Sbh1-Phosphorylierung verantwortliche Kinase zu finden, ohne schlüssiges Ergebnis. Ich schlussfolgerte, dass Sbh1 den ER-Import von Substraten mit suboptimalen Targeting-Sequenzen fördert und seine Aktivität durch eine durch N-terminale Phosphorylierung induzierte Konformationsänderung reguliert werden kann, und ich schlug ein Modell für die Regulation der ER-Proteintranslokation vor.

1

Introduction

1 Introduction

1.1 Secretory pathway in eukaryotes

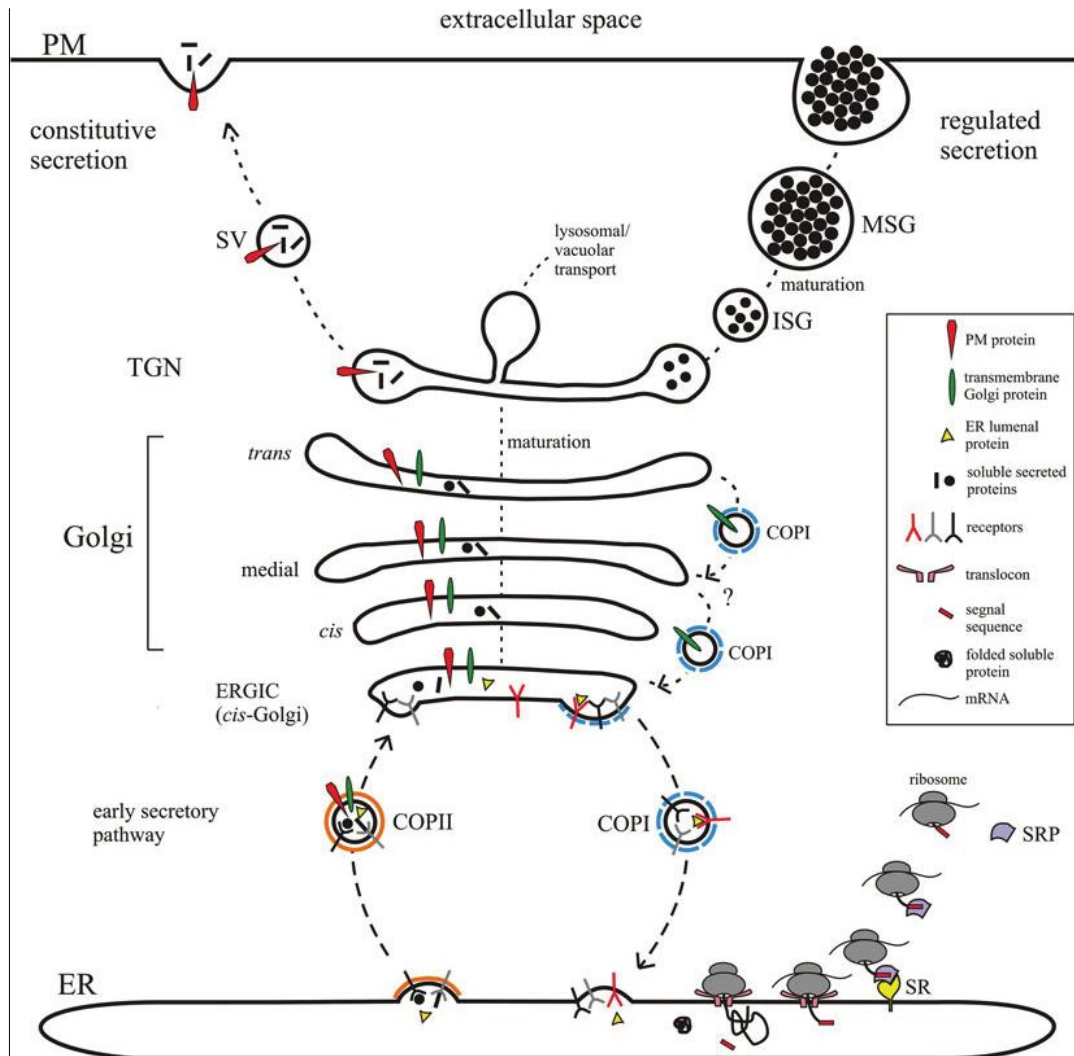


Figure 1.1: Schematic representation of protein secretion in eukaryotes. Figure from Viotti, 2016. Secretory proteins are translocated in the ER after the signal recognition particle (SRP) recognizes the signal sequence and interacts with its receptor (SR), leading to transport through the translocon and into the ER lumen. The signal sequence is cleaved off in the ER, and proteins are folded and packed in COPII vesicles upon receptor-ligand interaction. In animals, COPII vesicles are delivered to the ERGIC. In yeast or plants, to the cis-Golgi. Retro-transportation of escaped ER luminal proteins is done from the ERGIC or from the cis-Golgi to the ER via COPI vesicles. PM proteins and secreted proteins are transported via cisternal maturation to the TGN, whereas integral Golgi proteins are retrieved via intra-Golgi COPI mediated transport. At the TGN, proteins destined to be secreted are sorted in secretory vesicles (SVs) or immature secretory granules (ISGs). SVs are constitutively delivered toward the PM, whereas ISGs accumulate in the cytoplasm. ISGs form mature secretory granules (MSGs) and are transported to the PM.

Protein secretion, schematically represented in Figure 1.1, is an essential highly regulated process in both prokaryotes and eukaryotes. Cell regulation of its homeostasis and communication with the extracellular environment depend on protein secretion (Delic et al., 2013). One basic principle that can be found in both eukaryotes and prokaryotes is the compartmentalization of cells (Martin, 2010). Eukaryotic cells possess a complex

endomembrane system (the organelles) that is functionally interconnected (*Viotti, 2016*). This system allows processes, that in different circumstances would be incompatible, to occur simultaneously inside one cell by providing it with diverse environments that facilitates precise metabolic functions (*Hammer and Avalos, 2017*). It also eliminates metabolic cross-talk and enhance compartmentalized pathway efficiency (*Hammer and Avalos, 2017*). This results in the high specificity and regulation of cellular processes. In a typical eukaryotic cell, around 30% of protein synthesized on cytosol ribosomes enter the secretory pathway to be secreted or retained in the subcellular compartments of the pathway (*Delic et al., 2013; Tsukazaki et al., 2008*). Functions of the eukaryotic secretory pathway includes transport of newly synthesized proteins and lipids from the endoplasmic reticulum (ER) to cellular organelles, the plasma membrane, and the extracellular space via the Golgi complex, and modification those proteins and lipids in the process (*Delic et al., 2013*).

The secretory pathway in eukaryotes consists of different cellular compartments and starts with protein translocation into the ER, either co-translationally or post-translationally (*Zimmermann et al., 2011*). In mammalian, cells regardless of their final destination, most transmembrane and secretory proteins are translocated from the cytosol into the ER via the Sec61 complex as they emerge from the translating ribosome (*Simon and Blobel 1992; Rapoport, 2007*). In yeast, protein translocation across the ER membrane is mediated mainly by the Sec61 channel, either by the Sec61 trimeric complex (Sec61, Sbh1 and Sss1) when the translocation is done co-translationally or by the heptameric Sec complex (Sec trimeric complex plus Sec63 heptameric complex: Sec62, Sec63, Sec71 and Sec72) when the translocation is done post-translationally (*Rapoport, 2007*). For both, the pore forming sub-unit of the complex is Sec61 (*Zimmermann et al., 2011; Ng et al., 1996*). This subject will be addressed deeply further ahead in Section 1.2.3.

The ER is the main site of protein maturation and biosynthesis. After ER translocation into the ER lumen, proteins are targeted by a series of chaperones that facilitate folding (like the molecular chaperon Kar2), or undergo a series of modifications which include signal peptide cleavage by the signal peptidase complex (SPC), glycosylation by the oligosaccharyl-transferase (OST) complex and disulphide bond formation by Pdi1 (*Hatahet and Ruddock,*

2009; Goto 2007; Brodsky et al., 1995). At this point, proteins go through different steps of processing and quality control (QC) that assures correct folding. Proteins that are not able to reach their native conformation are retained in the ER lumen where they can form aggregates with toxic effects (Dobson, 2001; Kabani et al., 2003). Many of the chaperons involved in protein maturation are used as check-points. When there is any signal of misfolding protein, there are mechanisms that either remediate or degrade the misfolded form, preventing the unfolded and misfolded proteins from aggregating and allowing them to achieve their native folded state (Walter et al., 2006). They do that by the induction of the unfolded protein response (UPR) leading to upregulation of chaperone expression, which promotes protein folding (Gardner et al., 2013). Another mechanism known as ER associated degradation (ERAD) is used by the cell as a response to the accumulation of misfolded proteins. During ERAD, misfolded proteins are retro-translocated to the cytosol for subsequent proteasomal degradation (Ruggiano et al., 2014).

Some proteins going through this process are ER residents, and after being translocated and processed they stay in the ER. However, membrane or soluble proteins targeted for other cellular compartments or for secretion must continue further through this pathway and enter the Golgi apparatus. After being correctly processed by ER quality control, they are ready for continuing their traffic through the secretory pathway (Figure 1.1).

The series of compartments forming the secretory pathway are interconnected by vesicular transport steps, that occur not only in a forward direction (anterograde), but also in a retrograde manner (Pelham and Munro, 1993; Lewis and Pelham, 1996). Secretory proteins that are exported from the ER accumulate at specialized regions known as ER exit sites (ERES) or transitional ER (tER) (Shindiaipina and Barowle, 2010; Rossanese et al., 1999). These proteins are then packaged in coated transport vesicles, process driven by the derived coat protein complex II (COPII) which is assembled on the ER surface and bud from the ribosome-free ER subdomains (Barlowe et al., 1994). COPII, form by five subunits (Sar1-GTP, dimeric Sec23/Sec24, and tetrameric Sec13/Sec31), is responsible not only for budding of the cargo vesicle but also for incorporating correctly folded secretory and membrane proteins into the formed vesicles (Barlowe et al., 1994; Stagg et al., 2006). In *Saccharomyces cerevisiae* (*S. cerevisiae*) there is no discrete tER sites and budding appears to occur

stochastically across the entire ER membrane with many small tER distributed all over the ER (Rossanese *et al.*, 1999; Castillon *et al.*, 2009). In mammalian cells, the COPII vesicles bud from the ER forming the vesicular-tubular clusters (VTCs) by homotypic fusion events (Hughes and Stephens, 2008). These clusters are cargo-rich compartments that mediate the trafficking of secretory cargo between the ER and the Golgi (Viotti, 2016). After budding, vesicles have to move towards the target membrane proceeding through defined and progressive steps: tethering, docking, and fusion (Figure 1.2; Cai *et al.*, 2007). In *S. cerevisiae*, however, COPII-coated vesicles have not been shown to form VTCs, but instead they fuse directly with the cis-Golgi complex assisted by a large tethering complex known as TRAPPI (Bonifacino and Glick, 2004; Sacher *et al.*, 1998). The soluble NSF attachment protein receptors (SNARE), a related family of integral membrane proteins mediates the fusion of the vesicle with the membranes (Cao and Barowle, 2000). Monomeric SNARE proteins have their SNARE motif unstructured, but when they associate into a complex, they form elongated four-helical bundles that mechanically pull the membranes closer together and open a fusion pore (Figure 1.2) (Jahn and Scheller, 2003; Ferro-Novick and Brose, 2013).

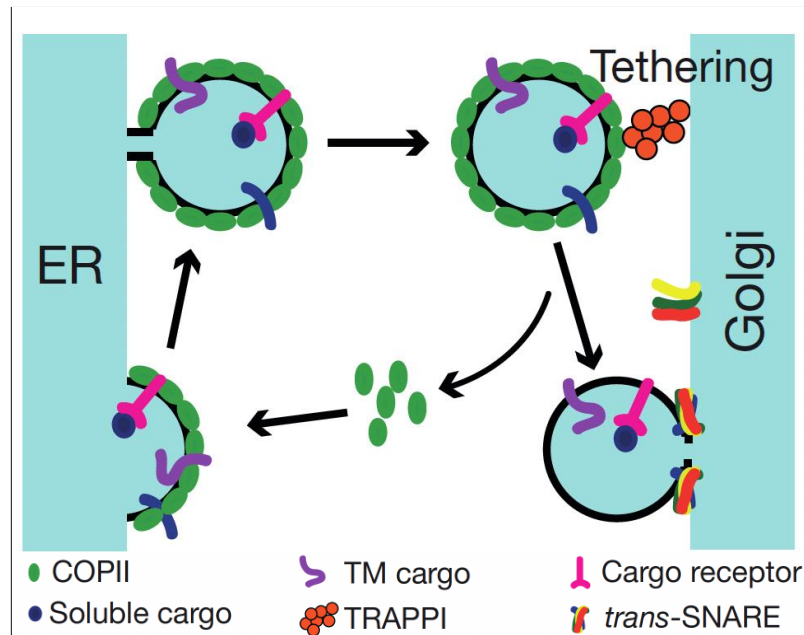


Figure 1.2: SNARE mediated vesicle fusion. Modified figure from Cai *et al.*, 2007. Schematic representation of SNARE mediated vesicle fusion.

After budding from the ER, vesicles must fuse with the target downstream organelle, the Golgi. The Golgi apparatus in higher eukaryotes consists of a series of flattened functionally distinct cisternal membranes that closely apposed and aligned in parallel to form a stack,

whereas in *S. cerevisiae* vesicles corresponding to Golgi sub-compartments are typically seen as single, randomly distributed, isolated cisternae, generally not arranged into parallel stacks (Preuss et al., 1992; Rossanese et al., 2001). These cisternae can be classified as cis, medial, or trans-Golgi Network (TGN), each containing a compartment-specific set of enzymes (Lowe, 2011). Proteins reaching the Golgi apparatus undergo further modifications (O-glycosylation, proteolytic processing, sulfation and formation of high-mannose oligosaccharides) that allows functional diversification of mature proteins so they can exit from the TGN (Shorter and Warren, 2002). When the trans-Golgi cisternae is reached, the properly folded secretory proteins are packaged into clathrin coated vesicles and are sent to their correct final destination with the help of different adaptor proteins (Viotti, 2016; Tooze et al., 2001; Nakatsu and Ohno, 2003).

As mentioned before, a central characteristic of this system is its bidirectionality, with cargo vesicles moving in the ER-Golgi direction in COPII-coated vesicles (anterograde transport) for further processing and secretion, while transport machinery or escaped ER resident proteins return in the Golgi-ER direction (retrograde transport) by COPI-coated vesicles (Figure 1.3) (Gomez-Navarro and Miller, 2016; Viotti, 2016; Emr et al., 2009). The COPI complex, which in addition to the retrograde transport have complex functions in intra-Golgi trafficking (Duden, 2003), is composed by seven stoichiometric subunits (α , β , β' , γ , δ , ε and ξ -COP), which enter the coated vesicles as an intact unit (Hara-Kuge et al., 1994).

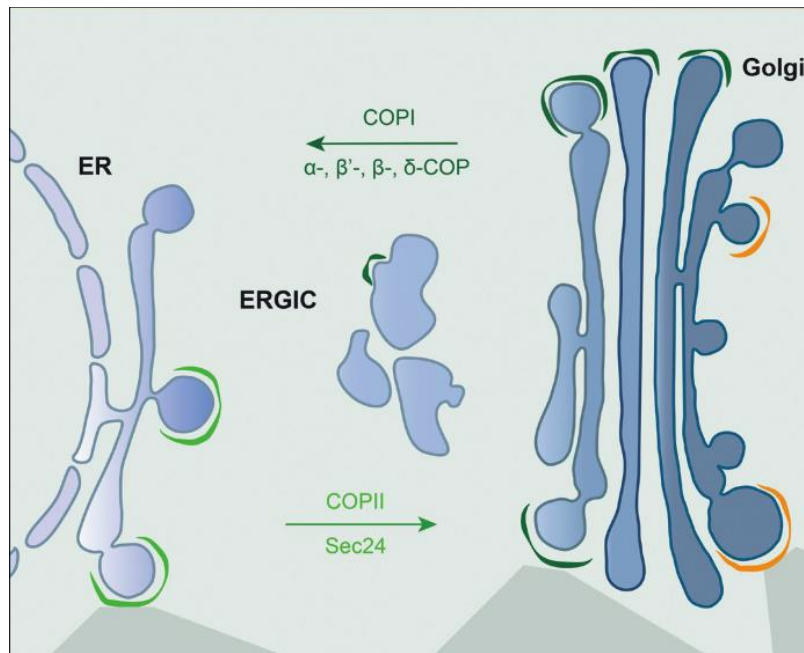


Figure 1.3: Anterograde and retrograde transport pathways. Modified figure from *Gomez-Navarro and Miller, 2016*. Schematic representation of anterograde and retrograde transport pathways. Secretory cargoes are trafficked in an anterograde direction from the ER to the Golgi in COPII-coated vesicles. Sec24 is the cargo adaptor. The COPI coat mediates retrograde transport from Golgi to the ER between Golgi compartments.

1.2 Protein translocation

1.2.1 The endoplasmic reticulum

In eukaryotic cells, the ER membrane is a major site of protein biogenesis and the entry point into the compartments of the exocytic and endocytic pathways and the extracellular space (*Dudek et al., 2015*). The ER coordinates the biosynthesis, maturation, quality control and degradation of secretory and membrane protein via multiple pathways, playing a central role in the cell (*Powell and Latterich, 2000*). It is also a major site for storage of intracellular calcium, and takes part in different cellular processes such as signalling and lipid biogenesis (*Clapham, 2007; Fagone and Jackowsky, 2009*). The ER is considered one of the most complex organelles of the eukaryotic cells, and the complexity of the ER is reflected in an equally complex physical architecture (*Powell and Latterich 2000; Du et al., 2004; West et al., 2011*). The ER consists of the nuclear envelope and the peripheral ER, which includes smooth tubules and rough sheets. While the ER is defined as an interconnected network with a continuous membrane, the different structures that make up the ER perform very diverse and specialized functions within the cell (*Schwarz and Blower, 2016*). In *S. Cerevisiae* the appearance of the ER network differs from the highly

organized stacks of ER cisternae that are normally observed in mammalian cells that are specialized for secretion (*Preuss et al., 1991*). The Yeast tubules are not abundant near the nuclear envelope and appear to be highly convoluted, since long sections of tubules are rarely observed. Most of the peripheral ER, known as cortical ER, appears as a simple ring juxtaposed with the plasma membrane and is actually a network of highly dynamic tubules, similar in structure to the ER in higher eukaryotes (*Preuss et al., 1991; Prinz et al., 2000; Fehrenbacher et al., 2002*).

1.2.2 Targeting

Protein synthesis in the cytosol is directed towards the appropriate organelles by specific targeting sequences (*Pool et al., 2022*). A prerequisite of protein translocation into the ER, either co- or post-translational, is the recognition of the peptide to be translocated and its targeting to the translocon (*Hegde and Bernstein, 2006*). The recognition of a signal sequence (SS), which was first identified experimentally by Milstein, is essential for these two processes to happen (*Milstein et al., 1972; Yim et al., 2018*). N-terminally positioned SSs are conventionally referred to as signal peptides (SPs) and are cleaved by signal peptidase. ER-targeting can also be achieved by more internally located, uncleaved signal sequences (so-called signal-anchored (SAs) sequences) or first transmembrane domains of a protein (*Mandon et al., 2013; Spiess et al., 2019*). Most SPs have a recognizable three-domain structure (Figure 1.4): a net positive charge in the N-terminal region, that facilitates their initial insertion and subsequent inversion; a central hydrophobic H-region; and a conserved polar C-terminal region containing the cleavage site for signal peptidase (*O'Keefe and High, 2020; von Heijne, 1984; Gierasch, 1989; Hegde and Bernstein, 2006; Von Heijne, 1985*). Even if the general architecture of signal peptides is conserved, their primary sequence and length vary substantially (*von Heijne, 1986*). The consensus cleavage site is determined by small residues at positions -1 and -3 relative to the cleavage site (*von Heijne, 1986*). Both SPs and SAs are hydrophobic, but transmembrane helices typically have longer hydrophobic regions. Also, transmembrane helices do not have cleavage sites, but the cleavage-site pattern is in itself not sufficient to distinguish the two types of sequences (*Petersen et al., 2011*). This makes it difficult to distinguish between SPs and SAs (*Yim et al., 2018*).

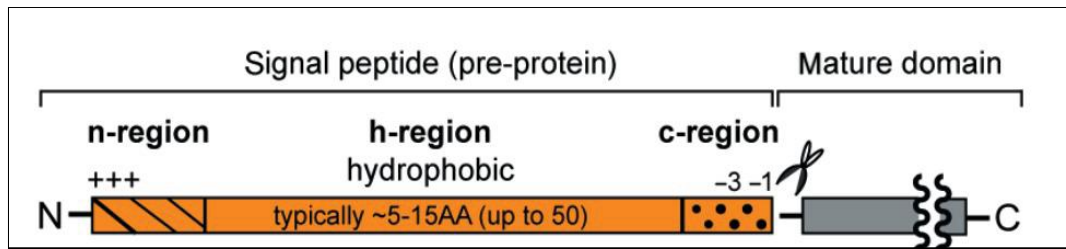


Figure 1.4: Schematic representation of a typical signal peptide. Modified figure from *O'Keefe and High, 2020*. Most ER signal peptides have an N-terminal polar n-region (dashed orange) that facilitates their initial 'head-on' insertion and subsequent inversion; a central hydrophobic H-region (plain orange); and a polar C-terminal c-region (dotted orange) containing the residues that direct signal sequence cleavage.

Even if two signal sequences are equally efficient in their ability to initiate translocation, they can differ in other aspects of their interaction with either the translocation pore or the signal sequence cleavage machinery (*Hegde and Bernstein, 2006*). The composition of a signal sequence can similarly influence the transmembrane integration of a downstream transmembrane domain or the post-translational maturation of the translocated protein (*Ott and Lingappa, 2004; Rutkowski et al., 2003*). The timing of signal sequence cleavage, which vary considerably among substrates, might influence the use of glycosylation sites near the N terminus (*Chen et al., 2001; Hegde and Bernstein, 2006*). Conversely, the presence of downstream sequence elements, like transmembrane domains or glycosylation sites, can influence the functionality of a signal sequence at the N terminus (*Pool et al., 2022; Shaffer et al., 2005; Kim and Hegde, 2002; Hegde and Bernstein, 2006*). Signal sequences seem to regulate the timing of cleavage, and by doing this it controls not only downstream protein folding and glycosylation events, but also the exit of proteins from the ER (*Hegde and Bernstein, 2006*).

Several features make a signal sequence optimal for ER translocation through the Sec61 channel. Since helices consist largely of hydrophobic amino acids with their hydrophobic side chains exposed to the outside and the hydrophilic peptide backbone hidden inside, helicity is an important aspect for insertion into the translocation pore (*Spiess et al., 2019*). This helix propensity can be disturbed though by high glycine/proline content in the H-region (*Nguyen et al., 2018*). Also, hydrophobicity of the H-region, which is the main driving force for transmembrane integration and has a great diversity in terms of length, is as well among the most important features that make a signal sequence optimal; In addition, charge bias between N-region and C-region is important to help the peptide orientate when

inserting to the channel. The transmembrane orientation of the initial signal and to a weaker extent also the downstream transmembrane segment is affected by charge flanking residues according to the so-called positive-inside rule (*Spieß et al., 2019; Yim et al., 2018*).

Signal sequence inefficiency might have pathological consequences under some conditions (*Hegde and Bernstein, 2006*). The prion protein (PrP), which is a cell-surface glycoprotein whose altered metabolism is implicated in causing neurodegeneration, provides one example of this phenomenon (*Kim and Hegde, 2002; Ma et al., 2002; Rane et al., 2004*). Moreover, point mutations adjacent to the SP cleavage site of pre-proteins may impair SP cleavage (*Lyko et al., 1995*) and downstream folding (*Beuret et al., 1999*), and can cause ER stress, cytotoxicity and a series of pathological events (*Kang et al., 2006*). Missense mutations upstream of pre-pro-insulin's signal peptide cleavage site causing mutant INS gene and inducing diabetes of youth is one example of this kind of anomalies (*Liu et al., 2012*).

In co-translational translocation, targeting begins when the signal recognition particle (SRP) recognizes and binds the signal sequence of a nascent polypeptide as it emerges from the ribosome (*Pool et al., 2022; Walter et al., 1981; Halic and Beckmann, 2005; Shan and Walter, 2005*). This binding of SRP leads to retardation of chain elongation, increasing the length of time that the nascent polypeptide remains in an unfolded conformation compatible with an efficient translocation through the Sec61 complex (*Walter et al., 1981; Wolin and Walter, 1989*). SRP is a ribonucleoprotein complex that binds to predominantly very hydrophobic signal sequences as they emerge from the ribosome (*Hegde and Bernstein, 2006; Ng et al., 1996*). Signal sequence binding is mediated primarily by a deep, flexible hydrophobic groove in the 54-kDa subunit of SRP, and also by electrostatic interactions between the phosphate backbone of SRP RNA and basic amino acids in the N domain of signal sequences (*Keenan et al., 1998; Batey et al., 2000; Hegde and Bernstein, 2006*). After recognition and slowing translation, SRP targets the ribosome-nascent chain (RNC) complex to the ER via the SRP receptor (SR) (*Pool et al., 2022; Gilmore et al., 1982; Meyer et al., 1982*). After docking to the membrane, the RNC is transferred to the translocon (*Halic and Beckmann, 2005*). The initial contact between the large ribosomal subunit and the Sec61 complex is important for efficient insertion of the nascent

polypeptide into the translocation pore (*Cheng et al., 2005*). The Sec61 pore aligns with the exit of the tunnel traversing the large ribosomal subunit, allowing both structures to function together and promoting the direct movement of the nascent chain through or into the ER membrane (*Beckmann et al., 1997, Beckmann et al., 2001*). The SRP-SR complex dissociates then from the ribosome and, as result of GTP hydrolysis, SRP and SR dissociates from each other (*Gilmore and Blobel, 1983; Wild et al., 2004, Jiang et al., 2008, Song et al., 2000*).

The targeting of proteins during post-translational translocation is less well understood. They escape recognition and targeting by SRP, possibly because the substrates are too short to engage SRP before their synthesis is completed, or because they have less hydrophobic signal peptides (*Rapoport et al., 2017*). These substrates need to be kept in an unfolded or loosely folded conformation before their transfer through the membrane (*Rapoport et al., 2017*). Post-translational translocation in yeast requires both the Sec61 translocation channel and a complex of four additional proteins: Sec63, Sec62, Sec71 and sec72 (*Tripathi et al., 2017; Pool et al., 2022*). Sec62 has been suggested to act as a targeting receptor for the secretion of small proteins and provides cells with the opportunity to regulate secretion of small proteins independent to the SRP pathway (*Lakkaraju et al., 2012, Lang et al., 2012*).

1.2.3 Translocation

Protein translocation across the ER membrane was for a long time a controversial topic of scientific debate and for many years various models were proposed. Back in 1975, the existence of a protein conducting channel from where the proteins emerging from the ER bound ribosomes were translocated into the ER was proposed by Blobel and Dobberstein (*Blobel and Dobberstein, 1975*), but it was not until two decades later that their hypothesis was confirmed and components of the Sec61 complex were characterised (*Deshaies and Schekman, 1987; Gorlich et al., 1992; Gorlich and Rapoport, 1993; Hartmann et al., 1994*).

As mentioned previously, translocation through the Sec61 channel can happen either co-translationally (i.e concomitant with protein synthesis) or post-translationally (i.e after termination of protein synthesis). Translocation of proteins across the ER membrane takes

place co-translationally in all organisms, whereas in eukaryotes post-translational translocation can also occur (*Mandon et al., 2013; O'Keefe and High, 2020; Corsi and Schekman, 1996*). In yeast, the selection of the pathway used depends on the hydrophobicity of the signal peptide of each protein: for proteins with more hydrophobic signal peptides the translocation tends to happen co-translationally, while those with less hydrophobic signal peptides preferentially use post-translationally translocation (*Corsi and Schekman 1996; Ng et al., 1996*). When the translocation is done co-translationally, a trimeric complex (Figure 1.8) is formed by the association of Sec61 (Sec61 α in mammals) with sbh1 (Sec61 β in mammals) and Sss1 (Sec61 γ in mammals) (*Panzner et al., 1995a; Helmers et al., 2003*). As mentioned before, when the translocation is done post-translationally, the association of the Sec61 complex with the Sec63 complex is required (*Meyer et al., 2000; Panzner et al., 1995b*). The Sec63 complex is composed of Sec63, Sec62, sec71 and Sec72 (*Cox and Walter, 1996; Brodsky and Schekman, 1993*), forming the heptameric Sec complex (Figure 1.10).

1.2.3.1 Co-translational Translocation

The initial trigger for channel priming during cotranslational translocation is ribosome arrival. The SRP-RNC targeting complex itself is unable to interact directly with the translocon due to overlapping binding sites of SRP and translocon at the ribosomal tunnel exit. The presence of the SR, however, allows translocon binding and leads to structural rearrangements of the SRP, such that a ribosomal binding site for the translocon became exposed (*Halic et al., 2006*). Once SRP has dissociated from the RNC, the complex can bind to the translocon and protein translocation resumes.

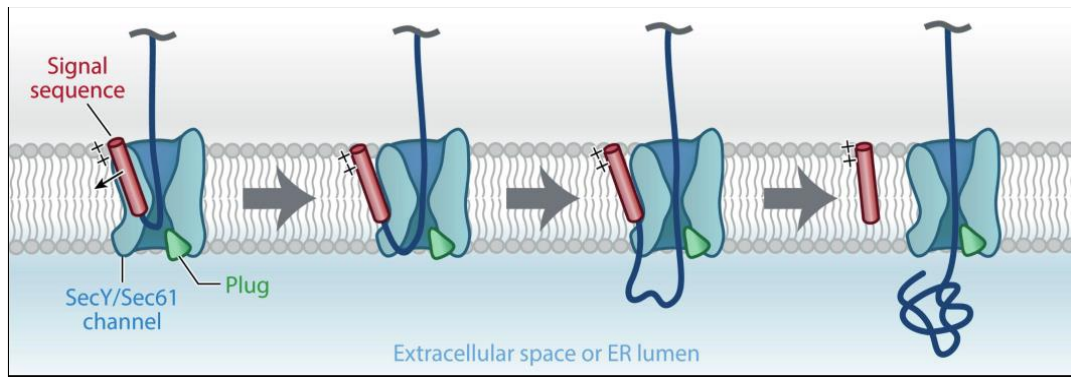


Figure 1.5: Schematic representation of translocation of a secretory protein. Modified figure from *Rapoport et al., 2017*. In all modes of translocation, the secretory protein inserts as a loop, with the positively charged N-terminus of the signal sequence staying in the cytosol. The signal sequence is eventually cleaved off by signal peptidase. In the schematic representation the lateral gate is to the left.

The ribosome binds to the C-terminal half of the Sec61, interacting with the cytosolic loops between TM8 and TM9, and TM6 and TM7 (*Rapoport et al., 2017; Cheng et al., 2005; Becker et al., 2009; Voorhees et al., 2014*). Ribosomal binding to these loops constrains this region of Sec61 in a defined position, and this propagates a conformational change through the structure of the channel. This both disrupts the interaction between the polar cluster residues and exposes a seam of hydrophilic residues to the hydrophobic bilayer, resulting in a partial destabilization and cracking of the lateral gate (*Voorhees and Hegde, 2016b*). As the signal sequence approaches the channel, its positively charged N-terminus interacts with the positively charged head groups of phospholipids, retaining the N-terminus on the cytosolic side of the membrane and allowing for loop insertion (*Rapoport et al., 2017*). The hydrophobic part of the signal sequence moves then into the partially opened lateral gate of the primed channel and binds to a hydrophobic binding site in the space between helices 2 and 7, created by a conformational change caused by the ribosome binding (*Plath et al., 1998; Voorhees and Hegde, 2016a*). At the same time, the segment following the signal sequence would move into the pore in a loop-like manner as shown in Figure 1.5 (*Shaw et al., 1988, Plath et al., 1998, Rapoport et al., 2017*).

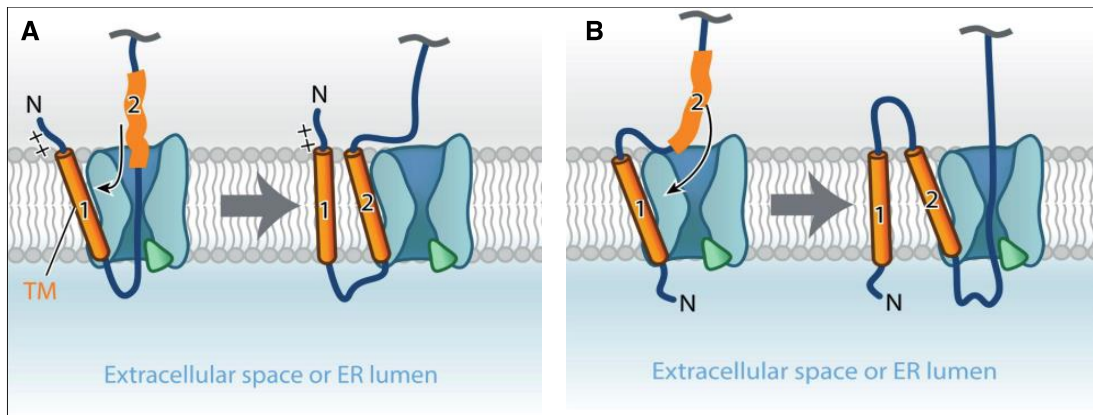


Figure 1.6: Schematic representation of membrane insertion of a protein. Modified figure from *Rapoport et al., 2017*. (A) Membrane insertion of a protein that retains the N terminus in the cytosol. The nascent membrane protein inserts as a loop into the channel, with the positively charged N terminus preceding the first transmembrane (TM) segment staying in the cytosol. The next TM segment aborts translocation of the polypeptide across the membrane. (B) Membrane insertion of a protein with its N terminus on the extracellular side. The N terminus preceding the first TM segment flips across the membrane. The next TM segment causes loop insertion of the polypeptide into the channel and initiates translocation.

Lipid partitioning is a universal mechanism for signal sequence recognition and explains how diverse hydrophobic signal and TM sequences can be recognized (*Plath et al., 1998, Rapoport et al., 2017*). Signal sequence recognition may also involve some amino acid side chain interactions, particularly between hydrophobic residues from the signal sequence and the outside of TM2 (*Voorhees and Hegde, 2016a*). In contrast to signal sequences, the more hydrophobic TM segments displaces TM2, which results in a further destabilization of the lateral gate and widening of the central pore (*Voorhees and Hegde, 2016a, Hizlan et al., 2012, Park et al., 2014*). This allows the TM segments to move away from the channel into the lipid phase once the connecting loop to the polypeptide segment inside the channel reach sufficient length (*Briggs et al., 1986; McKnight et al., 1991; Voorhees and Hegde, 2016a*). TM domains are inserted into the membrane in a sequential manner, starting with an N-terminal signal or TM sequence that determines the orientation of all downstream TM segments. In a generic model for transmembrane domain insertion, the relative orientation of the integration follows the ‘positive-inside rule’ (*von Heijne and Gavel., 1988*) (Figure 1.6).

The Sec61 channel is a passive pore with an aqueous interior, so the polypeptide chain located in the translocon can slide in either direction inside the channel by Brownian motion. In co-translational translocation, the elongating polypeptide chain goes directly from the ribosome tunnel to the channel, and the translating, channel bound ribosome restricts any back movement of the polypeptide chain back out of the channel (*Rapoport et al., 2017*). The driving force during co-translational protein import into the ER is the

elongation of the nascent polypeptide chain on the translating ribosome. (Rapaport *et al.*, 2017).

During the translocation process, the signal sequence would tend to remain in the binding pocket of the Sec61 complex until is cleaved off by a translocon associated signal peptidase, realising the translocated peptide into the ER lumen (Figure 1.5) (Rapaport *et al.*, 2017). This is not the case for most membrane proteins, since they lack SP and their highly hydrophobic N-terminal signal anchor sequences or first transmembrane domains serve as a recognition signal instead (von Heijne, 1990). However, most membrane proteins use the co-translational pathway for their integration (Schibich *et al.*, 2016; Ast *et al.*, 2013; Ng *et al.*, 1996).

1.2.3.2 Post-translational Translocation

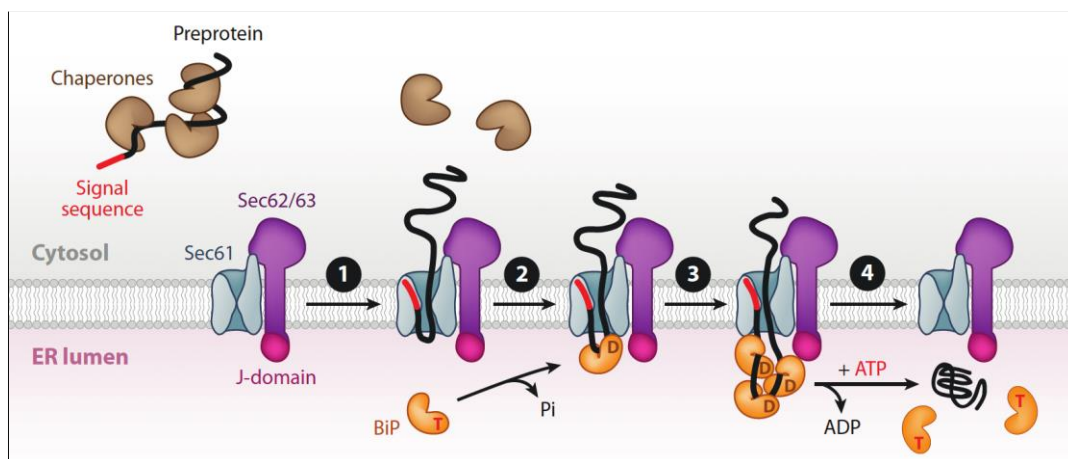


Figure 1.7: Schematic representation of post-translational translocation in eukaryotes. Modified figure from Park and Rapoport, 2011. Different steps in the post-translational translocation of a eukaryotic secretory protein. Step 1: Binding of a completed polypeptide chain to the Sec complex, form by Sec61 channel and the Sec62/Sec63 complex. Chaperones associated with an already synthesised polypeptide chain are released during insertion into the channel. Step 2: The ER-luminal BiP ATPase starts out in its ATP-bound state (T) with an open peptide-binding pocket. Interaction with the J-domain (J) of Sec63 introduces ATP hydrolysis, converting BiP to the ADP-bound state (D) and causing the binding pocket to close around the translocating polypeptide chain. BiP binding prevents the polypeptide chain from moving back into the cytosol but does not impede forward movement. Step 3: When the polypeptide chain has moved a sufficient distance into the ER lumen, the next BiP molecule binds. This process is repeated until the polypeptide has completely traversed the channel. Step 4: Finally, ADP is exchanged for ATP, which opens the binding pocket and causes BiP to dissociate from the translocating chain.

In post-translational translocation, the secretory proteins are completely synthesised and realised from ribosomes before they are targeted to the ER membrane (Rapaport *et al.*, 2017; Wu *et al.*, 2019). In the cytosol, the newly synthesized proteins are maintained in a translocation-competent state, a function that in yeast is performed by cytosolic heat shock

(Hsp70) proteins which helps keeping them in an unfolded or loosely folded conformation (Figure 1.7) (*Corsi and Schekman, 1996*).

Post-translational translocation, represented schematically in Figure 1.7, occurs in two well-defined steps. The first involves the recognition and binding of SP from soluble fully translated substrates to the Sec63 complex (*Barlowe and Miller, 2013; Hassdenteufel et al., 2018*). In the second step the polypeptide chain is translocated through the protein conducting channel by an ATP-dependent mechanism that involves the lumenally associated chaperone Kar2 (the yeast orthologue of BiP) (*Park and Rapoport, 2011; Plath et al., 1998; Matlack et al., 1999*). Similar to what happens in co-translational translocation, the signal peptide binds to the translocon near the lateral gate and induces the pore opening, allowing the hydrophilic polypeptide to transverse the membrane (Figure 1.7) (*Plath et al., 1998, Voorhees and Hegde, 2016a*). Afterwards, the protein to be secreted associates with Kar2 which promotes the directed movement of the polypeptide chain through the channel (*Matlack et al., 1999, Panzner et al., 1995a*). Kar2 starts out in its ATP-bound state with an open peptide-binding pocket. After an interaction with the luminal J-domain of Sec63, which stimulates the ATP hydrolysis and closure of the peptide-binding pocket, Kar2 binds to the translocated polypeptide preventing it from moving back into the cytosol. When the polypeptide has moved a sufficient distance in the forward direction, the next Kar2 molecule can bind and the process repeats (*Rapoport et al., 2017; Feldheim et al., 1992; Misselwitz et al., 1999; Griesemer et al., 2014; Ramirez et al., 2017*).

1.3 Sec61 channel

As mentioned previously, protein translocation across the eukaryotic ER membrane or across the prokaryotic plasma membrane is a decisive step in the biosynthesis of secretory and transmembrane proteins (*Cheng et al., 2005; Mandon et al., 2013; Park and Rapoport, 2012; Rapoport et al., 2017; Shao and Hegde, 2011; Nyathi et al., 2013*). These proteins are moved through a conserved protein-conducting channel, the Sec61 channel, either in a co- or post-translational manner (*Park and Rapoport, 2012*).

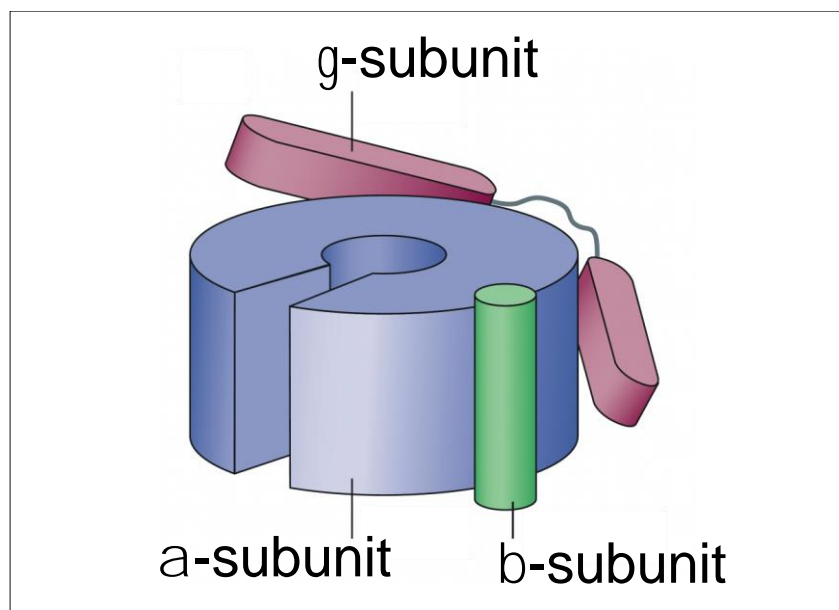


Figure 1.8: Sec61 complex in yeast. Schematic representation of sec61 complex in yeast. Modified figure from *Cross et al., 2009*.

The Sec61 channel (Figure 1.8) consists of a large α -subunit (Sec61 α in eukaryotes and SecY in archaea and bacteria) with both termini on the cytosol, and 10 transmembrane domains; and two small, usually single-spanning, β - and γ -subunits (Sec61 β and Sec61 γ in eukaryotes and SecG and SecE in bacteria). Much of what is known about the Sec complex function was obtained from the crystal structure of an archaeal SecY complex (*van den Berg et al., 2004*). The structure (Figure 1.9) showed that SecY (Sec61 in yeast and Sec α in mammals) is divided into two N- and C-terminal halves of five transmembrane (TM) segments, which are pseudo-symmetrical and form a central pore between TM5 and TM6 (*van den Berg et al., 2004; Tsukazaki et al., 2008, Egea and Stroud, 2010*). The channel pore has an hourglass shape with a constriction in the centre of the membrane, called the pore ring (Figure 1.9A and B, green), that consists in a ring of six aliphatic amino acids that projects their hydrophobic side chains to the inside of the ring. The cytosolic side of the pore is not sealed, but the luminal cavity is occupied by a plug domain (Figure 1.9A and B, yellow) (*Reithinger et al., 2014; Park and Rapoport, 2017*), that together with the pore ring restrict the passage of ions and other small molecules through the membrane and maintain its integrity (*Park and Rapoport, 2011*). The pore has a lateral gate, located opposite to the hinge, that is bordered by segments TM2 and TM3 on one side of the interface and by segments TM7 and TM8 on the other side (*van den Berg et al., 2004; Mandon et al., 2013*). The lateral gate functions as signal peptide binding site during translocation early stages and

allows transmembrane domains to partition into the lipid bilayer (Plath *et al.*, 1998; Heinrich *et al.*, 2000; Gogala *et al.*, 2014). The α -subunit has been shown to interact with polypeptide residues during translocation and integration (Nyathi *et al.*, 2013) and has been also proposed to be the core component of the export channel of misfolded proteins and the receptor of the proteasome during ERAD (Kalies *et al.*, 2005; Römisch, 2005).

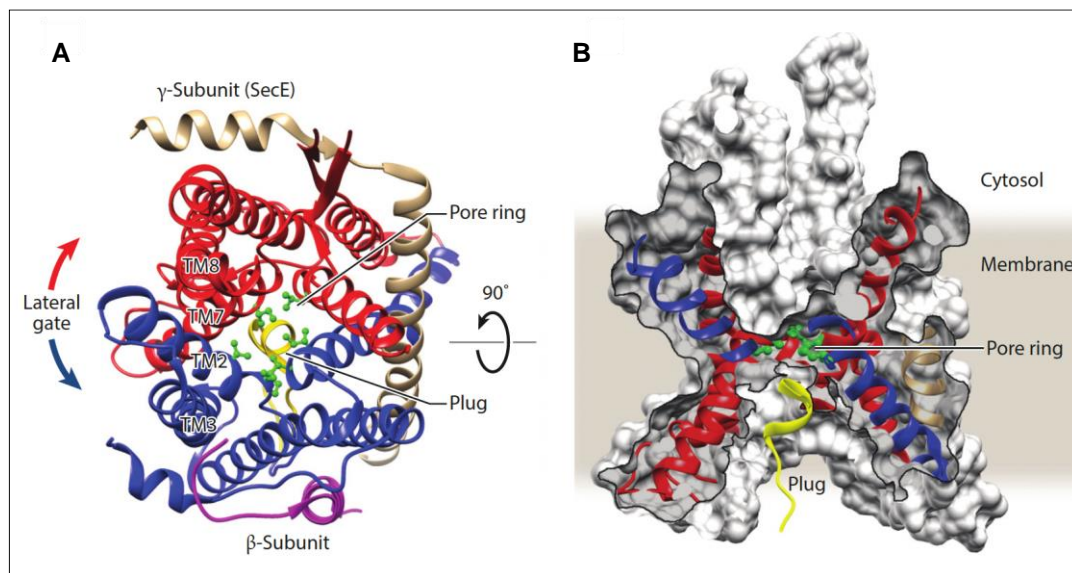


Figure 1.9: Sec61 structure. Modified figure from Rapoport *et al.*, 2017. Crystal structure of the idle SecY channel from *Methanocaldococcus jannaschii*. (A) view from the cytosol. (B) cutaway side view of a space-filling model of the channel in the membrane. For both (A) and (B): β -subunit is shown in purple, γ -subunit in beige, the N- and C-terminal halves of the α -subunit are shown in blue and red, respectively, the plug domains in yellow, and the pore ring residues are shown in green.

For co-translational translocation, the α -subunit associates in a trimeric complex with the β -subunit (Sbh1 in yeast, Sec61 β in mammals; Figure 1.9A and B, purple) and the γ -subunit (Sss1 in yeast, Sec61 γ in mammals Figure 1.9A and B, beige) (Panzner *et al.*, 1995b, Wilkinson *et al.*, 1997; Kalies *et al.*, 1998; Helmers *et al.*, 2003). Sbh1 and Sss1, both conserved through evolution, are small tail-anchored proteins with their N-termini on the cytoplasmic face of the ER membrane (Hartmann *et al.*, 1994; Van dem Berg *et al.*, 2004). Sss1 is an essential component of the translocon (Mandon *et al.*, 2013; Wilkinson *et al.*, 1997). It contains an amphipathic helix that lies flat on the cytosolic surface of the ER membrane, and a TM segment that diagonally crosses the membrane, forming a “clamp” that stabilizes the channel by keeping the two halves of the Sec61 together (van den Berg *et al.*, 2004; Voorhees and Hegde, 2016b). An overview of Sbh1, which has been the protein of main interest for my project, will be given in the following section (Section 1.3.1).

As mention earlier, a requirement for post-translational transport in eukaryotes is the association of the trimeric Sec61 complex with the tetrameric Sec63 complex (*Meyer et al., 2000; Panzner et al., 1995a*), form by Sec63, Sec62, sec71 and Sec72 (*Wu et al., 2019; Cox and Walter, 1996; Brodsky and Scheckman, 1993*). This association give place to the heptameric Sec complex (Figure 1.10), with sec62 and sec63 being essential for cell growth (*Plath et al., 1998; Meyer et al., 2000*). Orthologs of yeast Sec62 and Sec63 have been also identified in the mammalian ER membrane (*Skowronek et al., 1999; Meyer et al., 2000*), suggesting that these proteins may be playing additional roles in the secretory pathway. Also, overexpression of Sec63 decreases steady state levels of multi-spanning membrane proteins, suggesting a substrate specific and regulatory functions of Sec63 in ER import (*Mades et al., 2012*). Recent studies shows that proper sorting of single- and double-pass membrane proteins was severely impaired in *sec63* mutants, suggesting that sec63 is required for proper insertion and topogenesis of membrane proteins in the ER (*Jung et al., 2019; Jung and Kim, 2021*).

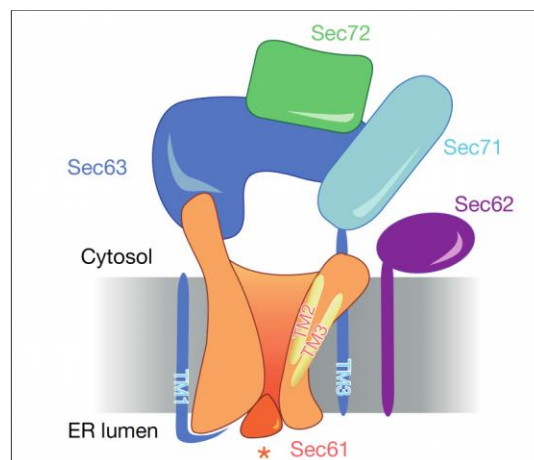


Figure 1.10: Heptameric Sec complex. Modified figure from *Wu et al., 2019*. Schematic representation of the Sec62-Sec63-primed channel. The lateral gate is open caused as Sec63 serving as a scaffold. The plug (*) is closing the channel across the membrane. The Sec61 channel is shown in orange, Sec63 in blue, Sec62 in purple, Sec71 in light blue and Sec72 in green.

S. cerevisiae has a homologue of Sec61, called Ssh1, that shares around 30% identity with Sec61 (*Osborne et al., 2005*). Ssh1 associates with a homologue of Sbh1, called Sbh2, and Sss1 to form the Ssh1 trimeric complex (*Finke et al., 1996*). The non-essential Ssh1 complex does not assemble with the Sec62-sec63 complex, but it associates with ribosomes with an affinity similar to the Sec61 complex (*Jan et al., 2014; Prinz et al., 2000*). This, together with the evidence that Ssh1 binds to the signal sequences of some co-

translationally translocated proteins (Wittke *et al.*, 2002), suggests that the Ssh1 complex might function exclusively in co-translational import of proteins into the ER (Becker *et al.*, 2009; Finke *et al.*, 1996; Wittke *et al.*, 2002).

1.3.1 Sbh1

Sbh1 or Seb1, the β -subunit of yeast Sec61 complex was identified in parallel biochemically by Panzner *et al.* (1995) and by Toikkanen *et al.* (1996), and shares 30% identity with its mammalian counterpart as shown by the multiple alignments in Figure 1.11 (Panzner *et al.*, 1995A; Toikkanen *et al.*, 1996).

Sbh1 is a small tail-anchored protein of 82 amino acids with one transmembrane span integrated into the ER membrane, peripherally associated with the Sec61 channel (Toikkanen *et al.*, 1996; Borgese *et al.*, 2019; Park and Rapoport, 2012; Panzner *et al.*, 1995A). The helical transmembrane span is preceded by a 54 amino acid-long cytosolic domain consisting of a membrane-proximal, conserved, and structured part of about 16 amino acids and an intrinsically unstructured, poorly conserved N-terminal domain of 38 amino acids (Kinch *et al.*, 2002). The transmembrane span is followed by a C-terminal short tail of a few amino acids facing the lumen (van den Berg *et al.*, 2004). Sbh1 interacts with Sec61 both via its transmembrane helix, through the transmembrane domain 4 of Sec61, and via its cytosolic domain (Voorhees and Hegde, 2016b; Zhao and Jäntti, 2009; Elia *et al.*, 2019).

S. cerevisiae contains a homologue of Sbh1, called Sbh2, which is part of the trimeric Ssh1 complex and is around 50% identical to Sbh1 (Finke *et al.*, 1996; Toikkanen *et al.*, 1996). Even though Sbh1 and Sbh2 are quite similar in sequence (Figure 1.11), they do not appear to replace each other in their respective complexes when their original α -subunit partner is present (Finke *et al.*, 1996). However, when they both lack their original partners, so when Sbh1 and Ssh1 are missing, Sbh2 can associate with Sec61 (Finke *et al.*, 1996). Neither Sbh1, nor Sbh2 are essential in yeast, but deletion of both genes makes cells temperature-sensitive at 37°C (Toikkanen *et al.*, 1996; Finke *et al.*, 1996; Feng *et al.*, 2007; Soromani *et al.*, 2012). Previous data on the translocation defect in the $\Delta sbh1\Delta sbh2$ strain were

somewhat contradictory (Finke et al., 1998; Feng et al., 2007). Finke et al. showed that this double deletion mutant has no detectable general ER protein import defects at 30°C, and results only in moderate accumulation of unprocessed precursors of the post-translationally translocated α -factor and Kar2 at 37°C (Finke et al., 1996). Later on, Feng et al. showed that the $\Delta sbh1\Delta sbh2$ strain has only a modest post-translational translocation defect into the ER for the α -factor precursor at 37°C, and the import defect was more pronounced when co-translational import was examined (Feng et al., 2007). In addition, $\Delta sbh1\Delta sbh2$ mutant cells showed a glycan trimming defect, due to reduced mannosidase 1 (Mns1) and glucosidase 1 (Gls1) translocation into the ER lumen at all temperatures (Feng et al., 2007).



Figure 1.11: Sequence alignments of Sbh1 with Sbh2 and mammalian Sec61β. (A) Alignment of amino acid sequences of yeast Sbh1 and its mammalian homologue Sec61β. (B) Alignment of amino acid sequences of yeast Sbh1 and its yeast homologue Sbh2. For both (A) and (B): Sites found phosphorylated in phosphoproteome screens in Sbh1 are shown red (Touati et al., 2019; Gnad et al., 2009; Soufi et al., 2009; Yachie et al., 2011; Amoutzias et al., 2012; Soramani et al., 2012; Swaney et al., 2013); Sites conserved in Sbh2, but not proven to be phosphorylated so far, are shown in blue; Sites found phosphorylated in phosphoproteome screens in Sec61β are shown in orange (PhosphoSitePlus). Transmembrane domains are shown in green. The top lines of each alignment (amino acids 1-38 of Sbh1, 1-45 of Sbh2 and 1-54 of Sec61β) show the intrinsically disordered regions of the cytosolic domains according to IUPred and PrDOS.

The TM domains of Sbh1 or Sbh2 has been shown to be sufficient to rescue $\Delta sbh1\Delta sbh2$ mutant strain from the temperature-sensitive growth phenotype (Feng et al., 2007). It was also reported by Feng et al. that the Sbh1 TM domain was able to rescue the associated co-translational translocation defect, and the reported glycan trimming defect (Feng et al., 2007). In addition, the Sbh1 TM domain was also sufficient for association with Sec61 and Sss1 (Feng et al., 2007). Although Sbh1 and Sbh2 share around 50% of their amino acid

identity, and both can interact with Sec61 or Ssh1, they have distinct functions in translocation as shown by distinct patterns of synthetic lethality (*Toikkanen et al., 1996; Schuldiner et al., 2005; Jonikas et al., 2009; Costanzo et al., 2016*).

A physical and functional link between Sbh1 and members of the exocyst complex has been proposed (*Toikkanen et al., 2003*). The exocyst is a conserved octameric protein complex involved in vesicle tethering to the plasma membrane (*Guo and Novick, 2004*), and so interaction between the ER translocation complex and the exocyst components are intriguing because functionally they are located at opposite ends of the secretory pathway (*Toikkanen et al., 2003*). Overexpression of *SBH1* has been shown to suppress the growth defect of exocyst mutants (*Toikkanen et al., 2003*). In addition, Sbh1 coimmunoprecipitates with Sec15 and Sec8, two subunits of the exocyst complex, and with Sec4, a secretory vesicle associated Rab GTPase that binds to Sec15 and is essential for exocytosis (*Toikkanen et al., 2003*). The β -subunit of the mammalian Sec61 complex can as well coimmunoprecipitate with subunits with the exocyst complex (*Lipschutz et al., 2003*). Sbh1 can also exist in the ER membrane independently of the Sec61 complex and on its own interacts with Rtn1, a resident ER TM protein that localizes preferentially to peripheral ER membrane, copurifies with the exocyst, contributes to formation tubular ER and regulates ER inheritance under stress (*Feng et al., 2007; De Craene et al., 2006; Voeltz et al., 2006; Piña et al., 2016*). At the same time the TM or cytosolic domains of Sbh1 alone did not suppress temperature-sensitive growth phenotypes of exocyst mutants, suggesting that the Sbh1 cytosolic domain plays a role in the functional interaction with the exocyst, and its association with the ER membrane is critical for retain this function (*Feng et al., 2007*).

The cytosolic domain of the β -subunit of Sec61 has been shown to interact directly with ribosomes in a specific manner, in contrast to previous findings that suggested the presence of the β -subunit is non-essential for ribosome binding (*Kalies et al., 1994; Levy et al., 2001*). However, this binding may occur at a post-targeting stage, after a first interaction of the ribosome with another ER component (*Levy et al., 2001*). In addition, it has been demonstrated that even if it is not essential, the β -subunit kinetically facilitates co-translational translocation by participating in a rapid insertion of the ribosome-bound nascent chain into the translocon (*Kalies et al., 1998; Jiang et al., 2008*). Data form

crosslinking experiments have also identified a tight interaction between the β -subunit and the 25kDa component of the SPC complex, indicating an SPC recruitment function of the β subunit during co-translational translocation at least in mammalian cells (*Kalies et al., 1998*). In yeast, SPC interaction with the β -subunit of the Sec61 complexes in the absence of ribosomes has been reported (*Antonin et al., 2000*). Coupling of the RNC-SRP targeting to translocation is another proposed function of both Sbh1p and Sbh2p. Despite their small sizes, the cytosolic domains of Sbh1 and Sbh2 are proposed to function as the guanine nucleotide exchange factors (GEF) for the β -subunit of the signal recognition particle receptor (SR β) (*Helmerts et al., 2003*). Both Sbh1 and Sbh2 efficiently promote the exchange of nucleotide for SR β , required to complete its GTP switch cycle (*Schwartz and Blobel, 2003; Helmerts et al., 2003*). This is supported by the fact that a protein interaction screen has found the trimeric Sec61 complex and its homologue Ssh1 complex to be in the proximity of SR β (*Wittke et al., 2002*). When part of the post-translational transport heptameric complex, however, the same Sec61 β is inactive as the GEF for SR β (*Helmerts et al., 2003*). Nevertheless, SR heterodimer formation is not compromised in cells lacking the β -subunits and the expression of a short segment of Sbh2, that lacks the majority of the GEF domain partially suppress the abnormal translocon gating kinetics (*Jiang et al., 2008*).

Sbh1 is central to the Sec complex required for post-translational protein import into the yeast ER which, as mentioned before, consists of the Sec61 channel and the heterotetrameric Sec63 complex (*Wu et al., 2019*). Even though Sbh1 makes extensive contact with the Sec71 subunit of the Sec complex, it is dispensable for stability of the Sec complex and general post-translational translocation into the ER in *Saccharomyces cerevisiae* (*Allen et al., 2019; Bhadra et al., 2021; Feng et al., 2007*). Reconstitution of Sec61 channels lacking Sec61 β into proteoliposomes still allows protein translocation, but only if the time for protein insertion is extended (*Kalies et al., 1998*). The Sec61 β cytosolic domain makes contact with targeting sequences in the vestibule of the Sec61 channel, and this contact is enhanced if substrates are prevented from inserting into the lateral gate (*Laird and High, 1997; MacKinnon et al., 2014*). Taken together, the data suggest that Sec61 β /Sbh1 recognizes some ER targeting sequences in the Sec61 channel vestibule and promotes their insertion into the lateral gate, but that its activity is not essential for most proteins.

1.4 Translocational regulation

Cells need to adapt to changes in environmental conditions and cellular demands, by tightly regulating different biological processes. This includes protein translocation through the ER membrane, process of which not much is known (*Hegde and Kang, 2008*).

As mentioned before, in co-translational translocation, a prerequisite of protein translocation into the ER is the recognition of the peptide to be translocated and its targeting to the translocon (*Hegde and Bernstein, 2006*). Targeting begins when the signal recognition particle (SRP) recognizes and binds the signal sequence of a nascent polypeptide as it emerges from the ribosome (*Walter et al., 1981; Halic and Beckmann, 2005; Shan and Walter, 2005*). This binding of SRP leads to retardation of chain elongation, increasing the length of time that the nascent polypeptide remains in an unfolded conformation compatible with an efficient translocation through the Sec61 complex (*Walter et al., 1981; Wolin and Walter, 1989*). After recognition and slowing translation, SRP targets the ribosome-nascent chain (RNC) complex to the ER via SRP receptor (SR) (*Gilmore et al., 1982; Meyer et al., 1982*). After targeting, the substrates must also interact with the Sec61 channel and induce its opening with their signal sequence (*Halic and Beckmann, 2005*). This interaction serves as a “proofreading” step, which can prevent translocation of proteins that are erroneously targeted to the ER, and also allows proper positioning of the nascent chain into the channel (*Hegde and Kang, 2008*).

1.4.1 Potential mechanisms

Regulatory systems contain accessory factors, that can selectively activate or inhibit specific reactions along the pathway. All proteins that enter the ER have distinguishing elements (e.g., signal sequences) with functional differences that can be exploited by cell modulated accessory components to influence key steps in translocation and effect regulatory control in a substrate-specific manner (*Hegde and Kang, 2008*).

As mentioned in section 1.2.2, natural signal sequences are notably diverse, and this diversity may be biologically important for differential modulation of ER translocation to mediate regulation (von Heijne, 1986; Hegde and Bernstein, 2006). Since signal sequences are recognized first by the SRP and later by the Sec61 channel (Walter et al., 1981; Halic and Beckmann, 2005), both are potential sites for regulation. Signal sequence recognition by SRP is typically considered to happen rapidly and efficiently, bringing all potential substrates constitutively to the translocon (Halic et al., 2006). To the contrary, Sec61 complex recognition is clearly more stringent and less efficient (Gorlich and Rapoport, 1993). The variability in translocation efficiencies could be due to the efficiency with which different signals sequences adopt their correct orientation in the Sec61 channel, influenced by the features of the signal sequence itself and its surroundings (Spiess et al., 2019; Yim et al., 2018). These configurations seem to be dynamic, but this would change as the nascent chain gets longer, eventually resulting in a forward or failed translocation (Figure 1.12). This crucial point result would vary between substrates and would be influenced by properties of both the signal sequence and the mature region (Hegde and Kang, 2008).

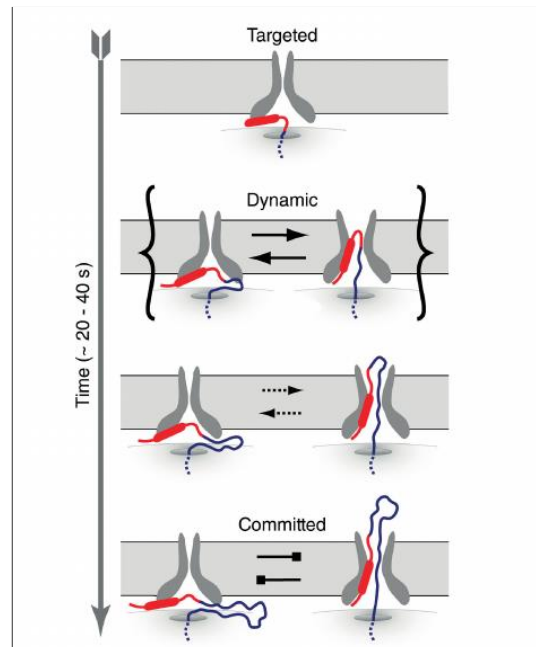


Figure 1.12: Signal sequence-Sec61 complex dynamic interaction. Modified figure from Edge and Kang., 2008. The Signal sequence is proposed to interact with a weak and dynamic manner after targeting the Sec61 channel (Top). The two configurations (looped, right; non-looped, left) have a higher interconvertibility with shorter nascent chain than longer ones.

Basal interaction activity of most signal sequences for the Sec61 complex is very low, because the substrate correct configuration in the channel is not achieved or not

maintained for long enough to allow the mature domain to enter the ER lumen before translocation competence is lost (*Hegde and Kang, 2008*). This suggests that additional substrate-specific factors operating in combination with each other are required for productive ER protein translocation. One possibility is that these additional factors interact directly with the nascent chain to stabilize the looped orientation (Figure 1.13, A), like what happens for example with the translocating chain-associating membrane protein (TRAM) and the translocon-associated protein complex (TRAP) in mammals (*Gorlich et al., 1992*), where both proteins stimulate translocation in a signal sequence-dependent manner, but neither is absolutely required (*Hegde and Kang, 2008*). Alternatively, the engaged nascent chain could be trapped in a transiently sampled configuration, preventing it from fully interconvert into another configuration (Figure 1.13, B). This trapping mechanism could be performed by a chaperone, or simply by nascent chain folding or glycosylation (*Goder et al., 1999*). Substrate specificity of this mechanism would be conferred by features of the mature domain, like appropriately positioned glycosylation sites, or the presence of high affinity chaperone binding sites (*Hegde and Kang, 2008*). A third possibility could be an indirect alteration on Sec61 functionality (Figure 1.13, C), by factors that influence the dynamic conformational changes needed for signal recognition and gating of the channel. For example, interactions of Sec61 with different factors could enhance or obstruct the movement of the plug domain, altering the open/close state of the channel, and affecting the translocation, which would happen to different degrees for different substrates (*Van dem Berg et al., 2004*). This mechanism would alter the basal translocation activity for many specific substrates, altering their relative dependence on stabilization and trapping, and tuning the substrate range of the Sec61 channel (*Hegde and Kang, 2008*). In addition, this mechanism is supported by the idea that the ribosome may loosen the plug domain (*Lizak et al., 2008*), and may explain how factors like BiP can influence gating and conductivity of the channel (*Hamman et al., 1998*).

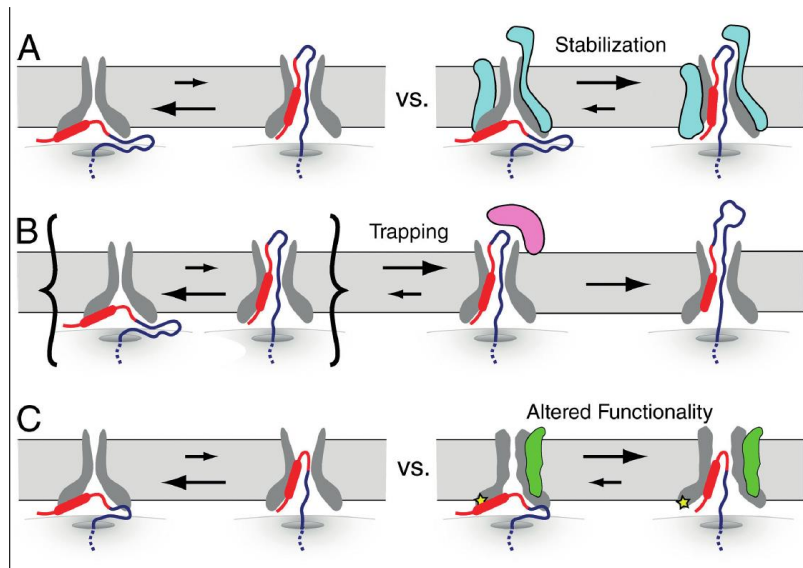


Figure 1.13: Translocational regulation mechanisms. Modified figure from *Edge and Kang., 2008*. (A) Selective stabilization of the looped conformation by accessory factors. (B) Trapping of transiently sampled conformation by nascent chain binding proteins, like chaperones. (C) Alterations of Sec61 channel functionality by an accessory factor or by a modification of the channel that changes its signal recognition properties.

Finally, opposite effects of all three mentioned mechanisms (factors that selectively obstruct some signal sequences, as well as proteins that trap the non-translocated conformation of the nascent chain or factors that stabilize the close conformation of the Sec61 channel) can act as counterparts contributing to the selective and graded general regulation of protein translocation (*Hegde and Kang, 2008*). This can be also illustrated by the fact that there are small molecules that inhibit translocation in a signal-specific manner (*Garrison et al., 2005; Besemer et al., 2005*).

1.4.2 Physiological implications

One general reason for regulating the translocation of proteins into the ER is quality control. A precise control of the amount of protein that engage the biosynthetic versus the degradation machinery can be done by simply regulating the access of proteins into the ER (*Hegde and Kang, 2008*). One example of these can be seen in stress-dependent translocation attenuation, where the amounts of certain substrates that are allowed to engage the biosynthetic machinery in the ER are controlled during stress, to prioritize the limited maturation capacity of the stressed ER for the most essential secretory and membrane proteins (*Kang et al., 2006*). This changes in translocation efficiency are substrate specific, reversible, physiological important and determined by the signal

sequence diversity of the substrates (*Kang et al., 2006*). Another purpose for translocational regulation is to regulate protein function, by controlling their localization. For this to happen, the protein that is not being translocated would have to avoid degradation and be functional for a determined cellular process (*Hegde and Kang, 2008*). One example can be seen with the ER luminal protein calreticulin, which has a role as molecular chaperone and calcium binding protein (*Michalak et al., 1999*). This protein has as well a minor cytosolic population involved in regulation of steroid hormone receptor function, nuclear export and integrin function (*Michalak et al., 1999*). The extent of partitioning between these two populations is controlled by the signal sequence of this protein and factors in the ER lumen and membrane that can regulate its ER translocation and so, modulate the actual function of the protein (*Shaffer et al., 2005*). Because regulation in ER translocation generates multiple products in different cellular compartments, a misregulation can result in inappropriate interactions between secretory pathway proteins and cytosolic components (*Hegde and Kang, 2008*). Such adverse interactions have been seen in certain diseases, including Alzheimer's (*Devi et al., 2006*).

1.4.3 Selective regulation of ER translocation

A selective change in the translocation of some but not other substrates is needed to modulate and adapt protein secretion to changes in cellular needs and environmental conditions. For doing this, contextual inputs from the environment or other cellular pathways can be translated into proper outputs through different mechanisms (*Hegde and Kang, 2008*). One simple possibility is differential expression of different components of the translocation machinery, either in a developmental or tissue-specific manner (*Hegde and Kang, 2008*). For example, components of the TRAP complex appear to be under regulatory control in some organisms, where alternative splicing events lead to isoforms of different TRAP components that are differentially expressed developmentally and tissue selectively (*Holthuis et al., 1995; Mesbah et al., 2006*). Alternatively, the availability of regulatory factors could be regulated simply by titration (*Hegde and Kang, 2008*). An example is what occurs during ER stress with luminal chaperones, where there is only a translocation reduction for proteins whose signal sequences dictate their dependence on the titrated factor, minimizing the risk of excessive protein misfolding (*Kang et al., 2006*). In addition,

phosphorylation of the translocon components, typically on the cytosolic side, can also modulate ER protein translocation, perhaps by manipulating the stability, functional activity or the association with the translocon or ribosome (*Prehn et al., 1990; Gruss et al., 1999*). The N-terminal region of signal sequences is very variable in terms of length and charge, and the same region of TMDs regulates its determinates is relative orientation on the membrane (*Spiess et al., 2019*), and so charge alterations in components of the translocon could alter the stability or/and the orientation of signal sequences or TMDs (*Goder et al., 2004*). This effect could be extremely selective depending the region of the translocon being altered, the nature of the signal sequence and other factors influencing this interaction (*Hegde and Kang, 2008*).

1.4.4 Mitochondrial example

For a long time, mitochondria were considered autonomous organelles with only a partial integration into cellular signaling networks (*Opalinska and Meisinger, 2014*). However, over the past few years this view has changed due to findings in mitochondrial biology, showing that mitochondrial activity can be modified according to cellular needs at various levels (*Opalinska and Meisinger, 2014*). They could adapt to cellular demands, by adjusting the ratio between fission and fusion events within the mitochondrial network, by modifying the rates of organelle turnover, or by adjusting either the mitochondrial protein content or activity of the mitochondrial enzymes (*Mcbride et al., 2006; Galluzzi et al., 2012*). They have also the capacity to control distinct molecular cascades leading to cell death and the ability to sense and react to cellular stress promoting the induction of cell-intrinsic or systemic adaptive responses (*Galluzzi et al., 2012*). Several studies have shown that mitochondrial protein import is tightly controlled by cytosolic and outer membrane bound kinases, via the phosphorylation of the translocase of the outer membrane (TOM complex) (*Opalinska and Meisinger, 2014*). One example of that is what happens when *S. cerevisiae* grow under glucose-rich conditions, and mitochondrial respiratory function is reduced due to a metabolic switch into fermentation (*Gerbeth et al., 2013*). In this situation, function and biogenesis of the TOM complex are tightly controlled by two kinases involved in glucose-induced signal transduction (*Schmidt et al., 2011; Gerbeth et al., 2013*): casein kinase 1 (CK1) and cAMP-dependent protein kinase (PKA). PKA negatively regulates import of the channel

forming subunit Tom40, by phosphorylating Tom40 and Tom22; and also, directly modulates the function of the mature TOM complex by phosphorylating Tom70 (*Gerbeth et al., 2013*). CK1 on the contrary, specifically modifies Tom22, supporting the assembly of TOM complex and alleviating the inhibitory effects of PKA (*Schmidt et al., 2011*), perhaps to maintain crucial mitochondrial functions that are essential under all metabolic conditions. These examples show the signaling pathway complexity involved in the adaptation of mitochondrial activity by directly controlling the mitochondrial proteome at the level of the translocase of the outer membrane in response to specific cellular demands (*Opalinska and Meisinger, 2014*).

1.5 Phosphorylation of the Sec61 translocon

1.5.1 Protein phosphorylation

Generally, cells use transcription regulation to control the distribution of protein resources, but this is a relatively slow process and post-translational modifications can therefore be used to rapidly modify the activity of proteins for adapting to temporal metabolic changes (*Cheng and Nielsen, 2016*). Such modifications not only allow for rapid alteration of enzyme activity, but are also reversible, enabling a cell to have tunable control of its basic cellular processes (*Cheng and Nielsen, 2016; Mok et al., 2011*). Protein phosphorylation is one of the most important and wide-spread types of post-translational modifications used in signal transduction, and is involved in the regulation of virtually every basic cellular process, affecting protein's activity, localization, stability, conformation, and/or interaction with other proteins (*Mok et al., 2011*). The interactions of protein kinases and phosphatases with their regulatory subunits and substrates, support cellular regulation and form complex self-regulating networks essential for cellular signal processing (*Breitkreutz et al., 2010; Abd-Rabbo and Michnick, 2017*). Abnormal phosphorylation has been associated with a wide variety of diseases phenotypes, including various leukemias, the development of different types of tumors, vascular diseases, diabetes mellitus and immune/inflammatory disorders (*Mok et al., 2011; Cohen, 2002*). In yeast, there are around 130 protein kinases and 32 protein phosphatases and each kinase can phosphorylate many different phosphorylation sites (*Breitkreutz et al., 2010; Sharifpoor et al., 2012; Bhandari et*

al., 2013). Protein kinases catalyze the transfer of the gamma-phosphate from ATP to specific amino acids in proteins (in eukaryotes, usually Ser, Thr, and Tyr residues) and several mechanisms are used to contribute to the specificity of phosphorylation, including catalytic site structure, local and distal interactions Kinase/substrate, and the formation of complexes that regulate the kinase (*Ubersax and Ferrell, 2007*).

1.5.2 Phosphorylation of ER translocation-relevant components

Sec61 β /Sbh1 and Sec63 are the only ER protein import channel subunits whose phosphorylation has been experimentally investigated (*Gruss et al., 1999; Wang and Johnsson, 2005; Soromani et al., 2012*). In yeast, Sec63 is phosphorylated in threonines 652 and 654, at its C-terminal domain and this phosphorylation strengthens the interaction between the cytosolic domains of Sec63 and Sec62, important for the formation of the Sec62/Sec63 complex (*Wang and Johnsson, 2005*). Sec63 phosphorylation is essential for tightly recruiting Sec62 to the Sec complex, which is part of the signal-sequence receptor, to efficiently deliver the signal sequence to the pore-forming Sec61 subunit of the translocation channel (*Plath et al., 1998; Wittke et al., 2002; Wang and Johnsson, 2005*). The disruption of the phosphorylation-dependent Sec62-Sec63 interaction impairs but does not prohibit protein translocation, probably due to a residual interaction between Sec62 and Sec63 that is independent of this phosphorylation (*Wang and Johnsson, 2005*). Since the turnover of Sec63 phosphorylation is slow, a phosphorylation-dependent regulation of Sec complex assembly is rather improbable (*Wang and Johnsson, 2005*). Nevertheless, a signal-induced dephosphorylation of Sec63 could cause the Sec62/Sec63 complex dissociation, and free the subunits for alternative tasks, such as cotranslationally protein translocation for Sec63 (*Wang and Johnsson, 2005*). Sec63 is phosphorylated by casein kinase 2 (CK2) which is highly expressed in fast growing cells and also enhances protein import capacity of mitochondria by phosphorylating the TOM complex (*Wang and Johnsson, 2005; Gerbeth et al., 2013*). CK2 was also found to phosphorylate Sec63 in mammals, at serines 574, 576 and 748, which also enhances its binding to Sec62 (*Ampofo et al., 2013*). These three amino acids and their surrounding sequences are highly conserved from yeast to man, indicating their importance for Sec63 function (*Ampofo et al., 2013*). In addition, CK2 has been associated with ER stress mediating signaling pathways (*Schneider et al., 2012*).

1.5.3 Phosphorylation β -subunit of the Sec61 complex

The phosphorylation of the β -subunit of the Sec61 complex has been shown both in mammals and in yeast (*Gruss et al., 1999; Soromani et al., 2012*). All known phosphorylation sites of Sbh1 and all but one of mammalian Sec61 β are located in their N-terminal unstructured region (Figure 1.11). Due to their flexibility, intrinsically disordered regions or proteins can interact with different partners in different circumstances, playing an important role in intracellular signaling (*Wright and Dyson, 2015*). Since phosphorylation can induce a conformational switch in an intrinsically disordered domain, generating or burying different binding sites for different interaction partners (*Valk et al., 2014; Bah and Forman-Kay, 2016; Bah et al., 2015; Ubersax and Ferrell, 2007*), differential phosphorylation of the Sbh1 cytosolic intrinsically disordered domain can therefore potentially regulate its differential association with different interaction partners.

1.5.3.1 Phosphorylation of mammalian Sec61 β

The cytoplasmatically-exposed segment of the mammalian Sec61 β include 70 amino acid residues and contain two putative phosphorylation sites with consensus sites for phosphorylation by (Ca²⁺)-dependent protein kinase C (PKC) (*Hartmann et al., 1994; Gruss et al., 1999*). The phosphorylation sites were not identified at the time, and the potential phosphorylation sites are poorly conserved between the mammalian and the yeast subunits (Figure 1.11), with the exception of the proline-flanked T5 (*Gruss et al., 1999*). The β subunit of Sec61 is phosphorylated in intact cells and pretreatment of purified dog pancreas membrane with PKC in vitro resulted in stimulation of cotranslational protein import into the ER, but since PKC phosphorylates as well others ER membrane proteins that are relevant for ER-import (SR α and TRAM), it is not clear whether the enhanced import is due to the phosphorylation of Sec61 β (*Gruss et al., 1999*).

1.5.3.2 Phosphorylation of Yeast Sbh1

In the 54-amino acid long cytosolic domain of yeast Sbh1, 8 sites have been found phosphorylated in different combinations in a number of phosphoproteome screens (*Touati et al., 2019; Gnad et al., 2009; Soufi et al., 2009; Yachie et al., 2011; Amoutzias et al., 2012; Soromani et al., 2012; Swaney et al., 2013*). It remains unclear though, how many sites are modified simultaneously in individual Sbh1 molecules, or in different Sbh1 populations (*Soromani et al., 2012*). In disordered proteins or disordered domains, transient contacts may predominantly occur at clustered charged residues functioning as promiscuous binding interfaces (*Theillet et al., 2014*). Also, phosphorylation sites in disordered proteins or disordered domains are often clustered, which can enhance multisite cooperativity (*Theillet et al., 2014*). This is indeed the case for phosphorylation sites in Sbh1 (Figure 1.11), which are organized in 2 defined clusters: one proximal to the N-terminal region including S2, S3, T5, T12, S20 and S21, and another one closer to the conserved transmembrane domain including S35 and S38 (*Soromani et al., 2012; Swaney et al., 2013*). T5 is conserved in Sbh1 and mammalian Sec61 β , but not present in Sbh2, lower vertebrates or invertebrates suggesting convergent evolution and a particularly important Sbh1-specific role, since the site evolved twice independently (*Soromani et al., 2012*). T5 was also confirmed to be phosphorylated in purified Sec61 complexes by mass spectrometry (*Soromani et al., 2012*). In addition, phosphorylation of the cellular pool of Sbh1 was found to be dynamic, strongly suggesting a regulatory function, perhaps to regulate its interactions with its various partners (*Soromani et al., 2012*). Neither the kinases responsible for Sbh1 phosphorylation, nor the effects on protein translocation have been identified yet.

Mutation of S35 to alanine led to a complete destabilization of Sbh1 and in inability to complement the temperature-sensitivity of the $\Delta sbh1\Delta sbh2$ strain (*Soromani et al., 2012*). Mutation of S35 to aspartate (Phospho-mimetic residue), left the protein stable and complementation competent (*Soromani et al., 2012*). Mutation of S5 to alanine did not affect the ability of Sbh1 to complement the temperature-sensitivity of the $\Delta sbh1\Delta sbh2$ strain at 37°C and did not result in detectable hypophosphorylation of Sbh1 in yeast cells (*Soromani et al., 2012*). Later work done by this lab showed that individual mutation on S3 and T5 individually had no effects on growth at 37°C or pGls1 ER import defect, but

mutation on both S3 and T5 together to A resulted in poor growth at 37°C, and a pGls1 ER import defect similar at the one found in the $\Delta sbh1\Delta sbh2$ strain (Simon, BSc thesis, 2015; Feng et al., 2007). The phosphor-mimetic mutations S3E and T5E individually or together had no effects on growth at 37°C or pGls1 ER import defect (Simon, BSc thesis, 2015).

1.5.3 Phosphorylation-dependent prolyl cis-trans isomerization of Sbh1

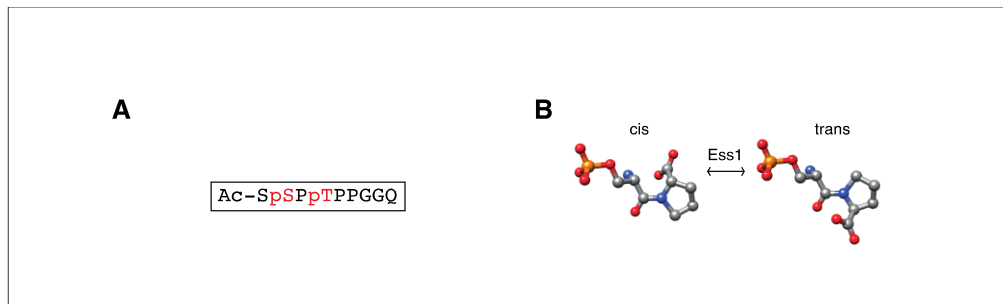


Figure 1.14: Ess1 isomerization scheme. (A) Schematic representation of the phosphorylated-S3/T5 Sbh1 N-terminus. Phosphorylated amino acids shown in red. (B) Schematic representation of Ess1-catalyzed phosphoserine-proline isomerization. Carbon atoms in grey, oxygen atoms in red, nitrogen atoms in blue, phosphorous atom in orange, hydrogen atoms not shown.

The highly conserved yeast enzyme Ess1 catalysed the cis-trans isomerization of proline residues that are preceded by phosphorylated serine or threonine (Hanes, 2014). Both S3 and T5 in Sbh1 are proline-flanked (Figure 1.14A), so the phosphorylated N-terminus of Sbh1 is a potential Ess1 target (Hanes et al., 2014). Extensive research in the past 25 years has shown that, the mammalian Ess1 orthologue, Pin1, has profound effects on several cellular events and human diseases by controlling the fate of a wide variety of phosphorylated proteins (Liou et al., 2011). For example, *PIN1* is over-expressed and/or activated by multiple mechanisms in many common human cancers, and acts on multiple signal pathways to promote tumorigenesis, by disrupting the balance of oncogenes and tumor suppressors (Driver et al. 2015; Zhou and Lu, 2016). In contrast, *PIN1* is down-regulated or inactivated by multiple mechanisms in neurons from Alzheimer’s Disease brains (Driver et al. 2015). In addition, Pin1 is required for insulin secretion from pancreatic β -cells (Nakatsu et al., 2017), and is involved in the regulation of neuronal excitability, and cognitive flexibility (Hu et al., 2020). A secreted Pin1 orthologue of the intracellular parasite *Theileria* is targeted to the host cell ER, probably via its retained signal sequence, where it isomerizes so far uncharacterized target proteins to control host oncogenic signaling (Marsolier et al., 2015).

Ess1 is essential, and its isomerase activity is required for growth, but only at vanishing levels (Gemmil *et al.*, 2005). Higher levels of Ess1 are required for growth in the presence of certain metabolic inhibitors, suggesting the importance of Ess1 for tolerance to environmental challenge (Gemmil *et al.*, 2005). A catalytic site mutant of Ess1, *ess1H164R*, encodes a catalytically deficient mutant enzyme with its isomerase activity reduced 10.000-fold at all temperatures, and cells with this mutation are temperature-sensitive at 37°C (Gemmil *et al.*, 2005; Hanes *et al.*, 2014; Atencio *et al.* 2014). The direct cause of the temperature-sensitivity remains unclear, but is likely linked to a specific Ess1 substrate whose function is essential at high temperature (Hanes *et al.*, 2014). In a synthetic genetic array with all viable yeast deletion mutants, *ess1H164R* mutation was synthetically lethal with the deletion of the genes for the *SEC61* homologue *SSH1*, and the cytosolic N-glycanase *PNG1* required for glycoprotein ERAD (Atencio *et al.*, 2014). In addition, *ess1* is synthetically lethal with a mutation in the gene for the ER-resident oxidoreductase *PDI1* (Kim *et al.*, 2009). Isomerization by Ess1 can alter substrate protein activity, localization, or substrate ubiquitylation and thus protein degradation by proteosomes (Hanes *et al.*, 2014; Siepe and Jentsch, 2009).

Previous data generated by this lab showed that about 30% of both wildtype and mutant Ess1 was associated with a crude yeast microsomal fraction, suggesting that Ess1 has membrane-bound targets (Lupusella, *MSc thesis*, 2015). It was also seen that *ess1H164R* does not cause any general translocation defects (Lupusella, *MSc thesis*, 2015). In contrast, it was found that translocation of Gls1 into the ER of *ess1H164R* cells was reduced to about 50% of the wildtype, comparable to the reduction seen in the *sbh1S3A/T5A* strain (Lupusella, *MSc thesis*, 2015). This indicates that transport of Gls1 into the ER is dependent not only on the phosphorylation at S3 and T5 of Sbh1, but also on the isomerization by Ess1.

2

Material and Methods

2 Material and Methods

2.1 Material

2.1.1 Laboratory equipment and their Suppliers

All Laboratory equipment used in this study are listed in table 2.1

Company	Product
AGFA Healthcare GmbH	CP1000 X-ray film processor
Beckman Coulter Inc.	Optima L-90K ultracentrifuge Optima MAX-XP benchtop ultracentrifuge Avanti® J-E high-speed centrifuge
Bio-Rad Laboratories Inc.	583 gel dryer PowerPac HC power supply PowerPac 3000 power supply Trans-Blot electrophoretic transfer cell
BioSpec Products Inc.	Mini-BeadBeater-24
Eppendorf AG	Microcentrifuge 5415R Temperature Freezer C340 MiniSpin Plus Centrifuge Thermomixer 5436 Thermomixer Compact
GE Healthcare	Amersham autoradiography Hypercassettes Amersham Ultrospec 2100 pro UV/VIS Spectrophotometer ImageQuant TL software Storage Phosphor Screens and cassettes Typhoon TRIO phosphorimager Amersham Imager 600 RGB
Gilson Inc.	Pipette PIPERTMAN Classic set
Gram A/S	BioBasic 410 Lab-Refrigerator

Heidolph Instruments Gmbh & Co. KG	Duomax 1030 platform Shaker
Hellma Analytics	Quartz cuvettes
Hirschmann Gmbh & Co. KG	Pipet-Aid pipette controller
IKA-Werke GmbH	EUROSTAR power-b overhead stirrer RCT basic magnetic stirrer
Infors AG	Multitron Standard incubation shaker
Invitrogen	Mini Gel Tank
Liebherr-Hausgeräte Ochsenhausen GmbH	Freezer 20190930
Merck KGaA	MilliQ Integral water purification system
NeoLab Migge gmbH	Overhead rotator Rocking shaker
Roth GmbH & Co. KG	Neubauer Hemocytometer
Sartorius AG	Analytical balance
Scientific Industries Inc.	Vortex-Genie 2
Sigma Laborzentrifugen GmbH	4K15 refrigerated centrifuge
Systec	DX-150 autoclave
Thermo Fisher Scientific Inc.	XCell SureLock Mini-Cell electrophoresis system 3UV-Lamp
VWR/PEQLAB	E-BOX VX2 gel documentation system peqSTAR 2X gradient thermocycler PerfectBlue Gelsystem Mini S
Zeiss Microscopy & GmbH	Axioskop microscope

Table 2.1: Laboratory equipment used in this study

2.1.2 Reagents, consumables and Chemicals

All reagents, consumables and chemicals used in this study are listed in table 2.2

Company	Product
AGFA HealthCare GmbH	AGFA Developer G153

	AGFA Fixer G354
Applichem GmbH	Ampicillin Sodium Salt (BioChemica) DEPC (BioChemica) Kanamycin Sulfate (BioChemica) Tunicamycin HEPES-Sodium Salt Sodium Chloride Magnesium Chloride Sodium Acetate Magnesium Acetate Ammonium Acetate
B. Braun Melsungen AG	Surgical Disposable Scalpel Sterican hypodermic needle 0.9 x 40 mm
BD	Bacto™ Casamino Acids Bacto™ Peptone Bacto™ Yeast Extract Difco™ Yeast Nitrogen Base without Amino Acids & Ammonium Sulfate Difco™ Yeast Nitrogen Base without Amino Acids
Beckman Coulter GmbH	Polycarbonate Bottles, thick-walled, 70 ml (rotor type 45 Ti) Polyallomer Tubes, thin-walled, 4.4 ml (rotor type SW 60 Ti) Polycarbonate Tubes, thick-walled, 1.0/1.4 ml (TLS55) Polycarbonate Tubes, thick-walled, 3.0/3.5 ml (TLA100.3) Microfuge® Tubes, Polyallomer, 1.5 ml
Bemis Company	Parafilm M
Bernd Kraft GmbH	Hydrochloric Acid 37%

Bio-Rad Laboratories Inc.	Nitrocellulose Membrane (0.2 µM, 0.45 µM pore size) Precision Plus Protein™ All Blue Standards
Biozym Scientific GmbH	SurPhob pipette Tips SurPhob Gelloader Tips
Carbolution Chemicals GmbH	1,4-Dithiol-DL-threit, 98% (DTT)
Carl Roth GmbH	PMSF (>99%) Roti®-Aqua-Phenol (RNA extraction) Rotiphorese® Gel 30 (37,5:1) β-Mercaptoethanol (99 %, p.a.) TEMED (99 %, p.a.) Roti®-Phenol/Chloroform/Isoamyl-Alcohol (Nucleic acid extraction) Peptone (from Casein) Yeast Extract Glycine (PUFFERAN, >99 %, p.a.) Agar-Agar, Kobe I Ammonium Peroxydisulfate (>98 %, p.a.) SDS Pellets (>99 %) RNase AWAY® Glycerol (>98 %) Triton X 100, pure Sodium Carbonate Sodium Azide Urea Potassium Acetate 2-Nitrophenyl-β-D-Galactopyranoside Aluminium Foil
Corning Life Sciences	Inoculating loop with bubble end, length 195 mm
Costar	Stripette 5 ml, 10 ml, 25 ml, 50 ml Serological Pipettes

DWK Life Sciences GmbH	<p>Graduated cylinders</p> <p>Erlenmeyer flasks</p> <p>Beakers</p> <p>Solution bottles</p>
Eppendorf AG	Safe-Lock Tube
Fisher Scientific	Isopropanol
Fermentas	<p>Conventional and FastDigest® Restriction Enzymes</p> <p>T4 DNA Ligase</p> <p>FastAP™ Thermosensitive Alkaline Phosphatase</p> <p>GeneRuler™ 1 kb DNA Ladder</p> <p>GeneRuler™ 100 bp DNA Ladder</p> <p>GeneRuler™ 1 kb Plus DNA Ladder</p> <p>GeneRuler™ 100 bp Plus DNA Ladder</p> <p>PageRuler™ Prestained Protein Ladder</p> <p>PageRuler™ Plus Prestained Protein Ladder</p> <p>RNase A, DNase and Protease-free (10 mg/ml) 5-Fluoroorotic Acid</p>
Formedium™	<p>Synthetic Complete Drop-Out Mixture, (SC) (-Ade, -His, Leu, -Lys, -Trp, -Ura), (Kaiser Mixture)</p> <p>Yeast Nitrogen Base</p> <p>Yeast Nitrogen Base Without Amino Acids</p>
FujiFilm	Medical X-ray Film (Super HR-E30)
GE Healthcare	<p>Protein A Sepharose™ CL-4B</p> <p>Whatman Chromatography paper</p> <p>Amersham Hypercassette Autoradiography Cassette</p> <p>Amersham Protram 0.2µm Nitrocellulose Blotting Membrane</p>

Greiner Bio-One International GmbH	Cellstar 15 ml and 50 ml polypropylene tubes Petri Dish, PS, 94 x 16 mm
Grüssing GmbH	Glycerin 99% Potassium Acetate Potassium Hydroxide 85% Sodium Carbonate Anhydrous
Invitrogen™	NuPAGE® Novex 4-12 % Bis-Tris Gel 1.5 mm, 10 Well (Novex®) NuPAGE® MOPS SDS Running Buffer (20X) (Novex®) NuPAGE® MES SDS Running Buffer (20X) (Novex®)
Merck K GaA	Sodium Hydrogen Carbonate
New England BioLabs® (NEB)	Conventional Restriction Enzymes
PanReac AppliChem ITW Reagents	D-(+)-Glucose anhydrous BioChemica Tween-20 Sodium Dodecyl Sulfate (SDS)
PEQLAB Biotechnologie GmbH	KAPA HiFi™ PCR Kit
PerkinElmer Inc.	Express Protein Labeling Mix, [³⁵ S]-, 50mM Tricine (pH 7.4), 10mM BME Easy Tides Adenosine 5'-triphosphate, [³² P]-, 50mM Tricine (pH 7.4) Protein Molecular Weight Markers [Methyl- ¹⁴ C] Methylated COUNT-OFF Liquid Concentrate
Promega GmbH	Recombinant RNasin® Ribonuclease Inhibitor
Rockland™	HRP-conjugated anti-rabbit
Sartorius AG	Minisart® Plus Syringe Filters (0.2, 0.45 µm pore size)

Sigma-Aldrich®

Adenine (>99 %)
L-Cysteine (>98 %)
L-Histidine (Sigma)
Uracil (>99 %)
L-Leucine (>98.5 %)
L-Tryptophan (>98 %)
L-Methionine (>99 %)
L-Cysteine (>99 %)
DL-Dithiothreitol, BioUltra, >99.0 %
Sucrose BioXtra, >99.5 %
Tryptone, enzymatic digest from casein
D-(+)-Glucose (>99.5 %)
Deoxyribonucleic Acid Sodium Salt
Absolute Ethanol
Bromophenol Blue Sodium Salt
Trizma® Base, for molecular biology, >99.8
%
Urea
Metsulfuron-Methyl, Analytical standard
Sodium Azide, BioUltra, >99.5 %
Tween® 20
DMSO
Glass Beads, acid-washed 425-600 µm
EDTA, anhydrous, >99 %
Lithium Acetate Dihydrate, BioXtra
Polyethylene Glycol, BioXtra, average mol
wt 3,350
D-(+)-Galactose (>99 %)
Sodium Chloride, for molecular biology
(>98 %)
GenElute™ PCR Clean-Up Kit

	GenElute™ Gel Extraction Kit Corning® Cryogenic Vials, internal thread (2.0 mL) Tunicamycin
Sucofin	Skimmed Milk Powder
Thermo Fisher Scientific	Pierce 660 nm Protein Assay Reagent SuperSignal West Dura Extended Duration Chemiluminescent Substrate (ECL) Filter Units – 115/250/500 ml capacity, MF75™ Series, 0.45 µm pore size DMSO PageRuler Plus Prestained Protein Ladder Halt Protease and Phosphatase single use Inhibitor Cocktail (100 x)
VWR® International	Cloridric Acid 99 % GPR RECTAPUR® Ethanol Absolut AnalaR NORMAPUR® Glycine Methanol Vacuum filtration system
ZChL	All other chemicals not mentioned above but mentioned in the respective sections of this chapter

Table 2.2: Reagents, chemicals and consumables used in this study

2.1.3 Software

All Software used in this study are listed in table 2.3

Name	Use
BibDesk	Bibliography Software

Chimera	Draw chemical structures
Illustrator	Image editing
Image J	Image editing
ImageQuant	Band intensity quantitation
Photoshop	Image editing
SnapGene	DNA sequence editing

Table 2.3: Software used in this study

2.1.4 *Saccharomyces cerevisiae* strains

All *Saccharomyces cerevisiae* strains used in this study are listed in table 2.4

Name	Genotype	Source/Reference
KRY37	<i>MATa his4 trp1-1 leu2-3,112 ura3-52 hoc1-1 sec61-3</i>	<i>Stirling et al., 1992</i>
KRY61	<i>MATα sec23-1 ura3-52 his4-619</i>	<i>Paccaud et al., 1996</i>
KRY200	<i>MATα can1-100 leu2-3,112 his3-11,15 trp1-1 ura3-1 ade2-1 sec61::HIS3 [pDQ1sec61-32]</i>	<i>Pilon et al., 1998</i>
KRY585	<i>MATa leu2-3,113 ura3-52</i>	<i>Toikkanene et al., 2003</i>
KRY586	<i>MATa seb1::KanMx leu2-3,112 ura3-52 GAL+</i>	<i>Soromani et al., 2012</i>
KRY587	<i>MATa seb2::hphMx leu2-3,112 ura3-52 GAL+</i>	<i>Soromani et al., 2012</i>
KRY588	<i>MATa seb1::KanMx seb2::hphMx leu2-3,112 ura3-52 GAL+</i>	<i>Soromani et al., 2012</i>
KRY996	<i>MATa ura3-1 leu2-3,112 trp1-1 can 1-100 ade2-1 his3-11,15 (phi+)</i>	<i>Wu et al., (2000)</i>
KRY997	<i>MATa ess1H164R ura3-1 leu2-3,112 trp1-1 can 1-100 ade2-1 his3-11,15 (phi+)</i>	<i>Wu et al., (2000)</i>
KRY1077	<i>MATα his3Δ1 leu2Δ0 lys2Δ0 ura3Δ0 (BY4742)</i>	<i>Giaever et al., 2002</i>
KRY1080	<i>MATα his3Δ1 leu2Δ0 lys2Δ0 ura3Δ0 ire1::kanMX4</i>	<i>Giaever et al., 2002</i>

KRY1156	<i>MATα his3Δ1 leu2Δ0 lys2+/lys+ met15Δ0 ura3Δ0 can1Δ::STE2pr-sp HIS5 lyp1Δ::STE3pr-LEU2"</i>	<i>Cohen and Schuldiner, 2011</i>
KRY1157	<i>MATα Tef2-Cherry::NATr his3Δ1 leu2Δ0 lys2+/lys+ met15Δ0 ura3Δ0 can1Δ::STE2pr-sp HIS5 lyp1Δ::STE3pr-LEU2</i>	<i>Cohen and Schuldiner, 2011</i>
KRY1158	<i>MATα his3Δ1 leu2Δ0 lys2+/lys+ met15Δ0 ura3Δ0 can1Δ::STE2pr-sp HIS5 lyp1Δ::STE3pr-LEU2"ΔSbh1::Kan</i>	<i>This work</i>
KRY1159	<i>MATα Tef2-Cherry::NATr his3Δ1 leu2Δ0 lys2+/lys+ met15Δ0 ura3Δ0 can1Δ::STE2pr-sp HIS5 lyp1Δ::STE3pr-LEU2 ΔSbh1::Kan</i>	<i>This work</i>
KRY1160	<i>MATα his3Δ1 leu2Δ0 lys2+/lys+ met15Δ0 ura3Δ0 can1Δ::STE2pr-sp HIS5 lyp1Δ::STE3pr-LEU2" ΔSbh1::Kan ΔSbh2::Hygro</i>	<i>This work</i>
KRY1161	<i>MATα Tef2-Cherry::NATr his3Δ1 leu2Δ0 lys2+/lys+ met15Δ0 ura3Δ0 can1Δ::STE2pr-sp HIS5 lyp1Δ::STE3pr-LEU2 ΔSbh1::Kan ΔSbh2::Hygro</i>	<i>This work</i>
KRY1169	<i>MATα ess1H164R ura3-1 leu2-3,112 trp1-1 can1-100 ade2-1 his3-11,15 (phi+) ΔSbh1::Kan ΔSbh2::Hygro</i>	<i>Römisch Lab</i>
KRY1170	<i>MATα his3Δ1 leu2Δ0 met15Δ0 ura3Δ0 (BY4741)</i>	<i>Brachmann et al., 1998</i>
KRY1171	<i>MATα his3Δ1 leu2Δ0 met15Δ0 ura3Δ0 fus3::kanMX4</i>	<i>Giaever et al., 2002</i>
KRY1172	<i>MATα his3Δ1 leu2Δ0 met15Δ0 ura3Δ0 kss1::kanMX4</i>	<i>Giaever et al., 2002</i>
KRY1173	<i>MATα his3Δ1 leu2Δ0 met15Δ0 ura3Δ0 hog1::kanMX4</i>	<i>Giaever et al., 2002</i>

KRY1174	<i>MATa his3Δ1 leu2Δ0 met15Δ0 ura3Δ0 slt2::kanMX4</i>	<i>Giaever et al., 2002</i>
KRY1175	<i>MATa his3Δ1 leu2Δ0 met15Δ0 ura3Δ0 smk1::kanMX4</i>	<i>Giaever et al., 2002</i>
KRY1176	<i>MATa his3Δ1 leu2Δ0 met15Δ0 ura3Δ0 ctk1::kanMX4</i>	<i>Giaever et al., 2002</i>
KRY1177	<i>MATa his3Δ1 leu2Δ0 met15Δ0 ura3Δ0 ssn3::kanMX4</i>	<i>Giaever et al., 2002</i>
KRY1178	<i>MATa his3Δ1 leu2Δ0 met15Δ0 ura3Δ0 mck1::kanMX4</i>	<i>Giaever et al., 2002</i>
KRY1179	<i>MATa his3Δ1 leu2Δ0 met15Δ0 ura3Δ0 yjk3::kanMX4</i>	<i>Giaever et al., 2002</i>
KRY1180	<i>MATa his3Δ1 leu2Δ0 met15Δ0 ura3Δ0 rim11::kanMX4</i>	<i>Giaever et al., 2002</i>
KRY1181	<i>MATa his3Δ1 leu2Δ0 met15Δ0 ura3Δ0 mrk1::kanMX4</i>	<i>Giaever et al., 2002</i>
KRY1182	<i>MATa his3Δ1 leu2Δ0 met15Δ0 ura3Δ0 ime2::kanMX4</i>	<i>Giaever et al., 2002</i>
KRY1183	<i>MATa his3Δ1 leu2Δ0 met15Δ0 ura3Δ0 yak1::kanMX4</i>	<i>Giaever et al., 2002</i>
KRY1184	<i>MATa his3Δ1 leu2Δ0 met15Δ0 ura3Δ0 kns1::kanMX4</i>	<i>Giaever et al., 2002</i>
KRY1185	<i>MATa his3Δ1 leu2Δ0 met15Δ0 ura3Δ0 sky1::kanMX4</i>	<i>Giaever et al., 2002</i>
KRY1186	<i>MATa his3Δ1 leu2Δ0 met15Δ0 ura3Δ0 rck1::kanMX4</i>	<i>Giaever et al., 2002</i>
KRY1187	<i>MATa his3Δ1 leu2Δ0 met15Δ0 ura3Δ0 rck2::kanMX4</i>	<i>Giaever et al., 2002</i>
KRY1188	<i>MATa his3Δ1 leu2Δ0 met15Δ0 ura3Δ0 rim15::kanMX4</i>	<i>Giaever et al., 2002</i>

KRY1189	<i>MATa his3Δ1 leu2Δ0 met15Δ0 ura3Δ0 (BY4741)</i>	<i>Li et al., 2011</i>
KRY1190	<i>MATa his3Δ1 leu2Δ0 met15Δ0 ura3Δ0 cdc28-1 kanMX4</i>	<i>Li et al., 2011</i>
KRY1191	<i>MATa his3Δ1 leu2Δ0 met15Δ0 ura3Δ0 cdc28-13 kanMX4</i>	<i>Li et al., 2011</i>
KRY1192	<i>MATa his3Δ1 leu2Δ0 met15Δ0 ura3Δ0 kin28-ts kanMX4</i>	<i>Li et al., 2011</i>
KRY1193	<i>MATa his3Δ1 leu2Δ0 met15Δ0 ura3Δ0 sgv1-80 kanMX4</i>	<i>Li et al., 2011</i>
KRY1195	<i>MATα his3D1 leu2D0 lys2D0 ura3D0 pho85::kanMX4</i>	<i>Giaever et al., 2002</i>
KRY1196	<i>MATα his3D1 leu2D0 lys2D0 ura3D0 kdx1::kanMX4</i>	<i>Giaever et al., 2002</i>
KRY1197	<i>MATα his3D1 leu2D0 lys2D0 ura3D0 cka1::kanMX4</i>	<i>Giaever et al., 2002</i>
KRY1198	<i>MATα his3D1 leu2D0 lys2D0 ura3D0 cka2::kanMX4</i>	<i>Giaever et al., 2002</i>
KRY1199	<i>MATa Δura Δhis Δleu Δmet Δcan1::STE2pr-spHIS5 Δlyp1::STE3pr-LEU2 NATR-TEF2pr-mCherry-KNS1</i>	<i>Weill et al., 2018</i>
KRY1200	<i>MATa Δura Δhis Δleu Δmet Δcan1::STE2pr-spHIS5 Δlyp1::STE3pr-LEU2 NATR-TEF2pr-mCherry-RCK1</i>	<i>Weill et al., 2018</i>
KRY1201	<i>MATa Δura Δhis Δleu Δmet Δcan1::STE2pr-spHIS5 Δlyp1::STE3pr-LEU2 NATR-TEF2pr-mCherry-RCK2</i>	<i>Weill et al., 2018</i>
KRY1202	<i>MATa Δura Δhis Δleu Δmet Δcan1::STE2pr-spHIS5 Δlyp1::STE3pr-LEU2 NATR-TEF2pr-mCherry-PHO85</i>	<i>Weill et al., 2018</i>

KRY1203	<i>MATa Δura Δhis Δleu Δmet Δcan1::STE2pr-spHIS5 Δlyp1::STE3pr-LEU2 NATR-TEF2pr-mCherry-IME2</i>	<i>Weill et al., 2018</i>
KRY1204	<i>MATa Δura Δhis Δleu Δmet Δcan1::STE2pr-spHIS5 Δlyp1::STE3pr-LEU2 NATR-TEF2pr-mCherry-SSN3</i>	<i>Weill et al., 2018</i>
KRY1205	<i>MATa Δura Δhis Δleu Δmet Δcan1::STE2pr-spHIS5 Δlyp1::STE3pr-LEU2 NATR-TEF2pr-mCherry-HOG1</i>	<i>Weill et al., 2018</i>
KRY1206	<i>MATa Δura Δhis Δleu Δmet Δcan1::STE2pr-spHIS5 Δlyp1::STE3pr-LEU2 NATR-TEF2pr-mCherry-MCK1</i>	<i>Weill et al., 2018</i>
KRY1207	<i>MATa Δura Δhis Δleu Δmet Δcan1::STE2pr-spHIS5 Δlyp1::STE3pr-LEU2 NATR-TEF2pr-mCherry-SKY1</i>	<i>Weill et al., 2018</i>
KRY1208	<i>MATa Δura Δhis Δleu Δmet Δcan1::STE2pr-spHIS5 Δlyp1::STE3pr-LEU2 NATR-TEF2pr-mCherry-YAK1</i>	<i>Weill et al., 2018</i>
KRY1209	<i>MATa Δura Δhis Δleu Δmet Δcan1::STE2pr-spHIS5 Δlyp1::STE3pr-LEU2 NATR-TEF2pr-mCherry-MRK1</i>	<i>Weill et al., 2018</i>
KRY1210	<i>MATa Δura Δhis Δleu Δmet Δcan1::STE2pr-spHIS5 Δlyp1::STE3pr-LEU2 NATR-TEF2pr-mCherry-SGV1</i>	<i>Weill et al., 2018</i>
KRY1211	<i>MATa Δura Δhis Δleu Δmet Δcan1::STE2pr-spHIS5 Δlyp1::STE3pr-LEU2 NATR-TEF2pr-mCherry-CAK1</i>	<i>Weill et al., 2018</i>
KRY1212	<i>MATa Δura Δhis Δleu Δmet Δcan1::STE2pr-spHIS5 Δlyp1::STE3pr-LEU2 NATR-TEF2pr-mCherry-CDC28</i>	<i>Weill et al., 2018</i>

KRY1213	<i>MATa Δura Δhis Δleu Δmet Δcan1::STE2pr-spHIS5 Δlyp1::STE3pr-LEU2 NATR-TEF2pr-mCherry-CTK1</i>	Weill et al., 2018
KRY1214	<i>MATa Δura Δhis Δleu Δmet Δcan1::STE2pr-spHIS5 Δlyp1::STE3pr-LEU2 NATR-TEF2pr-mCherry-SMK1</i>	Weill et al., 2018
KRY1215	<i>MATa Δura Δhis Δleu Δmet Δcan1::STE2pr-spHIS5 Δlyp1::STE3pr-LEU2 NATR-TEF2pr-mCherry-KSS1</i>	Weill et al., 2018
KRY1216	<i>MATa Δura Δhis Δleu Δmet Δcan1::STE2pr-spHIS5 Δlyp1::STE3pr-LEU2 NATR-TEF2pr-mCherry-RIM15</i>	Weill et al., 2018
KRY1217	<i>MATa Δura Δhis Δleu Δmet Δcan1::STE2pr-spHIS5 Δlyp1::STE3pr-LEU2 NATR-TEF2pr-mCherry-FUS3</i>	Weill et al., 2018
KRY1218	<i>MATa Δura Δhis Δleu Δmet Δcan1::STE2pr-spHIS5 Δlyp1::STE3pr-LEU2 NATR-TEF2pr-mCherry-SLT2</i>	Weill et al., 2018
KRY1219	<i>MATa Δura Δhis Δleu Δmet Δcan1::STE2pr-spHIS5 Δlyp1::STE3pr-LEU2 (yMS2085)</i>	Weill et al., 2019
KRY1220	<i>MATa shr3Δ6 ura3-52</i>	Martins et al., 2019
KRY1223	<i>MATa ade2-101 his3-Δ200 leu2-Δ1lys2-801 trp1-Δ1 ura3-52 cka1-Δ1::HIS3 cka2-Δ1::TRP1 (CEN6/ARSH4 LEU2 CKA2)</i>	Hanna et al., 1995
KRY1224	<i>MATa ade2-101 his3-Δ200 leu2-Δ1lys2-801 trp1-Δ1 ura3-52 cka1-Δ1::HIS3 cka2-Δ1::TRP1 (CEN6/ARSH4 LEU2 cka2-13)</i>	Hanna et al., 1995
KRY1226	<i>MATα his3Δ1 leu2Δ0 lys2+/lys+ met15Δ0 ura3Δ0can1Δ::STE2pr-sp HIS5 lyp1Δ::STE3pr-LEU2" ess1H154R:NatRx</i>	Römisch Lab

Table 2.4: *E. coli* strains used in this study

The libraries used for the screens were:

1. The mini "Secretome-GFP" library, genotype: BY4741 Δ met Δ ura Δ his Δ leu MATa XXX-GFP-HIS (Won-Ki Huh *et al.*, 2003).
2. The Δ kinases/ Δ phosphatases deletion library, genotype: BY4741 Δ met Δ ura Δ his Δ leu MATa Δ xxx::G418R (Giaever *et al.*, 2002)
3. The TEF2-Cherry Overexpression library, genotype: Δ ura Δ his Δ leu Δ met MATa Δ can1::STE2pr-spHIS5 Δ lyp1::STE3pr-LEU2 NATR-TEF2pr-mCherry-XXX (Weil *et al.*, 2018)

2.1.5 *Escherichia coli* strains and Plasmids

All *Escherichia coli* strains and plasmids used in this study are listed in table 2.5

Strain	Plasmid	Genotype	Use/Description	Source/Reference
KRB3	-	Lyticase expressing E. coli (in DH5 α)	Lyticase expression and purification	<i>Shen et al., 1991</i>
KRB46	-	F- endA1 glnV44 thi-1 recA1 relA1 gyrA96 deoR nupG Φ 80dlacZ Δ M15 Δ (lacZYA- argF)U169,hsdR17(rKmK+), λ -	DH5 α	<i>Hanahan, D. 1983</i>
KRB125	p416	CEN plasmid for expression under MET25 promoter. URA3, amp	Empty P416 plasmid	<i>Mumberg et al. 1994</i>

KRB351	p416pΔgpαF	CEN plasmid for expression under MET25 promoter. URA3, amp	pΔgpαF integrated in p416 plasmid	<i>Mumberg et al. 1994</i>
KRB536	pRS415	CEN, LEU2, amp	Empty pRS415 plasmid	<i>Sikorski and Hieter, 1987</i>
KRB546	pRS416 PEX3	PEX6 in pRS416	Expression of PEX6	<i>Dominic Hoepfner/Henk Tabak</i>
KRB689	SBH1pRS415	SBH1 in pRS415 vector	Expression of SBH1	<i>Römisch Lab</i>
KRB746	sbh1S3ApRS415	sbh1S3A in pRS415	Expression of sbh1S3A	<i>Römisch Lab</i>
KRB747	Sbh1T5ApRS415	Sbh1T5A in pRS415	Expression of Sbh1T5A	<i>Römisch Lab</i>
KRB748	Sbh1T12ApRS415	Sbh1T12A in pRS415	Expression of Sbh1T12A	<i>Römisch Lab</i>
KRB752	Sbh1S35DpRS415	Sbh1S35D in pRS415	Expression of Sbh1S35D	<i>Römisch Lab</i>
KRB1032	Sbh1S3A/T5ApRS415	Sbh1S3A/T5A in pRS415	Expression of Sbh1S3A/T5A	<i>Römisch Lab</i>
KRB1033	Sbh1S3EpRS415	Sbh1S3E in pRS415	Expression of Sbh1S3E	<i>Römisch Lab</i>
KRB1034	Sbh1T5EpRS415	Sbh1T5E in pRS415	Expression of Sbh1T5E	<i>Römisch Lab</i>
KRB1035	Sbh1S3E/T5EpRS415	Sbh1S3E/T5E in pRS415	Expression of Sbh1S3E/T5E	<i>Römisch Lab</i>
KRB1087	P502.8	ess1H164R in PCR2.1	Genomic replacement of ESS1 into ess1H164R	<i>Atencio et al. 2014</i>

KRB1136	Ylp α L	α -amylase expression cassette with ADL1 promoter and terminator	Expression of α -amylase	<i>Feng et al., 2007</i>
KRB1138	pYEX4T-1-GLS1	GST-GLS1 fusion in pYEX4T	Expression of GST-GLS1	<i>Shibuya et al., 2015</i>
KRB1221	p416Mns1 Δ gp α F	Mns1 SP Δ gp α F fusion in p416	Reporter for Sbh1 phosphorylation	<i>This Work</i>
KRB1125	pRS416sbh1S3A/T5A	sbh1S3A/T5A in pRS416 plasmid	For microscopic screen	<i>This work</i>
KRB1127	pKT209-GFP	pKT209-GFP(codon optimized) URA	For C-Terminal GFP fusion of proteins	<i>Schuldiner Lab</i>

Table 2.5: *S. cerevisiae* strains used in this study

2.1.6 Primers

All primers used in this study are listed in table 2.6

Name	Sequence (5'-3')	Tm	Application
24	GTAAAACGACGGCCAGT	53°C	M13 primer (Frw). Used in sequencing or Colony PCR and in Mns1 Δ gp α F construct generation
25	CAGGAAACAGCTATGAC	47°C	M13 primer (Rev). Used in sequencing or Colony PCR
59	CAAAAAGAAAAATGTGAATTTAGC G	52°C	Sbh1_5' -296. SBH1 deletion, and deletion confirmation

60	AAATGAACATGGAATTGAGAAACA T	53°C	Sbh1_3'_+332. SBH1 deletion, and deletion confirmation
118	GTGGTGAACGATAGATGGAC	60°C	ACT1. HAC1 mRNA splicing assay
119	ATTCTGAGGTTGCTGCTTTG	58°C	ACT1. HAC1 mRNA splicing assay
120	CTGGCTGACCACGAAGACGC	66°C	HAC1. HAC1 mRNA splicing assay
121	TTGTCTTCATGAAGTGATGA	54°C	HAC1. HAC1 mRNA splicing assay
124	TTTTTTTTTTTTTTTTTT	36°C	Oligo-dT. cDNA synthesis
Sbh2ExtFw	GTTACCCGTTTCCTTAGCC	60°C	SBH2 deletion, and deletion confirmation
Sbh2ExtRv	ATTGCTGTCTCCATCTCG	58°C	SBH2 deletion, and deletion confirmation
OW38	CATAACCGACTACGGCAC	59°C	<i>ess1</i> mutant generation
OW989	TGTTTACAAAAAATACAAGAATCC GTTACTAAAGATTCAGTATAGCGA CCAGCATTAC	60°C	<i>ess1</i> mutant generation
checkess1Fw	AAGTCCAAGAAAAGAGAG	51°C	<i>ess1</i> mutant confirmation
checkess1Rv	CAAGAATCCGTTACTAAAG	47°C	<i>ess1</i> mutant confirmation
FwMns1-F5	TCAACACCGCAAGCTCATCCTTTTC CAGTATTAGACGAAGAAATATTAA AATCGCAGTCTCTGACCACAGGTT GGTCGTTGGGTGACGGTGCTGGTT TA	65°C	Mns1 C-Ter GFP tagging
RvMns1-R3	TGGAAAAATGGTATAGCACATCA TCACACCGCATAGTGAATTTTAAAA GGCGAATCTGGCCACTATATAGCA CACTAACTCGATGAATTCGAGCTCG	65°C	Mns1 C-Ter GFP tagging

FwMns1Chck	CACAGAAGCTCATCCTTTTCCAG	53°C	Mns1 C-Ter GFP tagging checking
RvMns1Chck	ATGGTATAGCACATCATCACACCG	53°C	Mns1 C-Ter GFP tagging checking
EcoRIMns1AlphaFFW	TGAAGCGAATTCGATTCTATGAAG AACTCTGTGGTATTTCAATTGCAA CCATTGTTGCTATCATAGCAGCTAT ACCAGTCAACACTACAACA	59°C	Mns1ΔgpaF construct generation

Table 2.6: Primers used in this study

2.1.7 Antibodies

All antibodies used in this study are listed in table 2.7

Antibody	Dilution	Source
Anti-Rpn12	Western Blot 1:2.500	<i>Pereira et al., 2019</i>
Anti-ppαF	Western Blot 1:2.500	<i>Soromani et al., 2012</i>
Anti-DPAPB	IP 1:100	<i>Pereira et al., 2019</i>
Anti-Sbh1 ₍₁₋₁₈₎	Western Blot 1:2.500	<i>Soromani et al., 2012</i>
Anti-Sbh1 ₍₁₀₋₂₃₎	Western Blot 1:2.500	<i>This work</i>
Anti-Sbh1 ₍₃₉₋₄₈₎	Western Blot 1:2.000	<i>This work</i>
Anti-Sbh1 _(Pi)	Western Blot 1:2.500; IP 1:100	<i>This work</i>
Anti-GFP	Western Blot 1:5.000; IP 1:100	<i>Ab290, abcam</i>
Anti-α-Amy	Western Blot 1:1.000	<i>EC3211, Sigma-Aldrich</i>
Anti-Gas1	Western Blot 1:10.000	<i>Horvath et al., 1994</i>
Anti-Kar2	Western Blot 1:10.000; IP 1:100	<i>Gillece et al., 1999</i>
Anti-Gls1	Western Blot 1:2.000	<i>Shibuya et al., 2015</i>
Anti-rabbit (HRP)	Western Blot 1:10.000	<i>AP182P, Sigma-Aldrich</i>

Table 2.7: Antibodies used in this study

2.1.8 Enzymes

All enzymes used in this study are listed in table 2.8

Class	Enzyme	Company
Restriction Enzymes	EcoRI	NEB
	KpnI	
	Sall	
	SacI	
Polymerase	OneTaq	NEB
	KAPA HiFi	Peqlab
Reverse Transcriptase	Maxima RT	Fermentas
Ligase	T4 DNA Ligase	Fermentas
Other Enzymes	FastAP	Thermo Fisher Scientific
	T4 Polynucleotide Kinase	NEB
	Lyticase	Römisch lab

Table 2.8: Enzymes used in this study

2.1.9 Media and Buffers

All media and buffers used in this study are listed in table 2.9, 2.10 and 2.11

Medium	Composition
YPD (Yeast Extract, Peptone, Dextrose)	1% Yeast Extract, 2% Peptone, 2% Glucose (For solid media: 2% Agar-Agar)
YPD-Kan	YPD with 100 µg/ml Kanamycin (For solid media: 2 % Agar-Agar)
YPD-Nat	YPD with 100 µg/ml Nourseothricin (For solid media: 2 % Agar-Agar)
YPD-Hph	YPD with 200 µg/ml Hygromycin (For solid media: 2 % Agar-Agar)

Minimal Medium	0.67% Yeast Nitrogen Base without Amino Acids, 0.13% Synthetic Complete Drop-Out Mixture (-Ade, -His, -Leu, -Lys, -Trp, -Ura), 2% Glucose, Amino Acids according auxotrophies (Table 1.10) (For solid media: 2% Agar-Agar)
----------------	--

Table 2.9: *S.cerevisiae* growth media used in this study

Compound	Concentration
Adenine	18 mg/l
L-Alanine	76 mg/l
L-Asparagine	
L-Aspartic Acid	
L-Cysteine	
L-Glutamine	
L-Glutamic acid	
Glycine	
L-Histidine	
L-isoleucine	
L-Leucine	380 mg/l
L-Lysine	76 mg/l
L-Methionine	
L-Phenylalanine	
L-Proline	
L-Serine	
L-Threonine	
L-Tryptophan	
L-Tyrosine	
Uracil	
L-Valine	

Table 2.10: Composition of synthetic complete amino acid drop-out mixture for *S. cerevisiae* used in this study

Medium	Composition
LB (Lysogeny Broth)	0.5 %Yeast Extract, 1 %Tryptone, 0.05 %NaCl, 1.0 mM NaOH (For solid media: 2 % Agar-Agar)
LB-Amp	LB with 100 µg/ml Ampicillin (For solid media: 2 % Agar-Agar)
LB-Kan	LB with 100 µg/ml Kanamycin (For solid media: 2 % Agar-Agar)

Table 2.11: *E. coli* growth media used in this study

2.2 Methods

2.2.1 Sterilization

All glassware were sterilized by autoclaving at 100 kPa and 134 °C for 20 min. LB media, YPD media, and all autoclavable solutions were sterilized by autoclaving at 100 kPa and 121°C for 20 min. Drop out media, and all the non-autoclavable solutions were sterilized by filtration.

2.2.2 Growth cultures

2.2.2.1 Growth of *S. cerevisiae*

S. cerevisiae cells were grown either in full or minimal media at 30°C (if not stated otherwise) with continuous shaking at 200 rpm, and cells were harvest in early exponential phase and washed with sterile deionized water. For drop dilution assays an OD₆₀₀ of 0.5 was harvested, washed and serial 1:10 dilution was done. For each dilution, 5 µl (containing 10⁴-10 cells/5 µl) were dropped on to the respective media plates. To test tunicamycin (TM) (Sigma) sensitivity, cells were grown on YPD plates supplemented with 0.5 µg/ml TM. To

test Methylsulfonyl-methyl (MM) (Sigma) sensitivity, cells were grown on YPD plates supplemented with 200 µg/ml MM. To test the effect of sorbitol on growth recovery, cells were grown on YPD plates supplemented with 1,2 M sorbitol. The growth was documented after 3.

2.2.2.2 Growth of *E. coli*

E. coli cells were grown at 37°C in LB medium with continuous shaking at 180 rpm or on LB medium plates. When needed, cells were grown on LB media, both liquid and solid, supplemented with adequate concentration of appropriate antibiotic (Table 1.11).

2.2.3 DNA Extraction

2.2.3.1 Isolation of plasmidic DNA from *E. coli*

For the isolation of plasmidic DNA from *E. coli*, the Gen Elute Plasmid Miniprep Kit (Sigma) was used. Cells (2 ml) of an over-night culture of *E. coli* grown as described in Section 2.2.2.2, were collected. Pellet was then resuspended in 200 µl Resuspension Solution, 200 µl of Lysis Solution was added, and sample incubated at room temperature for 5 min. This step is responsible for the cell lysis. After incubation, 350 µl of Neutralization Solution was added, as to stop the lysis process. Sample was then centrifuged at 14.000 x g for 10 min, supernatant applied to a previously prepared binding column and respective collector tube, and submitted to new centrifugation step. Flow-through was discarded, as DNA stays trapped in the cellulose-based membrane. DNA was then washed with Wash solution, flowthrough discarded, and membrane properly dry. Column was fixed into a clean collector tube and DNA was eluted by applying 50 µl of 60°C MQ-water onto the membrane and spinning it for 30 sec at 14.000 x g. Plasmid DNA was quantified using the NanoDrop spectrophotometer (Thermo Scientific) and stored at -20°C.

2.2.3.2 Isolation of plasmidic DNA from *S. cerevisiae*

For isolation of plasmidic DNA from *S. cerevisiae* strains, a phenol/chloroform extraction protocol was used. Cells were grown overnight as described in Section 2.2.2.1, in 10 ml

cultures. Cells were collected by centrifugation for 5 min at 3.000 rpm, supernatant was discarded, and pellet was disrupted by vortexing. Cells were resuspended in 200 µl of Breaking Buffer (10 mM Tris Hcl, pH 8.0 / 2 % Tx-100 / 1 % SDS / 100 mM NaCl / 1 mM EDTA, pH 8.0) and glass beads (200 µl, acid washed, 1 mm, Sigma) and 200 µl phenol/chloroform/isoamyl alcohol (Roti-aqua-P/C/I, Roth) were added. Cells were then disrupted in a MiniBeadbeater-24 (Bio Spec Products Inc.) at 4°C for 3 x 1 min, with 1 min pause in between cycles and centrifuged for 5 min at 13.000 x g (RT). Supernatant was transferred to new tube, and 1/10 of the total volume of cold sodium acetate (3 M, pH 5.2) and 3 volumes of cold 100 % ethanol were added. Samples were incubated for 1 h at -80°C and centrifuged at 16.000 x g for 30 min (4°C). Supernatant was discarded and pellet washed with 70 % ethanol. After centrifugation at 16.000 x g for 15 min (4°C), supernatant was discarded and pellet air dried. Finally, pellets were resuspended in 100 µl of TE Buffer (10 mM Tris-HCl, pH 7.5/1 mM EDTA) and quantified using a NanoDrop spectrophotometer (Thermo Scientific) and stored at 4°C.

2.2.3.3 Isolation of *S. cerevisiae* total DNA

For isolation of total DNA from *S. cerevisiae*, cells were grown overnight as described in Section 2.2.2.1, in 10 ml cultures. Cells were collected by centrifugation for 5 min at 3.000 rpm and washed with 0.5 ml of sterile deionized water. After sedimenting the cells for 5 sec at 16.000 x g (RT), supernatant was discarded, pellet disrupted by vortexing, and resuspended in 200 µl of Breaking Buffer (10 mM Tris Hcl, pH 8.0 / 2 % Tx-100 / 1 % SDS / 100 mM NaCl / 1 mM EDTA, pH 8.0). Glass beads (200 µl, acid washed, 1 mm, Sigma) and 200 µl phenol / chloroform / isoamyl alcohol (Roti-aqua-P/C/I, Roth) were added and samples were vortexed at highest speed for 3 min. After 200 µl of TE Buffer (10 mM Tris-HCl, pH 7.5 / 1 mM EDTA) were added, samples were vortexed briefly and centrifugated at 16.000 x g for 5 min (RT). Aqueous layer was transferred to new tube and, after the addition of 1 ml of 100 % ethanol, samples were mixed by inversion. After centrifugation at 16.000 x g for 3 min (RT), pellet was resuspended in 400 µl TE Buffer and 15 µl of DNase-free RNase A (10 mg/ml, Sigma) was added, sample was mixed and incubated for 15 min at 37°C. After incubation, 10 µl of 4 M ammonium acetate and 1 ml of 100 % ethanol were added, sample was mixed by inversion and centrifuged at 16.000 x g for 3 min (RT). Pellet was finally

washed with 15 % ethanol, air dried, resuspended in 100 µl of TE Buffer and quantified using a NanoDrop spectrophotometer (Thermo Scientific).

2.2.4 DNA manipulation

2.2.4.1 Polymerase Chain Reaction

Polymerase Chain Reaction (PCR) is a technique that allows the exponential amplification (i.e. increase of the copy number) of a targeted DNA sequence. For this process, there are three key elements: the template DNA (containing region to be amplified); the flanking primers (short single-stranded oligonucleotides designed to specifically bind to the template DNA at the 5' and 3' end of the target sequence); and the DNA polymerase, which will catalyse the polymerization of the new DNA copies. A standard PCR reaction consists of 20-35 cycles, depending on the polymerase used and is divided in three steps: denaturing, primer annealing, and primer extension. In the denaturing step, the PCR mix (Table 2.12) is heated at a high temperature (dependent on the polymerase used) to denature the double-stranded DNA and allow access of primers to their area of homology. The primer annealing step is performed at a lower (sequence-specific) temperature to assure specific binding of the primers to the template DNA. During the extension step, the DNA polymerase extends the primers and adds nucleotides complementary to the template DNA. During this study, PCR was performed in order to amplify multiple DNA targets. Kapa HiFi (Peqlab) was used for all cloning-purpose amplifications (Section 2.1.8, Table 2.8). The standard reaction composition and program used is described in Tables 2.12 and 2.13, respectively. Temperature and duration of each step (Table 2.13) were optimized for each reaction. Gene-specific primers (Table 2.6) were designed using the sequences acquired on www.yeastgenome.org. The peqSTAR 2X Gradient Thermocycler (Peqlab) was used routinely for PCRs. The correct size of each PCR product was verified by agarose gel electrophoresis (Section 2.2.4.3). Resulting PCR products were either cloned into a vector or used to directly transform *S. cerevisiae*.

Component	Volume	Final concentration
5X KAPA HiFi Reaction Buffer	10 μ l	1X
KAPA dNTP Mix (10 mM each) Forward primer (10 μ M) Reverse primer (10 μ M)	1.5 μ l	0.3 mM
Template DNA	1 μ l	10ng plasmid DNA
KAPA HiFi Polymerase	1 μ l	0.02 U/ μ l
dH2O	to 50 μ l	-

Table 2.12: Standard reaction mixture for PCR used in this study

Number of cycles	Operation	Temperature	Duration
1	Initial denaturation	95°C	
35	Denaturation	98°C	12 sec
	Primer annealing	(60-75)°C	15 sec
	Primer extension	72°C	30 sec/Kb
1	Final extension	72°C	5 min
1	Store	4°C	∞

Table 2.13: Standard thermal cycle program for PCR used in this study

2.2.4.2 Colony PCR

In colony PCR a sample of each transformant colony to be screen was resuspended in 50 μ l of MQ water, and denatured at 95°C for 5 min. After centrifugation at 16.000 x g for 1 min, 10 μ l of the supernatant (cell crude extract) was used as template DNA in a PCR reaction. In this study, colony PCRs were done in a final volume of 25 μ l, using the OneTaq[®] DNA polymerase (Table 2.8). Reaction composition and programs used with this setup are described in Table 2.14 and 2.15, respectively. Adequate primers were used for these reactions (Table 2.6). Full volume of the reaction was then resolved in an agarose gel of

appropriate concentration as described in Section 2.2.4.3, and positive clones were selected by band-size confirmation. Positive clones were then verified by sequencing.

Component	Volume	Final concentration
2X OneTaq Master Mix	12.5 μ l	1X
Forward primer (10 μ M) Reverse primer (10 μ M)	0.5 μ l	0.2 μ M
Template DNA	10 μ l (of crude extract)	-
dH ₂ O	1.5 μ l	-

Table 2.14: Standard colony PCR reaction mixture used in this study

Number of Cycles	Operation	Temperature	Duration
1	Initial denaturation	94°C	5 min
30	Denaturalization	94°C	30 sec
	Primer annealing	(45-68) °C	30 sec
	Primer extension	68°C	1 min/Kb
1	Final extension	68°C	5 min
1	Store	4°C	∞

Table 2.15: Standard thermal cycle program for colony PCR used in this study

2.2.4.3 Agarose Gel Electrophoresis

Agarose gel electrophoresis was performed to separate, identify and purify DNA fragments. DNA samples were mixed with DNA Loading buffer (6X: 50 % Sucrose / 0.15 % Bromophenol Blue / 0.02 M EDTA), unless OneTaq[®] DNA polymerase was used (Which has the loading buffer already incorporated in the mix) and loaded onto a 1 % Agarose Gel (1 % Agarose / 2 % 50X TAE / 90 % dH₂O) containing 0.5 μ g/ml Ethidium Bromide (EtBr). Gels were placed in a Peqlab gel tank containing 1X TAE buffer (Tris Acetate EDTA / 50X: pH 8.4 / 20 M Tris- HCl / 10 M Acetic Acid / 0.05 M EDTA) and electrophoresis was then carried out at 100 - 120 V for 1-2 h. GeneRuler™ 1 kb DNA ladder (Fermentas) was used as the size

standard (0.5 µg loaded). Gels were placed over a transilluminator for visualization of the DNA, which was photographed using the E-Box VX2 Gel Documentation System (Peqlab).

2.2.4.4 Recovery of DNA Fragments

For recovering DNA from agarose gels, the GenElute™ Gel Extraction Kit (SigmaAldrich) was used. DNA band was excised from the agarose gel using a x-tracta gel extraction tool (SigmaAldrich), and then transferred into a 2 ml microcentrifuge tube. The gel slice was resuspended in 3 gel volumes of Gel Solubilization Solution. The mixture was incubated at 65°C until the gel was dissolved and 1 gel volume of 100 % isopropanol was added. The mix was loaded onto a binding column and centrifuged for 1 min at max. speed in a benchtop centrifuge (MiniSpin®, Eppendorf). The flow-through liquid was discarded, 700 µl of Wash Solution were added to the binding column and the column centrifuged for 1 min at max. speed (RT). Once all of the solution had been passed through the binding column, the column was centrifuged as before in order to remove residual Wash Solution. The DNA was eluted by addition of 50 µl MQ water (65°C) to the membrane of the binding column and incubated for 1 min at RT, followed by centrifugation for 1 min at max. speed. DNA was then stored at -20°C for future usage.

2.2.4.5 Restriction Digestion of PCR Products and Plasmid DNA

All endonuclease restriction digestions were carried out in a 50 µl reaction mixture containing the appropriate buffer, as recommended by the supplier (NEB), and 10 units of enzyme per µg of DNA. Reaction mixtures were incubated for 5 min or 1 h at 37°C, depending if fast-digest enzyme was used. Afterwards, reaction mixtures were heat-inactivated as recommended and cleaned with the PCR cleaning Kit (Sigma). DNA was then analyzed by gel electrophoresis (Section 2.2.4.3). In case of two-enzymes reactions, the buffer used was the one in which both enzymes exhibit the highest efficiency. The standard reaction mixture is outlined in Table 2.16.

Component	Volume
DNA	X µl (1 µg)

Buffer	5 μ l
Restriction Enzyme	1 μ l (10U)
dH ₂ O	to 50 μ l

Table 2.16: Standard reaction mixture for the restriction digestion of DNA used in this study

2.2.4.6 DNA cleaning

For linearized DNA cleaning after processing, the GenElute™ PCR Clean-Up Kit was used. The columns supplied by the kit were prepared by adding 500 μ l of Column Preparation Solution, centrifuging at 14,000 x g for 1 min and discarding the flowthrough. DNA sample was diluted by adding 5 volumes of Binding Solution to 1 volume of the DNA sample. The mix was applied to the column, centrifuged at 14,000 x g for 1 min and the flowthrough was discarded. Column was then washed with 750 μ l of Washing Solution, centrifuged sequentially twice at 14,000 x g exchanging collector tube in between, and left to dry for some minutes. For elution, 50 μ l of 65°C MQ water was added to the centre of the column, incubation for 1 min at RT, and then centrifuge the column at 14,000 x g for 1 min in a clean eppendorf. Sample was then quantified using a NanoDrop spectrophotometer (Thermo Scientific) and stored at -20 °C for future usage.

2.2.4.7 Dephosphorylation of Vector DNA

Hydrolyzation of 5' phosphate group prior to ligation in case of double blunt end cloning, is use in order to avoid re-ligation of the digested vector. FastAP™ Thermosensitive Alkaline Phosphatase (Thermo Fisher Scientific) was used for this purpose. The reaction mix (Table 2.17) consisted of 1 unit of FastAP™ Thermosensitive Alkaline Phosphatase, 0.1 volume of 10X FastAP™ buffer and 1 μ g of vector DNA. The sample was incubated at 37°C for 10 min and heat-inactivated at 65°C for 15 min.

Component	Volume
DNA	X μ l (1 μ g)
Buffer	2 μ l

FastAP	1 μ l
dH ₂ O	to 20 μ l

Table 2.17: Standard reaction mixture for the dephosphorylation of digested vector DNA used in this study

2.2.4.8 Phosphorylation of insert DNA

When double blunt end cloning was used, in order to allow ligation with the dephosphorylated digested vector, a 3' phosphate group was added to the insert prior ligation. T4 Polynucleotide Kinase (PKN) (NEB) was used for this purpose. The reaction mix (Table 2.18) consisted of 1 unit of PKN, 0.1 volume of 10X PKN buffer and 1 μ g of vector DNA. The sample was incubated at 37°C for 10 min and heat-inactivated at 65°C for 15 min.

Component	Volume
DNA	X μ l (1 μ g)
Buffer	2 μ l
T4 PKN	1 μ l
dH ₂ O	to 20 μ l

Table 2.18: Standard reaction mixture for the phosphorylation of digested vector DNA used in this

2.2.4.9 Ligation of Vector DNA and Insert DNA

Following digestion of vector and insert DNA with the appropriate enzymes to create matching sticky ends, ligation is usually needed. T4 DNA ligase (Fermentas) was used for this purpose. Reaction was carried out for 10 min at 22°C in a water bath using a mixture contained 10X T4 DNA ligase buffer, 2 units of T4 DNA ligase (2 U/ μ l) and a 3:1 ratio of insert to vector. Ligations were prepared according to the reaction mixture presented in Table 2.19. For transformation of *E. coli* cells, 10 μ l of the ligation were used.

Component	Volume
Buffer	2 μ l

Vector DNA	X μ l (50 ng)
Insert DNA	Y (relation 3:1 with Vector DNA)
dH ₂ O	to 20 μ l
T4 DNA Ligase	1 μ l

Table 2.19: Standard reaction mixture for the ligation of the vector and insert DNA used in this

2.2.5 Transformation of *E. coli* Cells with plasmidic DNA

2.2.5.1 Preparation of Chemically Competent *E. coli* Cells

E. coli DH5 α cells were grown to an OD₆₀₀ of approximately 0.6 and centrifuged at 4.000 rpm at 4°C for 6 min (Sigma 4K15 centrifuge, 12169-H rotor). After resuspending the pellet in 8.5 ml of 4°C sterile TFPI buffer, pH 5.8 (30 mM KOAc / 100 mM KCl / 10 mM CaCl₂ / 50 mM MnCl₂ / 10 % glycerol), cells were incubated on ice for 10 min. Cells were then sedimented by centrifugation at 4.000 rpm at 4°C for 6 min, the pellet was resuspended in 1 ml of 4°C and sterile TFPII buffer, pH 6.5 (10 mM KCl / 75 mM CaCl₂ / 10 % glycerol / 10 mM MOPS) and incubated on ice for 30 min. Resuspended cells were then divided into 100 μ l aliquots, flash frozen in liquid nitrogen and stored at -80°C for future usage.

2.2.5.2 Transformation of chemically competent *E. coli* cells

To generate recombinant bacteria, chemically competent *E. coli* DH5 α cells (section 2.2.5.1) was used. After adding 10-100 ng of plasmid DNA to the recently thawed aliquot of competent *E. coli*, cells were incubated for 20 min on ice and subsequently heat-shocked at 42°C for 2 min. Pre-warmed LB medium (700 μ l) was added and cells were incubated for 1 h at 37°C under shaking. Cells were centrifuged at 10.000 rpm for 1 min (Eppendorf 5415 R microcentrifuge), the supernatant was discarded and cells were resuspended in the residual LB medium. Finally, cells were plated onto LB agar plates containing the appropriate selection marker (table 2.11).

2.2.5.3 DNA Sequencing

For analysing cloned DNA sequences all plasmids were sequenced. Miniprep DNA samples (Section 2.2.3.1) of all transformants were sent for sequencing. Sequencing was performed by GATC Biotech AG (Konstanz) according to the sequencing method by Sanger et al. For the majority of plasmid sequencings, M13 primers (Table 2.6) were used if not stated otherwise. The results were analyzed with the Snapgene® software.

2.2.5.4 Transformation of *S. cerevisiae*

The Lithium Acetate method (LiAc / SSDNA / PEG) was used for the transformation of *S. cerevisiae*. Yeast strains (25 ml) were grown overnight at 30°C, 220 rpm. For each transformation, cells (2 ml) were harvested at 3.000 rpm for 2 min at RT (Minispinner, Table top) and washed with 1 ml of sterile LiAc / TE Solution (10 mM Tris -HCl, pH 7.5 / 100 mM LiAc / 1 mM EDTA). The pellet was resuspended in 100 µl of LiAc / TE Solution, and 20 µl of denatured carrier DNA (Salmon testes DNA, 10 mg/ml (Sigma)), 1 µg of DNA, 600 µl of PEG solution (10 mM Tris -HCl, pH 7.5 / 100 mM LiAc / 1 mM EDTA / 40 % PEG₂₀₀₀), and 50 µl of 1 M LiAc were added. Sample was mixed and incubated for 1 h at 30 °C, followed by 15 min at 42 °C after adding 20 µl of DMSO (this step was not performed when temperature sensitive strains were used). Cells were collected, by centrifuging at 3.000 rpm for 2 min and the pellet was washed in 1 ml of TE (10 mM Tris-HCl pH 8.0 / 1 mM EDTA pH 8.0). Cells were resuspended in 100 µl of TE Solution, plated onto the appropriate selective medium plates and incubated at 30°C for 2-4 days. The LiAc method was applied to transform all *S. cerevisiae* strains in this work with the appropriate plasmid DNA or linear DNA (Table 2.5) to create the desired strains.

2.2.5.5 Verification of *S. cerevisiae* Transformants

Positive transformants were picked and plated onto the appropriate selective medium plates and the genomic DNA was isolated (Section 2.2.3.3). This DNA was then used as template in a PCR reaction (Section 2.2.4.1) with specific primers to confirm proper integration of the desired sequence into the yeast genome. PCR products were sequenced

as verification of the procedure. When possible, gene knockouts were also verified by Western blotting using the appropriate antibody against the protein codified by the targeted gene being knocked out.

2.2.6 Isolation of *S.cerevisiae* RNA

Yeast strains (10 ml culture) were grown to early exponential phase at 30°C, 220 rpm. Cells were harvested for 5 min at 4°C, 5.700 x g. Pellets were resuspended in 1 ml of ice-cold RNase-free water (DEPC-treated). The cells were centrifuged at full speed, 4°C for 10 sec (5424-R Eppendorf microfuge) and the pellet was resuspended with 400 µl TES Solution (10 mM Tris-HCl, pH 7.7 / 10 mM EDTA / 0.5 % SDS). Acid Phenol (400 µl, Roti®-Aqua-Phenol, Carl Roth) was added and the sample vortexed for 10 sec and incubated at 65°C for 1 h with occasional vortexing. The samples were centrifuged at full speed, 4°C for 5 min. The aqueous phase was transferred to a clean microfuge tube. Roti®-Aqua-Phenol (400 µl) was added and the sample was vortexed for 20 sec, incubated on ice for 5 min and centrifuged as before. The aqueous phase was transferred to a clean microfuge tube and mixed with 400 µl chloroform, vortexed for 20 sec and centrifuged as before. The aqueous phase was transferred to a clean microfuge tube and 40 µl of 3 M sodium acetate (pH 5.3) and 1ml of ice-cold 100 % ethanol were added. The sample was vortexed and centrifuged as before. Pellets were washed with 1.5 ml 70 % ethanol, centrifuged as before and resuspended in 50 µl RNase-free water (DEPC-treated). RNA concentration was determined using a NanoDrop spectrophotometer (Thermo Scientific), and RNA was stored at -20 °C.

2.2.7 HAC1 mRNA Splice Assay

Upon induction of the UPR the HAC1 mRNA is spliced. Thus, the comparison of the two species, HAC1^u and HAC1ⁱ (u = uninduced; i = induced), allows for the evaluation of the UPR status of various yeast strains. Yeast strains were grown to early exponential phase at 30°C, 220 rpm. For positive controls each strain was incubated in the presence of TM (2 µg/ml), 3 h as above. A volume of 10 ml of each culture was pelleted, and used to isolate yeast RNA. The RNA was then diluted to a final concentration of 0.1 µg/µl, and used in reverse transcription reactions to generate cDNA using the Maxima® Reverse Transcriptase

(Fermentas), according to the manufacturer's instructions (Table 2.20). The samples were incubated for 30 minutes at 50 °C, followed by an inactivation at 85 °C for 5 minutes. Each cDNA (0.1 µg) was used in a PCR reaction using *HAC1* and *ACT1* specific primer sequences (Table 2.6). The thermal cycler program was as described in Table 2.13 with the following exceptions: primer annealing (step 3) was at 50 °C, primer extension (step 4) was for 45 sec, final primer extension was for 3 min and steps 2 to 4 were cycled 24 times. The PCR setup was as described in Table 2.12. The PCR products were resolved on a 1 % agarose gel in 1X TAE Buffer (50X TAE pH 8.4 / 20 M Tris-HCl / 10 M Acetic Acid / 0.05 M EDTA) at 100 V and RT for 1 hr (Section 2.2.4.3). Bands were visualized and photographed using the E-BOX VX2 gel documentation system (Peqlab).

Component	Volume	Final Concentration
RNA	1 µl	0.1 µg
Oligo-dT-Primer (100 mM)	1 µl	100 pmol
dNTP mix (10 mM)	1 µl	0.5 mM
RNase-free dH ₂ O	to 14.5 µl	-
5X RT Buffer	4 µl	1X
RNasin (40 U/µl)	0.5 µl	20 U
Maxima RT	1 µl	200 U

Table 2.20: Reverse transcription reaction mixture used in this

2.2.8 Protein Gel Electrophoresis and Western Blot Analysis

2.2.8.1 Preparation of Cell Extracts

Yeast strains were grown to an OD₆₀₀ of 1 at 30°C, 220 rpm. Cells 2 (OD₆₀₀) were harvested at 1.600 x g for 1 min (MiniSpin® Centrifuge, Eppendorf) and the supernatants were discarded. Pellets were washed with 1 ml of sterile deionized water, resuspended in 200 µl 2 X SDS sample buffer (100 mM Tris-HCl, pH 6.8 / 4 % SDS / 0.2 % bromophenol blue / 20 % glycerol / 200 mM DTT). Glass beads (100 µl, acid washed, 1 mm, Sigma) were added and the cells were disrupted in a MiniBeadbeater-24 (Bio Spec Products Inc.) at 4°C for 2 x 1

min, with 1 min pause in between cycles. Samples were incubated at 95°C for 5 min (10 min at 65°C for membrane proteins) and centrifuged at 11.000 x g for 1 min. Samples were then loaded onto SDS-PAGE gels.

2.2.8.2 Protein Gel Electrophoresis

Protein gel electrophoresis (SDS-PAGE) was routinely conducted using NuPAGE® Novex® Pre-Cast Bis-Tris gels (4-12 % gradient gels or 10% gels, 1.5 mm, 10 wells) and the XCell SureLock™ Mini-Cell (both Invitrogen) if not stated otherwise. After loading the appropriate volume of the protein sample onto the gel, samples were run in 1X NuPAGE® MOPS SDS Running Buffer (Invitrogen) or 1X NuPAGE® MES SDS Running Buffer (Invitrogen), depending on the size of the protein to be blot against, at 80V for 15 min and 160V for about 1 h, at RT using a Bio-Rad PowerPac™ HC power supply, until the gel front ran off the bottom of the gel. The PageRuler™ Prestained Protein Ladder (Fermentas) was used as the size standard according to the supplier's instructions.

2.2.8.3 High concentrated urea gel Electrophoresis

18% acrylamide, 4M urea SDS gels were prepared as followed:

For 40 ml the separating gel: 24 ml acrylamide, 10 ml of 1.5M Tris pH 8.8, 200 µl of 20 % SDS and 9.6 g urea were mixed with moderate heating, until urea was dissolved and then 16.7 µl TEMED and 200 µl 10 % APS were added. For 25 ml stacking gel: 4.15 ml acrylamide, 6.25 ml 0.5M Tris pH 6.8, 125 µl 20 % SDS, 6 g urea and 10 ml water were mixed with moderate heating until urea was dissolved, and then 15 µl TEMED and 200 µl 10 % APS were added. Samples were run in SDS running buffer (25 mM Tris / 200 mM Glycine / 0.2 % (w/v) SDS) at 90V, until the gel front ran off the bottom of the gel. After running and prior to transfer them to nitrocellulose membrane, gels were washed 4 times, 10 minutes, in 200 ml of transfer buffer (25 mM Tris / 200 mM Glycine / 20 % (v/v) Methanol / 0.2 % (w/v) SDS).

2.2.8.4 Coomassie Staining

For Coomassie gel staining, after SDS-PAGE, the gels were incubated with 50-100 ml of staining solution (0,025 % CBB G-250) in a closed box for 20 min at 65°C. After incubation, gel was rinsed multiple times with destaining solution (30% methanol / 10% acetic acid), and incubated in destaining solution, under shaking, until adequate background was reached. After destaining, gel was rinsed with MQ Water 3 times.

2.2.8.5 Western Blot Analysis

Western Blotting was employed to identify target proteins using appropriate antibodies. A “sandwich” containing the acrylamide gel and the nitrocellulose (NC) membranes (0.45 µm pore size, Bio-Rad), as well as 3 MM Chromatography Paper (Whatman®) and sponges soaked in Transfer Buffer (25 mM Tris / 200 mM Glycine / 20 % (v/v) Methanol / 0.2 % (w/v) SDS) were assembled. The protein transfer was then conducted in Transfer Buffer for 2 hr at 100 V in the cold room using a Trans-Blot® Electrophoretic Transfer Cell (with plate electrodes and super cooling coil, Bio-Rad). For the the second part of the Western Blot protocol, the immunoblot and detection phase, the membrane was blocked in Blotto (50 mM Tris-HCl, pH 7.4 / 150 mM NaCl / 2 % (w/v) Milk Powder / 0.1 % (v/v) Tween-20 / 5 mM Sodium Azide) for 1 hr under shaking (RT). The membrane was then incubated under shaking with the primary antibody (Table 2.7) diluted in Blotto for 2h at RT or overnight in the cold room. The membrane was then washed twice (10 min) in Blotto followed by 2 washes (also of 10 min) in 1X TBST (50 mM Tris-HCl, pH 7.4 / 150 mM NaCl / 0.1 % (v/v) Tween20 / 5 mM Sodium Azide). For the last step, the membrane was incubated with the secondary antibody (Table 2.7) diluted in 1X TBST shaking for 1 hr at RT. The membrane was washed 4 times for 10 min with TBST. The blot was prepared for detection using the SuperSignal™ West Dura Extended Duration Chemiluminescent Substrate (Pierce) according to the supplier’s instructions. Signals were detected using the Amersham Imager 600 (GE Healthcare).

2.2.9 Isolation of Membrane and Cytosolic Fractions

Yeast strains were grown to early exponential phase at 30°C, 220 rpm. Cells (7 OD₆₀₀) were harvested at 2.000 x g for 5 min and washed with 1 ml of 100 mM Tris-HCl, pH 9.4. After addition of 10 mM DTT, cells were incubated at RT for 10 min, and centrifuged at 4.300 x g for 1 min. Pellets were resuspended in 200 µl of JR lysis buffer (20 mM Hepes, pH 7.4 / 50 mM KOAc / 2 mM EDTA, pH 8 / 1 mM DTT / 1 mM PMSF / 1 X Phosphatase inhibitor cocktail, Thermo Scientific), 0.3 g of glass beads (acid washed, 1 mm, Sigma) were added and the cells were disrupted in a MiniBeadbeater-24 (Bio Spec Products Inc.) at 4°C for 2 x 1 min, with 1 min pause in between cycles. After short centrifugation (10 sec, 14.000 x g), the supernatant was transferred to a clean microfuge tube and the glass beads were washed with 100 µl B88 (20 mM Hepes, pH 6.8 / 250 mM sorbitol / 150 mM KOAc / 5 mM Mg(OAc)₂ / 1 X Phosphatase inhibitor cocktail, Thermo Scientific) and the new supernatant was added to the previous one. Membranes were sedimented for 15 min, 14.000 x g, 4°C. The supernatant corresponds to the cytosolic fraction and was transferred to a clean microfuge tube. The final volume was adjusted to 350 µl with 2X SDS sample buffer (100 mM Tris-HCl, pH 6.8 / 4 % SDS / 0.2 % bromophenol blue / 20 % glycerol / 200 mM DTT). Sedimented membranes were used for alkaline phosphatase treatment and subsequent TCA precipitation.

2.2.10 Alkaline Phosphatase Treatment and TCA Precipitation

Sedimented membranes were resuspended in 50 µl B88 (20 mM Hepes, pH 6.8 / 250 mM sorbitol / 150 mM KOAc / 5 mM Mg(OAc)₂ / 1 X Phosphatase inhibitor cocktail, Thermo Scientific) and 20 µl of Alkaline Phosphatase (1u/µl, FastAP, Thermo Scientific) was added together with 8 µl of the reaction buffer (10X Thermo scientific FastAP reaction buffer). The samples were incubated for 1h at 37°C. Membranes were then sedimented at 20.000 x g at 4°C for 10 min, and resuspended in 100 µl B88. Membranes were sedimented as before and resuspended in 100 µl B88. Samples were then ready for TCA precipitation. As non-AP treated control, sedimented membranes were directly resuspended in 100 µl B88, without any AP treatment. Proteins were precipitated with 20 % TCA on ice for 30 min and washed with ice-cold acetone. After centrifugation of the samples for 5 min, 14.000 x g, 4°C, pellet

was resuspended in 140 μ l 2X SDS sample buffer (100 mM Tris-HCl, pH 6.8 / 4 % SDS / 0.2 % bromophenol blue / 20 % glycerol / 200 mM DTT) and incubated at 65°C for 10 min.

2.2.11 Preparation of Rough Microsomal Membranes

2.2.11.1 Preparation of Lyticase

KRB3 *E. coli* strain (200 ml) was grown ON in LB-Amp medium at 37°C, 200 rpm. LB-Amp medium (10 L), divided in 8 flasks with 1.25 L each, was inoculated with 15 ml of the ON KRB3 culture per flask and cells were grown at 37°C, 200 rpm to an OD₆₀₀ of 0.5. The cultures were induced with 0.5 mM IPTG for 5 hr at 37°C, 200 rpm and cells were then harvested at 6.300 rpm for 5 min, 4°C (Avanti J-E Centrifuge, JLA-10.500 rotor, Beckman Coulter). Pellets were resuspended with 400 ml 25 mM Tris, pH 7.4 and centrifuged as before. Supernatant was discarded and the pellet was resuspended with 200 ml 25 mM Tris, pH 7.4 / 2 mM EDTA. Then, an equal volume of 25 mM Tris pH 7.4 / 40% sucrose was slowly added and the mix slowly stirred for 20 min at RT on a magnetic stirrer (RH basic 2 IKAMAG®, IKA®). The suspension was then centrifuged as before and the supernatant discarded. The pellet was resuspended with 150 ml of ice-cold 0.5 mM MgSO₄, slowly stirred in the cold room (4°C) for 20 min and centrifuged as before. The supernatant containing the lyticase was aliquoted in 15 ml falcon tubes, frozen in liquid nitrogen and stored at -80°C for future use. The activity of the lyticase was determined using the yeast strain KRY585 (Table 2.4). Cultures (50 ml) were grown in YPD to an OD₆₀₀ of 2, centrifuged for 5 min at 4.200 rpm (Sigma 4K15 centrifuge, 12169-H rotor), RT and resuspended in 50 mM Tris-HCl pH 7.4 / 10 mM DTT to an OD₆₀₀ of 2. Aliquots of 1 ml yeast culture (in duplicates) were incubated with different concentrations of lyticase (0.01, 0.02, 0.5, 1, 2 μ l). Samples were incubated at 30 °C for 30 min and the OD₆₀₀ was immediately measured. The activity of the lyticase was calculated based on the principle that a 10% decrease of OD₆₀₀ corresponds to 1U of lyticase activity. The two most diluted points of the curve were taken in consideration for the calculation of the activity.

2.2.11.2 Preparation Microsomal Membranes

Yeast culture (2.5-10 L) was grown ON either in full or minimal media at 30°C with continuous shaking at 200 rpm to an OD₆₀₀ of 2-4. Cells were harvested at 5.000 rpm and RT for 3 min (Avanti J-E Centrifuge, JLA-10.500 rotor, Beckman Coulter), the pellet was resuspended in 100 mM Tris-HCl pH 9.4 / 10 mM DTT to a concentration of 100 OD₆₀₀/ml and incubated for 10 min at RT in order to weaken the cell walls. Cells were centrifuged at 5.000 rpm and RT for 5 min and then resuspended in Lyticase Buffer (50 mM Tris-HCl, pH 7.5 / 0.75 X YP / 700 mM Sorbitol / 0.5 % Glucose / 10 mM DTT) to a concentration of 100 OD₆₀₀/ml. Lyticase (Section 2.2.11.1) was added to a final concentration of 40 U per OD₆₀₀ of cells, and the mix was incubated for 20 min at 30°C, 80 rpm (Multitron Standard Incubation Shaker, Infors HT). Cells were then transferred into ice for 2 min and then centrifuged for 5 min at 5.000 rpm, 4°C. The supernatant was discarded and the pellet washed with 2X JR Buffer (40 mM Hepes-KOH, pH 7.4 / 400 mM Sorbitol / 100 mM KOAc / 4 mM EDTA) to a concentration of 250 OD₆₀₀/ml and centrifuged at 10.000 rpm and 4 °C for 10 min (Avanti J-E Centrifuge, JA-25.50 rotor, Beckman Coulter). The pellet was then resuspended in 2X JR buffer to a concentration of 500 OD₆₀₀/ml and frozen at -80°C overnight. The spheroplasts were thawed in an ice-cold water bath and an equal volume of cold MQ water was added. After the addition of PMSF and DTT to a final concentration of 1 mM, the spheroplasts were disrupted with ten strokes of a motor-driven Potter Elvehjem homogenizer (EUROSTAR power basic, IKA®) at 4°C. The lysate was centrifuged for 5 min at 3.000 rpm, 4 °C (Avanti J-E Centrifuge, JA-25.50 rotor, Beckman Coulter) and the supernatant transferred to a clean polycarbonate tube and centrifuged at 17.500 rpm and 4°C for 15 min to pellet the membranes. The sample was then transferred into ice and the pellet was resuspended in a minimum volume (0.5 ml) of B88 (20 mM Hepes-KOH, pH 6.8 / 250 mM Sorbitol / 150 mM KOAc / 5 mM Mg(OAc)) and gently homogenized on ice using a small teflon pestle and carefully resuspended using a Gilson® pipette. The sample was then loaded into a 1.2 M / 1.5 M (1.5 ml of each sucrose solution previously layered into an SW60Ti tube (Beckman Coulter)) Sucrose Gradient (20 mM Hepes-KOH, pH 7.5 / 50 mM KOAc / 2 mM EDTA / 1 mM DTT / 1.2 M or 1.5 M Sucrose) and centrifuged at 44.000 rpm and 4°C for 70 min (Optima™ L-90 K Ultracentrifuge, SW 60 Ti rotor). ER-derived microsomes were collected at the interphase of the gradient and washed with 50 ml of cold B88. The sample was centrifuged

at 17.500 rpm and 4°C for 15 min (Avanti J-E Centrifuge, JA-25.50 rotor, Beckman Coulter). The pellet was carefully resuspended in the appropriate volume of B88 (usually around 0.2 ml). Membrane concentration was measured at OD₂₈₀ in 2% SDS at a 1:200 dilution. The concentration was adjusted to an OD₂₈₀ of 30 with B88 and the samples were aliquoted (25 µl or 50 µl), frozen in liquid nitrogen and stored at -80°C for future usage.

2.2.12 Radioactive labelling

2.2.12.1 Pulse Labelling

Yeast strains were grown either in full or selective media at 30°C, 220 rpm to an OD₆₀₀ of 0.5–1. Cells were harvested at 900 x g, RT for 5 min, washed twice with Labeling Medium (0.67 % YNB without amino acids and ammonium sulphate / 5 % glucose, supplements as required by the strain's auxotrophies), and resuspended in Labeling Medium to an OD₆₀₀ of 6. Aliquots of 1.5 OD₆₀₀ were transferred to clean 2 ml microfuge tubes. The samples were pre-incubated at the respective temperature, 800 rpm for 10 min to use up intracellular methionine and cysteine. Cells were then pulsed with 2.20 MBq per sample with Express Protein Labeling Mix (Perkin Elmer) and incubated for 2.5, 5, or 15 min (depending on the substrate) at 800 rpm, at the respective temperature. Cells were immediately transferred to ice and killed by adding 750 µl of cold Tris-Azide Buffer (20 mM Tris-HCl, pH 7.5 / 20 mM sodium azide). Cells were harvested for 1 min at full speed in a 5424-R Eppendorf microfuge at 4°C, the pellets were resuspended in 1 ml of Resuspension Buffer (100 mM Tris-HCl, pH 9.4 / 10 mM DTT / 20 mM ammonium sulphate) and incubated for 10 min at RT. The samples were centrifuged as before and resuspended in 150 µl of Lysis Buffer (20 mM Tris-HCl, pH 7.5 / 2 % SDS / 1 mM PMSF / 1 mM DTT). Glass beads (150 µl, acid washed, 1 mm, Sigma) were added and the cells were disrupted in a MiniBeadbeater-24 (Bio Spec Products Inc.) for 2 x 1 min with 1 min pause in between cycles at RT. Samples were denatured at 85°C for 5 min (10 min at 65°C for membrane proteins). Beads were washed 3 times with 250 µl of IP Buffer without SDS (15 mM TrisHCl, pH 7.5 / 150 mM NaCl / 1 % Triton X-100 / 2 mM sodium azide), and the combined supernatants from each sample were collected and submitted to immunoprecipitation.

2.2.12.2 Phosphate labelling of microsomal membranes

Microsomes were prepared as in section 2.12. Labelling reactions contained 5 eq of membranes (10 μ l, OD₂₈₀ of 30) in B88 with 2 μ l of 10 X Phosphatase inhibitor cocktail (Thermo Scientific), 0.1 μ M GTP (2 μ l of 1 μ M), 2 mM CaCl₂ (2 μ l of 20mM) and 40 μ Ci γ -[³²P]ATP (Perkin Elmer, 4 μ l of 10 μ Ci/ μ l). Reactions were incubated at 30°C for 30 minutes and then sedimented at 14.000 x g at 4°C for 5 minutes. Membranes were resuspended in 50 μ l of 2% SDS and incubated at 65°C for 10 minutes. Then Sbh1 was immunoprecipitated with anti-Sbh1 serum raised by this lab against the first 18 amino acids of Sbh1. Samples were analyzed by SDS-PAGE on 15% gels and autoradiography.

2.2.12.3 Immunoprecipitation

Samples were precleared by adding 60 μ l of 20 % Protein A Sepharose™ CL-4B (GE Healthcare) in IP Buffer (15 mM Tris-HCl, pH 7.5 / 150 mM NaCl / 1 % Triton X-100 / 2 mM Sodium Azide / 0.1 % SDS) incubating for 30 min under rotation at RT. Samples were centrifuged for 1 min at full speed at RT and each supernatant was transferred to a clean microfuge tube containing 60 μ l of 20 % Protein A Sepharose™ CL-4B as well as the appropriate antibody (Table 2.7). The samples were then incubated overnight at 4°C under rotation. Samples were centrifuged for 10 sec at full speed, RT, washed with 1 ml of IP Buffer with SDS and 1 ml of Urea buffer (2 M Urea / 200 mM NaCl / 1 % Triton X-100 / 100 mM Tris-HCl, pH 7.5 / 2 mM sodium azide) 2 times each, and washed once with 1 ml of ConA buffer (500 mM NaCl / 1 % Triton X-100 / 20 mM Tris-HCl, pH 7.5 / 2 mM NaN₃) and 1 ml of Tris-NaCl Wash (50 mM NaCl / 10 mM Tris-HCl, pH 7.5 / 2 mM NaN₃). Samples were centrifuged as before and the supernatants discarded. SDS-PAGE Protein Sample Buffer (25 μ l of 2X, 125 mM Tris-HCl, pH 6.8 / 4 % SDS / 10 % β -Mercaptoethanol / 0.002 % bromophenol Blue / 20 % glycerol) was added and the samples incubated at 95°C for 5 min (10 min at 65 °C for membrane proteins). Samples were loaded onto a 10 % or 7.5% Bis-Tris gel (Invitrogen) and, following the electrophoresis, gels were fixed (10 % acetic acid / 40 % methanol) for 30 min under shaking. After washing with deionized water, gels were dried at 80°C for 1 h in a gel dryer (Model 583, Bio-Rad), exposed to phosphorimager plates and

signal acquired in Typhoon Trio™ Variable Mode Imager, GE Healthcare. Signals were analysed and quantified using the ImageQuant™ TL software (GE Healthcare).

2.2.13 Mutant construction

2.2.13.1 Integration of Ylp α -L plasmid into KRY585 and KRY588 strains

First I extracted the Ylp α -L plasmid from KRB1136 (Table 2.5), as described in section 2.2.3.1. Ylp α -L plasmid encodes *Bacillus amyloliquefaciens* α -amylase expression cassette with the ADH1 promoter and terminator, and it is used to integrate this cassette into the *leu2* locus of the target strain. After extraction of the plasmid, I transformed wildtype (KRY585) and $\Delta sbh1/\Delta sbh2$ (KRY588) strains (Table 2.4) with it, as described in section 2.2.5.4. After transformation, I plated the transformed yeast cells in minimal media (-Leu). Since this plasmid has no replication origin, only cells that have integrated the plasmid into the *leu2* locus can grow in -Leu media. After 5 days, I replated (in -leu plates) the colonies that were able to grow, and I checked the integration by Western blotting, using α -amylase specific antibodies. The generated strains were called KRY1128 and KRY1129 (Table 2.4).

2.2.13.2 SBH1 and SBH2 deletion in KRY1156 wildtype strain to make KRY1160 strain

In order to delete *SBH1* and *SBH2* I first extracted the genomic DNA from the KRY588 strain (Table 2.4) as described in section 2.2.3.3. Afterwards, I amplified the *seb1::KanMx* cassette (cassette for generating $\Delta sbh1$ by integration of the Kanamycin resistance). For this PCR reaction, done as described in section 2.2.4.1, I used as DNA template genomic DNA extracted from KRY588 (Table 2.4) and primers 59 and 60 (Table 2.6). I clean the PCR product as described in section 2.4.6 and transformed KRY1156 strain (Table 2.4) as described in section 2.2.5.4, plating the transformed KRY1156 in YPD plates supplemented with 100 μ g/ml Kanamycin. After 5 days, I replated (in YPD plates supplemented with 100 μ g/ml Kanamycin) the colonies that were able to grow, and I extracted the genomic DNA from this strains as described in section 2.2.3.3. I used this DNA to check the deletion of *SBH1*. I made a PCR reaction and I resolved the amplicon in agarose gels as described in section 2.2.4.1, using as a positive control DNA extracted from KYR588 ($\Delta sbh1\Delta sbh2$) and as

a negative control DNA extracted from KYR585 (wildtype) (Table 2.4). Afterwards, I sent for sequencing the genomic DNA extracted from the positive colonies (GATC Biotech), for a double check. For both PCR check and sequencing, I used primers 59 and 60 (Table 2.6). The strain resulted from this deletion was called KRY1158. After deletion of *SBH1*, I proceeded by deleting *SBH2*. For doing this, first I amplified the *seb2::hphMx* cassette (cassette for generating $\Delta sbh2$ by integration of the hygromycin resistance). For this PCR reaction done as described in section 2.2.41, I used as DNA template genomic DNA extracted from KRY588 (Table 2.4) and primers Sbh2ExtFw and Sbh2ExtRv (Table 2.6). I clean the PCR product as described in section 2.4.6 and transformed the KRY1158 strain (Table 2.4) as described in section 2.2.5.4, plating the transformed cells in YPD plates supplemented with 200 $\mu\text{g}/\text{ml}$ Hygromycin. After 5 days, I replated (in YPD plates supplemented with 200 $\mu\text{g}/\text{ml}$ Hygromycin) the colonies that were able to grow, and I extracted the genomic DNA from this strains as described in section 2.2.3.3. I used this DNA to check the deletion of *SBH2* by PCR and resolving amplicon in agarose gels as described in section 2.2.4.1., using as a positive control DNA extracted from KYR588 ($\Delta sbh1\Delta sbh2$) and as a negative control DNA extracted from KYR585 (wildtype) (Table 2.4). Afterwards, I sent for sequencing the genomic DNA extracted from the positive colonies (GATC Biotech), for a double check. For both PCR check and sequencing, I used primers Sbh2ExtFw and Sbh2ExtRv (Table 2.6). When I finally had the KRY1156 strain with the double deletion $\Delta sbh1\Delta sbh2$ (KRY1160), I verified the deletions by checking for Sbh1/Sbh2 expression by Western blotting (Figure 3.19A), using Sbh1-specific antibodies (Table 2.7) and by temperature sensitivity growth test at 37°C (Figure 3.19B).

2.2.13.3 Subcloning of *sbh1S3A/T5A* from pRS415 to pRS416

To be able to transform KRY1160 strain with *sbh1S3A/T5A*, I had to subclone this mutant gene from a pRS415 plasmid (leucine marker) to a pRS416 (uracil marker), for making it suitable for the KRY1160 strain background. For doing that, I extracted the empty pRS416 and the pRS415*sbh1S3A/T5A* plasmids as described in section 2.2.3.1 from KRB125 and KRB1032 respectively (Table 2.5). After the extraction, I performed a restrictive digestion of them as described in section 2.2.4.5, using KpnI and SacI restriction enzymes (Table 2.8), and I run the fragments on an agarose gel as described in section 2.2.4.3. Then I recovered

the DNA fragments from the agarose gels as described in section 2.2.4.4 (from the empty pRS416 the fragment was about 4.800 bp, and from the pRS415*sbh1S3A/T5A* the fragment was about 2.500 bp). After recovery of the DNA fragments, I ligated them as described in section 2.2.4.9 and I transformed chemically competent *E. Coli* as described in section 2.2.5.1, and plated the transformed bacteria in LB plates supplemented with ampicillin (100 µg/ml) (Table 2.7). I then performed a colony PCR as described in section 2.2.4.1 with M13 primers and to verify, I extracted the plasmids from the positive clones and sent them for sequencing (GATC Biotech). Finally, I used this plasmid pRS416*sbh1S3A/T5A* (KRB1152) to transform KRY1160.

2.2.13.4 Genomic replacement of ESS1 into *ess1H164R* in KRY1156 wildtype strain to make KRY1126

In order to replace wildtype *ESS1* gene with *ess1H154R* mutant gene, I first extracted p502.8 plasmid from KRB1085 (Table 2.5), as described in section 2.2.3.1. Afterwards, I amplified the *ess1H154R:NatMx* cassette (cassette for generating *ess1H154R* mutant gene by using integration of the Nourseothricin resistance). For this PCR reaction (*Atencio et al., 2014*) done as described in section 2.2.4.1, I used as DNA template p502.8 plasmid extracted from KRB1085 (Table 2.5) and primers OW39 and OW989 (*Ma et al., 2012*) (Table 2.6). I clean the PCR product as described in section 2.4.6 and transformed KRY1156 strain (Table 2.4) as described in section 2.2.5.4, plating the transformed KRY1156 in YPD plates supplemented with 100 µg/ml Nourseothricin. After 5 days, I replated (in YPD plates supplemented with 100 µg/ml Nourseothricin) the colonies that were able to grow, and I extracted the genomic DNA from these strains as described in section 2.2.3.3. I used this DNA to check the *ess1H154R:NatMx* integration. I made a PCR reaction using primers CheckEss1mutFw and CheckEss1MutRv (Table 2.6), and I resolved the amplicon in agarose gels as described in section 2.2.4.1, (wildtype about 730 bp, mutant about 2.000 bp). Afterwards, I sent for sequencing the genomic DNA extracted from the positive colonies (GATC Biotech), using primers CheckEss1mutFw and CheckEss1MutRv (Table 2.6).

2.2.13.5 Mns1 GFP-tagging

In order to GFP-tag chromosomal Mns1 from KRY1156 strain, I first extracted pKT209-GFP (plasmid for making C-terminal GFP fusion proteins by PCR) from KRB1127 (Table 2.5), as described in section 2.2.3.1. Afterwards, I amplified the *C-terminalGFPMns1:URA3* cassette (cassette for C-terminally GFP-tagging Mns1 with the integration of the *URA3* gene). For this PCR reaction done as described in section 2.2.4.1, I used as DNA template the pKT209-GFP plasmid extracted from KRB1127 (Table 2.5) and primers FwMns1F5 and RvMns1R3 (Table 2.6). I clean the PCR product as described in section 2.4.6 and transformed KRY1156 strain (Table 2.4) as described in section 2.2.5.4, plating the transformed KRY1156 in -Leu plates. After 5 days, I replated (in -Leu plates) the colonies that were able to grow, and I extracted the genomic DNA from these strains as described in section 2.2.3.3. I used this DNA to check Mns1 GFP-tagging. I made a PCR reaction using primers FwMns1Check and RvMns1Check (Table 2.6), and I resolved the amplicon in agarose gels as described in section 2.2.4.1, (wildtype about 151 bp, GFP-tagged about 2.000 bp). Afterwards, I sent for sequencing the genomic DNA extracted from the positive colonies (GATC Biotech), using primers CheckEss1mutFw and CheckEss1MutRv (Table 2.6). In addition, I checked the Mns1-GFP fusion by fluorescent microscopy of the cells.

2.2.13.6 Mns1SP Δ gp α F construct

In order to screen for the kinase responsible for the S3/T5 Sbh1 phosphorylation, I made a reporter construct by fusing the signal sequence of the Sbh1 phosphorylation-dependent substrate Mns1 to a mutant alpha factor precursor without glycosylation sites (Mns1 Δ gp α F) (Figure 3.41). For doing that, I first extracted the empty p416 plasmid (CEN plasmid for expression) and p416p Δ gp α F from KRB125 and KRB551 respectively (Table 2.5), as described in section 2.2.3.1. Afterwards, I amplified the future insert: EcoRI recognition site, followed by the first 57 nucleotides of Mns1 (codifying for the Mns1 signal sequence), fused with mutant alpha factor precursor without glycosylation sites and without its signal sequence (Δ gp α F) (Figure 3.41). For this PCR reaction done as described in section 2.2.4.1, I used as DNA template the p416p Δ gp α F plasmid extracted from KRB551 (Table 2.5) and primers EcoRIMns1 α FFw and M13Fw (Table 2.6). EcoRIMns1 α FFw primer has the EcoRI

recognition site followed by the first 57 nucleotides of Mns1 (coding for the Mns1 signal sequence), fused to 18 nucleotides from pp α F gene (from nucleotide 61 to nucleotide 78). This 18-nucleotide region is the one annealing the p416p Δ gp α F plasmid. I then performed a restrictive digestion of the amplicon of the PCR reaction, as described in section 2.2.4.5, using Sall and EcoRI restriction enzymes (Table 2.8) and I clean the digested PCR product (about 1400 bp) as described in section 2.2.4.6. In parallel, I performed a restrictive digestion of the empty p416 plasmid extracted from KRB125, as described in section 2.2.4.5, using Sall and EcoRI restriction enzymes (Table 2.8), and I run the fragments on an agarose gel as described in section 2.2.4.3. Then I recovered the DNA fragment from the agarose gels as described in section 2.2.4.4 (about 4.870 bp). After recovery of the DNA fragments, I ligated them as described in section 2.2.4.9 and I transformed chemically competent *E. Coli* as described in section 2.2.5.1, and plated the transformed bacteria in LB plates supplemented with ampicillin (100 μ g/ml) (Table 2.7). I then performed a colony PCR as described in section 2.2.4.1 with M13 primers and to verify, I extracted the plasmids from the positive clones and sent them for sequencing (GATC Biotech).

2.2.14 Automated microscopic screen

Using automated cell manipulations and microscopy platforms, it is possible to easily screen entire genomes for genes that affect any cellular process that can be visualized (*Cohen and Schuldiner, 2011*). The first part of the process is to define the biological question to be addressed. For answering this question, the next step is to design the microscopic screen. There are different possible combinations of query strains and libraries that can be used (*Cohen and Schuldiner, 2011*). As an example, a query strain with a fluorescent marker can be crossed with a mutant library or with a fluorescent library. Alternatively, a mutant query strain can be crossed with a fluorescent library. In order to introduce a genetic marker into an entire yeast library of choice it is necessary to design a suitable query strain. There are different issues to be consider when creating your query strain, like having a suitable genetic background of the strain, the fluorophore of choice, the selection marker, expression level of the marker and the function of the tagged protein. Another important aspect of the screen is the design of the marker, which in most cases is a fluorescent label. Using synthetic genetic Array (SGA) technology, it is possible to integrate

the marker of choice into only a single query strain, which is easily crossed into any yeast library by the use of pinning tools. This simple method allows rapid insertion of any marker into an entire library of choice (*tong et al., 2001*). SGA method works by allowing the mating of the query strain to mutant libraries, generating diploids, inducing meiosis to retrieve haploid cells, and finally selecting for only haploid strains that contain the original genetic determinants from both the query strain and the library of choice. Once the library is done and with the help of a robotic system, the screening library can be inoculated from agar to liquid plates to allow growth in a shaking incubator. Then, a liquid handling device facilitates high throughput manipulations of growth conditions as well as preparation of microscope plates for image acquisition. It is possible to automatically transfer the plates for screening from the liquid handler to the microscope stage using a swap arm. Finally, images of systematic arrays of yeast cells can be acquired using a fully automated fluorescence microscope, and image analysis software can be used for rapid data extraction (*Cohen and Schuldiner, 2011*). The high-throughput fluorescence microscopy and correspondent image analysis was done as described extensively in *Cohen and Schuldiner, 2011*, using strains that were generated as described in section 3.3.1.1 and section 3.3.2.1 of results.

3

Results

3 Results

The core objective of this project was to understand the role of Sec61 channel β -subunit (Sbh1 in yeast) phosphorylation in ER protein import. To achieve that, I tried to identify the kinase or kinases responsible for the phosphorylation of Sbh1 and characterized the effect on function of phosphorylation. In addition, I investigated the range of proteins whose ER import is affected by Sbh1 phosphorylation.

3.1 Characterization of *sbh1* mutants

3.1.1 Temperature sensitivity test for *Sbh1* mutant strains

Based on previous data generated by this lab, in which they saw that the only combination of Sbh1 phosphorylation sites mutations that had an effect on Sbh1 function was the two proline-flanked sites at S3 and T5 mutated into A, I performed a temperature sensitivity test. Sensitivity to either higher (37°C) or lower (20°C) temperature when compared to the standard growth temperature (30°C) is a common indicator used to characterize yeast strains with ER translocation defects, as transport into the ER is essential (Rothblatt *et al.*, 1989). Since the aim of the experiment was to test the effect on the ability of the *sbh1* phosphorylation site mutant to complement the growth defect of the $\Delta sbh1/\Delta sbh2$ deletion strain at 37°C (Finke *et al.*, 1996; Feng *et al.*, 2007), I transformed the $\Delta sbh1/\Delta sbh2$ strain with a pRS415 vector expressing different *sbh1* mutants: single or combined S3 and T5 either to A (to prevent phosphorylation) or to E (to mimic the phosphorylated site) and I tested for growth defect at 37°C. For this purpose, I prepared sequential dilution of $\Delta sbh1/\Delta sbh2$, *sbh1S3A*, *sbh1T5A*, *sbh1S3A/T5A*, *sbh1S3E*, *sbh1T5E* and *sbh1S3E/T5E* mutant strains and the corresponding wildtype strain and grew them in duplicates on solid media (YPD (for wildtype and $\Delta sbh1/\Delta sbh2$ mutant strain) or minimal media (-leu; for *sbh1S3A*, *sbh1T5A*, *sbh1S3A/T5A*, *sbh1S3E*, *sbh1T5E* and *sbh1S3E/T5E* mutant strains, which are integrated on a pRS415 plasmid)). Each set was grown in duplicates either at 30°C or at 37°C for 3 days. All mutants were able to promote growth of the $\Delta sbh1/\Delta sbh2$ strain at the restrictive temperature, with the exception of the combination S3A/T5A, which resulted in reduced growth at 37°C (Figure 3.1). Neither single

mutants of these sites to A, nor the correspondent phospho-mimetic mutants, showed any growth defect at 37°C (Figure 3.1). These results suggest the phosphorylation of S3 and T5 is important for Sbh1 function and that the two sites operate together or phosphorylation of these sites is (partially) redundant.

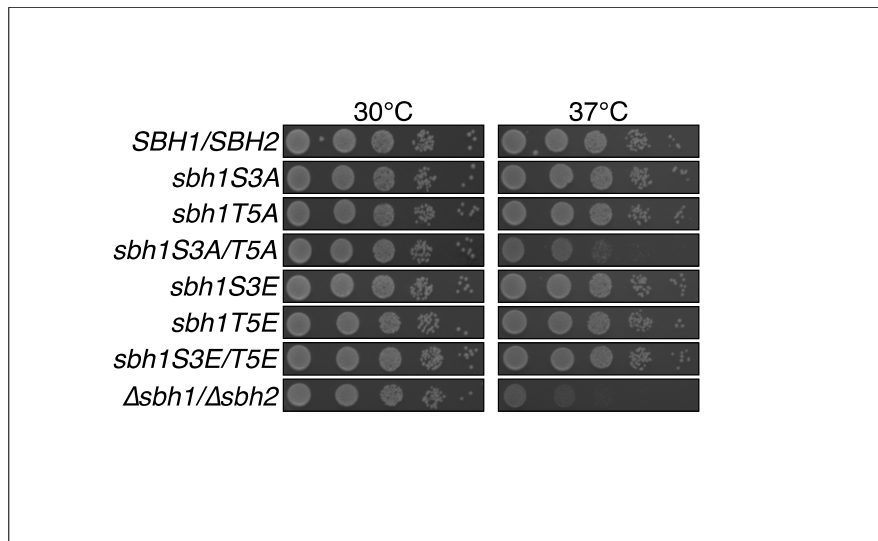


Figure 3.1: Temperature sensitivity of *sbh1* phosphorylation site mutant strains. Cells were grown overnight in YPD (for *SBH1* and $\Delta sbh1/\Delta sbh2$) or minimal medium (for *sbh1S3A*, *sbh1T5A*, *sbh1S3A/T5A*, *sbh1S3E*, *sbh1T5E*, *sbh1S3E/T5E*; all of them expressed form a pRS415 plasmid) at 30°C, 220 rpm. Then, cells were counted using a Neubauer chamber and sequentially diluted (10^4 - 10^7 cells/ 5μ l). Samples of each dilution (5μ l) were then plated side by side, on solid media (YPD or minimal media) and grown for 3 days. Each set was replicated 2 times in different plates and were incubated at 30°C or at 37°C (one replica per temperature).

3.1.2 Translocation of different substrates in $\Delta sbh1/\Delta sbh2$ mutant strain

3.1.2.1 Pre-pro- α -factor translocation in $\Delta sbh1/\Delta sbh2$ mutant strain

Previous data on the translocation defect in the $\Delta sbh1/\Delta sbh2$ strain were somewhat contradictory (Finke et al., 1996; Feng et al., 2007), so the next step was to test whether the deletion of both *SBH1* and *SBH2* resulted in a general protein translocation defect. For this purpose, I investigated the cytosolic precursor accumulation of ER translocation substrates. I first evaluated the translocation of a well characterized post-translationally translocated substrate pre-pro- α -factor (pp α F) by Western blotting with p α F-specific antibodies in the $\Delta sbh1/\Delta sbh2$ strain (Table 2.4). wildtype pp α F (18 KDa) is imported post-translationally into the ER where the signal sequence is cleaved off by a signal peptidase (Walters et al., 1988). The resulting pro- α -factor (p α F; 16 KDa) is N-glycosylated at three different sites upon entry into the ER and the glycosylated form is rapidly transported into the Golgi, where it is

proteolytically cleaved to release the 13 amino acid α -factor (α F). Hence the precursor form is only detectable in cells with ER import or ER-to-Golgi transport defects (Stirling *et al.*, 1992). For this experiment, I grew wildtype, $\Delta sbh1/\Delta sbh2$, and *sec61-32* mutant strains in YPD to an OD₆₀₀ of 0.25 at 30°C, 220 rpm, I then incubated them either at 20°C or 37°C, until cultures reached an OD₆₀₀ of 1. After incubation, I collected samples from each culture, made extracts, and resolved them by SDS-PAGE (Section 2.2.8). I then immunoblotted with pp α F-specific antibodies (Table 2.7). I used Rpn12 as a loading control. As can be seen in Figure 3.2, there was cytosolic accumulation of the precursor in the *sec61-32* mutant, that has a translocation defect at 20°C, but there was no accumulation of the cytosolic pp α F in the $\Delta sbh1/\Delta sbh2$ strain or in its correspondent wildtype (Figure 3.2).

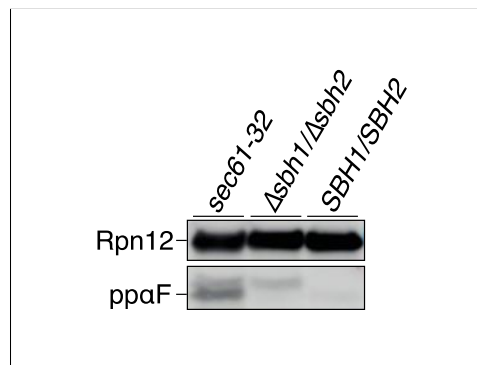


Figure 3.2: Analysis of pp α F ER import in $\Delta sbh1/\Delta sbh2$ strain. Cells were grown in YPD to an OD₆₀₀ of 0.25 at 30°C, 220 rpm, then incubated either at 20°C or 37°C, until cultures reached an OD₆₀₀ of 1. After incubation, 1 OD₆₀₀ of cells were collected from each culture, washed with sterile deionized water and extracts were prepared. For each sample, 0.4 OD₆₀₀ was resolved by SDS-PAGE, and protein detected by immunoblotting using a pp α F-specific antibodies and Rpn12-specific antibodies (loading control). Signal was acquired by chemiluminescence using an Amersham Imager 600.

3.1.2.2 Diaminopeptidase B translocation in $\Delta sbh1/\Delta sbh2$ mutant strain

Then, I looked at a co-translationally translocated substrate Diaminopeptidase B (DPAPB), which is a type II membrane protein with an N-terminal transmembrane domain (Pilon *et al.*, 1998). Upon co-translational integration into the ER membrane, the precursor protein (pDPAPB; 96 KDa) is core-glycosylated to form the mature protein (DPAPB; 120 KDa) (Roberts *et al.*, 1989). If DPAPB is efficiently integrated, its precursor form is undetectable, making it a typical substrate to test co-translational translocation impairments. To evaluate the translocation dynamics of DPAPB, I pulse-labelled the cells as follow: I grew wildtype, $\Delta sbh1/\Delta sbh2$, and *sec61-32* mutant strains in YPD at either 37°C or 20°C, 220 rpm, to an OD₆₀₀ of 0.5–1, I then labelled them with [³⁵S]-met/cys for 15 min, and I

immunoprecipitated DPAPB with specific antibodies (Table 2.7). After precipitation, I ran the samples on 7.5 % Bis-Tris SDS gel and I analysed specific signals by autoradiography (Section 2.2.12). Again, in the *sec61-32* mutant there was accumulation of the cytosolic DPAPB precursor at 20°C, but there was no accumulation of precursor in the $\Delta sbh1/\Delta sbh2$ strain or in its correspondent wildtype (Figure 3.3).

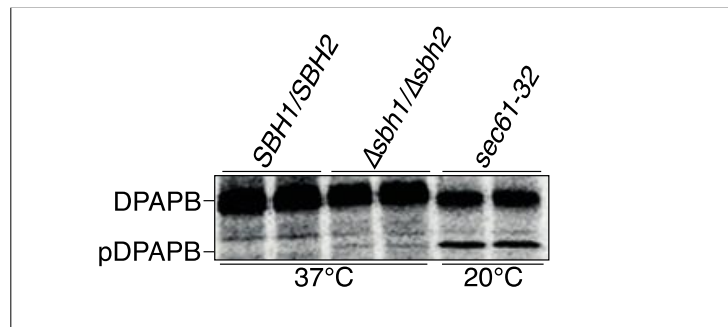


Figure 3.3: Analysis of the DPAPB ER translocation in $\Delta sbh1/\Delta sbh2$ strain. Cells were grown in YPD at either 37°C or 20°C, 220 rpm, to an OD₆₀₀ of 0.5–1, then labelled with [³⁵S]-met/cys for 15 min. 1.5 OD₆₀₀ of cells were lysed and proteins immunoprecipitated with specific antibodies against DPAPB. After SDS-PAGE, proteins were detected by exposing the gels to phosphorimager plates and signal acquired in Typhoon Trio™ Variable Mode Imager. All experiments were done in duplicates.

These results demonstrate that there is no general translocation defect either co-translationally or post-translationally in the absence of Sbh1 and Sbh2.

3.1.2.3 Gls1 translocation in $\Delta sbh1/\Delta sbh2$ mutant strain

There have been previous reports that indicate a specific translocation defect for glucosidase 1 (Gls1) and mannosidase 1 (Mns1) (*Feng et al., 2007*) and a moderate defect for the luminal chaperon Kar2 (BiP in mammals) translocation (*Finke et al., 1996*) in the $\Delta sbh1/\Delta sbh2$ strain, suggesting a precursor-specific effect. Gls1 is a soluble N-glycoprotein with a cleavable SP, involved in assembly of cell wall beta 1,6 glucan and asparagine-linked protein glycosylation; also involved in ER protein quality control and sensing of ER stress (*Hitt et al., 2004*). To test whether there is a specific Gls1 import defect in the $\Delta sbh1/\Delta sbh2$ strain, I looked at the steady state amount of Gls1 in wildtype vs. $\Delta sbh1/\Delta sbh2$ strain by Western blotting. For this experiment, I grew cells of each strain in YPD to an OD₆₀₀ of 0.25 at 30°C, 220 rpm. I then incubated them 37°C, until cultures reached an OD₆₀₀ of 1. After incubation, I collected samples from each culture, I made extracts, and resolved them by SDS-PAGE (Section 2.2.8). I detected Gls1 by immunoblotting using Gls1-specific antibodies

(Table 2.7). I used Rpn12 as a loading control. I could not distinguish the cytosolic precursor and the ER form of Gls1 on SDS gels, but $\Delta sbh1/\Delta sbh2$ cells had a reduced amount of Gls1 in the ER at steady state (Figure 3.4) compared to the correspondent wildtype, confirming the original observation (Feng *et al.*, 2007).

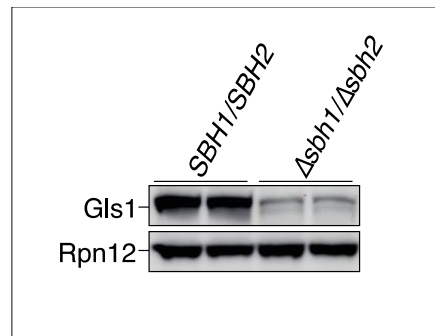


Figure 3.4: Analysis of the Gls1 ER translocation in $\Delta sbh1/\Delta sbh2$ strain. Cells were grown in YPD to an OD₆₀₀ of 0.25 at 30°C, 220 rpm. Then incubated at 37°C, until cultures reached an OD₆₀₀ of 1. After incubation, 1 OD₆₀₀ of cells were collected from each culture, washed with sterile deionized water and extracts were prepared. For each sample, 0.4 OD₆₀₀ was resolved by SDS-PAGE, and protein detected by immunoblotting using a Gls1-specific antibodies and Rpn12-specific antibodies (loading control). Signal was acquired by chemiluminescence using an Amersham Imager 600. All experiments were done in duplicates.

3.1.2.4 Kar2 translocation in $\Delta sbh1/\Delta sbh2$ mutant strain

Kar2 is an ATPase involved in protein import into the ER; it also acts as a chaperone to mediate protein folding in the ER, and may play a role in ER export of soluble proteins; it also regulates the unfolded protein response via interaction with Ire1 (Gillece *et al.*, 1999; Wang *et al.*, 2016). Upon translocation across the ER membrane, the precursor protein (pKar2; 74 KDa) is signal-cleaved to form the mature protein (Kar2; 72 KDa). I looked at pKar2 translocation by pulse-labelling. In this experiment, I grew wildtype, $\Delta sbh1/\Delta sbh2$, and *sec61-32* mutant strains in YPD at either 37°C or 20°C, 220 rpm, to an OD₆₀₀ of 0.5–1. I then labelled them with [³⁵S]-met/cys for 2.5 min, and I precipitated Kar2 with specific antibodies (Table 2.7). I ran the samples on 7.5 % Bis-Tris SDS gel and I analysed the specific signals by autoradiography (Section 2.2.12). I saw a strong translocation defect in the $\Delta sbh1/\Delta sbh2$ strain as well as in the control, the *sec61-32* mutant (Figure 3.5). These results show that Gls1 and Kar2 import into the ER are dependent on Sbh1 and Sbh2 and in contrast with the previous results (Feng *et al.*, 2007; Finke *et al.*, 1996), the defect I observed was more pronounced.

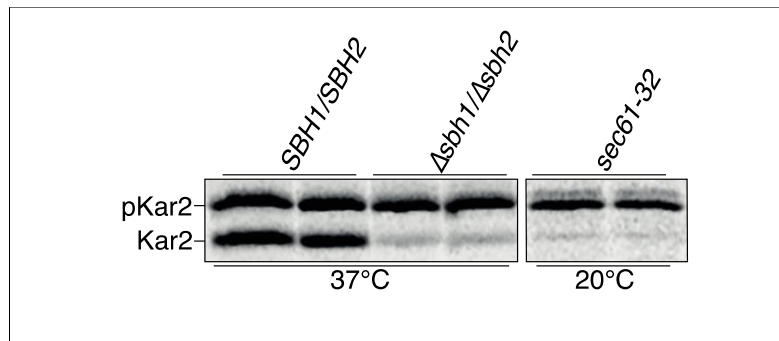


Figure 3.5: Analysis of the Kar2 ER translocation in $\Delta sbh1/\Delta sbh2$ strain. Cells were grown YPD at either 37°C or 20°C, 220 rpm, to an OD_{600} of 0.5–1, then labelled with [35 S]-met/cys for 2.5 min. 1.5 OD_{600} of cells were lysed and proteins immunoprecipitated with specific antibodies against Kar2. After SDS-PAGE, proteins were detected by exposing the gels to phosphorimager plates and signal acquired in Typhoon Trio™ Variable Mode Imager. All experiments were done in duplicates.

3.1.2.5 α -amylase translocation in $\Delta sbh1/\Delta sbh2$ mutant strain

3.1.2.5.1 α -amylase gene integration

In addition, bacterial α -amylase was previously used as a reporter secretory protein to characterize Sbh1 function in yeast (Toikkanen *et al.*, 1996; Feng *et al.*, 2007). Results published in Feng *et al.*, 2007 suggests that translocation of α -amylase is defective *in vivo* in $\Delta sbh1/\Delta sbh2$ cells at restrictive temperature (37°C). To test that, I first integrated Ylp α -L plasmid (Figure 3.6), encoding *Bacillus amyloliquefaciens* α -amylase gene with ADH1 promoter and terminator, in the *leu2* locus of wildtype (KRY585) and $\Delta sbh1/\Delta sbh2$ mutant (KRY588) strains, to generate KRY1128 and KRY1129, respectively (Table 2.4). For doing the integration, I first extracted Ylp α -L plasmid from KRB1136 (Table 2.5), then I transformed KRY585 and KRY588 with the Ylp α -L plasmid, and plated the transformed yeast cells in minimal media (-Leu, since Ylp α -L marker is LEU2). Since this plasmid has no replication origin, only cells that have integrated the plasmid into the *leu2* locus can grow in -Leu media.

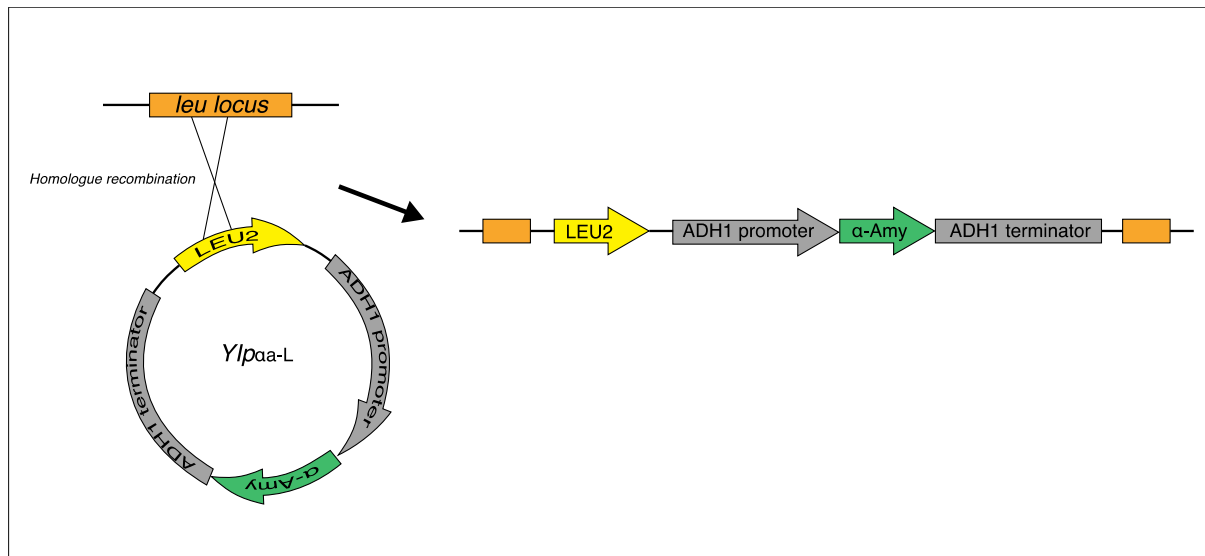


Figure 3.6: Bacillus amyloliquefaciens α -amylase integration Scheme: Schematic representation of the bacterial α -amylase integration process into KRY585 and KRY588 strains. Ylp α -L plasmid was used to integrate the α -amylase expression cassette (green) with ADH1 promoter and terminator (grey) in the *leu2* locus (orange) of KRY585 and KRY588 strains by integration of the *LEU2* gene (yellow). Integration of the cassette into the genome of KRY585 and KRY588 strains by homologue recombination was possible due to the overlapping sequences provided by the *leu2* locus (orange).

3.1.2.5.2 α -amylase translocation

After the integration, I looked at translocation of α -amylase by Western blotting with α -amylase-specific antibodies in wildtype and $\Delta sbh1/\Delta sbh2$ strains expressing the bacterial α -amylase. Upon translocation into the ER, the precursor protein (p α -amylase) gets glycosylated to form the mature protein (α -amylase), and that generates a visible change in migration (Feng *et al.*, 2007). For this experiment, I grew cells of each strain to an OD₆₀₀ of 0.25 at 30°C, 220 rpm and I then switched cultures to 37°C, 220 rpm, until cultures reached an OD₆₀₀ of 1. Then, I collected samples from each culture, I made extracts, and I resolved them by SDS-PAGE (Section 2.2.8). I detected α -amylase by immunoblotting using specific antibodies (Table 2.7). I used Rpn12 as a loading control. I saw cytosolic precursor accumulation of α -amylase in $\Delta sbh1/\Delta sbh2$ cells at 37°C (Figure 3.7), confirming that translocation of α -amylase is defective in $\Delta sbh1/\Delta sbh2$ cells at restrictive temperature.

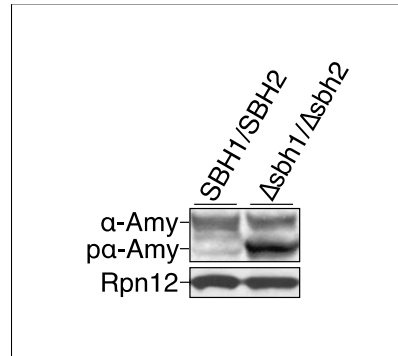


Figure 3.7: Analysis of the bacterial α -amylase ER translocation in $\Delta sbh1/\Delta sbh2$ strain. Cells were grown to an OD_{600} of 0.25 at 30°C, 220 rpm and then switched to 37°C, 220 rpm, until cultures reached an OD_{600} of 1. After incubation, 1 OD_{600} of cells were collected from each culture, washed with sterile deionized water and extracts were prepared. For each sample 0.4 OD_{600} was resolved by SDS-PAGE, and protein detected by immunoblotting using α -amylase-specific antibodies and Rpn12-specific antibodies (loading control). Signal was acquired by chemiluminescence using an Amersham Imager 600.

3.1.3 Translocation of different substrates in *sbh1S3A/T5A* mutant strain

3.1.3.1 Kar2 translocation in *sbh1* phosphorylation site mutant strains

3.1.3.1.1 Kar2 translocation in *sbh1S3A/T5A* mutant strain by pulse-labelling

To assess contribution of Sbh1 S3/T5 phosphorylation on ER translocation of the two Sbh1-dependent substrates, Gls1 and Kar2, I next investigated whether the *sbh1S3A/T5A* mutant was competent for translocation of pGls1 and pKar2. For testing pKar2 translocation, I grew wildtype, $\Delta sbh1/\Delta sbh2$, *sbh1S3A/T5A* and *sec61-32* mutant strains in YPD (for wildtype, $\Delta sbh1/\Delta sbh2$ and *sec61-32* mutant strains) or minimal media (-leu; for *sbh1S3A/T5A* mutant strain, which is integrated on a pRS415 plasmid) at either 37°C or 20°C, 220 rpm to an OD_{600} of 0.5–1. Then I labelled them with [³⁵S]-met/cys for 2.5 min, followed by an immunoprecipitation with Kar2-specific antibodies (Table 2.7). After precipitation, I ran the samples on 7.5 % Bis-Tris SDS gel and I analysed the specific signals by autoradiography (Section 2.2.12). I saw that in the *sbh1S3A/T5A* mutant there was as much pKar2 translocation as the wildtype, in contrast to the $\Delta sbh1/\Delta sbh2$ and *sec61-32* strains, where I saw cytosolic pKar2 accumulation (Figure 3.8). My data indicate that Kar2 is Sbh1-dependent, but not dependent on the S3/T5-phosphorylation of Sbh1.

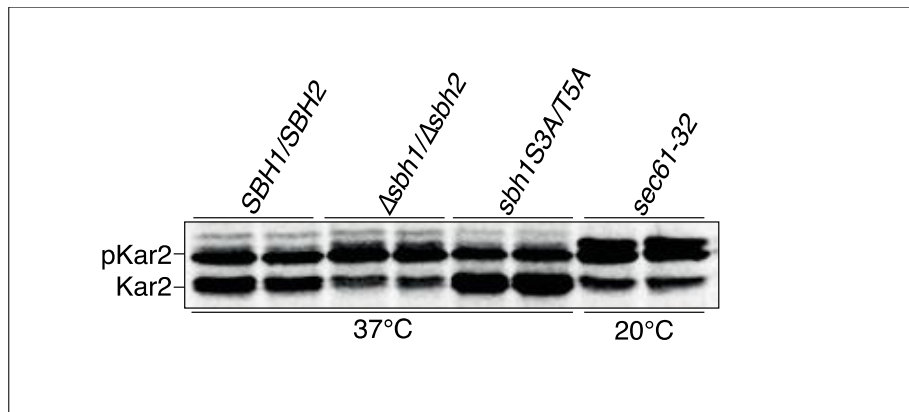


Figure 3.8: Analysis of the Kar2 ER translocation in *sbh1S3A/T5A* strain. Cells were grown in YPD (for wildtype, *Δsbh1/Δsbh2* and *sec61-32* mutant strains) or minimal media (-leu; for *sbh1S3A/T5A* mutant strain, which is integrated on a pRS415 plasmid) at either 37°C or 20°C, 220 rpm, to an OD₆₀₀ of 0.5–1, then labelled with [³⁵S]-met/cys for 2.5 min. 1.5 OD₆₀₀ of cells were lysed and proteins immunoprecipitated with specific antibodies against Kar2. After SDS-PAGE, proteins were detected by exposing the gels to phosphorimager plates and signal acquired in Typhoon Trio™ Variable Mode Imager. All experiments were done in duplicates.

3.1.3.1.2 Kar2 translocation in *sbh1S3A/T5A* mutant strain by Western blotting

I then verified this result by Western blotting using Kar2-specific antibodies in wildtype, *Δsbh1/Δsbh2* and *sbh1S3A/T5A* strains. For this experiment, I grew cells of each strain in YPD (for wildtype and *Δsbh1/Δsbh2* mutant strains) or minimal media (-leu; for *sbh1S3A/T5A* mutant strain, which is integrated on a pRS415 plasmid) to an OD₆₀₀ of 0.25 at 30°C, 220 rpm. I switched the cultures to 37°C, 220 rpm, until culture reached an OD₆₀₀ of 1. Then, I collected samples from each culture, made extracts, and resolved them by SDS-PAGE (Section 2.2.8). I detected Kar2 by immunoblotting with specific antibodies (Table 2.7). I used Rpn12 as a loading control. Again, I was able to see accumulation of Kar2 precursor on the *Δsbh1/Δsbh2* strain, but not in the *sbh1S3A/T5A* strain (Figure 3.9), confirming that pKar2 import into the ER is Sbh1-dependent, but independent of its phosphorylation at S3/T5.

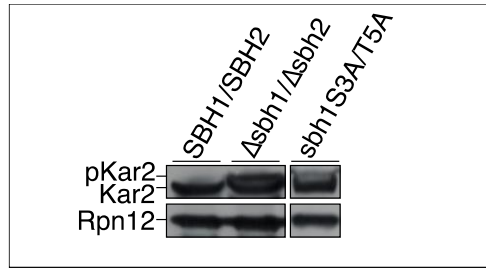


Figure 3.9: Analysis of Kar2 at steady state in $\Delta sbh1/\Delta sbh2$ and $sbh1S3A/T5A$ strains. Cells were grown either in YPD (for wildtype and $\Delta sbh1/\Delta sbh2$ mutant strains) or minimal media (-leu; for $sbh1S3A/T5A$ mutant strain, which is integrated on a pRS415 plasmid) to an OD_{600} of 0.25 at 30°C, 220 rpm and then switched to 37°C, 220 rpm, until cultures reached an OD_{600} of 1. After incubation, 1 OD_{600} of cells were collected from each culture, washed with sterile deionized water and extracts were prepared. For each sample 0.4 OD_{600} was resolved by SDS-PAGE, and protein detected by immunoblotting using a Kar2-specific antibodies and Rpn12-specific antibodies (loading control). Signal was acquired by chemiluminescence using an Amersham Imager 600.

3.1.3.2 Gls1 translocation in $sbh1S3A/T5A$ mutant strain

To assess the effect of Sbh1 S3/T5-phosphorylation on pGls1 import into the ER I looked at the steady state amount of Gls1 by Western blotting with Gls1-specific antibodies in wildtype, $sbh1S3A/T5A$, and individual $sbh1S3A$ and $sbh1T5A$ mutant strains. For this experiment, I grew cells of each strain in YPD (for wildtype strain) or minimal media (-leu; for $sbh1S3A/T5A$, $sbh1S3A$ and $sbh1T5A$ mutant strains, which are integrated on a pRS415 plasmid) to an OD_{600} of 0.25 at 30°C, 220 rpm. I then incubated them 37°C, until cultures reached an OD_{600} of 1. After incubation, I collected samples from each culture, I made extracts, and resolved them by SDS-PAGE (Section 2.2.8). I detected Gls1 by immunoblotting using specific antibodies (Table 2.7). I used Rpn12 as a loading control. I found that the amount of Gls1 in the ER of $sbh1S3A/T5A$ cells was substantially reduced compared to the wildtype or the single mutants (Figure 3.10), comparable to the reduction seen in $\Delta sbh1/\Delta sbh2$ strain (Figure 3.4). This indicates that transport of Gls1 into the ER is dependent not only on the presence of Sbh1, but also on its phosphorylation at S3 and T5.

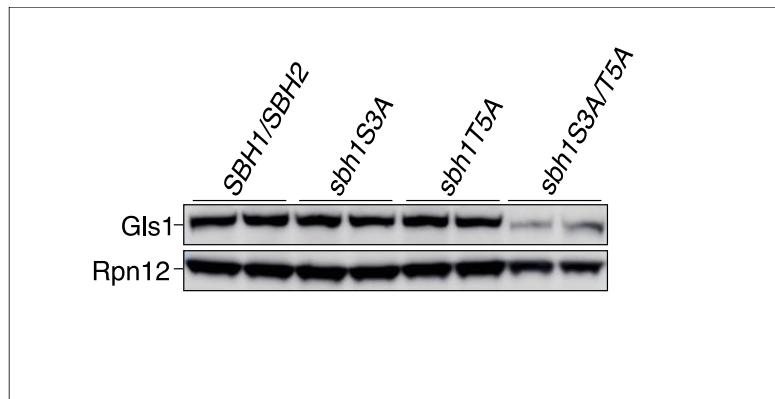


Figure 3.10: Analysis of the Gls1 ER translocation in *sbh1S3A/T5A*, *sbh1S3A* and *sbh1T5A* strains. Cells were grown in YPD (for wildtype strain) or minimal media (-leu; for *sbh1S3A/T5A*, *sbh1S3A* and *sbh1T5A* mutant strains, which are integrated on a pRS415 plasmid) to an OD₆₀₀ of 0.25 at 30°C, 220 rpm. Then incubated at 37°C, until cultures reached an OD₆₀₀ of 1. After incubation, 1 OD₆₀₀ of cells were collected from each culture, washed with sterile deionized water and extracts were prepared. For each sample 0.4 OD₆₀₀ was resolved by SDS-PAGE, and protein detected by immunoblotting using a Gls1-specific antibodies and Rpn12-specific antibodies (loading control). Signal was acquired by chemiluminescence using an Amersham Imager 600. All experiments were done in duplicates.

Taking together, my observations indicate that there are ER translocation substrates whose ER import is dependent on the presence of Sbh1, and there are ER translocation substrates whose ER import is dependent on S3/T5-phosphorylated Sbh1.

3.1.4 Tunicamycin sensitivity test in *Sbh1* mutant strains

As Kar2, Gls1, and the Sbh1-dependent mannosidase I (Mns1) contribute to protein quality control in the ER, I next determined whether *sbh1* mutants showed any tunicamycin (TM) sensitivity. Tunicamycin interferes with N-linked glycosylation in the ER which often is a prerequisite for protein folding. Hence tunicamycin-sensitivity is often indicative of perturbations in ER proteostasis (*Tran et al., 2011; Servas et al., 2013*). For this experiment I prepared sequential dilution of $\Delta sbh1/\Delta sbh2$, *sbh1S3A/T5A*, and $\Delta ire1$ mutant strains and the corresponding wildtype strains and grew them in duplicates on solid media. For $\Delta sbh1/\Delta sbh2$ and $\Delta ire1$ mutant strains as well as for SBH1/SBH2 and IRE1 wildtype strains I used YPD and YPD supplemented with TM (0.5 $\mu\text{g/ml}$). For *sbh1S3A/T5A* mutant strain, which has the *sbh1* mutant integrated on a pRS415 plasmid, I used minimal media (-leu) or minimal media (-leu) supplemented with TM (0.5 $\mu\text{g/ml}$). Plates grew at 30°C for 3 days. I used as a positive control the $\Delta ire1$ mutant, for which strong tunicamycin sensitivity has been widely reported (*Chawla et al., 2011; Servas et al., 2013*). IRE1, encoding Ire1, is the only signal transducer for the UPR in the yeast ER membrane (*Cox et al., 1993*). As expected, there was no growth of $\Delta ire1$ mutant in the presence of 0.5 $\mu\text{g/ml}$ of tunicamycin (Figure

3.11, bottom panel). My results show that none of the *sbh1* mutant strains were sensitive to TM (Figure 3.11).

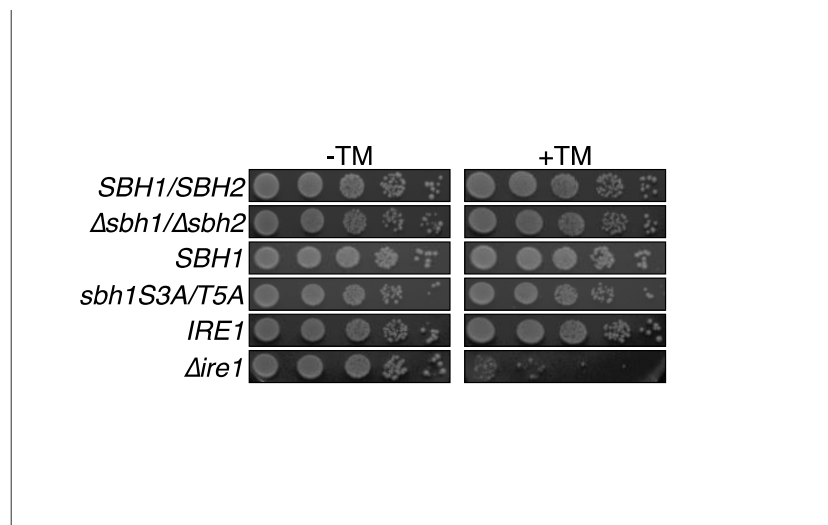


Figure 3.11: Tunicamycin sensitivity of *sbh1* mutant strains. Cells were grown overnight in YPD (for *Δsbh1/Δsbh2* and *Δire1* mutant strains as well as for *SBH1/SBH2* and *IRE1* wildtype) or minimal media (-leu; for *sbh1S3A/T5A* mutant strain, which is integrated on a pRS415 plasmid), at 30°C, 220 rpm. Then, cells were counted using a Neubauer chamber and sequentially diluted (10^4 -10 cells/5 μ l). Samples of each dilution (5 μ l) were then plated side by side, in solid media (YPD or minimal media) and grown for 3 days. Each set was replicated 2 times in different plates, one of the plates supplemented with tunicamycin (0.5 μ g/ml) and were incubated at 30°C.

3.1.5 UPR induction assay in *sbh1* mutant strains

I also tested these strains directly for induction of the UPR by doing a *HAC1* mRNA splicing assay. In yeast, misfolded-protein accumulation in the ER activates the UPR. For experimental induction of the UPR, a treatment with inhibitors of ER protein folding, like tunicamycin, can be done (Bernales et al., 2006). The UPR triggers an adaptive response to restore ER homeostasis through the action of *HAC1* (Travers et al., 2000; Schröder et al., 2008), a transcription-factor that is only produced after mRNA splicing by UPR-activated *Ire1* (Bernales et al., 2006; Sidrauski et al., 1997; Kawahara et al., 1997). For this assay, I grew cells in either YPD (for *SBH1/SBH2* wildtype strain or *Δsbh1/Δsbh2* mutant strain) or minimal media (-leu; for *sbh1S3A/T5A* mutant strain, which is integrated on a pRS415 plasmid) to an OD₆₀₀ of 1 at 30°C, 220 rpm and incubated them for 3 hours in either presence or absence of 2 μ g/ml of tunicamycin (30°C, 220 rpm). After isolation of the total RNA, I performed an RT-PCR for *HAC1* and *ACT1* mRNA, using *HAC1* specific primers and *ACT1* specific primers (Table 2.6). The amplification of *ACT1* was done as an internal control while the amplification of *HAC1* was used to detect the *Ire1*-spliced form of *HAC1* mRNA. I found that neither the

$\Delta sbh1/\Delta sbh2$ strain, nor the $sbh1S3A/T5A$ mutant, in the absence of TM, contained spliced HAC1 mRNA (Figure 3.12), indicating that there is no induction of the UPR nor a proteostasis defect in the $sbh1$ mutants.

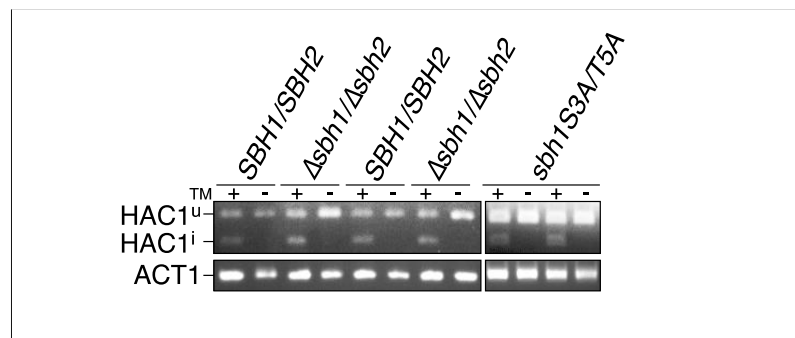


Figure 3.12: UPR activation in $sbh1$ mutants: wildtype and mutant strains were grown in YPD (for $\Delta sbh1/\Delta sbh2$ mutant strain as well as for SBH1/SBH2 wildtype strain) or minimal media (-leu; for $sbh1S3A/T5A$ mutant strain, which is integrated on a pRS415 plasmid) to an OD₆₀₀ of 1 at 30°C, 220 rpm and incubated for 3 hours in either presence (+) or absence (-) of 2 µg/ml of tunicamycin (30°C, 220 rpm). Total RNA (0.1 µg) was retrotranscribed to cDNA by RT-PCR using MaximaRT and Oligo(dT18)-dT primer. The resulting cDNA (1 µg) was subjected to PCR with a set of primers targeting ACT1 as an internal control and HAC1 to monitor the UPR induction state of the cell. PCR fragments derived from HAC1^u mRNA (HAC1^u = unspliced; 720 bp) and HAC1ⁱ mRNA (HAC1ⁱ = spliced; 470bp) are indicated. Samples were resolved on a 1% agarose gel.

3.2 Sbh1 antibodies

At the beginning of my project about Sbh1 phosphorylation and regulation of ER protein import, the lab had two different antibodies that could recognize Sbh1: Sbh1₍₁₋₁₈₎, raised against the first 18 residues of Sbh1 (Figure 3.13, blue) and Sbh1₍₁₀₋₂₃₎, raised against the residues 10 to 23 of Sbh1, so does not interact with the phosphorylation sites S3 and T5 of the protein (Figure 3.13, orange).

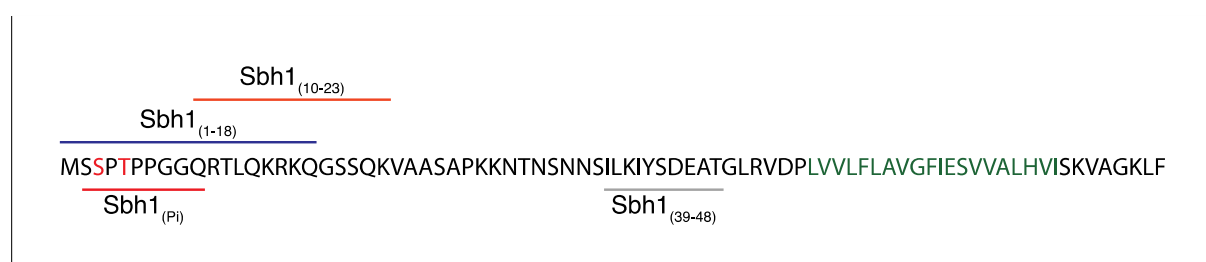


Figure 3.13: Sbh1 antibodies recognition scheme. Schematic representation of a Sbh1, with phosphorylation sites S3 and T5 (red) and hydrophobic transmembrane region (green). The schematic representation of different antibodies is also shown: Sbh1₍₁₋₁₈₎ (blue), raised against the first 18 residues of Sbh1; Sbh1₍₁₀₋₂₃₎ (orange), raised against the residues 10 to 23 of Sbh1; Sbh1₍₃₉₋₄₈₎ (grey), raised against the residues 39 to 48 of Sbh1; Sbh1_(Pi) (red), raised against a peptide made of residues 2 to 10 of Sbh1, which was N-acetylated and phosphorylated in the serine in position 3.

I first investigated whether these two antibodies (Sbh1₍₁₋₁₈₎ and Sbh1₍₁₀₋₂₃₎) recognize phosphorylated and unphosphorylated Sbh1 in the same manner. For this experiment, I

made microsomes from wildtype and $\Delta sbh1/\Delta sbh2$ mutant strains. I made these microsomes with a modification from the original protocol (Section 2.2.11): The homogenization of the spheroplasts and all the following steps were done preventing dephosphorylation of proteins, by adding phosphatase inhibitors to the mix in every step. Afterwards, I treated same amounts of microsomes of each strain with alkaline phosphatase (AP) to dephosphorylates microsomal proteins, including Sbh1. I resolved same amounts of this dephosphorylated microsomes (+) of each strain and same amounts of untreated microsomes (-) of each strain by SDS-PAGE (Section 2.2.8). I detected Sbh1 by immunoblotting using these two different specific antibodies: Sbh1₍₁₋₁₈₎, raised against first 18 residues of Sbh1; and Sbh1₍₁₀₋₂₃₎, raised against residues 10 to 23 of Sbh1. I found that both antibodies recognize mainly the N-terminally unphosphorylated form of Sbh1 (Figure 3.14).

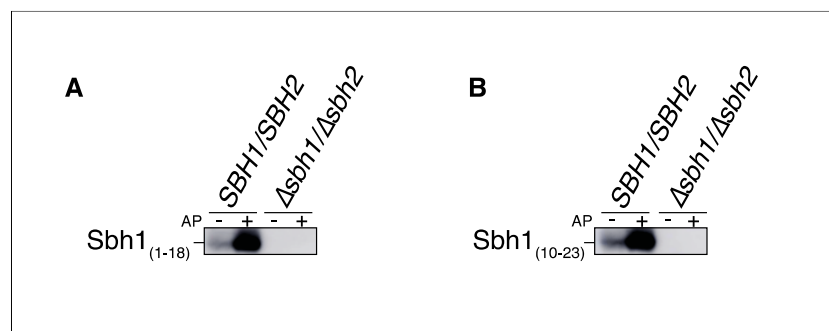


Figure 3.14: Sbh1₍₁₋₁₈₎ and Sbh1₍₁₀₋₂₃₎ antibodies recognition test. Microsomes from wildtype and $\Delta sbh1/\Delta sbh2$ mutant strains were prepared, with the microsome preparation protocol modified to prevent dephosphorylation of microsomal proteins. Phosphatase inhibitor was added to every step from the spheroplasts homogenization to the end of the protocol. Equal amounts (50 $\mu\text{g}/6 \mu\text{l}$) of microsomes ($\text{Abs}_{280}=30$) from each strain were treated with 10 U of alkaline phosphatase (AP), by adding 10 μl of AP and 2 μl of 10X buffer, and incubating the mix for 1 hour at 37°C. After incubation on ice, samples were centrifuged for 1 minute at 16.000 x g and resuspended in 50 μl of 2 x Sample buffer. In parallel, equal amounts (50 $\mu\text{g}/6 \mu\text{l}$) of microsomes ($\text{Abs}_{280}=30$) from each strain were resuspended in 50 μl of 2 x Sample buffer. Equal amounts (25 μl) of treated (+) and untreated (-) microsomes of each strain were then resolved by SDS-PAGE. Sbh1 was detected by immunoblotting using either the antibody against amino acids 1-18 of Sbh1 (Sbh1₍₁₋₁₈₎) or the antibody against amino acids 10-23 of Sbh1 (Sbh1₍₁₀₋₂₃₎). Signal was acquired by chemiluminescence using an Amersham Imager 600.

Later on, we raised an antibody against the phosphorylated N-terminus of Sbh1 (Sbh1_(Pi), Figure 3.13, red). This antibody was raised against a peptide made of residues 2 to 10 of Sbh1. In addition, the peptide was N-acetylated and the serine in the position 3 was phosphorylated. I then investigated how these two antibodies (Sbh1_(Pi) and Sbh1₍₁₀₋₂₃₎) recognize Sbh1 when S3/T5 sites are phosphorylated or unphosphorylated. For this experiment, I made microsomes from wildtype, $\Delta sbh1/\Delta sbh2$ and *sbh1S3A/T5A* mutant strains. I made these microsomes with a modification from the original protocol (Section

2.2.11): The homogenization of the spheroplasts and all the following steps were done preventing dephosphorylation of proteins, by adding phosphatase inhibitors to the mix in every step. Then, I resolved same amounts of microsomes of each strain by SDS-PAGE (Section 2.2.8). I detected Sbh1 by immunoblotting using these two different specific antibodies: Sbh1_(Pi), raised against the phosphorylated N-terminus of Sbh1; and Sbh1₍₁₀₋₂₃₎, raised against residues 10 to 23 of Sbh1. I found that Sbh1_(Pi) antibody recognizes mainly N-terminally phosphorylated Sbh1 (Figure 3.15A), while the Sbh1₍₁₀₋₂₃₎ antibody, recognizes primarily N-terminally unphosphorylated Sbh1 (figure 3.15B).

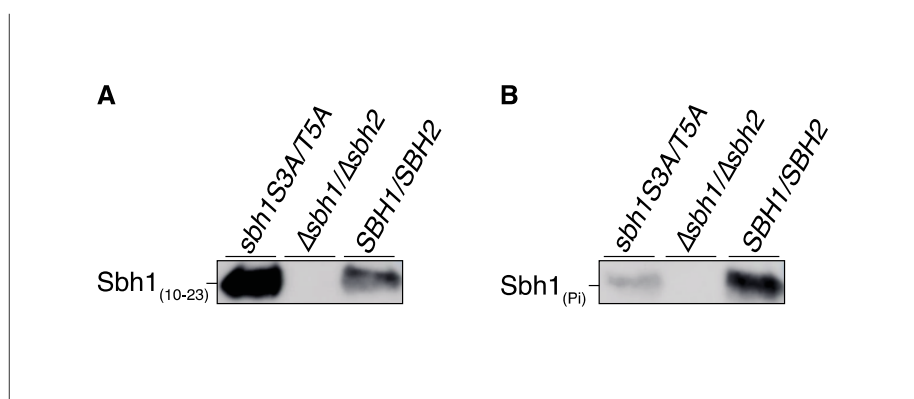


Figure 3.15: Sbh1₍₁₀₋₂₃₎ and Sbh1_(Pi) antibodies recognition test. Microsomes from wildtype, $\Delta sbh1/\Delta sbh2$ and *sbh1S3A/T5A* mutant strains were prepared, with the microsome preparation protocol modified to prevent dephosphorylation of microsomal proteins. Phosphatase inhibitor was added to every step from the spheroplasts homogenization to the end of the protocol. Equal amounts (50 μ g/6 μ l) of microsomes (Abs₂₈₀=30) from each strain were resuspended in 50 μ l of 2 x Sample buffer and resolved by SDS-PAGE. Sbh1 was detected by immunoblotting using either (A) the antibody against amino acids 10-23 of Sbh1 (Sbh1₍₁₀₋₂₃₎) or (B) the antibody against N-terminally phosphorylated Sbh1. Signal was acquired by chemiluminescence using an Amersham Imager 600.

Recently, the lab raised another antibody against Sbh1, Sbh1₍₃₉₋₄₈₎ (Figure 3.13, grey). This antibody was raised against the residues 39 to 48 of Sbh1, away from the N-terminal phosphorylation sites, and close to the transmembrane domain. With this antibody we are able to see the total amounts of Sbh1 in a more precisely way (Discussion, Section 4.2).

3.3 Automated microscopic screen

Using automated cell manipulations and microscopy platforms, it is possible to easily screen entire genomes for genes that affect any cellular process that can be visualized (Figure 3.16, *Schuldiner and Cohen, 2011*). The first step of the process consists in defining the biological question to be addressed. For answering this question, the next step is to design the microscopic screen. There are different possible combinations of query strains

and libraries that can be used (*Schuldiner and Cohen, 2011*). As an example, a query strain with a fluorescent marker can be crossed with a mutant library or with a fluorescent library. Alternatively, a mutant query strain can be crossed with a fluorescent library. In order to introduce a genetic marker into an entire yeast library of choice it is necessary to design a suitable query strain. There are different issues to be considered when creating your query strain, like having a suitable genetic background of the strain, the fluorophore of choice, the selection marker, expression level of the marker and the function of the tagged protein. Another important aspect of the screen is the design of the marker, which in most cases is a fluorescent label. Using Synthetic Genetic Array (SGA) technology, it is possible to integrate the marker of choice into only a single query strain, which is easily crossed into any yeast library by the use of pinning tools. This simple method allows rapid insertion of any marker into an entire library of choice (*Tong et al., 2001*). SGA method works by allowing the mating of the query strain to mutant libraries, generating diploids, inducing meiosis to retrieve haploid cells, and finally selecting for only haploid strains that contain the original genetic determinants from both the query strain and the library of choice. Once the library is done and with the help of a robotic system, the screening library can be inoculated from agar to liquid plates to allow growth in a shaking incubator. Then, a liquid handling device facilitates high throughput manipulations of growth conditions as well as preparation of microscope plates for image acquisition. It is possible to automatically transfer the plates for screening from the liquid handler to the microscope stage using a swap arm. Finally, images of systematic arrays of yeast cells can be acquired using a fully automated fluorescence microscope, and image analysis software can be used for rapid data extraction (*Schuldiner and Cohen, 2011*).

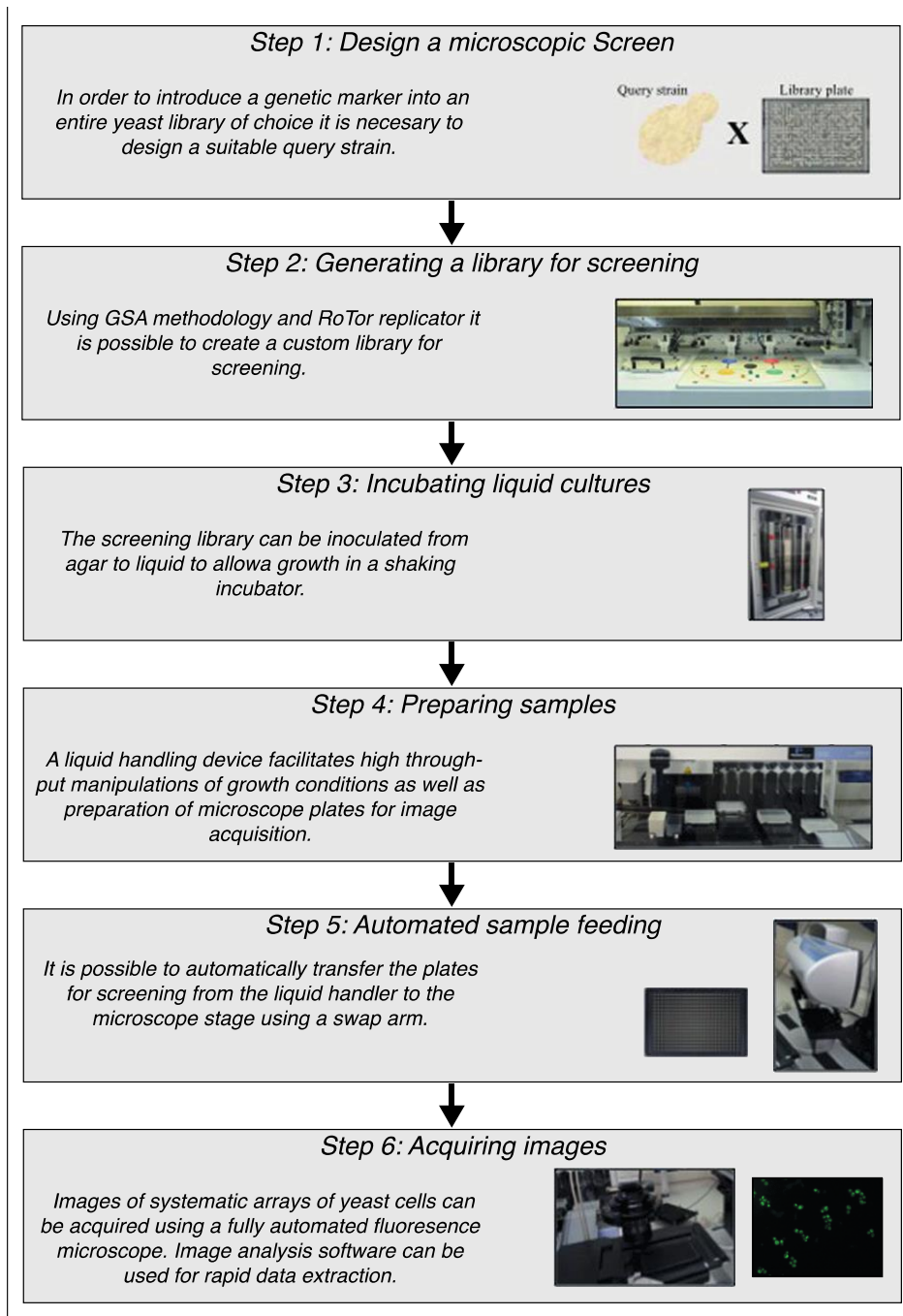


Figure 3.16: Automated microscopic screen in yeast Scheme: Modified from *Schuldiner and Cohen, 2011*. Schematic representation of the steps required to set up and perform a whole genome microscopic screen in yeast.

3.3.1 Identification of Sbh1-dependent, Sbh1 phosphorylation-dependent and Ess1-dependent ER translocation substrates

To identify in a systematic manner, proteins for which translocation depends on the presence of Sbh1, the S3/T5-phosphorylation of Sbh1, or the presence of active Ess1, I performed an automated microscopic screen (Figure 3.16, *Schuldiner and Cohen, 2011*, *Breker et al., 2013*). For this first part of my screens, the biological question to be addressed

was which substrates are Sbh1, Pi-Sbh1 or Ess1 dependent. For answering that question, the first step was to make the three query strains to be crossed with the fluorescent library: *Δsbh1/Δsbh2*, *sbh1S3A/T5A* and *ess1H164R* mutant strains. I generated them using KRY1156 (Table 2.4) as wildtype (control).

3.3.1.1 Query strains construction

3.3.1.1.1 SBH1 and SBH2 deletion in KRY1156 wildtype strain to make KRY1160 strain

In order to delete *SBH1* (Figure 3.17A) and *SBH2* (Figure 3.17B) I first extracted the genomic DNA from the KRY588 strain. Afterwards, I amplified the *seb1::KanMx* cassette (cassette for generating *Δsbh1* by integration of the Kanamycin resistance). For this PCR reaction I used as template genomic DNA extracted from KRY588 and primers 59 and 60 (Table 2.6). I cleaned the PCR product and transformed the KRY1156 strain with it. I then plated the transformed KRY1156 in YPD plates supplemented with 100 µg/ml Kanamycin. I extracted the genomic DNA from the colonies that were able to grow in YPD plates supplemented with 100 µg/ml Kanamycin. I used this DNA to check the *SBH1* deletion. I made a PCR reaction and I resolved the amplicon in agarose gels, using as a positive control DNA extracted from KRY588 (*Δsbh1/Δsbh2*), and as a negative control DNA extracted from KRY585 (wildtype). Afterwards, for a double check, I sent for sequencing the genomic DNA extracted from the positive colonies (GATC Biotech). For both, the PCR and the sequencing, I used primers 59 and 60. The resulting strain from this deletion was called KRY1158. After deletion of *SBH1*, I proceeded by deleting *SBH2*. For doing this, first I amplified the *seb2::hphMx* cassette (cassette for generating *Δsbh2* by integration of the hygromycin resistance). For this PCR reaction I used as template genomic DNA extracted from KRY588 and primers Sbh2ExtFw and Sbh2ExtRv (Table 2.6). I cleaned the PCR product and transformed the KRY1158 strain with it. I then plated the transformed cells in YPD plates supplemented with 200 µg/ml Hygromycin. I extracted the genomic DNA from the colonies that were able to grow in YPD plates supplemented with 200 µg/ml Hygromycin. I used this DNA to check the *SBH2* deletion by PCR and resolving amplicon in agarose gels, using as a positive control DNA extracted from KRY588 (*Δsbh1/Δsbh2*) and as a negative control DNA extracted from KRY585 (wildtype). Afterwards, for a double check, I sent for sequencing the

genomic DNA extracted from the positive colonies (GATC Biotech). For both, the PCR and the sequencing, I used primers Sbh2ExtFw and Sbh2ExtRv.

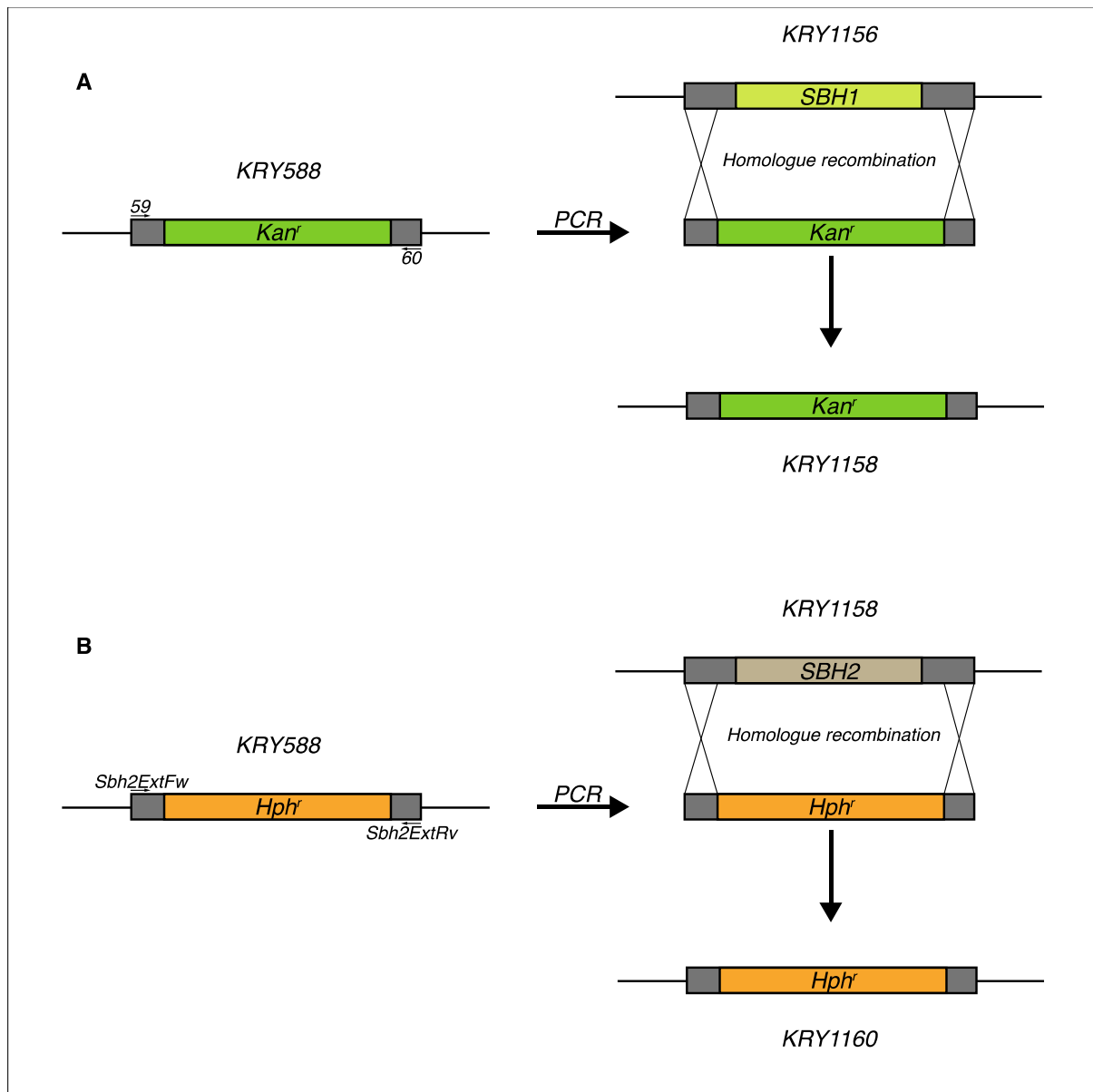


Figure 3.17: SBH2 and SBH1 deletion Scheme: Schematic representation of the *SBH1* and *SBH2* deletion process from KRY1156 strain. (A) Primers 59 and 60 were used in a PCR reaction using as template the genomic DNA extracted from KRY588. The amplified cassette was used to generate the *SBH1* (yellow) deletion by integration of the Kanamycin resistance (green). Integration of the cassette into the genome of KRY1156 by homologous recombination was possible due to the overlapping sequences provided by primers 59 and 60 (grey). (B) Primers Sbh2ExtFw and Sbh2ExtRv were used in a PCR reaction using as template the genomic DNA extracted from KRY588. The amplified cassette was used to generate the *SBH2* (beige) deletion by integration of the Hygromycin resistance (orange). Integration of the cassette into the genome of KRY1156 by homologous recombination was possible due to the overlapping sequences provided by primers Sbh2ExtFw and Sbh2ExtRv (grey).

When I finally had the KRY1156 strain with the double deletion $\Delta sbh1/\Delta sbh2$ (KRY1160), I verified the deletions, checking for Sbh1/Sbh2 expression by Western blotting (Figure 3.18A), and by temperature sensitivity growth test at 37°C (Figure 3.18B). For the Western

blot experiment, I grew KRY1160 ($\Delta sbh1/\Delta sbh2$) and KRY1156 (wildtype) strains to an OD₆₀₀ of 1 at 30°C, 220 rpm. I collected samples from each culture, made extracts, and resolved them by SDS-PAGE. I detected Sbh1 by immunoblotting using specific antibodies (Sbh1₍₁₋₁₈₎). I used Rpn12 as a loading control. I found that there was no expression of Sbh1 in KRY1160 cells (Figure 3.18A), confirming the double deletion $\Delta sbh1/\Delta sbh2$ in this strain. For the temperature sensitivity growth test, I prepared sequential dilutions of KRY1160 ($\Delta sbh1/\Delta sbh2$) and KRY1156 (wildtype) and grew them on solid media (YPD). Each set was grown in duplicates either at 30°C or at 37°C for 3 days. KRY1156 cells were able to grow at the restrictive temperature (37°C). KRY1160 resulted in reduced growth at 37°C (Fig 3.18B), comparable to the reduction seen in $\Delta sbh1/\Delta sbh2$ strain KRY585 (Fig 3.1). This result also confirms the double deletion $\Delta sbh1/\Delta sbh2$ in KRY1160 strain.

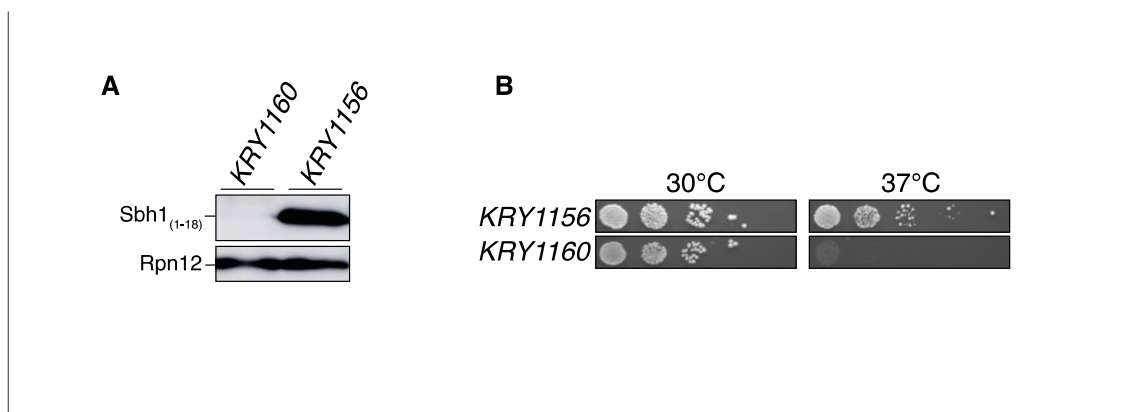


Figure 3.18: Analysis of Sbh1 expression and temperature sensitivity in KRY1156 and KRY1160 strains. (A) Cells were grown to an OD₆₀₀ of 1 at 30°C, 220 rpm in YPD. Then, 1 OD₆₀₀ of cells were collected from each culture, washed with sterile deionized water and extracts were prepared. For each sample, 0.4 OD₆₀₀ was resolved by SDS-PAGE, and protein detected by immunoblotting using antibody against N-terminal region of Sbh1 (Sbh1₍₁₋₁₈₎). Rpn12-specific antibodies were used for the loading control. Signal was acquired by chemiluminescence using an Amersham Imager 600. (B) Cells were grown overnight in at 30°C, 220 rpm. Then, cells were counted using a Neubauer chamber and sequentially diluted (10⁴-10 cells/5μl). Samples of each dilution (5 μl) were then plated side by side, on solid media (YPD) and grown for 3 days. Each set was replicated 2 times in different plates and were incubated at 30°C or at 37°C (one replica per temperature).

3.3.1.1.2 Subcloning of *sbh1S3A/T5A* from pRS415 to pRS416

To be able to transform KRY1160 strain with *sbh1S3A/T5A*, I had to subclone (Figure 3.19) this mutant gene from a pRS415 plasmid (leucine marker) to a pRS416 (uracil marker), for making it suitable for KRY1160 strain background. For doing that, I extracted the empty pRS416 and the pRS415*sbh1S3A/T5A* plasmids from KRB125 and KRB1032 respectively. After the extraction, I performed a restrictive digestion of them, using KpnI and SacI restriction enzymes, and I ran the fragments on an agarose gel. Then I recovered the DNA

fragments from the agarose gels (from the empty pRS416 the fragment was about 4.800 bp, and from the pRS415*sbh1S3A/T5A* the fragment was about 2.500 bp). After recovery of the DNA fragments, I ligated them, transformed chemically competent *E. Coli*, and plated the transformed bacteria in LB plates supplemented with ampicillin (100 µg/ml). I then performed a colony PCR with M13 primers. I then extracted the plasmids from the positive clones and sent them for sequencing (GATC Biotech), using M13 primers. Finally, I used this plasmid pRS416*sbh1S3A/T5A* (KRB1152) to transform KRY1160.

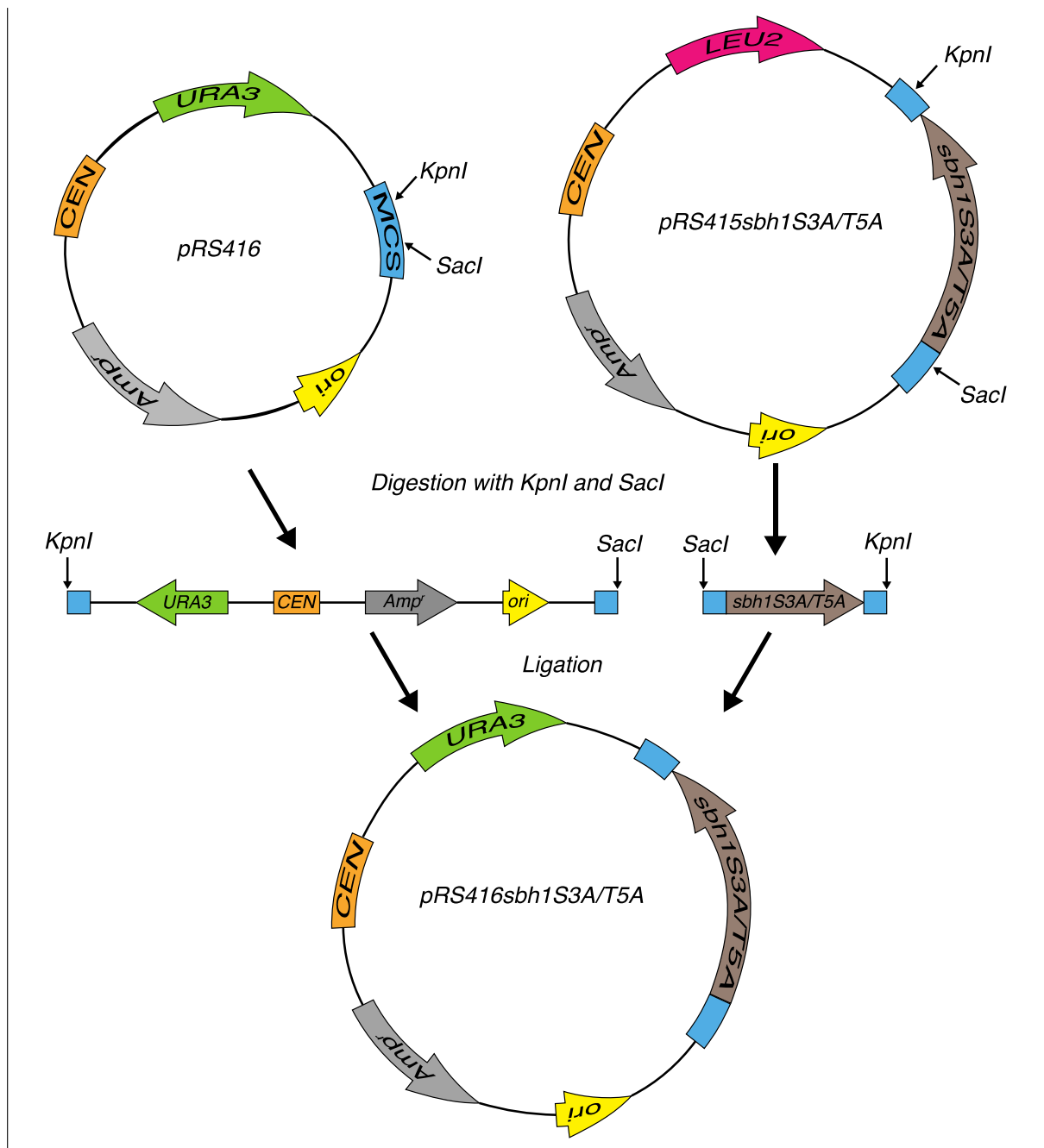


Figure 3.19: *sbh1S3A/T5A* subcloning Scheme: Schematic representation of the *Sbh1S3A/T5A* subcloning process from pRS415 to pRS416. Empty pRS416 and pRS415*sbh1S3A/T5A* were digested with KpnI and SacI restriction enzymes. After recovering, DNA fragments were ligated. Competent *E. coli* was transformed with resulting plasmid and plated in LB plates supplemented with ampicillin (100 µg/ml). *sbh1S3A/T5A* (brown), *URA3* gene (green), *LEU2* gene (pink), multiple cloning site (blue), replication origin (yellow), centromere (orange), ampicillin resistance (grey), and KpnI and SacI recognition sequences are shown.

3.3.1.1.3 Genomic replacement of *ESS1* with *ess1H164R* in KRY1156 wildtype strain to make KRY1126

In order to replace wildtype *ESS1* gene with *ess1H164R* mutant gene, which encodes a catalytically deficient mutant enzyme, to generate KRY1126 (Figure 3.20), I first extracted p502.8 plasmid form KRB1085. Afterwards, I amplified the *ess1H164R:NatMx* cassette

(cassette for generating *ess1H164R* mutant gene by using integration of the Nourseothricin resistance). For this PCR reaction (Atencio *et al.*, 2014) I used as DNA template p502.8 plasmid extracted from KRB1085 and primers OW39 and OW989 (Ma *et al.*, 2012). I cleaned the PCR product and transformed KRY1156 strain, plating the transformed KRY1156 in YPD plates supplemented with 100 µg/ml Nourseothricin. I extracted the genomic DNA from the colonies that were able to grow in YPD plates supplemented with 100 µg/ml Nourseothricin. I used this DNA to check the *ess1H164R:NatMx* integration. I made a PCR reaction using primers CheckEss1mutFw and CheckEss1MutRv, and I resolved the amplicon in agarose gels (wildtype about 730 bp, mutant about 2.000 bp). Afterwards, I sent for sequencing the genomic DNA extracted from the positive colonies (GATC Biotech), using primers CheckEss1mutFw and CheckEss1MutRv.

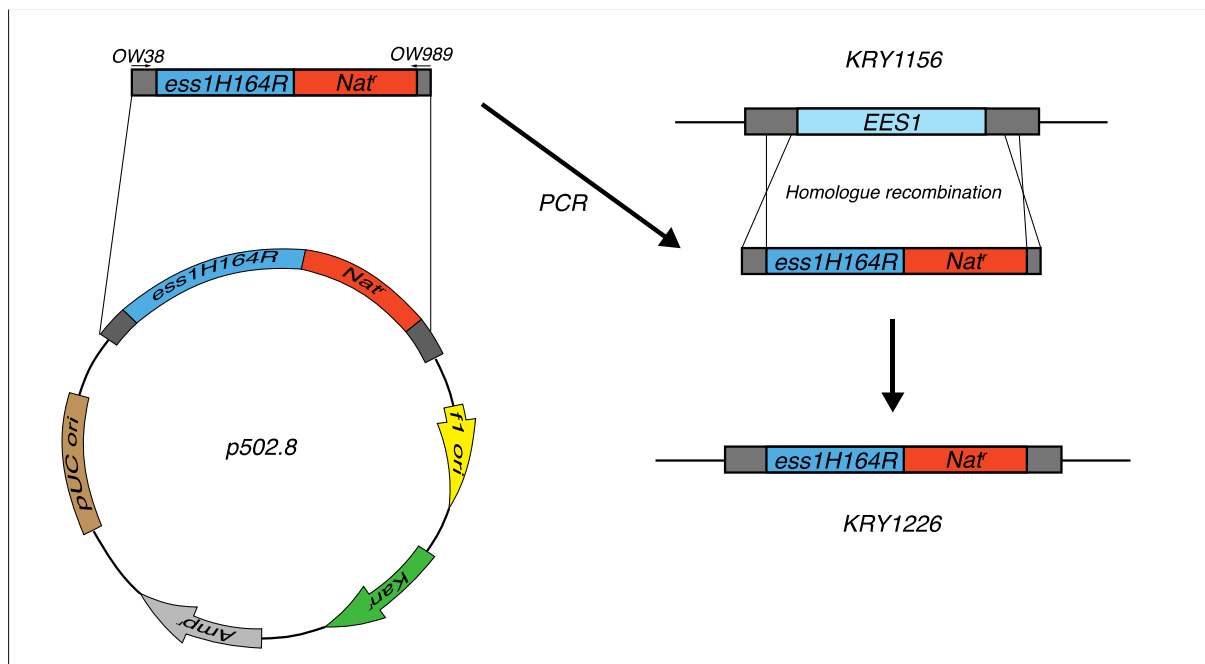


Figure 3.20: *ess1H164R* mutant construction Scheme: Schematic representation of the *ess1H164R* mutant construction process from KRY1156 strain. Primers OW38 and OW989 were used in a PCR reaction using as template p502.8 plasmid extracted from KRB1085. The amplified cassette was used to generate the *ess1H164R* (blue) mutant by integration of the Nourseothricin resistance (red). Integration of the cassette into the genome of KRY1156 by homologue recombination was possible due to the overlapping sequences provided by primers OW38 and OW989 (grey). *Ess1* gene (light blue), kanamycin resistance (green), f1 replication origin (yellow), pUC replication origin (brown), and ampicillin resistance (grey), are shown as well.

3.3.1.2 Generation of mutant libraries and screen

After the construction of the query strains, I crossed them ($\Delta sbh1/\Delta sbh2$, *sbh1S3A/T5A* and *ess1H164R* mutant strains) with a reporter library consisting of 382 secretory and

transmembrane proteins C-terminally fused to GFP (Geva *et al.*, 2017). I took images of the wildtype and mutant cells and looked for changes in the GFP signal pattern (increase or reduction of the signal, changes in localization of the signal, etc.). Here I show three examples (Figure 3.21): For Pmt1, an ER-localized multi-spanning protein mannosyl transferase, there was an increase of the fluorescence signal in the $\Delta sbh1/\Delta sbh2$ mutant (Figure 3.21, top). For Msb2, an osmosensor involved in signal transduction with a single transmembrane domain and that normally localizes to the vacuole, there was a reduction on the signal for the *sbh1S3A/T5A* mutant (Figure 3.21, middle). For Msc1, a protein of unknown function, whose mutant is defective in directing meiotic recombination events to homologous chromatids, there was an increase of the fluorescence signal in the *ess1H164R* mutant (Figure 3.21, bottom).

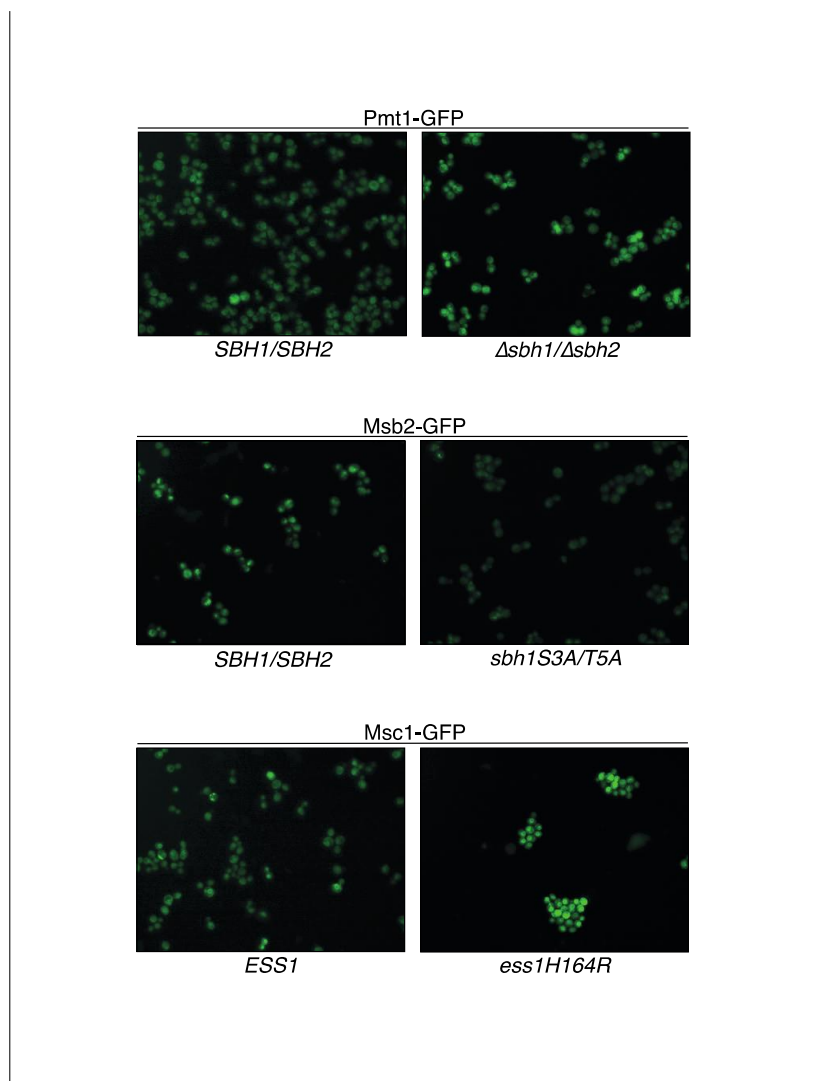


Figure 3.21: Image analysis from automated microscopic screen of secretome-GFP library in wildtype cells and the indicated mutants. $\Delta sbh1/\Delta sbh2$, *sbh1S3A/T5A* and *ess1H164R* mutant strains were crossed with a reporter library consisting of 382 secretory and transmembrane proteins C-terminally fused to GFP. The resulting library was inoculated from agar to liquid plates and grown in a shaking incubator. Plates for screening were transferred to the microscope stage. Images of cells were acquired using a fully automated fluorescence microscope and analysed for rapid data extraction.

Using this technology, I was able to identify 45 proteins that were dependent on the presence of Sbh1, 7 that were dependent on S3/T5-phosphorylation of Sbh1, and 45 that were dependent on isomerization by Ess1 (Table 3.1). From all these substrates: 5 are both dependent on the presence of Sbh1 and on S3/T5-phosphorylation of Sbh1 (Table 3.1, underlined); 19 are both dependent on the presence of Sbh1, and on isomerization by Ess1 (Table 3.1, bold); and 2 are dependent on the presence of Sbh1, on S3/T5-phosphorylation of Sbh1, and on isomerization by Ess1 (Table 3.1, underlined and bold).

<i>Δsbh1/Δsbh2</i>	<i>sbh1S3A/T5A</i>	<i>ess1</i>
Gpi13 ; Tda7; Yps7 ; Yhr202w ; Van1 ; Pst1 ; Sun4; Yol047c; Nus1 ; Sed1 ; Gpi14 ; Gpi11 ; Atg27; Sna2 ; Ybt1; Spf1 ; Pmt1; Cwh43 ; Gup1 ; Rsn1; Vph1 ; <u>Syg1</u> ; <u>Pmt2</u> ; Dip5 ; Atr1 ; Tat1 ; Hxt2; Ifa38; Erp3; Irc22 ; Lem3; Ypl162c ; Erd2 ; Gpi18 ; Mep1; Ice2 ; Kch1; Csg2; Yml018c ; Zrc1 ; Erp1; Yet3; Tsc3; Erv25 ; Yip3	Vph1 ; <u>Syg1</u> ; Dip5 ; Tat1 ; <u>Irc22</u> ; Msb2; Gaa1	Gpi13 ; Yhr202w ; Van1 ; Izh3; Pho11; Pho3; Tms1; Yjr015w; Msc1; Pst1 ; Ymr253c; Rtn2; Nus1 ; Gtt3; Fmp45; Sed1 ; Gpi14 ; Ayr1; Gpi11 ; Emc5; Yer053c-a; Sna2 ; Spf1 ; Pho91; Fui1; Hxt5; Bap3; Vph1 ; Ymr221c; Gab1; Ktr3; Dip5 ; Atr1 ; Pex3; Fen1; Ypl162c ; Erd2 ; Ice2 ; Ste2; Yjr054w; Tup38; Yml018c ; cos1; Zrc1 ; Erv25

Table 3.1: The Sbh1-dependent, Sbh1 phosphorylation-dependent and Ess1-dependent ER translocation substrates from the automated microscopic screen. Blue: proteins involved in cell wall biosynthesis, red: amino acid transporters, underlined: overlapping proteins between Sbh1-dependent and Sbh1 phosphorylation-dependent ER translocation substrates, bold: overlapping proteins between Sbh1-dependent and Ess1-dependent ER translocation substrates, bold and underlined: overlapping proteins between the three screens.

3.3.1.3 Biochemical verification of screen results

After identifying the proteins that were dependent either on the presence of Sbh1, on S3/T5-phosphorylation of Sbh1 or on the presence of Ess1, I verified biochemically for cytosolic precursor accumulation. First, I made a selection based on an expected clear size difference between cytosolic precursor and ER form. I ended up with two Sbh1-dependent ER translocation substrates: Erp-1 and Gpi-8; and one Sbh1 and Sbh1 phosphorylation-dependent ER translocation substrate: Irc22. Erp1 is a member of the p24 family involved in ER to Golgi transport. Upon translocation across the ER membrane, the precursor protein (pErp1-GFP; 51 KDa) is signal-cleaved to form the mature protein (Erp1-GFP; 48 KDa). Gpi8, is a catalytic subunit of the ER membrane GPI transamidase complex. Upon translocation across the ER membrane, the precursor protein (pGpi8-GFP; 74 KDa) is signal-cleaved, and 4 times glycosylated to form the mature protein (Gpi8-GFP; 81 KDa). Irc22 is a protein of unknown function, which localizes to the ER. Upon translocation across the ER membrane, the precursor protein (pIrc22-GFP; 52 KDa) is signal-cleaved, and 5 times glycosylated to form the mature protein (Irc22-GFP; 62 KDa). To test whether there was precursor accumulation in either the *Δsbh1/Δsbh2* mutant strain, or the *sbh1S3A/T5A* mutant strain, I looked at translocation of pErp1-GFP, pGpi8-GFP and pIrc22-GFP by Western blotting. For this experiment I grew wildtype, *Δsbh1/Δsbh2* and *sbh1S3A/T5A* mutant strains expressing either Erp1-GFP, Gpi-8-GFP or Irc22-GFP in either YPD (For wildtype and *Δsbh1/Δsbh2* mutant strain) or minimal media (-leu, for *sbh1S3A/T5A* mutant strain, expressed from a pRS415 plasmid) to an OD₆₀₀ of 0.25 at 30°C, 220 rpm, then I incubated them at 37°C, until cultures reached an OD₆₀₀ of 1. After incubation, I collected samples from each culture, made extracts, and resolved them by SDS-PAGE (Section 2.2.8). I detected Erp1-GFP, Gpi8-

GFP and Irc22-GFP by immunoblotting using GFP-specific antibodies (Table 2.7). As can be seen in Figure 3.22A and Figure 3.22B, I was able to detect cytosolic precursor accumulation for the Sbh1-dependent ER translocation substrates (pErp1-GFP, pGpi8-GFP) in the $\Delta sbh1/\Delta sbh2$ strain, but not in wildtype or *sbh1S3A/T5A* mutant cells. As for the Sbh1 and Sbh1 phosphorylation-dependent ER translocation substrate (Irc22-GFP), I was not able to see any precursor accumulation in neither $\Delta sbh1/\Delta sbh2$ nor *sbh1S3A/T5A* mutant cells. I saw though accumulation of a partially un-glycosylated form of Irc22-GFP in $\Delta sbh1/\Delta sbh2$ mutant strain (Figure 3.22C).

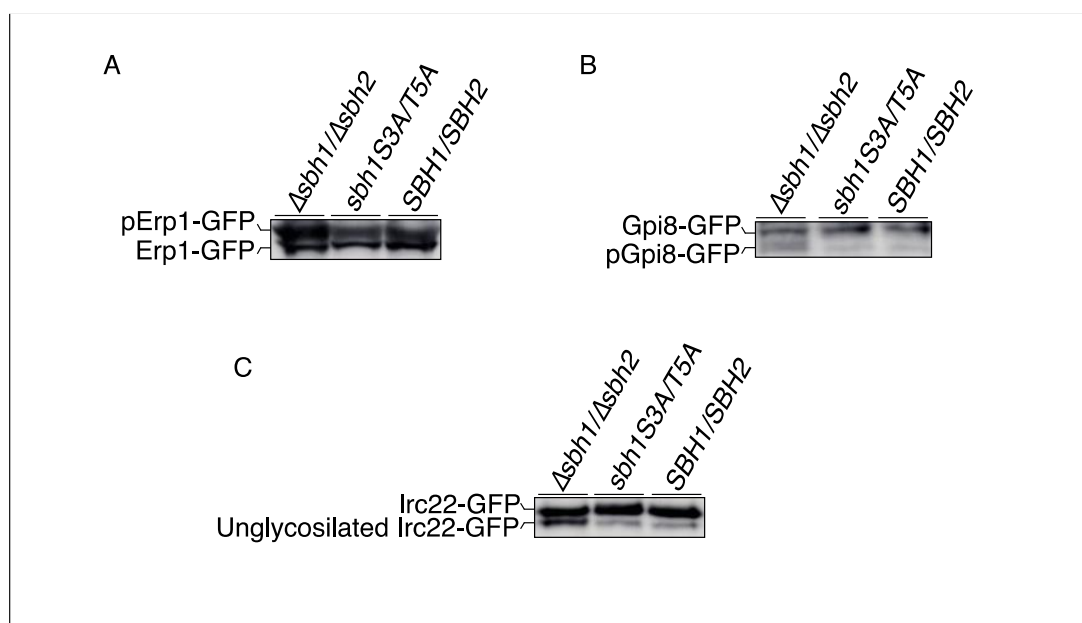


Figure 3.22: Analysis of the Erp1, Gpi8 and Irc22 ER translocation in $\Delta sbh1/\Delta sbh2$ and *sbh1S3A/T5A* strains. Wildtype, $\Delta sbh1/\Delta sbh2$ and *sbh1S3A/T5A* mutant strains were grown to an OD₆₀₀ of 0.25 at 30°C, 220 rpm and then cultures were switched to 37°C, 220 rpm, until cultures reached an OD₆₀₀ of 1. After incubation, 1 OD₆₀₀ of cells were collected from each culture, washed with sterile deionized water and extracts were prepared. For each sample 0.4 OD₆₀₀ was resolved by SDS-PAGE, and protein detected by immunoblotting using a GFP-specific antibodies. Signal was acquired by chemiluminescence using an Amersham Imager 600.

Then, I looked at pIrc22-GFP translocation by pulse-labelling, to check if I was able to see any precursor accumulation. For this experiment I grew wildtype, $\Delta sbh1/\Delta sbh2$ and *sbh1S3A/T5A* mutant strains expressing Irc22-GFP in either YPD (For wildtype and $\Delta sbh1/\Delta sbh2$ mutant strain) or minimal media (-leu, for *sbh1S3A/T5A* mutant strain, expressed from a pRS415 plasmid) at 37°C, 220 rpm, to an OD₆₀₀ of 0.5–1. I then labelled them with [³⁵S]-met/cys for 5 min, and I precipitated Irc22-GFP with GFP-specific antibodies (Table 2.7). I ran the samples on 7.5 % Bis-Tris SDS gel and analysed specific the signals by autoradiography (Section 2.2.12). Again, I was not able to see any precursor accumulation in

neither $\Delta sbh1/\Delta sbh2$ nor $sbh1S3A/T5A$ mutant cells, but I saw accumulation of a partially un-glycosylated form of Irc22-GFP in $\Delta sbh1/\Delta sbh2$ mutant strain (Figure 3.23).

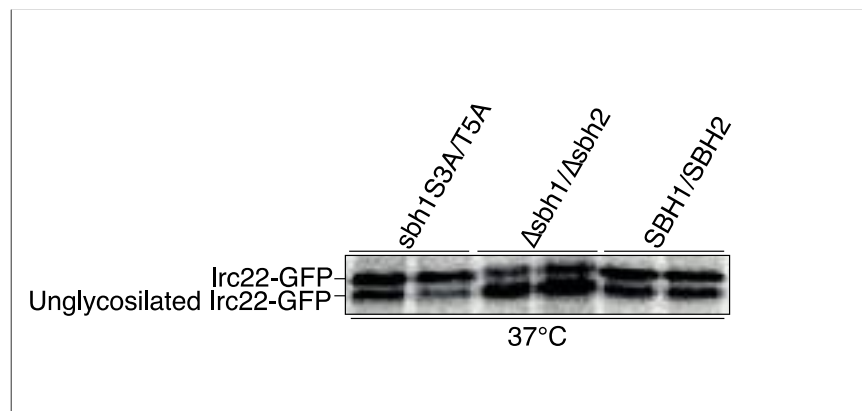


Figure 3.23: Analysis of the Irc22 ER translocation in $\Delta sbh1/\Delta sbh2$ and $sbh1S3A/T5A$ strains. Wildtype, $\Delta sbh1/\Delta sbh2$ and $sbh1S3A/T5A$ mutant strains were grown either in YPD (for wildtype or $\Delta sbh1/\Delta sbh2$ mutant strain) or minimal media (for $sbh1S3A/T5A$, expressed from a pRS415 plasmid) at 37°C, 220 rpm, to an OD_{600} of 0.5–1, then labelled with [35 S]-met/cys for 5 min. 1.5 OD_{600} of cells were lysed and proteins immunoprecipitated with specific antibodies against GFP. After SDS-PAGE, proteins were detected by exposing the gels to phosphorimager plates and signal acquired in Typhoon Trio™ Variable Mode Imager. All experiments were done in duplicates.

3.3.1.4 Statistical analysis of the signal peptides or transmembrane targeting sequences

The identification of a significant number of Sbh1-dependent proteins allowed me to investigate whether their signal sequences had specific common features compared to the total ER targeting sequences in *Saccharomyces cerevisiae*. With the help of the bioinformatics department of the University of Saarland (Duy Nguyen), I was able to compare different physicochemical properties of the signal sequences or the transmembrane targeting sequences from the Sbh1 dependent proteins I found on my screen with the total ER targeting sequences in yeast. My background dataset was the whole proteome of *Saccharomyces cerevisiae* (strain ATCC 204508 / S288c, a.k.a. Baker's yeast), retrieved from UniProtKB (date of retrieval: 16/01/2017), which contains 7904 protein entries. All information with respect to signal peptides (SPs) and transmembrane regions (TMDs), such as sequences, positions, etc. was taken using custom scripts. The signal peptides were segmented into three parts: the typical positively charged N-terminal region (N-region), the central hydrophobic helical region (H-region), and the slightly polar C-terminal region (C-region) (Figure 3.24). The parameters to be compare were: the total net charge of the N-region, the hydrophobicity and length of the core H-region, the polarity of the C-region, and the proline and glycine-proline content of the SP.

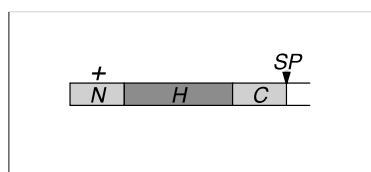


Figure 3.24: Signal peptide scheme. Schematic representation of a typical signal peptide, with a positively charged N-terminal region (N), hydrophobic region (H), C-terminal polar region (C), and signal peptide cleavage site (SP).

The well-established prediction tool Phobius (*Käll et al. 2004*) was used to identify the N-region, the H-region and the C-region of all SPs. Based on this, the total net charge of the N-region, the polarity of the C-region, and the hydrophobicity and absolute length of the H-region was calculated. The polarity score of the C-region of a single peptide was calculated as the averaged polarity of its amino acids according to the polarity propensity scale derived by *Radzicka et al. (1988)*. The hydrophobicity score of the H-region was calculated in the same fashion using the well-known Kyte-Doolittle propensity scale. Regarding the adjacent regions of the first transmembrane domain (TMD) of the Shb1-dependent proteins, the charges in both regions, upstream and downstream of the first TMD, were computed. However, only the region with the higher average positive charge was considered. All computations were normalised by length. After the analysis, I found that the Shb1-dependent signal sequences were slightly less hydrophobic (Figure 3.25A), but I detected no differences in charge distribution of the N-regions (Figure 3.25B), proline fraction of the SP (Figure 3.25C), polarity of the C-region (Figure 3.25D), glycine-proline fraction of the SP (Figure 3.25E) or H-region length (Figure 3.25F).

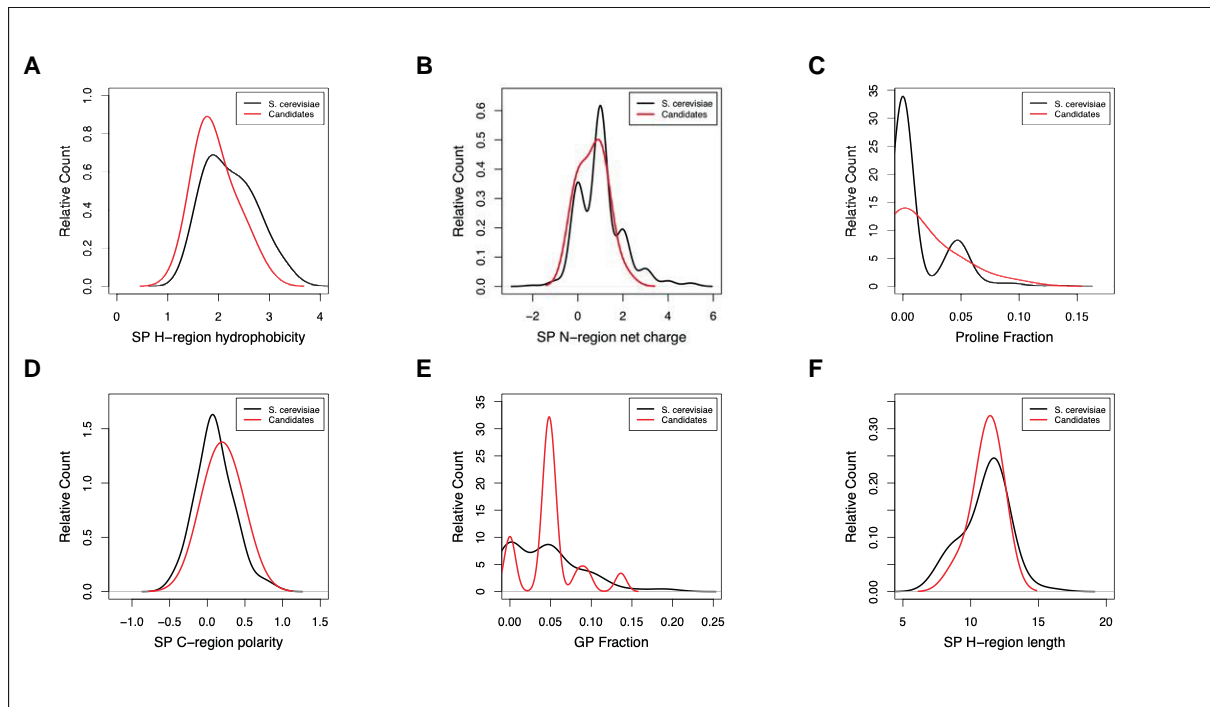


Figure 3.25: Statistical analysis of the signal peptides. Physicochemical properties of signal peptides of Sbh1-dependent candidates (red) and total ER targeting sequences in yeast (black): hydrophobicity of the core H-regions (A), net charge of the N-regions (B), proline content of the SP (C), polarity of the C-regions (D), glycine-proline content of the SP (E), and length of the H-region (F).

Regarding the hydrophobicity of the first TMD and the charge if the regions adjacent to the first TMD, there are no significant differences with respect to the hydrophobicity of the TMD or the charge of the regions adjacent to the TMD (Figure 3.26).

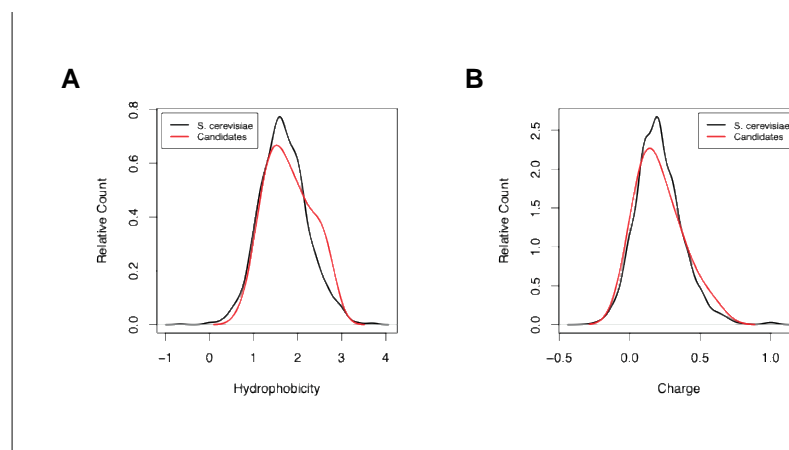


Figure 3.26: Statistical analysis of the transmembrane targeting sequences. Physicochemical properties of first TMD sequences of Sbh1-dependent candidates (red) and total first TMD sequences in yeast (black): hydrophobicity of the TMD (A), and Charges on both sides of TMD (B).

When I looked at Sbh1-dependent targeting sequences individually, however, I found that many targeting sequences had no charge bias (e.g., Yps7, Figure 3.27A) or an inverse charge bias (e.g., Gpi14, Figure 3.27A). This was true for both signal peptides (16) and

transmembrane (29) targeting sequences of Sbh1-dependent proteins. In addition, some transmembrane targeting sequences were unusually long or short (e.g., Yip3, Figure 3.27B), or contained a high number of glycine residues (e.g., Tat1, Figure 3.27B); all of these features would interfere with the efficient insertion of these targeting sequences into the lateral gate of Sec61 channel (*Nguyen et al., 2018; Spiess et al., 2019; Yim et al., 2018*). Targeting sequences of Sbh1 S3/T5-phosphorylation dependent proteins were similar to the Sbh1-dependent ones (Figure 3.27C), but I was unable to identify specific features, likely due to the small number of proteins identified.

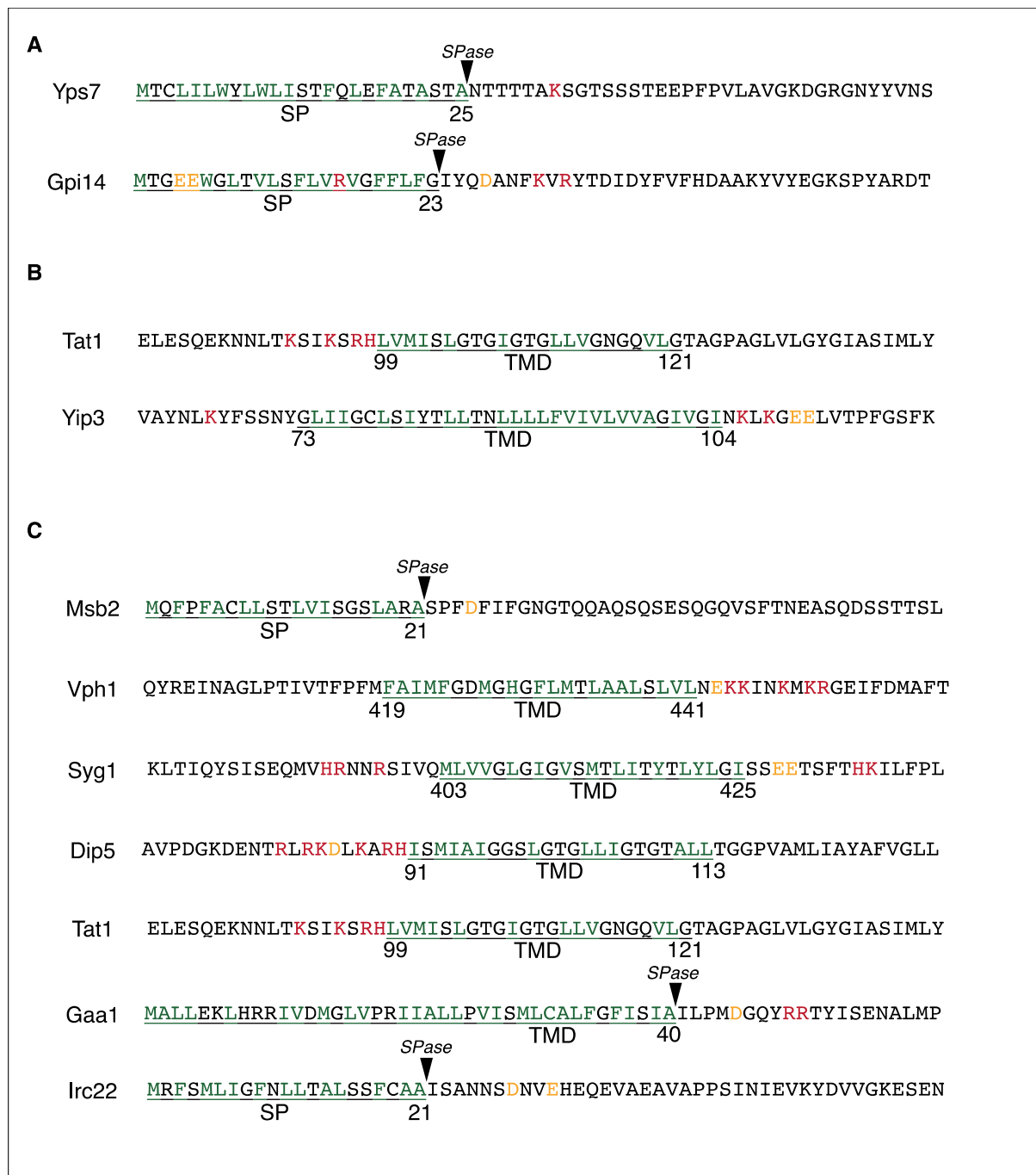


Figure 3.27: Examples of signal peptides or first transmembrane domain from the microscopic screen. (A) Examples of signal peptide (SP) or first transmembrane domain (TMD) and the neighbouring sequences from the Sbh1-dependent ER translocation substrates from the high content screen with either no charge bias or an inverse charge bias. Underlined: SP or first TMD from the substrates, green: Hydrophobic residues from the predicted SP or TMD, red: Positive charged residues from the SP or TMD 10 residues neighbouring sequences, yellow: negatively charged residues from the SP or TMD 10 residues neighbouring sequences. Signal peptidase cleavage site (SPase) is also shown. (B) Examples of the first TMD and the neighbouring sequences from the Sbh1-dependent ER translocation substrates from the high content screen with unusually long or short targeting sequences or a high number of glycine residues. Underlined: first TMD from the substrates, green: Hydrophobic residues from the predicted TMD, red: Positive charged residues from the TMD 10 residues neighbouring sequences, yellow: negatively charged residues from the TMD 10 residues neighbouring sequences. (C) The SP or first TMD and the neighbouring sequences from the Sbh1 phosphorylation-dependent ER translocation substrates from the automated microscopic screen. Underlined: SP or first TMD from the substrates, green: Hydrophobic residues from the predicted SP or TMD, red: Positive charged residues from the SP or TMD 10 residues neighbouring sequences, yellow: negatively charged residues from the SP or TMD 10 residues neighbouring sequences. Signal peptidase cleavage site (SPase) is also shown.

Signal peptides encoded with rare codons (suboptimal or slowly decoded codons), are more efficient in ER translocation because it takes more time for the ribosomes to synthesize the peptide. Since I wanted to know if that was the case for my Sbh1-dependent substrates, I did an analysis of codon usage in the signal peptide of our Sbh1-dependent targeting sequences. For doing that, I chose randomly 10 Sbh1-dependent substrates (Gls1, Pst1, Atg27, Erp3, Gpi8, Irc22, Sna2, Erp1, Erv25 and Sun4) and 10 non-Sbh1-dependent substrates (Pry3, Tos1, Fat1, Nhx1, Wsc4, Tat2, Mmp1, Msc7, Alg12 and Pmt4), and I calculated the codon adaptation index (CAI) for all of their signal sequences. The codon adaptation index is a simple, effective measure of synonymous codon usage bias (*Sharp and Li, 1987*). The index uses a reference set of highly expressed genes to assess the relative merits of each codon. A score for a gene is calculated from the frequency of use of all codons in that gene (*Sharp and Li, 1987*). After the calculation was done, I made an average of the CAI for the Sbh1-dependent substrates (CAI=0.548) and for the non-Sbh1-dependent substrates (CAI=0.474), having as a result no significant differences between the CAI for each set.

3.3.2 Identification of potential S3/T5 Sbh1 Kinases and Phosphatases

For the second screen, I had two biological questions to be addressed. The first one was which kinase or kinases are potentially phosphorylating Sbh1 in the S3 and T5 sites. For answering that, I performed two different Screens. Since the translocation of Mns1 into the ER is dependent on the phosphorylation of Sbh1, I used as a reporter for both screens Mns1 fused to GFP.

3.3.2.1 Mns1 GFP-tagging

In order to GFP-tag chromosomal Mns1 from KRY1156 strain (Figure 3.28), I first extracted pKT209-GFP (plasmid for making C-terminal GFP fusion proteins by PCR) from KRB1127. Afterwards, I amplified the *C-terminalGFPMns1:URA3* cassette (cassette for C-terminally GFP-tagging Mns1 by integration of the *URA3* gene). For this PCR reaction, I used as DNA template the pKT209-GFP plasmid extracted from KRB1127 and primers FwMns1F5 and RvMns1R3. I then clean the PCR product and transformed KRY1156 strain, plating the transformed

KRY1156 in -leu plates. I extracted the genomic DNA from the colonies that were able to grow in -leu plates. I used this DNA to check Mns1 GFP-tagging. I made a PCR reaction using primers FwMns1Check and RvMns1Check, and I resolved the amplicon in agarose gels, (wildtype about 151 bp, GFP-tagged about 2.000 bp). Afterwards, I sent for sequencing the genomic DNA extracted from the positive colonies (GATC Biotech), using primers CheckEss1mutFw and CheckEss1MutRv. In addition, I checked the Mns1-GFP fusion by fluorescent microscopy of the cells.

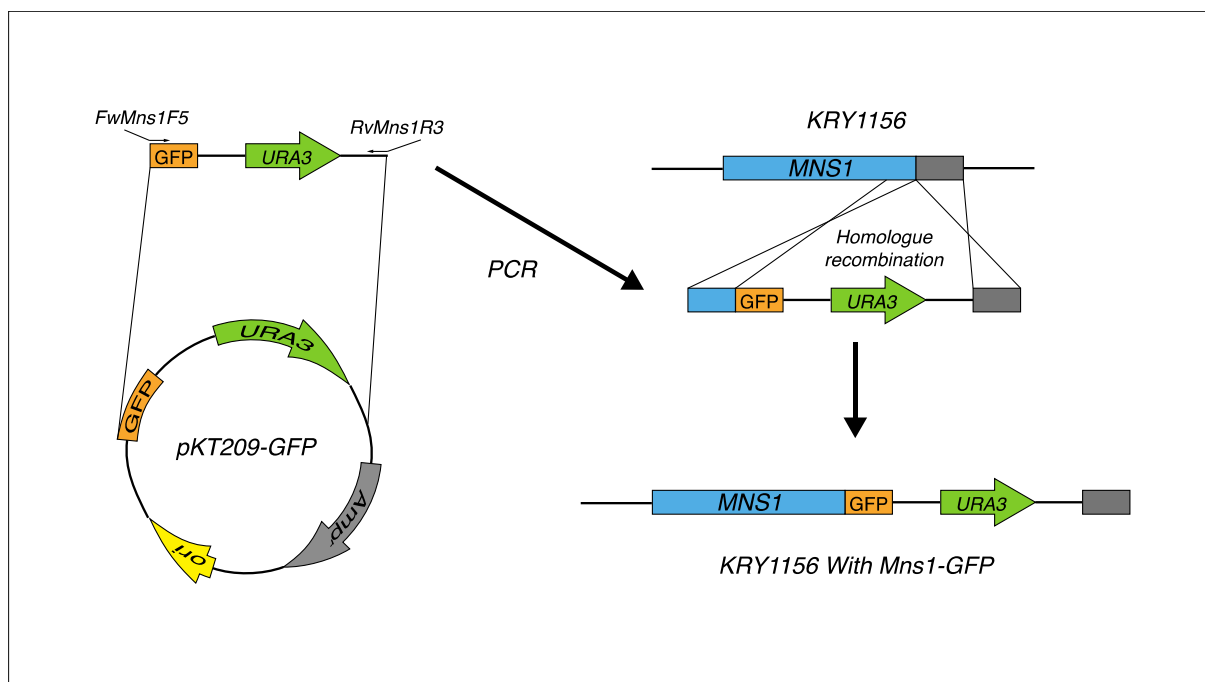


Figure 3.28: Mns1 GFP tagging Scheme: Schematic representation of the Mns1 GFP tagging process for KRY1156 strain. Primers FwMns1F5 and RvMns1R3 were used in a PCR reaction using as template pKT209-GFP plasmid extracted from KRB1127. The amplified cassette was used to GFP tag *MNS1* (blue) by integration of the *URA3* gene (green). Integration of the cassette into the genome of KRY1156 by homologue recombination was possible due to the overlapping sequences provided by primers FwMns1F5 and RvMns1R3. *MNS1* gene (blue), replication origin (yellow), and ampicillin resistance (grey), are shown as well.

3.3.2.2 Generation of mutant libraries and screen

For the first screen, I crossed the reporter Mns1-GFP strain with a mutant library consisting of 127 knockout Kinases. For the second screen, I used the same Mns1-GFP reporter strain and I crossed it with a mutant library consisting of 125 overexpressed Kinases. I took images of wildtype and mutant cells in both screens and looked for changes in the GFP signal pattern (increase or reduction of the signal, changes in localization of the signal, etc.). Here I show one example of each screen (Figure 3.29): For Mps1, a protein serine/threonine/tyrosine kinase involved in the phosphorylation of many mitotic regulators

and capable of auto-phosphorylation, there was an increase of the fluorescence signal in the overexpression mutant (Figure 3.29, top). For Yck2, Protein serine/threonine kinase involved in cell morphogenesis, endocytosis and glucose-mediated signalling, there was a reduction on the signal for the knockout mutant (Figure 3.29, bottom).

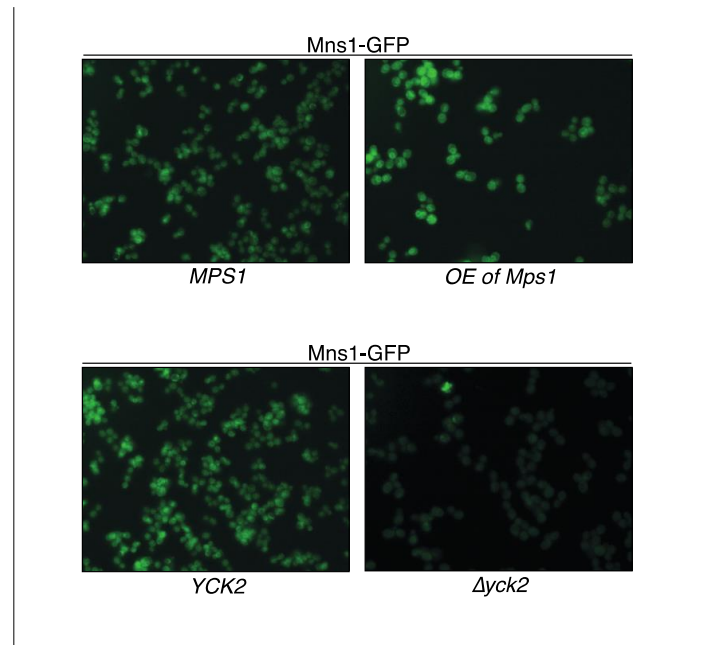


Figure 3.29: Image analysis from automated microscopic screen of Mns1-GFP cells in Wildtype, knockout and overexpression kinase mutant libraries. reporter Mns1-GFP strain was crossed with either a mutant library consisting of 127 knockout Kinases or a mutant library consisting of 125 overexpressed Kinases. The resulting libraries were inoculated from agar to liquid plates and grown in a shaking incubator. Plates for screening were transferred to the microscope stage. Images of cells were acquired using a fully automated fluorescence microscope and analysed for rapid data extraction.

With both screens, I was able to identify 13 kinases that were potentially responsible for the S3/T5-phosphorylation of Sbh1 (Table 3.2).

<i>Δkin screen</i>	<i>OE Kin screen</i>
<i>Δelm1; Δcka2; Δtda1; Δmek1; Δyck2; Δrim15; Δgcn2; Δtor2</i>	Mps1; Kin4; Kin3; Cka1; Prr2

Table 3.2: Results from Kinase identification Screen. The 13 Kinases that are potentially responsible for the S3/T5-phosphorylation of Sbh1, resulting from two automated microscopic screens.

The second biological question to be addressed from my second screen was which phosphatase or phosphatases are potentially de-phosphorylating Sbh1 in the S3 and T5 sites. For answering that, I did two different screens using again as a reporter for both screens Mns1 fused to GFP. In the first screen, I crossed the reporter Mns1-GFP strain with a mutant library consisting of 31 knockout phosphatases. In the second screen I used the

same Mns1-GFP reporter strain and I crossed it with a mutant library consisting of 31 overexpressed phosphatases. I took images of the wildtype and mutant cells in both screens and looked for changes in the GFP signal pattern (increase or reduction of the signal, changes in localization of the signal, etc.). Unfortunately, none of the 31 phosphatase mutants of neither screen resulted in a change in the signal pattern when compared to the correspondent wildtype and I was not able to identify any phosphatase as potential responsible for the de-phosphorylation of S3/T4-Sbh1.

3.4 Functional characterization of *sbh1* mutant strains

3.4.1 Sorbitol growth rescue assay for *sbh1* mutant strains

Since many of the Sbh1-dependent proteins I found in the automated microscopic screen play a role in cell wall biogenesis (Table 3.1, blue), I investigated whether the $\Delta sbh1/\Delta sbh2$ mutants had a cell wall defect. For this experiment, I prepared sequential dilution of wildtype, $\Delta sbh1/\Delta sbh2$, and *sec61-3* mutant strains and grew them in quadruplicates on solid media (YPD and YPD supplemented with 1,2M sorbitol (YPDS)) at either 30°C or 37°C for 3 days. Sorbitol stabilizes the plasma membrane if the cell wall is deficient (*Lommel et al., 2004*). I used as a positive control the *sec61-3* mutant strain, for which strong temperature sensitivity has been widely reported (*Biederer et al., 1996; Pilon et al., 1998*). I found that both $\Delta sbh1/\Delta sbh2$ and the *sec61-3* mutants were able to grow at 37°C in the presence of sorbitol (Figure 3.30), suggesting that a cell wall defect makes these mutant cells temperature sensitive.

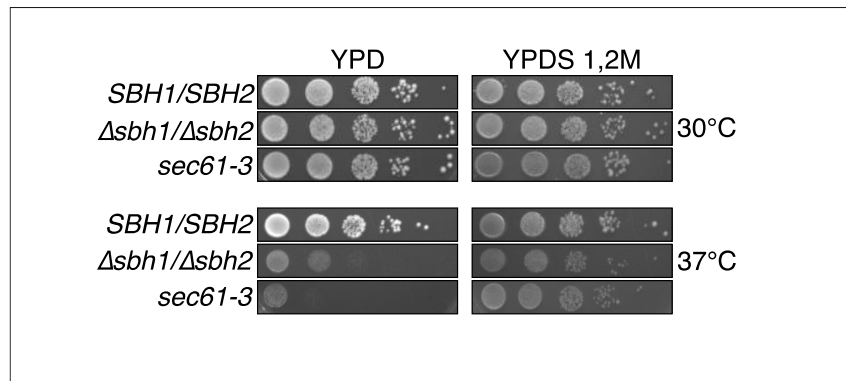


Figure 3.30: Sorbitol growth rescue assay for $\Delta sbh1/\Delta sbh2$ mutant strains. Wildtype, $\Delta sbh1/\Delta sbh2$ and *sec61-3* mutant strains were grown overnight in YPD, at 30°C, 220 rpm. Then, cells were counted using a Neubauer chamber and sequentially diluted (10^4 -10 cells/ 5μ l). Samples of each dilution (5μ l) were then plated side by side, in solid media (YPD or YPD supplemented with 1,2M sorbitol) and grown for 3 days. Each set was replicated 2 times in different plates and were incubated at 30°C or at 37°C (one replica per temperature).

In addition, since I also saw that the *sbh1S3A/T5A* mutant strain had a temperature sensitivity at 37°C, I investigated whether the *sbh1S3A/T5A* mutants had a cell wall defect as well. For this experiment, I prepared sequential dilution of wildtype and *sbh1S3A/T5A* mutant strains and grew them in quadruplicates on solid media (minimal media (-Leu) and minimal media supplemented with 1,2M sorbitol (-LeuS)) at either 30°C or 37°C for 3 days. I found that the *sbh1S3A/T5A* mutant strain was able to grow normally at 37°C in the presence of sorbitol (Figure 3.31), suggesting that a cell wall defect makes these mutant cells temperature sensitive as well.

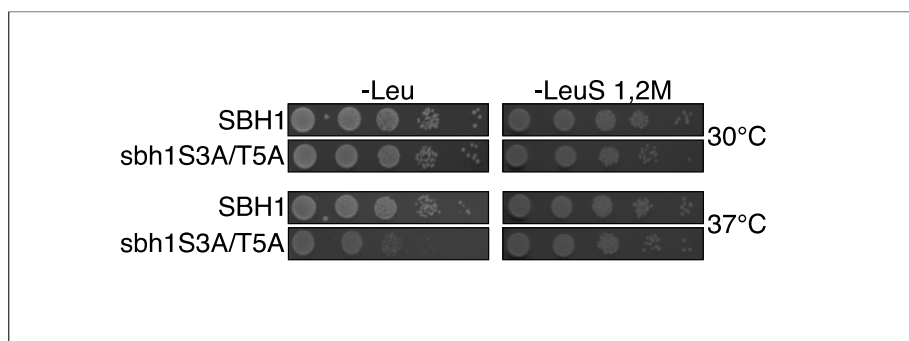


Figure 3.31: Sorbitol growth rescue assay for *sbh1S3A/T5A* mutant strains. Wildtype and *sbh1S3A/T5A* mutant strain were grown overnight in minimal media (-Leu, since *sbh1S3A/T5A* and *SBH1* were expressed from a pRS415 plasmid), at 30°C, 220 rpm. Then, cells were counted using a Neubauer chamber and sequentially diluted (10^4 -10 cells/ 5μ l). Samples of each dilution (5μ l) were then plated side by side, in solid media (-Leu or -Leu supplemented with 1,2M sorbitol) and grown for 3 days. Each set was replicated 2 times in different plates and were incubated at 30°C or at 37°C (one replica per temperature).

3.4.2 Sbh1 phosphorylation pattern in plasma membrane stabilized cells

My next step was to investigate whether the phosphorylation of Sbh1 is a response to the osmotic stress. I studied the change in the phosphorylation pattern of Sbh1

(phosphorylated Sbh1 vs. total Sbh1) in wildtype cells when they are grown with and without stabilization of the plasma membrane. For this experiment, I grew wildtype strain to an OD₆₀₀ of 1 at 30°C, 220 rpm in either YPD, YPD supplemented with 1M sorbitol, or YPD supplemented with 1,2M sorbitol. I collected samples from each culture, made the protein extracts, and resolved them by SDS-PAGE (Section 2.2.8). I detected Phosphorylated-Sbh1 using specific antibodies against the phosphorylated N-terminus of Sbh1 (Sbh1_(Pi), Figure 3.13), that recognizes mainly N-terminally phosphorylated. I detected total Sbh1 by immunoblotting using specific antibodies that was raised against the amino acids 39 to 48 of Sbh1 (Table 2.7), and recognizes the total Sbh1 (Sbh1₍₃₉₋₄₈₎, Figure 3.13). I used Rpn12 as a loading control. After normalization with the loading control, I was not able to see any difference in the pattern of phosphorylation of Sbh1 between the different conditions (Figure 3.32).

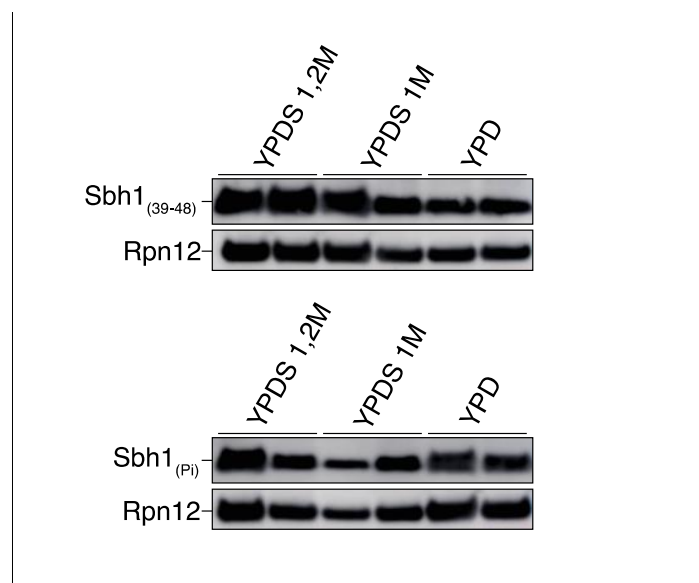


Figure 3.32: Analysis of the Sbh1 phosphorylation pattern in wildtype cells with and without stabilization of the plasma membrane. Cells were grown to an OD₆₀₀ of 1 at 30°C, 220 rpm in either YPD, YPD supplemented with 1M sorbitol or YPD supplemented with 1,2M sorbitol. Then, 1 OD₆₀₀ of cells were collected from each culture, washed with sterile deionized water and extracts were prepared. For each sample, 0.4 OD₆₀₀ was resolved by SDS-PAGE, and protein detected by immunoblotting using either antibody against amino acids 39-48 of Sbh1 (Sbh1₍₃₉₋₄₈₎) or antibody against the phosphorylated N-terminus of Sbh1 (Sbh1_(Pi)). Rpn12-specific antibodies were used for the loading control. Signal was acquired by chemiluminescence using an Amersham Imager 600. All experiments were done in duplicates.

3.4.3 Sbh1 expression and Sbh1 phosphorylation pattern in different growth phases

In addition, I studied the Sbh1 expression and the Sbh1 phosphorylation pattern in different yeast growth phases. For this experiment I grew wildtype strain in YPD to either an OD₆₀₀ of 0.5 (early exponential phase), an OD₆₀₀ of 4, or an OD₆₀₀ of 8 (Stationary phase) at

30°C, 220 rpm. I collected samples from each culture, made the protein extracts, and resolved them by SDS-PAGE (Section 2.2.8). I detected Phosphorylated-Sbh1 using specific antibodies against the phosphorylated N-terminus of Sbh1 (Sbh1_(Pi), Figure 3.13), that recognizes mainly N-terminally phosphorylated. I detected total Sbh1 by immunoblotting using specific antibodies that was raised against the amino acids 39 to 48 of Sbh1 (Table 2.7), and recognizes the total Sbh1 (Sbh1₍₃₉₋₄₈₎, Figure 3.13). I used Rpn12 as a loading control. After normalization with the loading control, I found that Sbh1 expression and Sbh1-Phosphorylation is considerably higher in early exponential phase, compared to later stages (Figure 3.33), consistent with its requirement for cell wall biosynthesis.

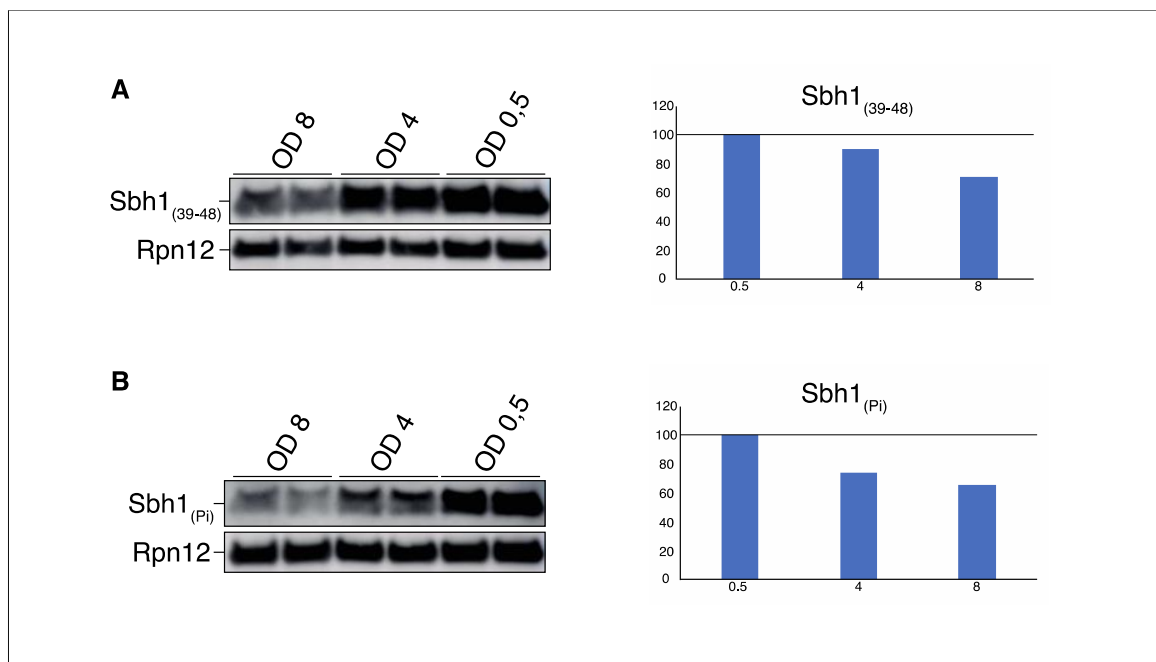


Figure 3.33: Analysis of Sbh1 phosphorylation pattern and Sbh1 expression in different growth phases. Wildtype cells were grown to either an OD₆₀₀ of 0.5, an OD₆₀₀ of 4 or an OD₆₀₀ of 8 at 30°C, 220 rpm in YPD. Then, 1 OD₆₀₀ of cells were collected from each culture, washed with sterile deionized water and extracts were prepared. For each sample, 0.4 OD₆₀₀ was resolved by SDS-PAGE, and protein detected by immunoblotting using either antibody against amino acids 39-48 of Sbh1 (A, left; Sbh1₍₃₉₋₄₈₎) or antibody against the phosphorylated N-terminus of Sbh1 (B, left; Sbh1_(Pi)). Rpn12-specific antibodies were used for the loading control. Signal was acquired by chemiluminescence using an Amersham Imager 600. All experiments were done in duplicates. Quantitation and graphs were done for total Sbh1 (A, right) and Phosphorylated Sbh1 (B, right). The amounts calculated for the cells grown until an OD₆₀₀ of 0.5 were taken as reference, and the arbitrary value of 100 was given them.

3.4.4 Gas1 maturation in $\Delta sbh1/\Delta sbh2$ mutant strain

Since several of the Sbh1-dependent proteins found in the automated microscopic screen are involved in GPI-anchored biosynthesis (Table 3.1, blue), I asked whether the $\Delta sbh1/\Delta sbh2$ strain was effective in GPI-anchor synthesis. The GPI-anchored protein Gas1 accumulates in the ER if its GPI-anchor is not appropriately processed (Horvath et al., 1994).

Maturation of Gas1p, which decreases its mobility in SDS-PAGE due to extensions of N- and O-linked carbohydrate chains (Golgi Gas1; 125 KDa), depends upon addition of a GPI anchor (Horvath et al., 1994; Nuoffer et al., 1993) and upon transport to the Golgi. If anchoring and/or transport was inefficient during the incubation period we would expect to find an accumulation of immature (ER Gas1; 105 kDa) Gas1. For this experiment I used as a control *sec23-1* mutant strain, an ER exit temperature sensitive mutant, which would allow me to see the immature ER Gas1 form when grown at restrictive temperature. I grew wildtype, $\Delta sbh1/\Delta sbh2$ and *sec23-1* mutant strains to an OD₆₀₀ of 0.25 at 30°C, 220 rpm. I then incubated them either at 37°C (for wildtype and $\Delta sbh1/\Delta sbh2$ mutant), 25°C (for *sec23-1* mutant strain, permissive temperature) or 33°C (for *sec23-1* mutant strain, restrictive temperature) until cultures reached an OD₆₀₀ of 1. After incubation, I collected samples from each culture, made extracts, and resolved them by SDS-PAGE (Section 2.2.8). I detected Gas1 by immunoblotting using specific antibodies (Table 2.7). As expected, in *sec23-1* cells grown at restrictive temperature there was accumulation of the ER form of Gas1 (Figure 3.34), in contrast to *sec23-1* cells grown at permissive temperature. Cells lacking *SBH1* and *SBH2*, however, did not accumulate the ER form of Gas1 after a 3-hour shift to the restricted temperature (Figure 3.34), suggesting no general defect in GPI-anchored biosynthesis.

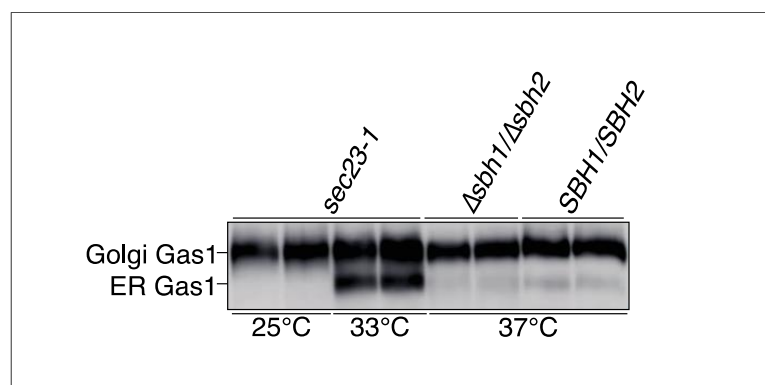


Figure 3.34: Analysis of Gas1 maturation in wildtype, $\Delta sbh1/\Delta sbh2$ and *sec23-1* strains. Cells were grown to an OD₆₀₀ of 0.25 at 30°C, 220 rpm and then cultures were switched to either 37°C (for wildtype and $\Delta sbh1/\Delta sbh2$ mutant strain), 33°C (for *sec23-1* mutant strain, restrictive temperature), or 25°C (for *sec23-1* mutant strain, permissive temperature), 220 rpm, until cultures reached an OD₆₀₀ of 1. After incubation, 1 OD₆₀₀ of cells were collected from each culture, washed with sterile deionized water and extracts were prepared. For each sample 0.4 OD₆₀₀ was resolved by SDS-PAGE, and protein detected by immunoblotting using a Gas1-specific antibodies. Signal was acquired by chemiluminescence using an Amersham Imager 600. All experiments were done in duplicates.

3.4.5 Amino acids transport integrity in $\Delta sbh1/\Delta sbh2$ mutant strain

Several of the *Sbh1*-dependent proteins found in the automated microscopic screen are amino acid transporters in the plasma membrane (Table 3.1, red). I therefore investigated whether the $\Delta sbh1/\Delta sbh2$ mutant had a defect in amino acid transport across the plasma membrane by testing its ability to survive on plates supplemented with metsulfuron-methyl (MM), which is toxic in strains lacking amino acid transporters (Jørgensen *et al.*, 1996). Metsulfuron-methyl blocks the biosynthesis of isoleucine, leucine and valine, which is not an issue for wildtype strains, because YPD is rich in amino acids, so the cells can just import the ones that cannot synthesize. However, if a strain has a defect in the biosynthesis of amino acids transporters, cells cannot grow in YPD supplemented with MM. For this experiment, I used as a control $\Delta shr3$ mutant strain. *Shr3* is a chaperone required for amino acid transporter biosynthesis, and strains lacking *SHR3* cannot grow in YPD supplemented with MM (Kuehn *et al.*, 1998). I prepared sequential dilution of wildtype, $\Delta sbh1/\Delta sbh2$, and $\Delta shr3$ mutant strains and I grew them in duplicates on solid media (YPD and YPD supplemented with MM (200 $\mu\text{g}/\text{ml}$)) at 30°C for 3 days. As expected, $\Delta shr3$ mutant strains was not able to grow in plates of YPD supplemented with MM. I found that $\Delta sbh1/\Delta sbh2$ strain was not sensitive to MM (Figure 3.35), suggesting that amino acid transporter biogenesis was not affected in these cells.

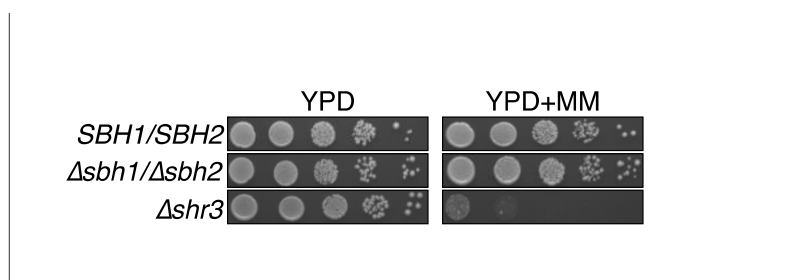


Figure 3.35: Metsulfuron-methyl (MM) sensitivity of $\Delta sbh1/\Delta sbh2$ mutant strains. Wildtype, $\Delta sbh1/\Delta sbh2$ and $\Delta shr3$ mutant strains were grown overnight in YPD at 30°C, 220 rpm. Then, cells were counted using a Neubauer chamber and sequentially diluted (10^4 - 10 cells/ $5\mu\text{l}$). Samples of each dilution ($5\mu\text{l}$) were then plated side by side, in solid media (YPD) and grown for 3 days. Each set was replicated 2 times in different plates, one of the plates supplemented with metsulfuron-methyl (200 $\mu\text{g}/\text{ml}$) and were incubated at 30°C.

3.5 Identification of potential S3/T5 Sbh1 Kinases

3.5.1 High concentrated Urea SDS gels for the Kinase screen

The resolution power of SDS-PAGE for small proteins can be further increased by using high-acrylamide gels and adding urea. Urea, in addition to its general effects on the electrophoretic mobility of proteins in acrylamide gels, seems to alter SDS binding to proteins in a protein-dependent way (*Schägger, 2006*). For unknown reasons, urea reduces the electrophoretic mobility of proteins in general, but the migration of small proteins in particular. Therefore, the resolution of proteins in the low mass range is improved at the cost of a lower resolution for larger proteins (*Rais et al., 2004; Swank et al., 1971*). In my first attempt to identify the kinase responsible for the S3/T5-Sbh1 phosphorylation, I performed electrophoresis on 18% polyacrylamide, 4M urea SDS gels to try to see a difference in the migration pattern of Sbh1, due to the phosphorylation of S3/T5 Sbh1. For this experiment, I first transformed the $\Delta sbh1/\Delta sbh2$ mutant strain with the empty pRS415 plasmid, with pRS415 expressing the wildtype *SBH1*, and with pRS415 expressing different *sbh1* mutants: *sbh1S3A*, *sbh1T5A*, *sbh1T12A*, *sbh1S35D*, and *sbh1S3A/T5A*. Then, I grew cells of each strain to an OD₆₀₀ of 1 at 30°C, 220 rpm. I collected samples from each culture, made protein extracts, and resolved them by electrophoresis on 18% polyacrylamide, 4M urea SDS gels (Section 2.2.8.3). I detected Sbh1 by immunoblotting using specific antibodies that were raised against the first 18 residues of Sbh1 (Sbh1₍₁₋₁₈₎, Figure 3.13) (Table 2.7). I was able to see a change in the migration pattern of Sbh1 in the *sbh1S3A/T5A* mutant strain compared to the wildtype *SBH1* strain (Figure 3.36). That was not the case for any of the other mutants, where no change in migration pattern was seen (Figure 3.36). This may indicate that electrophoresis on 18% polyacrylamide, 4M urea SDS gels could be a useful tool for the Identification of potential S3/T5 Sbh1 Kinases.

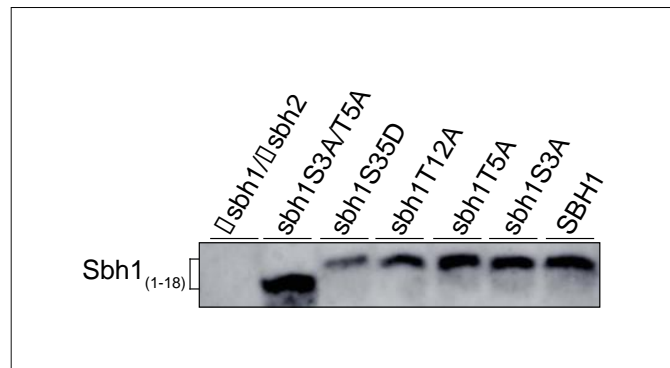


Figure 3.36: Analysis of Sbh1 migration in high concentrated Urea SDS gels for different *sbh1* mutant strains. Cells of wildtype and different *sbh1* mutant strains were grown to an OD₆₀₀ of 1 at 30°C, 220 rpm in minimal media (-Leu, all strains were made by transforming KRY585 ($\Delta sbh1/\Delta sbh2$) with either an empty pRS415 plasmid, or a pRS415 plasmid for expression of wildtype or different mutant versions of *sbh1*). Then, 1 OD₆₀₀ of cells were collected from each culture, washed with sterile deionized water and extracts were prepared. For each sample, 0.4 OD₆₀₀ was resolved by electrophoresis on 18% polyacrylamide, 4M urea SDS gels, and protein detected by immunoblotting using antibody against amino acids 1-18 of Sbh1 (Sbh1₍₁₋₁₈₎). Signal was acquired by chemiluminescence using an Amersham Imager 600.

Since I was not able to see a change in the migration pattern of Sbh1 in any of the *sbh1* mutants, with the exception of *sbh1S3A/T5A*, I investigated whether this change in migration pattern was due to the lack of phosphorylation of S3 and T5 of Sbh1, or is a consequence of the lack on proline isomerization of the P4 and P6. For this experiment, I grew *sbh1S3A/T5A* and *ess1H164R* mutant strains and their correspondent wildtypes, *SBH1* and *W303-1A* strains, either in YPD (for *ess1H164R* mutant strain and *W3031A* wildtype strain) or minimal media (-Leu, since *sbh1S3A/T5A* and *SBH1* were expressed from a pRS415 plasmid) to an OD₆₀₀ of 0.25 at 30°C, 220 rpm. Then I incubated the cultures at 35°C, until cultures reached an OD₆₀₀ of 1. After incubation, I collected samples from each culture, made protein extracts, and resolved them by electrophoresis on 18% polyacrylamide, 4M urea SDS gels (Section 2.2.8.3). I detected Sbh1 by immunoblotting using specific antibodies that were raised against the first 18 residues of Sbh1 (Sbh1₍₁₋₁₈₎, Figure 3.13) (Table 2.7). Again, I was able to see a change in the migration pattern of Sbh1 in the *sbh1S3A/T5A* mutant strain compared to the wildtype *SBH1* strain (Figure 3.37). No change in migration pattern of Sbh1 was observe for *ess1H164R* mutant strains, compared to its wildtype strain, *W303-1A* (Figure 3.37). This indicates that the change in the migration pattern of Sbh1 for *sbh1S3A/T5A* mutant strain is likely due to the lack of phosphorylation of S3 and T5 of Sbh1, and not due to the lack on proline isomerization on the P4 and P6 of Sbh1.

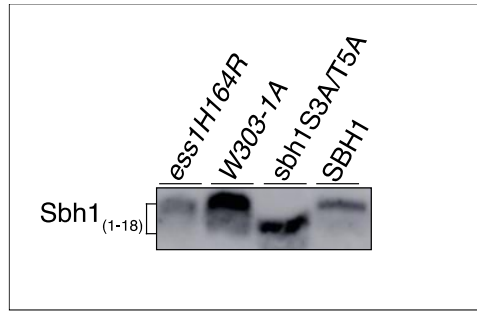


Figure 3.37: Analysis of Sbh1 migration in high concentrated Urea SDS gels for the *ess1H164R* mutant strain. *ess1H164R* and *sbh1S3A/T5A* mutant strains, and their respective wildtypes were grown to an OD_{600} of 0.25 at 30°C, 220 rpm in either YPD (for *ess1H164R* mutant strain and W303-1A wildtype strain) or minimal media (-Leu, *SBH1* wildtype strain and *sbh1S3A/T5A*, expressed from a pRS415 plasmid). Then cultures were switched to 35°C, 220 rpm, until cultures reached an OD_{600} of 1. After incubation, 1 OD_{600} of cells were collected from each culture, washed with sterile deionized water and extracts were prepared. For each sample, 0.4 OD_{600} was resolved by electrophoresis on 18% polyacrylamide, 4M urea SDS gels, and protein detected by immunoblotting using antibody against amino acids 1-18 of Sbh1 (Sbh1₍₁₋₁₈₎). Signal was acquired by chemiluminescence using an Amersham Imager 600.

After several unsuccessful attempts to use Tom22 (phosphorylated by CK1 and dephosphorylated by alkaline phosphatase (AK)) as a proper phosphorylation/dephosphorylation control for this 18% polyacrylamide, 4M urea SDS gels, I decided to change the approach for finding the kinase that phosphorylates S3 and T5 of Sbh1.

3.5.2 Identification of potential S3/T5 Sbh1 Kinase by screening through proline-directed kinases

In order to identify the kinase responsible for the phosphorylation of S3/T5 of Sbh1, my next step was to use the Sbh1_(P) antibody, that recognizes primarily the N-terminal phosphorylated Sbh1, and the Sbh1₍₁₀₋₂₃₎ antibody, that recognizes primarily N-terminally unphosphorylated Sbh1, to screen through loss of function mutants or overexpression mutants of the proline-directed kinases. *Saccharomyces cerevisiae* has 27 different proline-directed kinases (Table 3.3, *Kanshin et al., 2017; Zhang et al., 2019; Zhu et al., 2005; Bradley et al., 2019; Liu et al., 2000; Lin et al., 1996*).

Proline-directed Kinases
Fus3, Kss1, Hog1, Slt2, Smk1, Kdx1, Cdc28 , Pho85, Kin28 , Sgv1, Ctk1, Ssn3, Cak1, Mck1, Ygk3, Mrk1, Ime2, Yak1, Kns1, Sky1, Rck1, Rck2, Rim11, Rim15, Ire1, Cka1, Cka2

Table 3.3: Proline-directed Kinases and other kinases of interest: The 27 different proline-directed kinases and other kinases of interest that are potentially responsible for the S3/T5-Sbh1 phosphorylation, and were tested in different screens.

3.5.2.1 Sbh1 phosphorylation pattern in proline-directed kinases mutants

Initially, a bachelor student from this lab used the Sbh1_(Pi) and the Sbh1₍₁₀₋₂₃₎ antibodies to screen through loss of function mutants in all 27 proline-directed kinases in yeast (Table 3.3). For the non-essential kinases (Slt2, Hog1, Kss1, Fus3, Smk1, Ssn3, Ctk1, Ygk3, Mrk1, Ime2, Rck2, Rck1, Rim15, Rim11, Yak1, Mck1, Kns1, Sky1, Kdx1, Ire1, Pho85, Cka1 and Cka2), knockout mutants were used. For the essential ones (Sgv1, Kin28, Cdc28 and Cak1), different temperature sensitive mutants were used (sgv1-80, kin28-ts and cdc28-1, with 37°C as restrictive temperature; cak1-23 and cdc28-13, with 35°C as restrictive temperature). Unfortunately, she was unable to identify a kinase mutant in which N-terminal Sbh1 phosphorylation was reduced (BSc, Hahn, 2020). I then used the same antibodies to screen for Sbh1 N-terminal hyperphosphorylation in strains overexpressing 20 of these proline-directed kinases. For this experiment, I grew 20 kinase overexpression mutant strains (mutants overexpressing the following kinases: Kns1, Rck1, Rck2, Pho85, Ime2, Ssn3, Hog1, Mck1, Sky1, Yak1, Mrk1, Sgv1, Cak1, Cdc28, Ctk1, Smk1, Kss1, Rim15, Fus3 and Slt2) and their correspondent wildtype strain in YPD to an OD₆₀₀ of 1 at 30°C, 220 rpm. I collected samples from each culture, made the protein extracts, and resolved them by SDS-PAGE (Section 2.2.8). I detected Phosphorylated-Sbh1 using specific antibodies against the phosphorylated N-terminus of Sbh1 (Sbh1_(Pi), Figure 3.13), that recognizes mainly N-terminally phosphorylated Sbh1. I detected unphosphorylated Sbh1 by immunoblotting using specific antibodies that was raised against the amino acids 10 to 23 of Sbh1 (Table 2.7), and recognizes mainly unphosphorylated Sbh1 (Sbh1₍₁₀₋₂₃₎, Figure 3.13). I used Rpn12 as a loading control. I was not able to see any difference between any of the kinase overexpression mutants and the wildtype in neither phosphorylated or unphosphorylated Sbh1 (Figure 3.38).

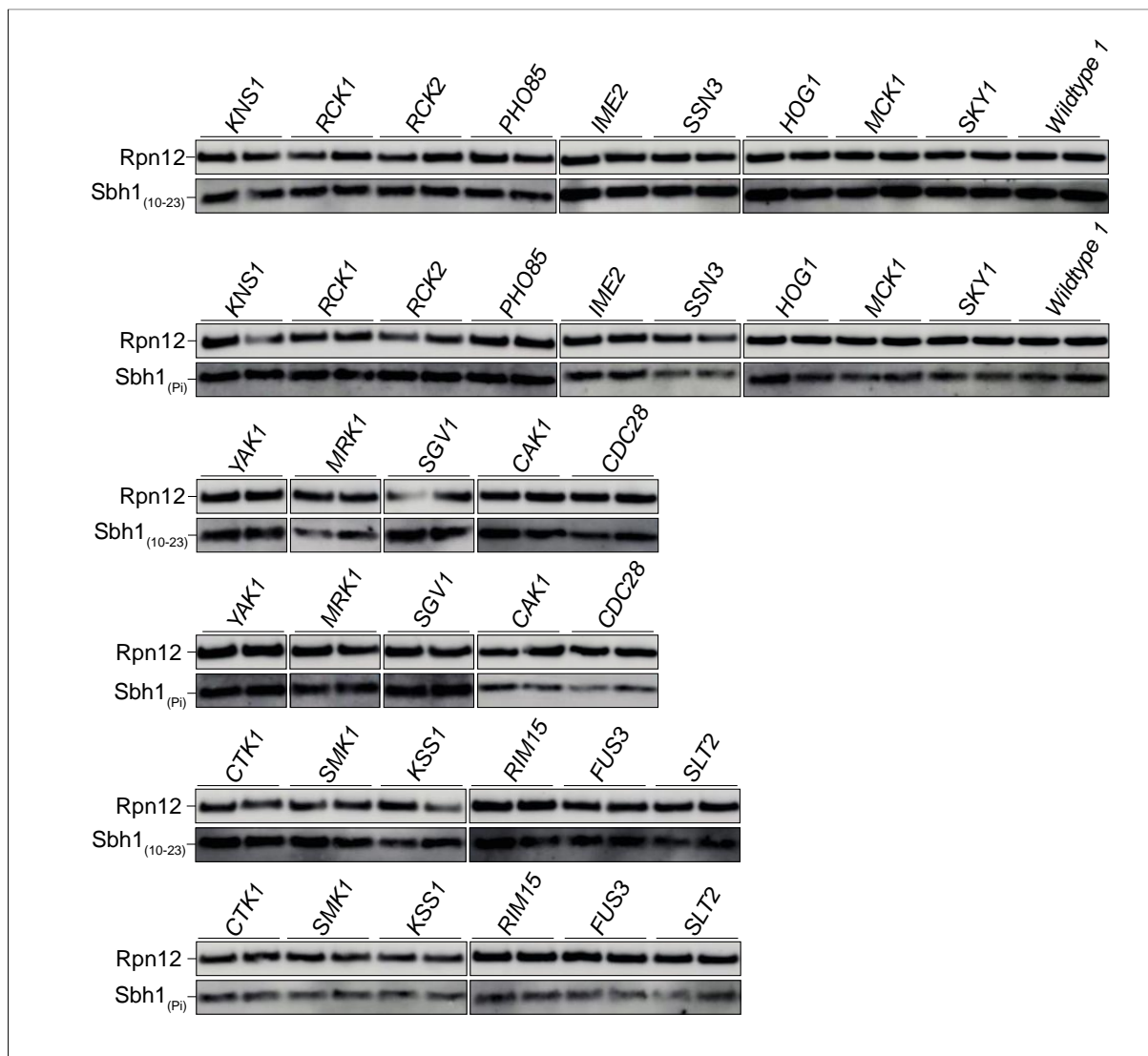


Figure 3.38: Analysis of the Sbh1 phosphorylation pattern in proline-directed kinases overexpression mutants. Cells from 20 kinase overexpression mutant strains were grown to an OD₆₀₀ of 1 at 30°C, 220 rpm in YPD. Then, 1 OD₆₀₀ of cells were collected from each culture, washed with sterile deionized water and extracts were prepared. For each sample, 0.4 OD₆₀₀ was resolved by SDS-PAGE, and protein detected by immunoblotting using either antibody against amino acids 10-23 of Sbh1 (Sbh1₍₁₀₋₂₃₎) or antibody against the phosphorylated N-terminus of Sbh1 (Sbh1_(Pi)). Rpn12-specific antibodies were used for the loading control. Signal was acquired by chemiluminescence using an Amersham Imager 600. All experiments were done in duplicates.

3.5.2.2 Sbh1 phosphorylation pattern in *cka1/cka2* double mutant strain

Casein Kinase II (CKII) of *Saccharomyces cerevisiae* contains two distinct catalytic subunits, α and α' , that are encoded by *CKA1* and *CKA2* genes, respectively (Chester *et al.*, 1995). Disruption of either catalytic subunit gene has no obvious genotype, but disruption of both is lethal (Chen-Wu *et al.*, 1988). I then used a strain with the double mutation $\Delta cka1/\Delta cka2$ transformed with a CEN plasmid expressing either the wildtype *CKA2* gene ($\Delta cka1/CKA2$, KRY1223) or the *cka2-13* temperature sensitive allele ($\Delta cka1/cka2-ts$,

KRY1224) with temperature-sensitivity at 37°C (Rethinaswamy et al., 1996), to check for Sbh1 phosphorylation pattern when there is a loss of function in both subunits. For this experiment, I grew $\Delta cka1/cka2-ts$ mutant strain and its correspondent control, $\Delta cka1/CKA2$ strain; as well as $sbh1S3A/T5A$ mutant strains and its correspondent wildtype strain in minimal media (-leu since $cka2-ts$, and its wildtype $CKA2$, as well as $sbh1S3/T5$ and its wildtype $SBH1$ are express from plasmids with Leu as marker) to an OD₆₀₀ of 0.25 at 30°C, 220 rpm. Then I switched the cultures to 37°C, 220 rpm, until culture reached an OD₆₀₀ of 1. I collected samples from each culture, made extracts, and resolved them by SDS-PAGE (Section 2.2.8). I detected Phosphorylated-Sbh1 using specific antibodies against the phosphorylated N-terminus of Sbh1 (Sbh1_(Pi), Figure 3.13), that recognizes mainly N-terminally phosphorylated Sbh1. I detected unphosphorylated Sbh1 by immunoblotting using specific antibodies that was raised against the amino acids 10 to 23 of Sbh1 (Table 2.7), and recognizes mainly unphosphorylated Sbh1 (Sbh1₍₁₀₋₂₃₎, Figure 3.13). I used Rpn12 as a loading control. As expected, I was able to see a reduction in the Sbh1_(Pi) signal for $sbh1S3A/T5A$ mutant strains, since Sbh1_(Pi) antibody recognizes mainly N-terminally phosphorylated Sbh1 (Figure 3.15A), and a more intense Sbh1₍₁₀₋₂₃₎ signal for $sbh1S3A/T5A$ mutant strains, since the Sbh1₍₁₀₋₂₃₎ antibody recognizes primarily N-terminally unphosphorylated Sbh1 (figure 3.15B). I was not able to see any difference between $cka1/cka2-ts$ and its control, $\Delta cka1/CKA2$ in neither phosphorylated or unphosphorylated Sbh1 (Figure 3.39).

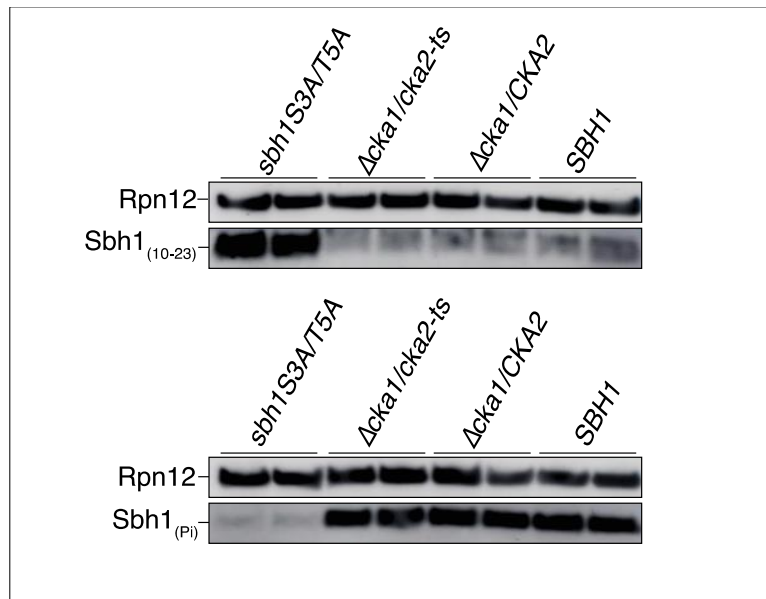


Figure 3.39: Analysis of the Sbh1 phosphorylation pattern in *cka1/cka2* mutant strain. Cells from $\Delta cka1/cka2-ts$, *sbh1S3A/T5A* mutant strains and their respective controls were grown to an OD_{600} of 0.25 at 30°C, 220 rpm in minimal media (-leu, since *cka2-ts* and its wildtype *CKA2*; as well as *sbh1S3/T5* and its wildtype *SBH1* are expressed from plasmids with Leu as marker). Cultures were switched to 37°C, 220 rpm, until cultures reached an OD_{600} of 1. Then, 1 OD_{600} of cells were collected from each culture, washed with sterile deionized water and extracts were prepared. For each sample, 0.4 OD_{600} was resolved by SDS-PAGE, and protein detected by immunoblotting using either antibody against amino acids 10-23 of Sbh1 ($Sbh1_{(10-23)}$) or antibody against the phosphorylated N-terminus of Sbh1 ($Sbh1_{(Pi)}$). Rpn12-specific antibodies were used for the loading control. Signal was acquired by chemiluminescence using an Amersham Imager 600. All experiments were done in duplicates.

3.5.2.3 Sbh1 phosphorylation pattern using γ -[^{32}P]ATP

In order to identify the kinase responsible for the phosphorylation of S3/T5 of Sbh1, my next step was to use γ -[^{32}P]ATP to phosphate label Sbh1 and screen through all the loss of function proline-directed kinase mutants. For doing this, first I investigated whether I would be able to see a difference in phosphate labelled Sbh1, after immunoprecipitation with Sbh1 specific antibodies and resolving by SDS-PAGE and autoradiography. For this experiment, I first transformed the $\Delta sbh1/\Delta sbh2$ mutant strain with pRS415 expressing the wildtype *SBH1*, and with pRS415 expressing the *sbh1S3A/T5A* mutant. I then prepared microsomes from these strains and I labelled the membranes using γ -[^{32}P]ATP and phosphatase inhibitors. After labelling, I performed an immunoprecipitation of Sbh1 with anti-Sbh1 serum raised by this lab against the first 18 amino acids of Sbh1. After precipitation, I resolved the samples by SDS-PAGE and I analysed the specific signals by autoradiography (Section 2.2.12). As can be seen in Figure 3.40, I was not able to see a reduction in the signal for the *sbh1S3A/T5A* mutant strain, compare to the wildtype *SBH1* strain, suggesting that the phosphorylated residues of Sbh1 are not only S3 and T5. Since I was not able to use this

method for the screen of the kinase responsible for the phosphorylation of S3/T5 of Sbh1, I decided to change the approach of my screening.

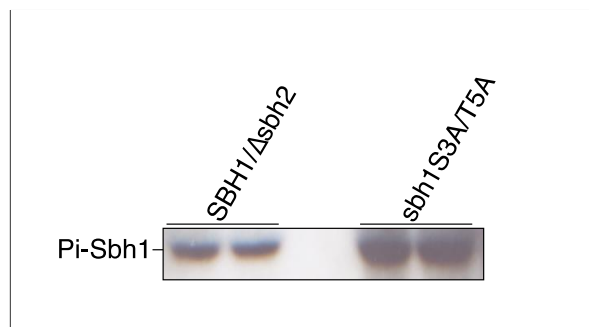


Figure 3.40: Analysis of Sbh1 phosphorylation pattern in *sbh1S3A/T5A* mutant strain. Equal amounts of microsomes (5eq) of each strain were labelled using γ -[32 P]ATP (40 μ Ci) and phosphatase inhibitors for 30 minutes at 30°C and then sedimented. After sedimentation, membranes were resuspended in 2% SDS and incubated at 65°C for 10 minutes. proteins were immunoprecipitated with specific antibodies against N-terminal Sbh1 (Sbh1₍₁₋₁₈₎). After SDS-PAGE, proteins were detected by exposing the gels to phosphorimager plates and signal acquired in Typhoon Trio™ Variable Mode Imager. All experiments were done in duplicates.

3.5.2.4 Screen with Mns1SP Δ gp α F reporter construct in proline-directed kinases mutants

3.5.2.4.1 Mns1SP Δ gp α F construct

In order to screen for the kinase responsible for the S3/T5 Sbh1 phosphorylation, I made a reporter construct by fusing the signal sequence of the Sbh1 phosphorylation-dependent substrate Mns1 to a mutant alpha factor precursor without glycosylation sites (Mns1 Δ gp α F) (Figure 3.41).

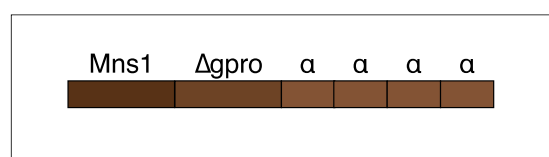


Figure 3.41: Reporter construct scheme. Schematic representation of the Sbh1 S3/T5 phosphorylation-dependent reporter construct Mns1 Δ gp α F. Mns1 signal sequence (Mns1, dark brown), mutant pro region lacking N-glycosylation sites (Δ gpro, brown), alpha factor repeats (α , light brown) are indicated.

For doing that, I first extracted the empty p416 plasmid (CEN plasmid for expression) and p416p Δ gp α F from KRB125 and KRB551 respectively. Afterwards, I amplified the future insert. The insert has the EcoRI recognition site, followed by the first 57 nucleotides of Mns1 (codifying for the Mns1 signal sequence), fused with the mutant alpha factor precursor without glycosylation sites and without its signal sequence (Δ gp α F). For this PCR reaction I used as DNA template the p416p Δ gp α F plasmid, extracted from KRB551 and primers

EcoRIMns1 α FFw and M13Fw. EcoRIMns1 α FFw primer has the EcoRI recognition site followed by the first 57 nucleotides of Mns1 (codifying for the Mns1 signal sequence), fused to 18 nucleotides from pp α F gene (from nucleotide 61 to nucleotide 78). This 18-nucleotide region is the one annealing the p416 Δ gp α F plasmid. I then performed a restrictive digestion of the amplicon from the PCR reaction using Sall and EcoRI restriction enzymes, and clean the digested PCR product (about 1400 bp). In parallel, I performed a restrictive digestion of the empty p416 plasmid, extracted from KRB125, using Sall and EcoRI restriction enzymes, and I ran the fragments on an agarose gel. I recovered the DNA fragment form the agarose gels (about 4.870 bp). After recovery of both DNA fragments (empty p416 and insert), I ligated them generating the vector with my insert, p416Mns1 Δ gp α F (Figure 3.42). I transformed chemically competent *E. Coli* with the ligation mix, and plated the transformed bacteria in LB plates supplemented with ampicillin (100 μ g/ml). I then performed a colony PCR using the M13 primers. Finally, to verify I extracted the plasmids form the positive clones and sent them for sequencing (GATC Biotech).

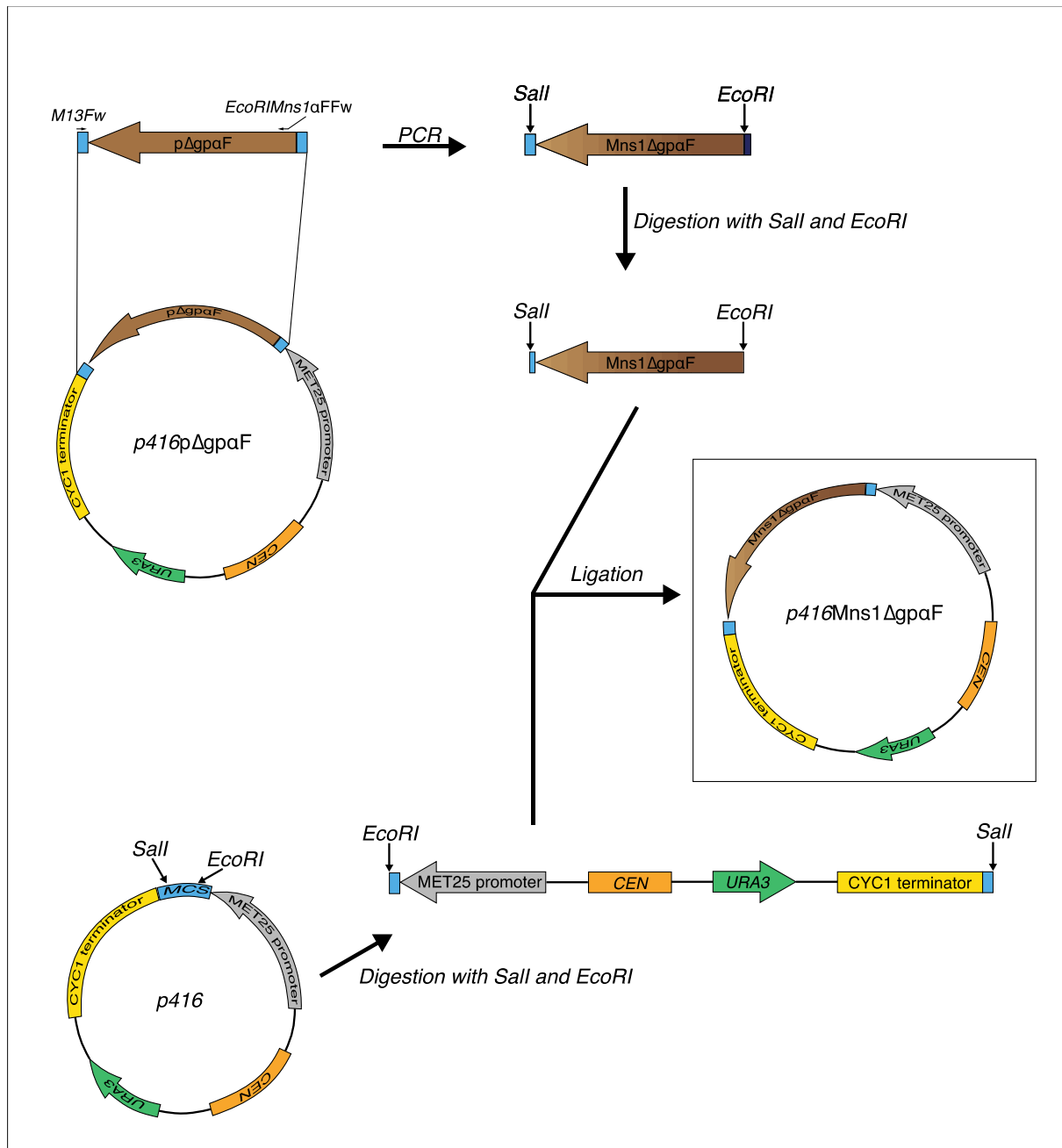


Figure 3.42: Mns1ΔgpaF reporter construct construction scheme. Schematic representation of p416Mns1ΔgpaF construction process. Primers M13Fw and EcoRIMns1αFFw were used in a PCR reaction using as template p416pΔgpaF plasmid extracted from KRB551. The amplicon generated has the EcoRI recognition site, followed by the first 57 nucleotides of Mns1 (codifying for the Mns1 signal sequence), fused with mutant alpha factor precursor without glycosylation sites and without its signal sequence (ΔgpaF) and finally the Sall recognition site. Empty p416 and amplicon generated in the PCR reaction were digested with EcoRI and Sall restriction enzymes. After recovering, DNA fragments were ligated to generate the p416Mns1ΔgpaF plasmid. pΔgpaF (brown), Mns1ΔgpaF (gradient brown), URA3 gene (green), multiple cloning site (blue), CYC1 terminator (yellow), centromere (orange), MET25 promoter (grey), and EcoRI and Sall recognition sequences are shown.

3.5.2.4.2 Characterization of Mns1SPΔgpaF construct in *sbh1* mutant strains

After making the reporter construct, I characterize it in our *sbh1* mutant strains. For this experiment, I first transformed wildtype, $\Delta sbh1/\Delta sbh2$, $\Delta sbh1/SBH2$, $SBH1/\Delta sbh2$ and

sbh1S3A/T5A mutant strains with my p416Mns1 Δ gpaF vector. I grew cells of each strain in minimal media (-ura for all the strains transformed with the reporter construct vector, with the exception of *sbh1S3/T5*; -ura-leu for *sbh1S3/T5*, that also express the mutant Sbh1 from a pRS415 plasmid) to an OD₆₀₀ of 0.25, at 30°C, 220 rpm and then I switched the cultures to 37°C, 220 rpm, until culture reached an OD₆₀₀ of 1. Then, I collected samples from each culture, made extracts, and resolved them by SDS-PAGE (Section 2.2.8). I detected p α -Factor by immunoblotting with specific antibodies (Table 2.7). I was able to see precursor accumulation in Δ *sbh1*/ Δ *sbh2*, Δ *sbh1*/*SBH2* and *sbh1S3A/T5A* mutant strains (Figure 3.43, upper band), but not in wildtype and *SBH1*/ Δ *sbh2* mutant strain.

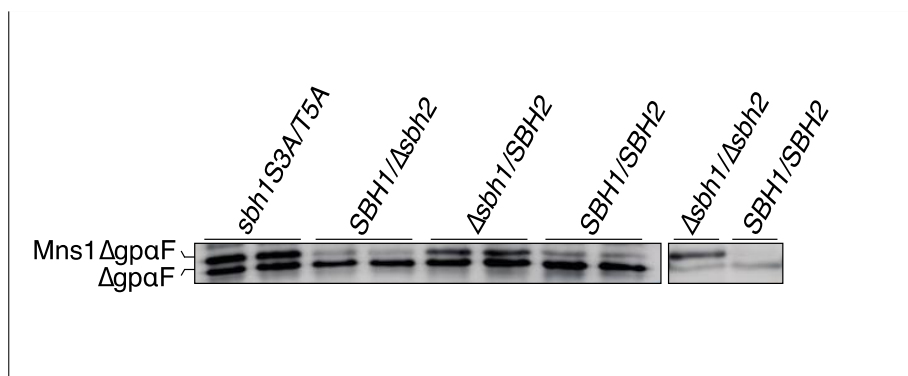


Figure 3.43: Characterization of Mns1 Δ gpaF reporter construct in *sbh1* mutant strains. Cells were grown in minimal media (-ura for all the strains transformed with the reporter construct vector, with the exception of *sbh1S3/T5*; -ura-leu for *sbh1S3/T5*, that express the mutant *sbh1* from a pRS415 plasmid) to an OD₆₀₀ of 0.25 at 30°C, 220 rpm, then incubated at 37°C, until cultures reached an OD₆₀₀ of 1. After incubation, 1 OD₆₀₀ of cells were collected from each culture, washed with sterile deionized water and extracts were prepared. For each sample, 0.4 OD₆₀₀ was resolved by SDS-PAGE, and protein detected by immunoblotting using a p α F-specific antibodies. Signal was acquired by chemiluminescence using an Amersham Imager 600.

3.5.2.4.3 Screen with Mns1SP Δ gpaF construct

For this experiment, I first transformed *sbh1S3A/T5A* mutant strain, and the 27 proline-directed kinase (Table 3.3) deficient mutants with their respective wildtype strains with my vector expressing the reporter construct (p416Mns1 Δ gpaF). I then grew cells of each strain in minimal media (-ura for all the strains transformed with the reporter construct vector, with the exception of *sbh1S3/T5*; -ura-leu for *sbh1S3/T5*, that also express the mutant Sbh1 from a pRS415 plasmid) to an OD₆₀₀ of 0.25, at 30°C, 220 rpm. For non-essential kinases, I continued growing cells in minimal media to an OD₆₀₀ of 1, at 30°C, 220 rpm. For *sbh1S3A/T5A* mutant strain and the essential kinases, for which I used temperature sensitive mutants, I switched cultures to either 35°C or 37°C, 220 rpm, until culture reached

an OD₆₀₀ of 1. Then, I collected samples from each culture, made extracts, and resolved them by SDS-PAGE (Section 2.2.8). I detected p α -Factor by immunoblotting with specific antibodies (Table 2.7). I found cytosolic precursor accumulation in Δ kns1, Δ mck1, and *cdc28-1* at the restrictive temperature (Figure 3.44), suggesting that these kinases might be involved in Sbh1 N-terminal phosphorylation.

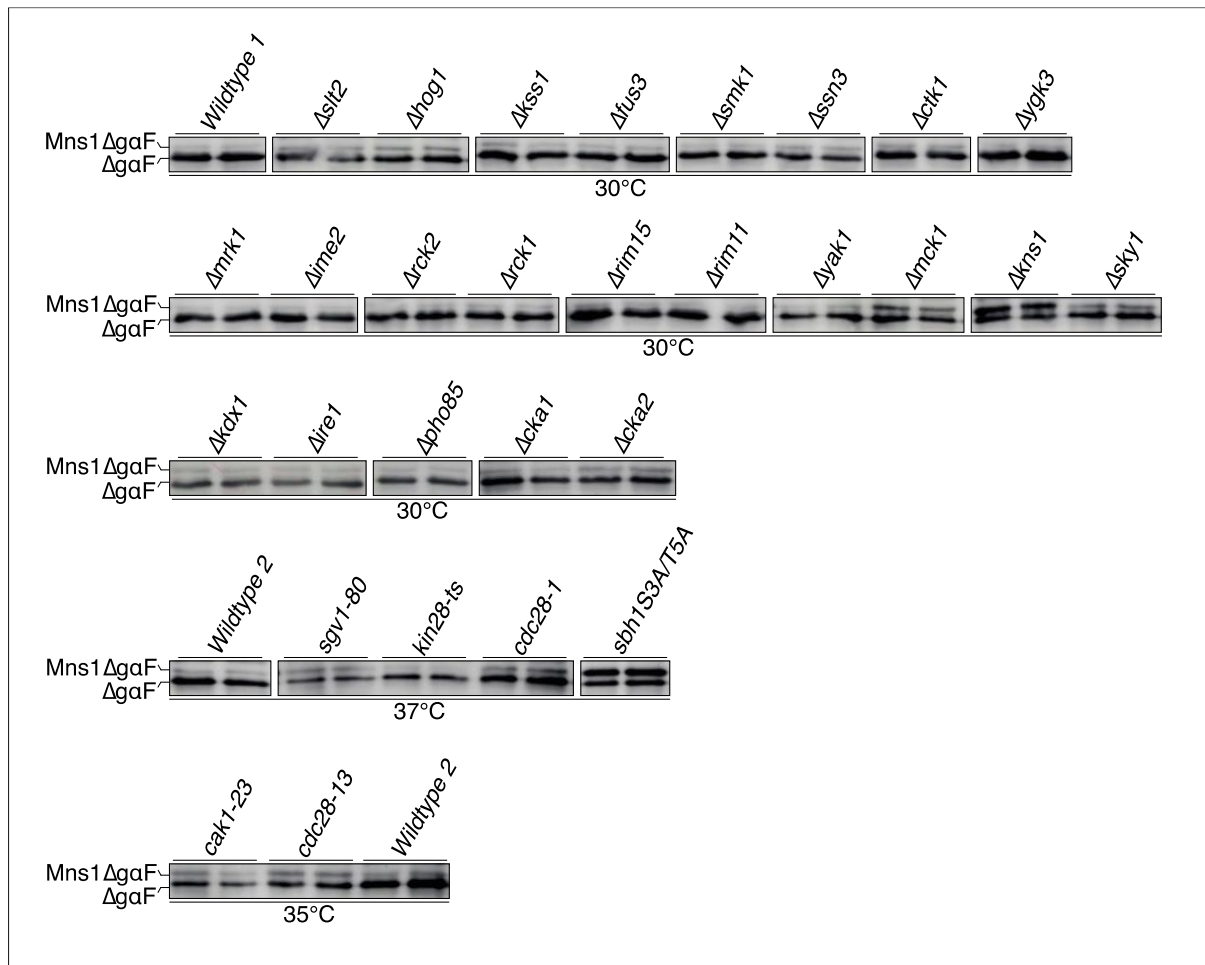


Figure 3.44: Analysis of Mns1 Δ g α F ER import in the proline-directed kinases loss of function mutants. Cells were grown in minimal media (-ura for all the strains transformed with the reporter construct vector, with the exception of *sbh1S3/T5*; -ura-leu for *sbh1S3/T5*, that express the mutant *sbh1* from a pRS415 plasmid) to an OD₆₀₀ of 0.25 at 30°C, 220 rpm. For non-essential kinases, cells were continued growing in minimal media to an OD₆₀₀ of 1, at 30°C, 220 rpm. For *sbh1S3A/T5A* mutant strain and the essential kinases, for which I used temperature sensitive mutants, cultures were switched either to 35°C or 37°C, 220 rpm, until culture reached an OD₆₀₀ of 1. After incubation, 1 OD₆₀₀ of cells were collected from each culture, washed with sterile deionized water and extracts were prepared. For each sample, 0.4 OD₆₀₀ was resolved by SDS-PAGE, and protein detected by immunoblotting using a p α F-specific antibodies. Signal was acquired by chemiluminescence using an Amersham Imager 600. All experiments were done in duplicates.

3.5.2.4.4 Mns1SP Δ g α F construct precursor accumulation in *cka1/cka2* double mutant strain

For this experiment, I first transformed KRY1223 (Δ *cka1*/ Δ *cka2* strain previously transformed with a CEN plasmid expressing the wildtype *CKA2* gene (Δ *cka1*/*CKA2*)),

KRY1224 ($\Delta cka1/\Delta cka2$ strain previously transformed with a CEN plasmid expressing the *cka2-13* temperature sensitive allele ($\Delta cka1/cka2-ts$)), *sbh1S3A/T5A* mutant strains and its correspondent wildtype strain with my vector expressing the reporter construct (p416Mns1 Δ gp α F). I then grew these strains in minimal media (-leu-ura, since *cka2-ts*, and its wildtype *CKA2*, as well as *sbh1S3/T5* and its wildtype *SBH1* are express from plasmids with Leu as marker; and the reporter construct comes from a p416 plasmid) to an OD₆₀₀ of 0.25 at 30°C, 220 rpm. Then I switched the cultures to 37°C, 220 rpm, until culture reached an OD₆₀₀ of 1. I collected samples from each culture, made extracts, and resolved them by SDS-PAGE (Section 2.2.8). I detected p α -Factor by immunoblotting with specific antibodies (Table 2.7). As expected, I was able to see precursor accumulation in *sbh1S3A/T5A* mutant strain, but not in its corresponding wildtype (Figure 3.45). I was not able to see any Mns1 Δ gp α F precursor accumulation in *cka1/cka2-ts* mutant strain and its control, $\Delta cka1/CKA2$ (Figure 3.45), consistent with the lack of change in Sbh1 phosphorylation pattern (Figure 3.39).

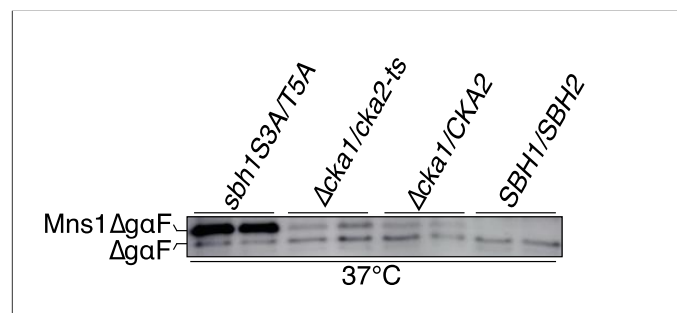


Figure 3.45: Analysis of Mns1 Δ gp α F ER import in *cka1/cka2* mutant strain. Cells from $\Delta cka1/cka2-ts$, *sbh1S3A/T5A* mutant strains and their respective controls, previously transformed with p416Mns1 Δ gp α F, were grown in minimal media (-leu-ura, since *cka2-ts*, and its wildtype *CKA2*, as well as *sbh1S3/T5* and its wildtype *SBH1* are express from plasmids with Leu as marker; and the reporter construct comes from a p416 plasmid) to an OD₆₀₀ of 0.25 at 30°C, 220 rpm. Cultures were switched to 37°C, 220 rpm, until cultures reached an OD₆₀₀ of 1. Then, 1 OD₆₀₀ of cells were collected from each culture, washed with sterile deionized water and extracts were prepared. For each sample, 0.4 OD₆₀₀ was resolved by SDS-PAGE, and protein detected by immunoblotting using a p α F-specific antibodies. Signal was acquired by chemiluminescence using an Amersham Imager 600. All experiments were done in duplicates.

3.6 Kinases mutants potentially involved in Sbh1 N-terminal phosphorylation

3.6.1 Kar2 ER translocation in kinases mutants potentially involved in Sbh1 N-terminal phosphorylation

Next, I investigated whether the effect I saw with the Mns1 Δ gp α F reporter, was specific to the Mns1 signal peptide. For this, I subsequently investigated translocation of the Sbh1-

dependent, but N-terminal phosphorylation-independent translocation substrate pKar2 in these kinase mutants by pulse-labelling. Upon translocation across the ER membrane, the precursor protein (pKar2; 74 KDa) is signal-cleaved to form the mature protein (Kar2; 72 KDa). For this experiment I used $\Delta kns1$, $\Delta mck1$, $cdc28-1$ mutant strains and their respective wildtype strains, as well as the control, $sec61-32$ mutant strain, that has a translocation defect at 20°C. I grew cells of each strain in YPD at either 30°C (for $\Delta kns1$, $\Delta mck1$, and their correspondent wildtype), 37°C (for $cdc28-1$ mutant strain and its correspondent wildtype), or 20°C (for $sec61-32$ mutant strain), 220 rpm, to an OD₆₀₀ of 0.5–1. I then labelled them with [³⁵S]-met/cys for 2.5 min, and I precipitated Kar2 with specific antibodies (Table 2.7). I ran the samples on 7.5 % Bis-Tris SDS gel and I analysed the specific signals by autoradiography (Section 2.2.12). As expected, I saw a strong pKar2 translocation defect in the $sec61-32$ control strain. nevertheless, none of the kinase mutants had defects in pKar2 translocation (Figure 3.46), suggesting that the observed effect with the reporter was specific to the Mns1 signal peptide.

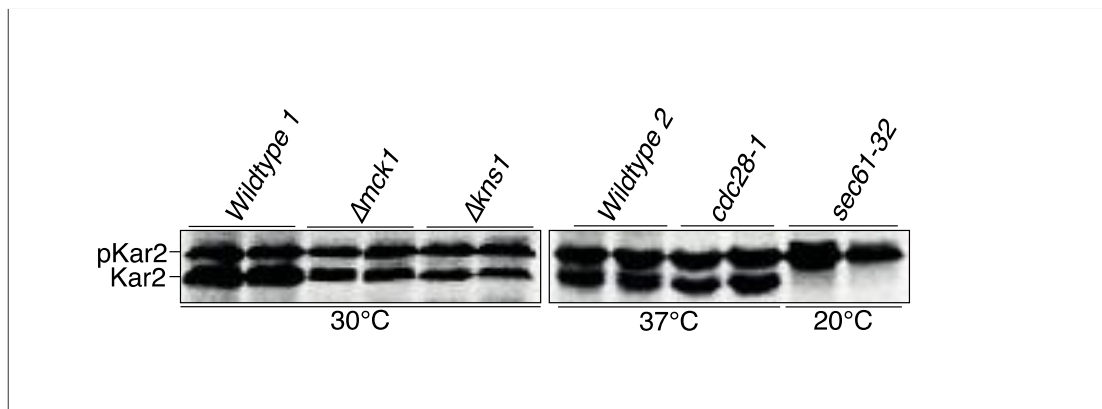


Figure 3.46: Analysis of the Kar2 ER translocation in proline-directed kinase deficient mutants potentially involved in Sbh1 N-terminal phosphorylation. Cells were grown in YPD at 30°C (for $\Delta kns1$, $\Delta mck1$, and their correspondent wildtype), 37°C (for $cdc28-1$ mutant strain and its correspondent wildtype), or 20°C (for $sec61-32$ mutant strain), 220 rpm, to an OD₆₀₀ of 0.5–1. Then cells were labelled with [³⁵S]-met/cys for 2.5 min. 1.5 OD₆₀₀ of cells were lysed and proteins immunoprecipitated with specific antibodies against Kar2. After SDS-PAGE, proteins were detected by exposing the gels to phosphorimager plates and signal acquired in Typhoon Trio™ Variable Mode Imager. All experiments were done in duplicates.

3.6.2 General protein translocation defect check in kinases mutants potentially involved in Sbh1 N-terminal phosphorylation

3.6.2.1 Post-translationally translocated substrate: pre-pro- α -factor

Next, I investigated whether these kinase mutations resulted in a general protein translocation defect. For this purpose, I investigated the cytosolic precursor accumulation of ER translocation substrates. I first evaluated the translocation of a well characterized post-translationally translocated substrate pre-pro- α -factor (pp α F) by Western blotting with pp α F-specific antibodies in these kinase mutant strains. wild-type pp α F (18 KDa) is imported post-translationally into the ER where the signal sequence is cleaved off by a signal peptidase (*Walter et al., 1988*). The resulting pro- α -factor (p α F; 16 KDa) is N-glycosylated at three different sites upon entry into the ER and the glycosylated form is rapidly transported into the Golgi, where it is proteolytically cleaved to release the 13 amino acid α -factor (α F). Hence the precursor form is only detectable in cells with ER import or ER-to-Golgi transport defects (*Stirling et al., 1992*). For this experiment, I used $\Delta kns1$, $\Delta mck1$, *cdc28-1*, *cdc28-13* (another *cdc28* temperature sensitive mutant) mutant strains and their respective wildtype strains, as well as the control (*sec61-32* mutant strain). I grew cells of each strain to an OD₆₀₀ of 0.25 at 30°C, 220 rpm. I then incubated them either at 30°C (for $\Delta kns1$, $\Delta mck1$, and their correspondent wildtype), 37°C (for *cdc28-1*, *cdc28-13* and their correspondent wildtype), or 20°C (for *sec61-32* mutant strain), until cultures reached an OD₆₀₀ of 1. After incubation, I collected samples from each culture, made extracts, and resolved them by SDS-PAGE (Section 2.2.8). I then immunoblotted with pp α F-specific antibodies (Table 2.7). I used Rpn12 as a loading control. As can be seen in Figure 3.47, there was cytosolic accumulation of the precursor in a *sec61-32* mutant, that has a translocation defect at 20°C, but there was no accumulation of the cytosolic pp α F in any of the kinase mutants or in their correspondent wildtypes.

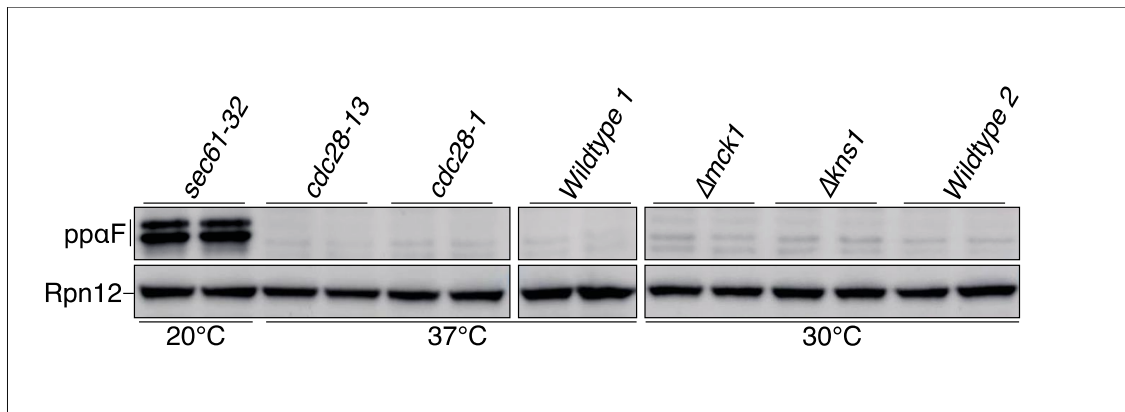


Figure 3.47: Analysis of ppaF ER import in proline-directed kinase deficient mutants potentially involved in Sbh1 N-terminal phosphorylation. Cells were grown in YPD to an OD₆₀₀ of 0.25 at 30°C, 220 rpm, then incubated either at 30°C (for *Δkns1*, *Δmck1*, and their correspondent wildtype), 37°C (for *cdc28-1*, *cdc28-13* and their correspondent wildtype), or 20°C (for *sec61-32* mutant strain), until cultures reached an OD₆₀₀ of 1. After incubation, 1 OD₆₀₀ of cells were collected from each culture, washed with sterile deionized water and extracts were prepared. For each sample, 0.4 OD₆₀₀ was resolved by SDS-PAGE, and protein detected by immunoblotting using a ppaF-specific antibodies and Rpn12-specific antibodies (loading control). Signal was acquired by chemiluminescence using an Amersham Imager 600. All experiments were done in duplicates.

3.6.2.2 Co-translationally translocated substrate: Diaminopeptidase B

Then, I looked at a co-translationally translocated substrate Diaminopeptidase B (DPAPB), which is a type II membrane protein with an N-terminal transmembrane domain (Pilon *et al.*, 1998). Upon co-translational integration into the ER membrane, the precursor protein (pDPAPB; 96 KDa) is core-glycosylated to form the mature protein (DPAPB; 120 KDa) (Roberts *et al.*, 1989). If DPAPB is efficiently integrated, its precursor form is undetectable, making it a typical substrate to test co-translational translocation impairments. For this experiment I used *Δkns1*, *Δmck1*, *cdc28-1* mutant strains and their respective wildtype strains, as well as the control (*sec61-32* mutant strain). To evaluate the translocation dynamics of DPAPB, I pulse-labelled the cells as follow: I grew cells of each strain were grown in YPD at either 30°C (for *Δkns1*, *Δmck1*, and their correspondent wildtype strain; also, for *sec61-32* mutant strain, permissive temperature), 37°C (for *cdc28-1* mutant strain and its correspondent wildtype strain), or 20°C (for *sec61-32* mutant strain, restrictive temperature), 220 rpm, to an OD₆₀₀ of 0.5–1. I then labelled the cells with [³⁵S]-met/cys for 15 min After labelling, I immunoprecipitated DPAPB with specific antibodies (Table 2.7). After precipitation, I ran the samples on 7.5 % Bis-Tris SDS gel and I analysed the specific signals by autoradiography (Section 2.2.12). Again, in the *sec61-32* mutant there was accumulation of the cytosolic DPAPB precursor at 20°C, but there was no accumulation of

precursor in *sec61-32* grown at 30°C, in any of the kinase mutant strains or in their correspondent wildtype strains (Figure 3.48).

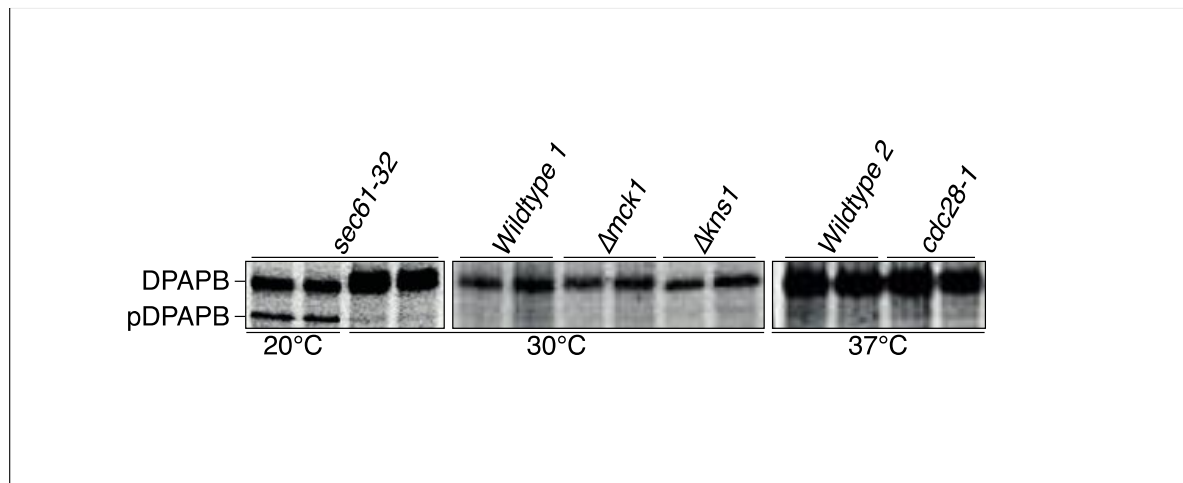


Figure 3.48: Analysis of the DPAPB ER translocation import in proline-directed kinase deficient mutants potentially involved in Sbh1 N-terminal phosphorylation. Cells were grown in YPD at either 30°C (for *Δkns1*, *Δmck1*, and their correspondent wildtype strain; also, for *sec61-32* mutant strain, permissive temperature), 37°C (for *cdc28-1* mutant strain and its correspondent wildtype strain), or 20°C (for *sec61-32* mutant strain, restrictive temperature), 220 rpm, to an OD₆₀₀ of 0.5–1, then labelled with [³⁵S]-met/cys for 15 min. 1.5 OD₆₀₀ of cells were lysed and proteins immunoprecipitated with specific antibodies against DPAPB. After SDS-PAGE, proteins were detected by exposing the gels to phosphorimager plates and signal acquired in Typhoon Trio™ Variable Mode Imager. All experiments were done in duplicates.

Both post-translational import of wildtype ppαF and co-translational import of pDPAPB was functional in these kinase mutants and I did not see any precursor accumulation (Figure 3.47 and Figure 3.48), suggesting the kinase mutations do not cause general translocation defects.

3.6.3 Tunicamycin sensitivity in kinases mutants potentially involved in Sbh1 N-terminal phosphorylation

Since mannosidase I (Mns1) contribute to protein quality control in the ER, I next investigated whether kinase mutants that have a defect in Mns1ΔgpαF translocation (*Δkns1*, *Δmck1*, and *cdc28-1*) showed any tunicamycin (TM) sensitivity. Tunicamycin interferes with N-linked glycosylation in the ER which often is a prerequisite for protein folding. Hence tunicamycin-sensitivity is often indicative of perturbations in ER proteostasis (Tran et al., 2011; Servas et al., 2013). For *cdc28-1* mutant strain, it was not possible to perform this experiment, because when growing at restrictive temperature (37°C), cells would not be able to grow since this kinase is essential. For the experiment using only non-essential kinase mutants (*Δkns1* and *Δmck1* mutant strains), I prepared sequential dilution

of $\Delta kns1$ and $\Delta mck1$ mutant strains, as well as the corresponding wildtype strain and grew them in duplicates on solid media (YPD and YPD+TM (0.5 $\mu\text{g/ml}$)) at 30°C for 3 days. My results show that there was a very mild effect in growth of $\Delta mck1$ mutant strain in the presence of 0.5 $\mu\text{g/ml}$ of tunicamycin, while $\Delta kns1$ mutant strain was not sensitive to TM (Figure 3.49).

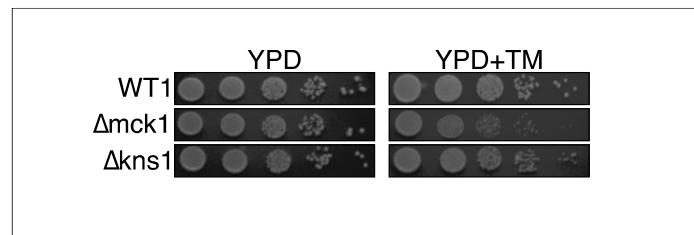


Figure 3.49: Tunicamycin (TM) sensitivity of proline-directed kinase deficient mutants potentially involved in Sbh1 N-terminal phosphorylation. Cells were grown overnight in YPD at 30°C, 220 rpm. Then, cells were counted using a Neubauer chamber and sequentially diluted (10^4 -10 cells/ $5\mu\text{l}$). Samples of each dilution (5 μl) were then plated side by side, in solid media (YPD) and grown for 3 days. Each set was replicated 2 times in different plates, one of the plates supplemented with tunicamycin (0.5 $\mu\text{g/ml}$) and were incubated at 30°C.

3.6.4 Gls1 ER import in kinases mutants potentially involved in Sbh1 N-terminal phosphorylation

I then investigated whether the proline-directed kinase mutants affected the levels of endogenous Gls1 in the ER. I tested whether there is a specific Gls1 import defect in any of the three proline-directed kinase deficient mutants that showed to be potentially involved in Sbh1 N-terminal phosphorylation. I used for this experiment these three mutant strains ($\Delta kns1$, $\Delta mck1$, $cdc28-1$), and three randomly chosen proline-directed kinase deficient mutant strains that showed not to be involved in Sbh1 N-terminal phosphorylation ($\Delta yak1$, $\Delta rim11$ and $\Delta rck2$). I also used the respective wildtype strains for the kinase mutants (as negative controls) and the $sbh1S3A/T5A$ mutant strain (as a positive control). I looked at the steady state amount of Gls1 by Western blotting with specific antibodies. For doing this, I grew cells of each strain either in YPD or minimal media (-leu for $sbh1S3A/T5A$ mutant strain) to an OD_{600} of 0.25, at 30°C, 220 rpm. For non-essential kinases, I continued growing cells to an OD_{600} of 1, at 30°C, 220 rpm. For $sbh1S3A/T5A$ mutant strain and the essential kinases, for which I used temperature sensitive mutants, I switched cultures to 37°C, 220 rpm, until culture reached an OD_{600} of 1. Then, I collected samples from each culture, made extracts, and resolved them by SDS-PAGE (Section 2.2.8). I detected Gls1 by immunoblotting using Gls1-specific antibodies (table 2.7). I used Rpn12 as a loading control. In contrast to

the *sbh1S3A/T5A* mutation which reduces Gls1 to around 50% of wildtype levels (Figure 3.10), none of the kinase mutants identified in my screen significantly affected Gls1 levels in the ER of the mutants (Figure 3.50).

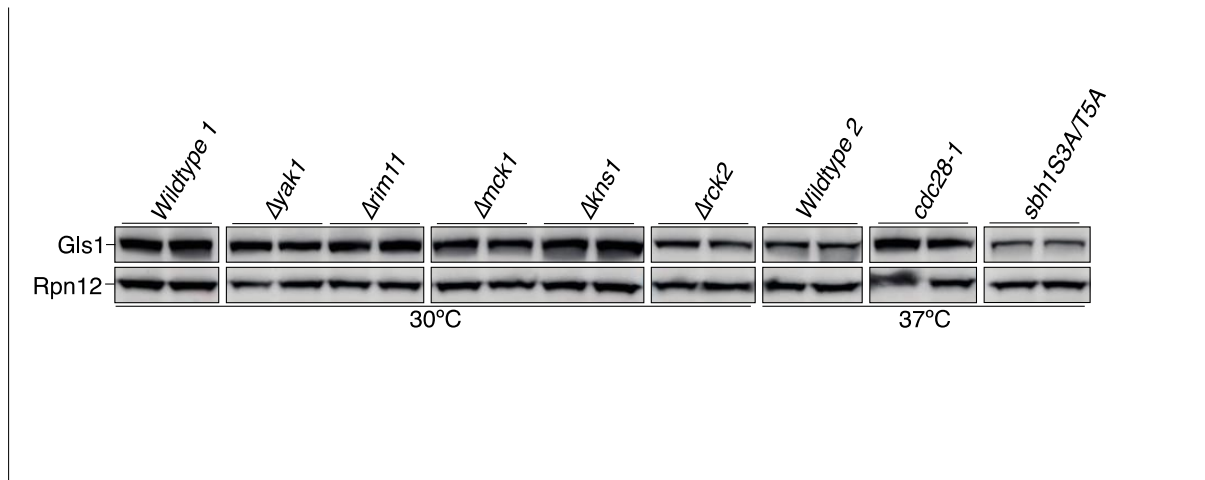


Figure 3.50: Analysis of the Gls1 ER translocation in proline-directed kinase deficient mutants potentially involved in Sbh1 N-terminal phosphorylation. Cells were grown in YPD (for wildtype strains and kinase mutant strains) or minimal media (-leu; for *sbh1S3A/T5A* mutant strain, which is integrated on a pRS415 plasmid) to an OD₆₀₀ of 0.25 at 30°C, 220 rpm, then incubated either at either 30°C (for non-essential kinases) or 37°C (for *sbh1S3A/T5A* mutant strain and the essential kinases, for which I used temperature sensitive mutants), until cultures reached an OD₆₀₀ of 1. Then, 1 OD₆₀₀ of cells were collected from each culture, washed with sterile deionized water and extracts were prepared. For each sample 0.4 OD₆₀₀ was resolved by SDS-PAGE, and protein detected by immunoblotting using a Gls1-specific antibodies and Rpn12-specific antibodies (loading control). Signal was acquired by chemiluminescence using an Amersham Imager 600. All experiments were done in duplicates.

3.6.5 GST-Gls1 ER import in kinases mutants potentially involved in Sbh1 N-terminal phosphorylation

In addition, since I could not distinguish the cytosolic precursor and the ER form of Gls1 on SDS gels, I investigated Gls1 translocation in these cells with a reporter that had glutathione-S-transferase (GST) fused to the N-terminus of the Gls1 signal peptide (Figure 3.51A) to generate a protein with a more pronounced size difference between cytosolic precursor and signal-cleaved ER-form (Figure 3.51B, *Shibuya et al., 2015*).

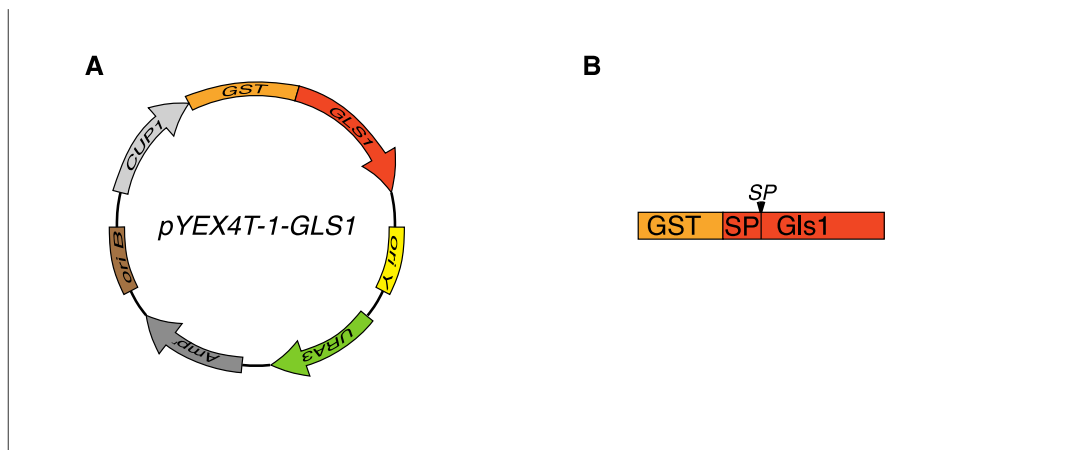


Figure 3.51: pYEX4T-1-GLS1 Scheme: (A) Schematic representation of pYEX4T-1-GLS1 plasmid. *URA3* gene (green), *GST* (orange), *GLS1* gene (red), yeast replication origin (yellow), bacterial replication origin (brown), CUP1 promoter (light grey), and ampicillin resistance (dark grey) are shown. (B) Schematic representation of GST-Gls1 fusion protein. *GST* (orange), *GLS1* gene with its signal peptide (SP) (red), and signal cleavage site (SP) are also shown.

First, I investigated whether I could see the GST-Gls1 accumulation on $\Delta sbh1/\Delta sbh2$ and *sbh1S3A/T5A* mutant strains. For doing this, I transformed wildtype, $\Delta sbh1/\Delta sbh2$ and *sbh1S3A/T5A* mutant strains with pYEX4T-1-GLS1 (reporter that had GST fused to the N-terminus of the Gls1 signal peptide). I then grew cells of each strain in minimal media (-Ura, for wildtype and $\Delta sbh1/\Delta sbh2$ mutant strain; -ura-leu, for *sbh1S3A/T5A* mutant strain) to an OD₆₀₀ of 0.25 at 30°C, 220 rpm and then I switched cultures to 37°C, 220 rpm, until culture reached an OD₆₀₀ of 1. Then, I collected samples from each culture, made extracts, and resolved them by SDS-PAGE (Section 2.2.8). I detected Gls1 by immunoblotting with specific antibodies (Table 2.7). As expected, I was able to see accumulation of GST-pGls1 precursor in the cytosol on the $\Delta sbh1/\Delta sbh2$ and *sbh1S3A/T5A* mutant strains, but not on the correspondent wildtype strain (Figure 3.52). This result confirmed that transport of Gls1 into the ER is dependent not only on the presence of Sbh1, but also on its phosphorylation at S3 and T5, and also provided me another method to test whether there is a specific Gls1 import defect in any of the three proline-directed kinase deficient mutants that showed to be potentially involved in Sbh1 N-terminal phosphorylation.

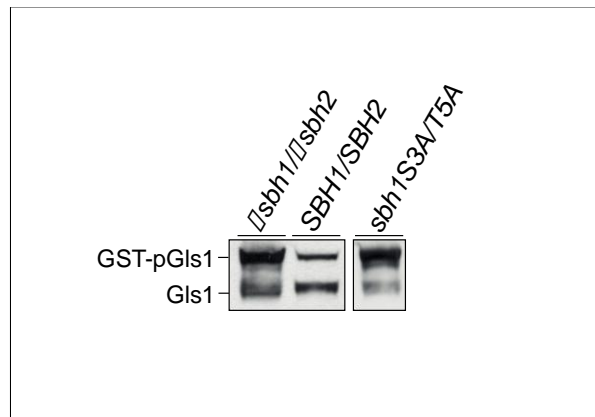


Figure 3.52: Analysis of the GST-Gls1 ER translocation in wildtype, *Δsbh1/Δsbh2* and *sbh1S3A/T5A* mutant strains. Cells were grown in minimal media to an OD₆₀₀ of 0.25 at 30°C, 220 rpm. For wildtype or *Δsbh1/Δsbh2* mutant strain, -ura media was used. For *sbh1S3A/T5A* mutant strain, which has the *sbh1* mutant gene integrated on a pRS415 plasmid, -ura-leu media was used. Cells were then incubated at 37°C for until OD₆₀₀ of 1. After incubation, 1 OD₆₀₀ of cells were collected from each culture, washed with sterile deionized water and extracts were prepared. For each sample 0.4 OD₆₀₀ was resolved by SDS-PAGE, and protein detected by immunoblotting using a Gls1-specific antibodies. Signal was acquired by chemiluminescence using an Amersham Imager 600.

Next, I investigated whether there was a specific GST-pGls1 import defect in any of the three proline-directed kinase deficient mutants that showed to be potentially involved in Sbh1 N-terminal phosphorylation. For doing this, I transformed these three mutant strains (*Δkns1*, *Δmck1*, *cdc28-1*), and three randomly chosen proline-directed kinase deficient mutant strains that showed not to be involved in Sbh1 N-terminal phosphorylation (*Δyak1*, *Δrim11* and *Δrck2*) with pYEX4T-1-GLS1 (reporter that had GST fused to the N-terminus of the Gls1 signal peptide). I also transformed the respective wildtype strains for the kinase mutants (as negative controls) and the *sbh1S3A/T5A* mutant strain (as a positive control) with the same vector, pYEX4T-1-GLS1. I then grew cells of each strain in minimal media (-Ura, for wildtype and all the kinase mutant strains; -ura-leu, for *sbh1S3A/T5A* mutant strain) to an OD₆₀₀ of 0.25 at 30°C, 220 rpm. For non-essential kinase mutants, I continued growing cells to an OD₆₀₀ of 1, at 30°C, 220 rpm. For *sbh1S3A/T5A* mutant strain and the essential kinase mutants, for which I used temperature sensitive mutants, I switched cultures to 37°C, 220 rpm, until culture reached an OD₆₀₀ of 1. Then, I collected samples from each culture, made extracts, and resolved them by SDS-PAGE (Section 2.2.8). I detected Gls1 by immunoblotting using Gls1-specific antibodies (Table 2.7). again, I was able to see accumulation of GST-pGls1 precursor in the cytosol on *sbh1S3A/T5A* mutant strains, but not in the proline-directed kinase mutants (Figure 3.53).

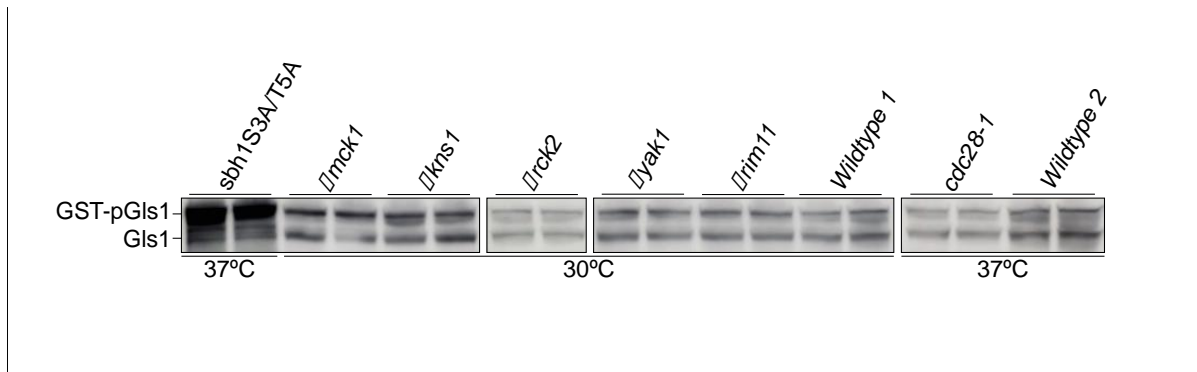


Figure 3.53: Analysis of the GST-Gls1 ER translocation in proline-directed kinase deficient mutants potentially involved in Sbh1 N-terminal phosphorylation. Cells were grown in minimal media to an OD₆₀₀ of 0.25 at 30°C, 220 rpm. For wildtype strains and kinase mutant strains, -ura media was used. For *sbh1S3A/T5A* mutant strain, which has the *sbh1* mutant gene integrated on a pRS415 plasmid, -ura-leu media was used. For non-essential kinase mutants, cells were continued growing to an OD₆₀₀ of 1, at 30°C, 220 rpm. For *sbh1S3A/T5A* mutant strain and the essential kinase mutants, for which I used temperature sensitive mutants, cultures were switched to 37°C, 220 rpm, until culture reached an OD₆₀₀ of 1. After incubation, 1 OD₆₀₀ of cells were collected from each culture, washed with sterile deionized water and extracts were prepared. For each sample 0.4 OD₆₀₀ was resolved by SDS-PAGE, and protein detected by immunoblotting using a Gls1-specific antibodies. Signal was acquired by chemiluminescence using an Amersham Imager 600. All experiments were done in duplicates.

Our results suggest that despite their defect in Mns1 Δ gp α F translocation $\Delta kns1$, $\Delta mck1$, and *cdc28-1* cells were competent for Gls1 import into the ER and hence none of these kinases is responsible for N-terminal Sbh1 phosphorylation.

3.7 Phosphorylation-dependent proline isomerase Ess1 contributes to Sbh1 regulation

3.7.1 Previous data on Ess1 contribution to Sbh1 regulation

Both S3 and T5 in Sbh1 are proline-flanked (Figure 1.14A). The conserved enzyme Ess1 (PIN1 in mammals) isomerizes proline residues that are preceded by phosphorylated serine or threonine (Figure 1.14B), so the phosphorylated N-terminus of Sbh1 is a potential Ess1 target (Hanes *et al.*, 2014). This lab therefore asked whether Ess1 contributes to Sbh1 regulation. For trying to answer this question, we used an active site mutant, *ess1H164R* (Gemmil *et al.*, 2005; Atencio *et al.*, 2014), which encodes a catalytically deficient mutant enzyme.

Previous data generated by this lab showed that about 30% of both wildtype and mutant Ess1 was associated with a crude yeast microsomes fraction, suggesting that Ess1 has membrane-bound targets. It was also seen that *ess1H164R* does not cause any general translocation defects. In contrast, it was found that translocation of Gls1 into the ER of *ess1H164R* cells was reduced to about 50% of the wildtype, comparable to the reduction

seen in the *sbh1S3A/T5A* strain. This indicates that transport of Gls1 into the ER is dependent not only on the phosphorylation at S3 and T5 of Sbh1, but also on the isomerization by Ess1.

3.7.2 Kar2 translocation in *ess1H164R* mutant strain

As mentioned before, Kar2 is an ATPase involved in protein import into the ER, acts as a chaperone to mediate protein folding in the ER, and may play a role in ER export of soluble proteins; it also regulates the unfolded protein response via interaction with Ire1 (Guillece *et al.*, 1999; Wang *et al.*, 2016). After being translocated across the ER membrane, the precursor protein (pKar2; 74 KDa) is signal-cleaved to form the mature protein (Kar2; 72 KDa). I looked at pKar2 translocation by pulse-labelling. In this experiment, I grew wildtype, *ess1H164R*, and *sec61-32* mutant strains in YPD at either 37°C (for Ess1 and *ess1H164R* mutant strain) or 20°C (for *sec61-32* mutant strain), 220 rpm, to an OD₆₀₀ of 0.5–1. I then labelled them with [³⁵S]-met/cys for 2.5 min, and I precipitated Kar2 with specific antibodies (Table 2.7). I ran the samples on 7.5 % Bis-Tris SDS gel and I analysed the specific signals by autoradiography (Section 2.2.12). As expected, I saw a clear translocation defect in the control, the *sec61-32* mutant, but no translocation defect was seen in the wildtype or the *ess1H164R* mutant strain (Figure 3.54). These results show that the *ess1H164R* mutant had no effects on pKar2 import into the ER in a pulse experiment, consistent with previous data showing no general translocation defect for this mutant.

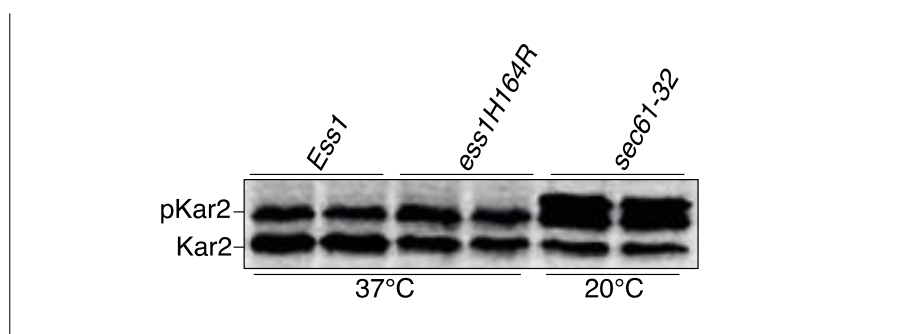


Figure 3.54: Analysis of the Kar2 ER translocation in *ess1H164R* mutant strain. Cells were grown YPD at either 37°C (for Ess1 and *ess1H164R* mutant strain) or 20°C (for *sec61-32* mutant strain), 220 rpm, to an OD₆₀₀ of 0.5–1, then labelled with [³⁵S]-met/cys for 2.5 min. 1.5 OD₆₀₀ of cells were lysed and proteins immunoprecipitated with specific antibodies against Kar2. After SDS-PAGE, proteins were detected by exposing the gels to phosphorimager plates and signal acquired in Typhoon Trio™ Variable Mode Imager. All experiments were done in duplicates.

3.7.3 Sorbitol growth rescue assay for *ess1H164R* mutant strain

The *ess1H164R* mutant strain has been shown to be temperature sensitive at 35°C (Atencio *et al.*, 2014), and since many of the Sbh1-dependent proteins, and Ess1 dependent proteins I found in the automated microscopic screen play a role in cell wall biogenesis (Table 3.1, blue), I investigated whether the *ess1H164R* mutant strain had a cell wall defect. For this experiment, I prepared sequential dilution of wildtype, and *ess1H164R* mutant strain and grew them in quadruplicates on solid media (YPD and YPD supplemented with 1,2M sorbitol (YPDS)) at either 30°C or 35°C for 3 days. Sorbitol stabilizes the plasma membrane if the cell wall is deficient (Lommel *et al.*, 2004). I found that temperature-sensitivity of the *ess1H164R* mutant at 35°C was suppressed in the presence of sorbitol (Figure 3.55), suggesting that a cell wall defect, similar to the one found in the $\Delta sbh1\Delta sbh2$ mutant strain (Figure 3.30), makes the *ess1H164R* mutant temperature-sensitive.

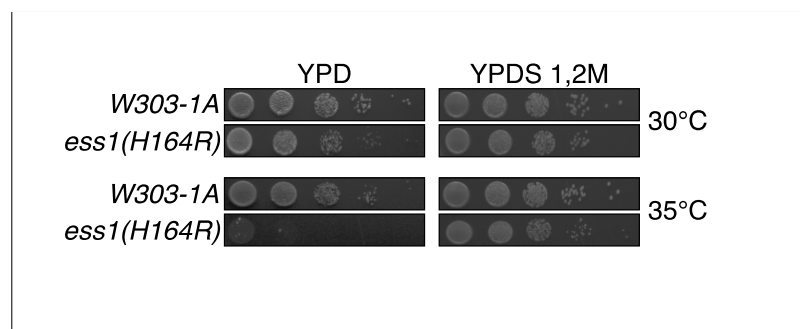


Figure 3.55: Sorbitol growth rescue assay for *ess1H164R* mutant strains. Cells were grown overnight in YPD, at 30°C, 220 rpm. Then, cells were counted using a Neubauer chamber and sequentially diluted (10^4 - 10^0 cells/ $5\mu\text{l}$). Samples of each dilution ($5\mu\text{l}$) were then plated side by side, in solid media (YPD or YPD supplemented with 1,2M sorbitol) and grown for 3 days. Each set was replicated 2 times in different plates and were incubated at 30°C or at 35°C (one replica per temperature).

3.7.4 Sbh1 phosphorylation pattern in *ess1H164R* mutant strain

I then used the Sbh1_(Pi) and the Sbh1₍₁₀₋₂₃₎ antibodies to investigate the Sbh1 N-terminal phosphorylation pattern in *ess1H164R* mutant strain, using $\Delta sbh1/\Delta sbh2$ mutant strain as a control. For this experiment, I grew wildtype strain, $\Delta sbh1/\Delta sbh2$ and *ess1H164R* mutant strains in YPD to an OD₆₀₀ of 0.25 at 30°C, 220 rpm. I then switched cultures to 35°C, 220 rpm, until culture reached an OD₆₀₀ of 1. I collected samples from each culture, made extracts, and resolved them by SDS-PAGE (Section 2.2.8). I detected Phosphorylated-Sbh1 using specific antibodies against the phosphorylated N-terminus of Sbh1 (Sbh1_(Pi), Figure

3.13), that recognizes mainly N-terminally phosphorylated Sbh1. I detected unphosphorylated Sbh1 by immunoblotting using specific antibodies that was raised against the amino acids 10 to 23 of Sbh1 (Table 2.7), and recognizes mainly unphosphorylated Sbh1 (Sbh1₍₁₀₋₂₃₎, Figure 3.13). I used Rpn12 as a loading control. I was not able to see any difference between the *ess1H164R* mutant strain and the wildtype strain in neither phosphorylated or unphosphorylated Sbh1 (Figure 3.56).

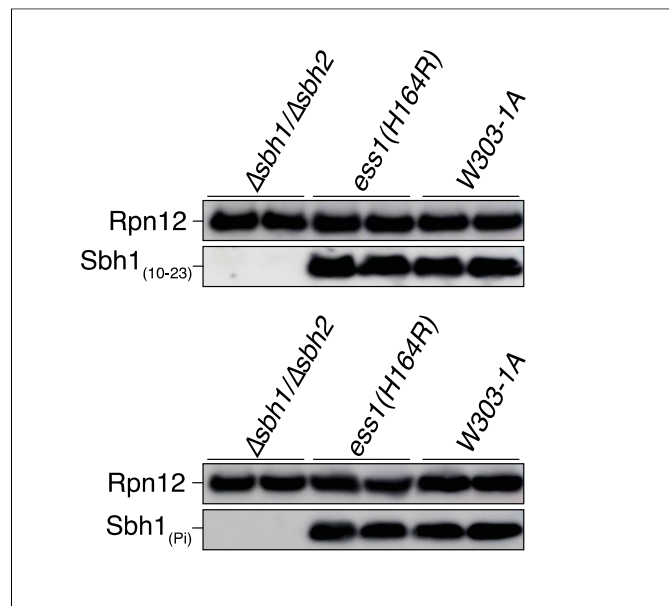


Figure 3.56: Analysis of the phosphorylation pattern of Sbh1 in *ess1H164R* mutant strain. Wildtype, *Δsbh1/Δsbh2* and *ess1H164R* mutant strains were grown an OD₆₀₀ of 0.25 at 30°C, 220 rpm, then incubated at 35°C, until cultures reached an OD₆₀₀ of 1. Then, 1 OD₆₀₀ of cells were collected from each culture, washed with sterile deionized water and extracts were prepared. For each sample, 0.4 OD₆₀₀ was resolved by SDS-PAGE, and protein detected by immunoblotting using either antibody against amino acids 10-23 of Sbh1 (Sbh1₍₁₀₋₂₃₎) or antibody against the phosphorylated N-terminus of Sbh1 (Sbh1_(Pi)). Rpn12-specific antibodies were used for the loading control. Signal was acquired by chemiluminescence using an Amersham Imager 600. All experiments were done in duplicates.

3.7.5 Epistasis assay for *ess1H164R* and *Δsbh1/Δsbh2* mutations

To investigate whether Ess1 and Sbh1 S3/T5 phosphorylation control the same step in ER translocation, I tested whether the effect on Gls1 translocation in *sbh1S3A/T5A* and *ess1H164R* was additive. I measured the amount of Gls1 in *Δsbh1/Δsbh2*, *ess1H164R*, a triple mutant containing *Δsbh1/Δsbh2* and *ess1H164R* mutations, and their respective wildtype strains by Western blotting. For this experiment, I grew *Δsbh1/Δsbh2*, *ess1H164R* and *Δsbh1/Δsbh2/ess1H164R* mutant strains, and their respective wildtype strains in YPD to an OD₆₀₀ of 0.25 at 30°C, 220 rpm. I then switched cultures to 35°C, 220 rpm, until culture reached an OD₆₀₀ of 1. I collected samples from each culture, made extracts, and resolved

them by SDS-PAGE (Section 2.2.8). I detected Gls1 by immunoblotting using Gls1-specific antibodies (Table 2.7). I used Rpn12 as a loading control. I found that the amount of Gls1 in the ER of all mutant cells was similarly reduced compared to wildtypes (Figure 3.57). This suggests that Ess1 and Sbh1 operate at the same stage of translocation.

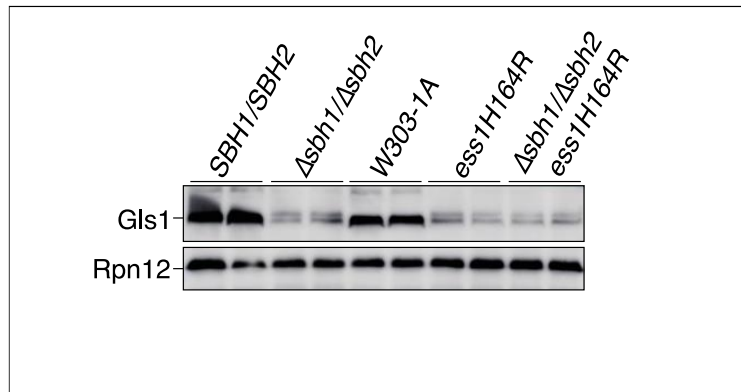


Figure 3.57: Analysis of the Gls1 ER translocation in *ess1H164R*, $\Delta sbh1/\Delta sbh2$, and $\Delta sbh1/\Delta sbh2/ess1H164R$ mutant strains. Cells were grown in YPD to an OD₆₀₀ of 0.25 at 30°C, 220 rpm, then incubated at 35°C, until cultures reached an OD₆₀₀ of 1. After incubation, 1 OD₆₀₀ of cells were collected from each culture, washed with sterile deionized water and extracts were prepared. For each sample 0.4 OD₆₀₀ was resolved by SDS-PAGE, and protein detected by immunoblotting using a Gls1-specific antibodies and Rpn12-specific antibodies (loading control). Signal was acquired by chemiluminescence using an Amersham Imager 600. All experiments were done in duplicates.

4

Discussion

4 Discussion

In the present work I aimed to understand the role of Sec61 channel β -subunit (Sbh1 in yeast) phosphorylation in ER protein import. To accomplish that, I tried to identify the kinase or kinases responsible for the phosphorylation of the serine in the position 3 (S3), and threonine in the position 5 (T5) of Sbh1 and characterized the effect on function of this phosphorylation. In addition, I investigated the range of proteins whose ER import is affected by Sbh1 phosphorylation.

Sbh1 is a small tail-anchored protein that interacts with different partners (Section 1.3.1). It is peripherally associated with the channel via its conserved TMD that contacts different TMDs of Sec61 (*Mandon et al., 2013; Zhao and Jäntti, 2009*). In addition, it makes extensive contact with Sec71, but it is dispensable for the stability of the Sec complex, required for post-translational translocation (*Wu et al., 2019; Allen et al., 2019; Bhadra et al., 2021; Feng et al., 2007*). It can bind ribosomes and the exocyst, but the role of these interactions is unclear (*Levy et al., 2001; Toikkanen et al., 2003*). Also, Sbh1 is the only non-essential subunit of the Sec61 channel, suggesting a potential regulatory role, enhancing the speed of translocation or the efficiency of the targeting (*Soromani et al., 2012*). In yeast, simultaneous deletion of SBH1 and the gene encoding its homolog in the Ssh1 channel, SBH2, results in temperature-sensitive growth, and affects ER translocation of different substrates differentially (*Finke et al., 1996; Feng et al., 2007*). $\Delta sbh1\Delta sbh2$ mutant cells showed as well a glycan trimming defect, due to reduced mannosidase 1 (Mns1) and glucosidase 1 (Gls1) translocation into the ER lumen at all temperatures (*Feng et al., 2007*). In addition, the Sbh1 cytosolic domain makes contact with targeting sequences in the vestibule of the Sec61 channel, and this contact is enhanced if substrates are prevented from inserting into the lateral gate (*Laird and High, 1997; MacKinnon et al., 2014*). Taken together, the data suggest that Sbh1 recognizes some ER targeting sequences in the Sec61 channel vestibule and promotes their insertion into the lateral gate, but that its activity is not essential for most proteins.

Transport of some proteins into the ER must be regulated during specific circumstances: for example, when cells are under ER stress, during certain developmental steps, or when

pathogens encounter a host cell and need to secrete virulence factors (Section 1.4). Regulation of this protein import into the ER can be possible not only if the ER targeting sequences have differences in how strong they are, but also if there are qualitative differences that determine the relative efficiency of insertion (*Hegde and Kang, 2008; O'Keefe and High, 2020*). In mammals, many targeting sequences require accessory proteins to achieve translocation through the Sec61 channel (*Hegde and Kang, 2008; O'Keefe and High, 2020*). An alternative from that could be an alteration of the channel function by posttranslational modifications (*Hegde and Kang, 2008*). A precedence is protein import into mitochondria, where phosphorylation of both substrates and translocation machinery regulates import (Section 1.4.4; *Opalinska and Meisinger, 2015*). Progressive phosphorylation of intrinsically disordered domains can act as a switch between one functional state and another, or induce formation of binding sites for specific interaction partners (*Valk et al., 2014; Bah and Forman-Kay, 2016*). Since the intrinsically unstructured domain of Sbh1 contains multiple phosphorylation sites (Section 1.5.3.2; Figure 1.11), most of which are not positionally conserved between yeast and mammals (*Gruss et al., 1999; Soromani et al., 2012*), modification of the phosphorylation state of this domain might have a role in ER import regulation under specific circumstances.

Mutation of all phosphorylation sites in Sbh1 individually to Alanine (A), including the highly conserved, proline-flanked Threonine (T) in position 5, had no effect on the ability of the mutant sbh1 to complement the temperature-sensitivity of a $\Delta sbh1\Delta sbh2$ deletion strain (*Soromani et al., 2012*). It has also been found that mutation of both S3 and T5 simultaneously to A results in poor growth at 37°C and a Gls1 precursor import defect, (*Barbarit, BSc thesis, 2015*). The phosphomimic mutation of both S3 and T5 simultaneously to Glutamic acid (E), however, rescues the growth phenotype of the $\Delta sbh1/\Delta sbh2$ strain (*Simon, BSc thesis, 2015*). Both sites are proline-flanked (Figure 1.14A), so the phosphorylated N-terminus of Sbh1 is a potential Ess1 target (Section 1.5.3; *Hanes et al., 2014*), which catalysed the cis-trans isomerization of proline residues that are preceded by phosphorylated serine or threonine (*Hanes et al., 2014*). It has been found that about 30% of both wildtype and mutant Ess1 is associated with a crude yeast microsome fraction, suggesting that Ess1 has membrane-bound targets (*Lupusela, MSc Thesis, 2015*). In addition, *ess1H164R* (Section 1.5.3) does not cause any general translocation defects, but ER import

of Gls1 is reduced to about 50% of the wildtype, comparable to the reduction seen in the *sbh1S3A/T5A* strain (Lupusela, MSc Thesis, 2015). This indicates that transport of Gls1 into the ER is dependent not only on the phosphorylation at S3 and T5 of Sbh1, but also on the isomerization by Ess1.

In the present work I characterized the *sbh1* mutant strains (Section 3.1 and 3.4), confirming that the mutation of two N-terminal, proline-flanked, phosphorylation sites in the Sbh1 cytosolic domain phenocopies the temperature-sensitivity of a yeast strain lacking SBH1/SBH2, and results in reduced translocation into the ER of an Sbh1-dependent substrate, Gls1. I also identified targeting signals that are generally Sbh1-dependent, dependent on Sbh1 phosphorylation, or dependent on Ess1 isomerization (Section 3.3). In a high content microscopic screen, I identified about 12% of secretory proteins assayed as Sbh1-dependent. With the data harvested from this setup, I was able to obtain a broader list of affected proteins, which enabled me to uncover their commonalities. I found that Sbh1-dependent proteins have suboptimal ER targeting sequences, with lower hydrophobicity and frequently without or with an inverse charge bias. A small fraction of the screened proteins (2%) was dependent on N-terminal phosphorylation of Sbh1 and on the phospho-S/T-dependent proline isomerase Ess1 for translocation into the ER. During the present work, I also developed and optimized different screens for finding the kinase or kinases responsible for S3/T5-Sbh1 phosphorylation, unfortunately with no conclusive result (Section 3.5 and 3.6). I conclude that Sbh1 promotes ER import of substrates with suboptimal targeting sequences and that its activity can be regulated by a conformational change induced by N-terminal phosphorylation (Section 3.1, 3.3, 3.4 and 3.7). Finally, I suggested a model for ER protein translocation regulation by Sbh1 N-terminal phosphorylation and conformational change induced by Ess1.

4.1 Characterization of *Sbh1* mutants

First, I wanted to verify whether the combination of Sbh1 phosphorylation site mutations, that was previously seen to being the only mutant combination unable to rescue the growth defect of the $\Delta sbh1/\Delta sbh2$ deletion strain at 37°C (Barbarit, BSc thesis, 2015; Finke et al., 1998; Feng et al., 2007), have an effect on sbh1 function. I used strains with

different sbh1 mutations: single or combined S3 and T5 either to A (to prevent phosphorylation) or to E (to mimic the phosphorylated site) and I tested for growth defect at 37°C. Sensitivity to either higher (37°C) or lower (20°C) temperature when compared to the standard growth temperature (30°C) is a common indicator used to characterize yeast strains with ER translocation defects, as transport into the ER is essential (*Rothblatt et al., 1989*). I confirmed that all the mutant strains (including the phosphomimic mutant *sbh1S3E/T5E*) promoted growth of the $\Delta sbh1\Delta sbh2$ strain at the restrictive temperature, with the exception of the combination *S3A/T5A*, which resulted in reduced growth at 37 °C (Figure 3.1). These results suggest the phosphorylation of S3 and T5 is important for Sbh1 function and that the two sites operate together or phosphorylation of these sites is (partially) redundant.

Previous data on the translocation defect in the $\Delta sbh1\Delta sbh2$ strain were somewhat contradictory (*Finke et al., 1996; Feng et al., 2007*). *Finke et al.* saw accumulation of the unprocessed precursor of Kar2 in the $\Delta sbh1\Delta sbh2$ mutant strain, although to a lesser extent than in their control (the *sec61-2* mutant strain). They saw precursor accumulation at the non-permissive temperature (37°C), as well as at the permissive temperature (30°C) (*Finke et al., 1996*). In the case of alpha factor, they did not see any precursor accumulation on wildtype cells, in which the precursor form of alpha factor (pre pro alpha factor; pp α F) is transported and processed rapidly (*Finke et al., 1996*). However, in the mutant lacking both Sbh1 and Sbh2, significant amounts of pp α F was detected, but not as much as in their control (*sec61-2* mutant cells) (*Finke et al., 1996*). *Feng et al.* showed that $\Delta sbh1\Delta sbh2$ mutant cells have a N-glycan trimming defect, explained by the reduced levels of mannosidase1 (Mns1) and glucosidase1 (Gls1) in $\Delta sbh1\Delta sbh2$ mutant cells, due to a constitutive ER translocation defect in these cells even at permissive temperature (30°C). *Feng et al.* show as well that translocation of bacterial α -amylase, previously used as a reporter secretory protein to characterize Sbh1 function in yeast (*Toikkanen et al., 1996; Feng et al., 2007*), is defective in vivo in $\Delta sbh1\Delta sbh2$ mutant cells at restrictive temperatures (37°C).

To test whether the deletion of both *SBH1* and *SBH2* resulted in a general protein translocation defect, I investigated cytosolic precursor accumulation of ER translocation substrates. Post-translationally translocated pre pro alpha factor (pp α F) accumulated in a *sec61-32* mutant that has an ER import defect at 20°C, but not in the Δ *sbh1* Δ *sbh2* strain at 37°C (Figure 3.2). Co-translationally translocated dipeptidylaminopeptidase B (DPAPB) also accumulated in the *sec61-32* mutant at the restrictive temperature, but not in the Δ *sbh1* Δ *sbh2* strain (Figure 3.3). These results demonstrate that yeast cells do not have a general translocation defect either co-translationally or post-translationally in the absence of Sbh1 and Sbh2.

Next, since the cytosolic precursor (pGls1) and the ER form of Gls1 cannot be distinguished on SDS gels, I looked at the steady state amount of Gls1 in wildtype vs. Δ *sbh1*/ Δ *sbh2* strain by Western blotting to test whether there is a specific Gls1 import defect in the Δ *sbh1*/ Δ *sbh2* strain and I saw that Δ *sbh1* Δ *sbh2* cells have a reduced amount of Gls1 in the ER at steady state (Figure 3.4). When I tested pKar2 translocation by performing a short pulse with [³⁵S]-methionine (met)/cysteine (cys) and immunoprecipitation with Kar2-specific antibodies in wildtype, Δ *sbh1* Δ *sbh2*, and *sec61-32* mutant strains, I saw a strong translocation defect in the Δ *sbh1*/ Δ *sbh2* strain as well as in the control, the *sec61-32* mutant (Figure 3.5). These results show that Gls1 and Kar2 import into the ER are dependent on Sbh1 and Sbh2 and in contrast with the previous results (Feng et al., 2007; Finke et al., 1996), the defect I observed was more pronounced. In addition, and after integrating the Ylp α -L plasmid (encoding *Bacillus amyloliquefaciens* α -amylase gene) in the *leu2* locus of my wildtype and Δ *sbh1*/ Δ *sbh2* mutant strains, I saw cytosolic precursor accumulation of α -amylase in Δ *sbh1*/ Δ *sbh2* cells at 37°C (Figure 3.7), confirming that translocation of α -amylase is defective in Δ *sbh1*/ Δ *sbh2* cells at restrictive temperature.

With the exception of Kar2, all the other translocation substrates for which an Sec61 β /Sbh1-dependence has been demonstrated so far have weak signal sequences with relatively short hydrophobic cores (green amino acids, Figure 4.1). These are: bacterial α -amylase, used as a reporter secretory protein for characterization (Toikkanen et al., 1996; Feng et al., 2007); Gls1, which was originally described as transmembrane protein, but has

now been shown to be a soluble protein in the ER with a cleaved signal peptide (*Shibuya et al., 2015*); Mns1, for which no cleavage site is predicted through standard prediction program (SignalP); and PC1 (polycystin-1), a large polytopic membrane protein, whose biogenesis has been shown to be dependent on the presence of Sec61 β (*Besse et al., 2017*). For efficient insertion into the lateral gate of the Sec61 channel these signal peptides might be particularly dependent on guidance by Sec61 β /Sbh1. The entry of these proteins to the ER could be therefore regulated by adjusting the interaction of their signal peptides with Sec61 β /Sbh1. The fact that ER entry can be regulated via different strength signal peptides, and that the majority of signal peptides is weak has been already demonstrated (*Kang et al., 2006*). The authors showed that in the context of acute ER stress, changes in translocation efficiency are substrate specific, reversible, and physiologically important, and the selectivity of translocational attenuation is determined by signal sequences, whose hydrophobicity, length, charge, and amino acid composition vary widely between substrates (*von Heijne, 1985*). Also, certain highly overproduced secretory proteins like prolactin may need to contain signal sequences that can escape stress-induced translocational attenuation mechanisms that might be generated during rapid changes in secretory activity (*Kang et al., 2006*). This rationale presumably applies to Kar2 as well, which sometimes requires effective translocation even at high expression levels during ongoing ER stress (*Kang et al., 2006*). This would mean that during ER stress only substrates with optimal signal peptides (like Kar2) enter the ER while substrates with weaker signal peptides are targeted to degradation via quality control pathway and whether or not proteins with weak signal peptides are translocated through the Sec61 channel is determined by the post-targeting interaction of the signal sequence with the Sec61 channel (*Kang et al., 2006*). The strength of this interaction might be enhanced by introducing negative charges into the Sbh1 N-terminal domain by phosphorylation, which could interact with the positively charged amino acids N-terminal of the hydrophobic core of the signal peptides (red amino acids, Figure 4.1). In a more general way, sequence differences among signal sequences may provide a means to adjust the translocation efficiency of some substrates separately of others for various physiological purposes.

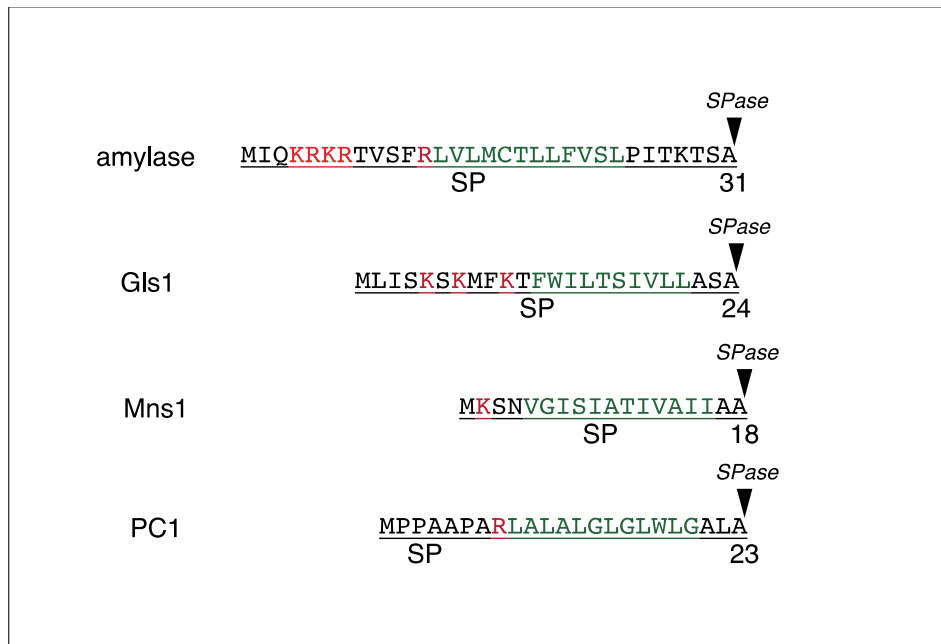


Figure 4.1: Signal sequences of Sec61 β /Sbh1-dependent ER translocation substrates demonstrated so far. Bacterial α -amylase, used as a reporter secretory protein for characterization (Toikkanen *et al.*, 1996; Feng *et al.*, 2007); Gls1, which was originally described as transmembrane protein, but has now been shown to be a soluble protein in the ER with a cleaved signal peptide (Shibuya *et al.*, 2015); Mns1, for which no cleavage site is predicted through standard prediction program (SignalP); PC1 (polycystin-1), a large polytopic membrane protein, whose biogenesis has been shown to be dependent on the presence of Sec61 β (Besse *et al.*, 2017). Signal peptide cleavage site (SPase) is also shown. Hydrophobic cores of signal peptides are in green, positively charged amino acids N-terminal of the hydrophobic core are in red.

I next investigated whether the *sbh1S3A/T5A* mutant was competent for translocation of these substrates. For testing pKar2 translocation, I performed a short pulse with [35S]-methionine (met)/cysteine (cys) and immunoprecipitation with Kar2-specific antibodies in wildtype, $\Delta sbh1\Delta sbh2$, *sbh1S3A/T5A*, and *sec61-32* mutant strains. I saw that in *sbh1S3A/T5A* yeast there was as much translocation of pKar2 as in the wildtype, in contrast to the $\Delta sbh1\Delta sbh2$ and *sec61-32* strains, where I saw cytosolic pKar2 accumulation (Figure 3.8), indicating that pKar2 is Sbh1-dependent, but not dependent on the S3/T5-phosphorylation of Sbh1. This was verified by Western blotting (Figure 3.9). I therefore quantified the amount of Gls1 in wildtype, *sbh1S3A/T5A*, and individual *sbh1S3A* and *sbh1T5A* strains by Western blotting. I found that the amount of Gls1 in the ER of *sbh1S3A/T5A* mutant was substantially reduced compared to the wildtype or the single mutants (Figure 3.10), comparable to the reduction seen in $\Delta sbh1\Delta sbh2$ strain (Figure 3.4). This indicates that transport of Gls1 into the ER is dependent not only on the presence of Sbh1, but also on its phosphorylation at S3 and T5.

As Gls1, Mns1, and Kar2 are involved in ER protein quality control, I next investigated the sensitivity to Tunicamycin (TM), of *sbh1* mutants. Tunicamycin is a glycosylation inhibitor that interferes with N-linked glycosylation in the ER which often is a prerequisite for protein folding. Since cells show greater difficulty to deal with misfolded protein clearing, tunicamycin-sensitivity leads to some misfolded protein response defect and is indicative of perturbations in ER proteostasis (*Tran et al., 2011; Römisch et al., 2005*). This means that cells that are defective in ER-associated degradation (ERAD) or the unfolded protein response (UPR) like the *Aire1* mutant are sensitive to TM in the growth media (*Tran et al., 2011*) and TM is known to induce the UPR. *IRE1*, encoding Ire1, is the only signal transducer for the UPR in the yeast ER membrane (*Cox et al., 1993*). I found that in contrast to the *Aire1* strain, the *sbh1* mutants were not sensitive to TM (Figure 3.11). I also tested these strains directly for induction of the UPR, by looking for the most proximal sign of induction - the splicing of the mRNA of the HAC1 transcription factor mRNA - using as a positive control, cells treated with TM. I found that neither the *Δsbh1Δsbh2* strain, nor the *sbh1S3A/T5A* mutant, in the absence of TM, contained spliced *HAC1* mRNA (Figure 3.12), indicating that there is no induction of the UPR nor a proteostasis defect in the *sbh1* mutants.

Taking together, these observations suggest that even if yeast cells lacking Sbh1 and Sbh2 do not have a general ER translocation defect either co-translationally or post-translationally, there is a substrate-specific ER import defect. These observations also suggest that there are two classes of Sbh1-dependent ER translocation substrates: some that are dependent on the presence of Sbh1 (e.g., Kar2), and a subset that are also dependent on S3/T5-phosphorylation of Sbh1 (e.g., Gls1). Levels of glycan-processing enzymes like Gls1 and Mns1 and the molecular chaperone Kar2 in the ER need to be tightly controlled (*Hosokawa et al., 2003*). *Hosokawa et al.* showed that overexpression of the processing α 1,2-mannosidase (ER Mns1) in mammalian cells leads to inappropriate targeting of wildtype proteins to ER-associated degradation. To prevent this, during recovery from ER stress mammalian Sec62 has an independent function from its conventional role in the translocation machinery by serving as an ER-resident autophagy receptor that delivers select ER constituents, like glycan processing machinery, to the autolysosomal pathway to re-establish physiological ER contents and contribute to maintain ER homeostasis (*Fumagalli et al., 2016*). In yeast, Gls1 and Mns1 concentrations in the ER

may be regulated by controlling their translocation into the ER via Sbh1 phosphorylation adjusting the ER glucan processing capacity to acute physiological requirements. The observations pointed out in this first part of my work suggests that Sbh1 plays a role in the regulation of the ER import of some proteins under specific physiological circumstances. During active growth cell would need to maximized the production of cell wall components whose synthesis depends on Gls1, Mns1 and Kar2 (*Simons et al., 1998; Orlean, 2012*). Also, during induction of the unfolded protein response (UPR), these proteins are essential for the promotion of appropriate protein folding in case of the molecular chaperone (*Kabani et al., 2003*) and the degradation of misfolded proteins in the case of the glycoproteins (*Jakob et al., 1998*). In these situations, ER import of these proteins would have to be maximized by phosphorylating Sbh1 (*Kabani et al., 2003; Hitt et al., 2004; Jakob et al., 1998; Simons et al., 1998; Orlean, 2012*), whereas in stationary phase or during recovery from the UPR their ER import needs to be limited by Sbh1 dephosphorylation to prevent excessive glycan-processing in the ER, which would lead to disturbed ER proteostasis (*Hosokawa et al., 2003*).

4.2 Sbh1 antibodies

At the beginning of the present work, the lab had two different antibodies that could recognize Sbh1: Sbh1₍₁₋₁₈₎, raised against the first 18 residues of Sbh1 (Figure 3.13, blue) and Sbh1₍₁₀₋₂₃₎, raised against the residues 10 to 23 of Sbh1, so does not interact with the phosphorylation sites S3 and T5 of the protein (Figure 3.13, orange). When I investigated whether these two antibodies (Sbh1₍₁₋₁₈₎ and Sbh1₍₁₀₋₂₃₎) recognize phosphorylated and unphosphorylated Sbh1 in the same manner, using microsomes and treating them with alkaline phosphatase (AP) to dephosphorylates microsomal proteins, I found that both antibodies recognize mainly the N-terminally unphosphorylated form of Sbh1 (Figure 3.14). Later on, we raised an antibody against the phosphorylated N-terminus of Sbh1 (Sbh1_(Pi), Figure 3.13, red). This antibody was raised against a peptide made of residues 2 to 10 of Sbh1 that was N-acetylated and with the serine in the position 3 phosphorylated. When I investigated how these two antibodies (Sbh1_(Pi) and Sbh1₍₁₀₋₂₃₎) recognize Sbh1 when S3/T5 sites are phosphorylated or unphosphorylated, using again microsomes prepared from wildtype, $\Delta sbh1/\Delta sbh2$ and *sbh1S3A/T5A* mutant strains, I found that Sbh1_(Pi) antibody

recognizes mainly N-terminally phosphorylated Sbh1 (Figure 3.15A), while the Sbh1₍₁₀₋₂₃₎ antibody, recognizes primarily N-terminally unphosphorylated Sbh1 (figure 3.15B).

A possible reason that would explain why both Sbh1₍₁₀₋₂₃₎ and Sbh1₍₁₋₁₈₎ antibodies recognize mainly the unphosphorylated form of Sbh1 could be that when Sbh1 is phosphorylated in positions S3 and T5, the negatively charged phosphate groups generated by this phosphorylation could interact with the positively charged residues K15, R16 and K17 of Sbh1. This interaction could generate a change in conformation that would interfere with the interaction between Sbh1 and these two antibodies (Figure 4.2).



Figure 4.2: Sbh1 phosphorylation/dephosphorylation and potential change in conformation scheme. Schematic representation of a Sbh1, with phosphorylation sites S3 and T5 (red) and hydrophobic transmembrane region (green). Schematic representation of phosphorylation and change in conformation due to interaction between negatively charged phosphate groups and positively charged K15, R16 and K17 of Sbh1.

For this reason, recently the lab raised another antibody against Sbh1, Sbh1₍₃₉₋₄₈₎ (Figure 3.13, grey). This antibody was raised against the residues 39 to 48 of Sbh1, away from the N-terminal phosphorylation sites, and close to the transmembrane domain. With this antibody we are able to see the total amounts of Sbh1 in a more precise way. In addition, I tried an antibody that specifically reacts to proteins containing phosphothreonine-proline motifs and phosphoserine-proline motifs (both pT-P and pS-P motifs reacts to a similar degree), but does not react to phosphothreonine, phosphoserine or phosphotyrosine (ab9344, abcam, not shown). Unfortunately, I was not able to detect Sbh1 with this antibody.

4.3 Secretome automated microscopic screen

To systematically identify proteins whose translocation depends on the presence of Sbh1, on the S3/T5-phosphorylation of Sbh1, or on Ess1 isomerization, I performed a high content screen (Breker *et al.*, 2014). I integrated the $\Delta sbh1\Delta sbh2$, *sbh1S3A/T5A* or *ess1H164R* backgrounds into a collection of yeast strains each expressing one of 382 secretory and transmembrane proteins C-terminally fused to a Green Fluorescent Protein (GFP) (Geva *et al.*, 2017). I imaged the wildtype and mutant cells and analysed them for changes in the signal pattern. By using automated cell manipulations and microscopy platforms, it is possible to easily screen entire libraries for genes that affect any cellular process that can be visualized (Schuldiner and Cohen, 2011). Since it is already established that Mns1 and Gls1 ER translocation is dependent on the presence of Sbh1, and is also dependent on the phosphorylation of S3/T5-Sbh1 (Feng *et al.*, 2007), it would have been useful to have these two proteins included in the screen library as a control. Unfortunately, these two proteins and several other secretome proteins were not included due to intrinsic experimental reasons in the library construction process. In section 3.3 (Results), I showed 3 examples (Figure 3.21) of different substrates C-terminally fused to GFP, from the secretome library where I was able to see differences in the GFP signal pattern between wildtype and mutant cells. More globally, I identified 45 proteins that were dependent on the presence of Sbh1, 7 proteins that were dependent on S3/T5-phosphorylation of Sbh1 and 45 that were dependent on isomerization by Ess1 (Table 3.1); From all these substrates: 5 are both dependent on the presence of Sbh1 and on S3/T5-phosphorylation of Sbh1 (Table 3.1, underlined); 19 are both dependent on the presence of Sbh1, and on isomerization by Ess1 (Table 3.1, bold); and 2 are dependent on the presence of Sbh1, on S3/T5-phosphorylation of Sbh1, and on isomerization by Ess1 (Table 3.1, underlined and bold). It is relevant to mention that two S3/T5-Sbh1 phosphorylation dependent substrates were not in the Sbh1 dependent list as well, not because they did not show a signal change between the wildtype and the $\Delta sbh1\Delta sbh2$ mutant strain, but rather because these cells did not grow at all in this background.

To verify the results from the screens, I biochemically analysed the translocation efficiency of proteins that had an expected clear size difference between cytosolic precursor

and ER form, by checking for cytosolic precursor accumulation. First, I made a selection between the different positive results, based on an expected clear size difference between cytosolic precursor and ER form. Initially, I ended up with 6 different protein-GFP from the screens that had an expected clear size difference and had also an absolute size, so the difference would be also visible by standard protein gel electrophoresis (protein-GFP molecular weight below 90 KDa): Erp1-GFP, Gpi8-GFP, Irc22-GFP, Sna2-GFP, Yet3-GFP and Erv25-GFP. From those, I was not able to see any precursor or mature form of 3 of these proteins-GFP (Sna2-GFP, Yet3-GFP and Erv25-GFP), possibly due to a rapid degradation of the precursors by the proteasome (*Ast et al., 2014*). I was able to detect different forms of the other 3 substrates: two Sbh1-dependent ER translocation substrates: Erp-1 and Gpi-8; and one Sbh1 and Sbh1 phosphorylation-dependent ER translocation substrate: Irc22. For both Erp1-GFP and Gpi8-GFP there was cytosolic precursor accumulation in the $\Delta sbh1\Delta sbh2$ strain, but not in wildtype or *sbh1S3A/T5A* mutant cells (Figure 3.22A, B). As for the Sbh1 and Sbh1 phosphorylation-dependent ER translocation substrate (Irc22-GFP), I was not able to see any precursor accumulation in neither $\Delta sbh1/\Delta sbh2$ nor *sbh1S3A/T5A* mutant cells. I saw though accumulation of a partially un-glycosylated form of Irc22-GFP in $\Delta sbh1/\Delta sbh2$ mutant strain (Figure 3.22C). Then, I looked at plrc22-GFP translocation by pulse-labelling, to check if I was able to see any precursor accumulation. Again, I was not able to see any precursor accumulation in neither $\Delta sbh1/\Delta sbh2$ nor *sbh1S3A/T5A* mutant cells, but I saw accumulation of a partially un-glycosylated form of Irc22-GFP in $\Delta sbh1/\Delta sbh2$ mutant strain (Figure 3.23).

SPs have a well-defined structure (Figure 1.4, Figure 3.24). ER-targeting can also be achieved by uncleaved SPs (signal anchors, SAs) or the first TMD of a protein (*Spiess et al., 2019*). Identification of a significant number of Sbh1-dependent proteins allowed me to investigate whether their ER targeting sequences had specific common features compared to the total ER targeting sequences in yeast. Several features make a SP optimal for ER translocation through the Sec61 channel. Because of their intrinsic hydrophobic amino acids disposition, with their hydrophobic side chains exposed to the outside and the hydrophilic peptide backbone hidden inside, helicity is an important aspect for insertion into the translocation pore (*Spiess et al., 2019*). This helix propensity can be disturbed though by

high glycine/proline content in the H-region (*Nguyen et al., 2018*). Connected to this, hydrophobicity of the H-region, which is the main driving force for transmembrane integration and has a great diversity in terms of length, is also a crucial feature that makes a signal sequence optimal. Charge bias between N-region and C-region, plays also an important role to help the peptide orientate when inserting to the channel. The transmembrane orientation of the initial signal and the downstream transmembrane segment is affected by charge flanking residues (positive-inside rule) (*Spiess et al., 2019; Yim et al., 2018*). Of the 45 Sbh1-dependent proteins, 16 had SPs, 5 had SAs, and 24 had TMDs as ER targeting signals. I found that the Sbh1-dependent SPs were slightly less hydrophobic (Figure 3.25A), but I detected no differences in charge distribution of the N-regions (Figure 3.25B), proline fraction of the SP (Figure 3.25C), polarity of the C-region (Figure 3.25D), glycine-proline fraction of the SP (Figure 3.25E) or H-region length (Figure 3.25F). When I looked at Sbh1-dependent targeting sequences individually, however, I found that many targeting sequences had no charge bias (e.g., Yps7, Figure 3.27A) or an inverse charge bias (e.g., Gpi14, Figure 3.27A). This was true for both SPs and transmembrane targeting sequences of Sbh1-dependent proteins. In addition, some transmembrane targeting sequences were unusually long or too short to span the membrane (e.g., Yip3, Figure 3.27B), or contained a high number of glycine residues (e.g., Tat1, Figure 3.27B); all of these features would interfere with the efficient insertion of these targeting sequences into the lateral gate of the Sec61 channel (*Nguyen et al., 2018; Spiess et al., 2019; Yim et al., 2018*). Targeting sequences of Sbh1 S3/T5-phosphorylation-dependent proteins were similar to the Sbh1-dependent ones (Figure 3.27C), but I was unable to identify specific features in these due to the small number of proteins identified. These observations suggest that Sbh1-dependent proteins have ER-targeting sequences that are suboptimal for insertion into the Sec61 lateral gate. Sbh1 may guide these targeting sequences into the Sec61 channel and thus enhance their insertion efficiency. These results would also reinforce the idea that for efficient insertion into the lateral gate of the Sec61 channel these signal peptides would be dependent on guidance by Sbh1, and that the entry of these proteins to the ER could be therefore regulated by adjusting the interaction of their signal peptides Sbh1. In addition, this diversity in sequence differences among signal sequences would provide a way to independently regulate the translocation efficiency of different substrates separately, depending on the physiological purposes. These results are consistent with the idea that

more efficient the signal sequences are, less sensitive to ER translocation regulation they are: signal sequences whose interactions with the translocon are highly efficient and less dependent on accessory factors are less susceptible to modulations by additional substrate-specific factors required for productive ER protein translocation (*Hegde and Kang, 2008*). In addition, the high diversity of the signal sequences whose ER translocation was found to be Sbh1-dependent, corroborates the idea that natural signal sequences diversity it is biologically important for differential modulation of ER translocation to mediate regulation (*von Heijne, 1986; Hegde and Bernstein, 2006*).

The cell wall in yeast, which is composed mainly by manno-proteins and β -glucans, is an elastic and essential structure that provides osmotic and physical protection and determines the shape of the cell (*Klis et al., 2002*). Many of the Sbh1-dependent proteins I found in my screen play a role in cell wall biogenesis (Table 3.1, blue). In addition to that, it has been shown that the production of cell wall components synthesis depends on Gls1, Mns1 and Kar2 (*Simons et al., 1998; Orlean, 2012*), whose ER import are Sbh1 and phospho-Sbh1 dependent (Figure 3.4, 3.5, 3.10; *Finke et al., 1996*). I then investigated whether the $\Delta sbh1\Delta sbh2$ and *sbh1S3A/T5A* mutants had a cell wall defect. I grew $\Delta sbh1\Delta sbh2$ and the *sec61-3* mutant (as a positive control) alongside the corresponding wildtype strains on rich media and on rich media supplemented with sorbitol, which stabilizes the plasma membrane if the cell wall is defective (*Lommel et al., 2004*), at permissive and restrictive temperature. I found that both the $\Delta sbh1\Delta sbh2$ strain and the *sec61-3* mutant grew at restricted temperature in the presence of sorbitol (Figure 3.30), suggesting that it is indeed the cell wall defect that makes the *Sbh1/2* mutant cells temperature sensitive. This was also the case for *sbh1S3A/T5A* mutant cells, which were also able to grow normally at restrictive temperature when in the presence of sorbitol (Figure 3.31), suggesting as well that is a cell wall defect what makes them temperature-sensitive. In addition, I found that Sbh1 expression and Sbh1 phosphorylation is considerably higher in early exponential phase, compared to later stages (Figure 3.33), consistent with its requirement for cell wall biosynthesis. When I investigate whether the phosphorylation of Sbh1 is a response to the osmotic stress, studying the change in the phosphorylation pattern of Sbh1 in wildtype cells when they are grown with and without stabilization of the plasma membrane (Figure 3.32), I was not able to see any difference in the pattern of phosphorylation of Sbh1 between the

different conditions, suggesting that osmotic stress does not induce phosphorylation of Sbh1. Taking together, these results show that both $\Delta sbh1\Delta sbh2$ and the *sec61-3* strain have a cell wall defect that results in temperature-sensitivity and since a large fraction of *S. cerevisiae* secretory activity is dedicated to cell wall biogenesis (Guo et al., 2021) it is likely that the temperature-sensitivity of most if not all secretory pathway mutants is due to an underlying cell wall defect (Novick and Schekman, 1983).

As several of the Sbh1-dependent proteins are involved in the biosynthesis of glycosylphosphatidylinositol anchors (GPI-anchor) that are glycolipid anchors enabling the presentation of proteins on the outer membrane or cell wall (Table 3.1, blue), I asked whether the $\Delta sbh1\Delta sbh2$ strain was affected in GPI-anchor synthesis. The GPI-anchored protein Gas1, the best characterized GPI-linked protein, accumulates in the ER if its GPI-anchor is not properly processed (Horvath et al., 1994). I took advantage of the difference in mobility on SDS-polyacrylamide gels of the mature and immature forms of Gas1 to check whether $\Delta sbh1\Delta sbh2$ strain disturb GPI anchoring and/or transport of GPI-anchored proteins. I found that cells lacking *SBH1* and *SBH2*, however, did not accumulate the ER form of Gas1 after a 3 h shift to the restrictive temperature (Figure 3.34). These data suggest that despite the reduction of components of the GPI-synthesis machinery in the ER of $\Delta sbh1\Delta sbh2$ mutants, the strain was competent for GPI anchor production. There is, however, a clear Sbh1-dependency of several proteins that are involve in the biosynthesis of GPI-anchor. This suggests that cells could be using Sbh1 to upregulate or downregulate GPI-anchor biosynthesis depending on the requirements of specific situations. For example, in transition to stationary phase, cells are no longer growing much anymore, and they don't need to produce as much cell wall as in exponential phase, and in consequence they wouldn't need as much GPI-anchor proteins, since they are largely part of the cell wall (Klis et al., 2002). GPI-anchor proteins have very special biosynthetic requirements: they not only have to coordinate the translocation of the protein with the formation of a new GPI-anchor (Lopez et al., 2019), but they also need to be O-mannosylated in the process and they have to reside in unique lipid environments for the anchor to be correctly modified and allowed export (Aguilera-Romero et al., 2021; Lopez et al., 2019). Finally, due to their special biophysical properties, they use a specialized COPII machinery (different from other

transmembrane domain proteins in the ER) to be exported from the ER (Lopez *et al.*, 2019). Because of that, another possible explanation of this Sbh1-dependency, is that Sbh1 could be marking specific translocons that are in translocational subdomains in the right maturation area for GPI-anchor proteins.

Since some of the Sbh1-dependent proteins found in my screen are amino acid transporters in the plasma membrane (Table 3.1, red), I investigated whether the $\Delta sbh1\Delta sbh2$ mutant had a defect in amino acid uptake. I tested its ability to survive on plates supplemented with metsulfuron-methyl (MM), which is toxic in strains lacking amino acid transporters (Jørgensen *et al.*, 1998). In contrast to an $\Delta shr3$ mutant (chaperone, required for amino acid transporter biogenesis, Kuehn *et al.*, 1998), I found that $\Delta sbh1\Delta sbh2$ was not sensitive to MM (Figure 3.35), suggesting that although amino acid transporter biogenesis was reduced in these cells, amino acid uptake was not critically affected.

4.4 Screening for the kinase responsible for Sbh1 S3/T5 phosphorylation

Initially I wanted to systematically identify which kinase or kinases are potentially phosphorylating Sbh1 in the S3 and T5 sites. For doing that I performed two different automated microscopic Screens using Mns1 fused to GFP as a reporter (Mns1 ER import is dependent on the phosphorylation of Sbh1). After generating the reporter Mns1-GFP strain (Section 3.3.2.1), I crossed it with a mutant library of knockout Kinases and also with a mutant library of overexpressed Kinases. When I took images of wildtype and mutant cells in both screens and looked for changes in the GFP signal pattern, I was able to identify 13 kinases that had a change in the GFP signal pattern (Table 3.2). From those 13 hits, only 9 would have a change in the GFP pattern that would logically correlate with them being potentially responsible for the S3/T5-phosphorylation of Sbh1 (increase in the GFP signal for overexpressed kinases, or decrease in GFP signal for knockout kinases): Mps1, Elm1, Cka2, Tda1, Mek1, Yck2, Rim15, Gcn2 and Tor2. In a second screen to identify the phosphatase or phosphatases that are potentially de-phosphorylating Sbh1 in the S3 and T5 sites, I did two different screens using as well the reporter Mns1-GFP strain and crossing it with a mutant library of knockout phosphatases and also with a mutant library of overexpressed

phosphatases. unfortunately, none of the phosphatase mutants of neither screen resulted in a change in the signal pattern when compare to the correspondent wildtype and I was not able to identify any phosphatase as potential responsible for the de-phosphorylation of S3/T4-Sbh1. Since these results were inconclusive, I decided to change the approach of my kinase screen, and because my studies focused of the phosphorylation of S3 and T5 of Sbh1, and both sites are proline-flanked, I decided to focus on the proline-directed kinases in yeast. Many serine/threonine kinases modify substrate sites that form integral or distal parts of kinase consensus motifs, and between these motifs, proline residues often define substrate site specificity (*Ubersax and Ferrel, 2007*). The proline-directed protein kinases phosphorylate proteins on a serine or threonine residue that is immediately preceding a proline residue and there are 27 different known proline-directed kinases in yeast (Table 3.3, *Kanshin et al., 2017; Zhang et al., 2019; Zhu et al., 2005; Bradley and Beltrao, 2019; Liu et al., 2000; Lin et al., 1997*). This would shorten the number of kinases to be tested and would allow me to use different strategies in order to find the one responsible for the Sbh1 S3/T5 phosphorylation. One proline-directed kinase, Slt2, is of special interest for these screens, since Sbh1 contains an Slt2 docking site (*Sacristan-Reviriego et al., 2014*). Slt2 is a serine/threonine kinase and is one of the five mitogen-activated protein (MAP) kinases in yeast that monitors cell wall integrity (CWI) (*Chen et al., 2005*). It also coordinates expression of all 19S regulatory particle assembly-chaperones (RACs) to control proteasome abundance, and is involved in cell cycle progression, nuclear mRNA retention in heat shock and septum assembly (*Carmody et al., 2010*). Cell wall perturbations in yeast triggers the activation of Slt2 by one of several sensors in the plasma membrane, and Slt2 phosphorylates and activates directly different transcription factors resulting in compensatory changes in the cell wall (*Chen et al., 2005; Nobel et al., 2000*), suggesting a potential connection between Sbh1 and Slt2.

For the next attempt to identify the kinase responsible for the phosphorylation of proline-flanked S3/T5 of Sbh1, our lab raised an antibody against the phosphorylated N-terminus of Sbh1 (Sbh1_(Pi)), that recognizes mainly the N-terminally phosphorylated Sbh1 (Figure 3.15B). Initially, a student from our lab (Paula Hahn) used the Sbh1_(Pi) antibody vs. the Sbh1₍₁₀₋₂₃₎ antibody that recognizes mainly the N-terminally unphosphorylated Sbh1 (Figure 3.15A) to screen through loss of function mutants in all 27 proline-directed kinases

in yeast. She was unable to identify a kinase mutant in which N-terminal Sbh1 phosphorylation was reduced. I then used these antibodies to screen for Sbh1 N-terminal hyperphosphorylation (Sopko *et al.*, 2006) in strains overexpressing 20 of these proline-directed kinases, again without a conclusive result. As mentioned previously, casein Kinase II (CKII) of *Saccharomyces cerevisiae* contains two distinct catalytic subunits, α and α' , that are encoded by *CKA1* and *CKA2* genes, respectively (Chester *et al.*, 1995). Disruption of either catalytic subunit gene has no obvious phenotype, but disruption of both is lethal (Chen-Wu *et al.*, 1988). When I used a strain with the double mutation $\Delta cka1/\Delta cka2$ transformed with a CEN plasmid expressing either the wildtype *CKA2* or the *cka2-13* temperature sensitive allele (Rethinaswamy *et al.*, 1998), to check for Sbh1 phosphorylation pattern when there is a loss of function in both subunits, I was not able to detect any difference between *cka1/cka2-ts* and its control, $\Delta cka1/CKA2$ in neither phosphorylated or unphosphorylated Sbh1 (Figure 3.39). Alternatively, we could have inhibited CK2 in yeast with 4,5,6,7-Tetrabromobenzotriazole (Kos-Braun *et al.*, 2017), but I decided to use temperature-sensitive mutant, due to time reasons.

I then generated a reporter construct, fusing the SP of the Sbh1 phosphorylation-dependent substrate Mns1 to mutant alpha factor precursor without glycosylation sites (Mns1 Δ gp α F, Figure 3.41 and 3.42). I first characterized the construct in my *sbh1* mutants. I detected reporter precursor accumulation in $\Delta sbh1\Delta sbh2$, $\Delta sbh1/SBH2$, and *sbh1S3A/T5A* strains (Figure 3.43). When I transformed the 27 proline-directed kinase deficient mutants (knockout non-essential, temperature sensitive for essential) and their respective wildtypes with a vector expressing this reporter construct (Mns1 Δ gp α F), I found some cytosolic precursor accumulation in $\Delta kns1$, $\Delta mck1$, and in temperature-sensitive *cdc28-1* at the restrictive temperature (Figure 3.44). I transformed as well the *cka1/cka2-ts* mutant strain and its respective control strains with Mns1 Δ gp α F vector and I was not able to see any Mns1 Δ gp α F precursor accumulation (Figure 3.45). These results suggest that Kns1, Mck1 and Cdc28 kinases might therefore be involved in Sbh1 N-terminal phosphorylation. I subsequently investigated translocation of the Sbh1-dependent, but N-terminal phosphorylation-independent, translocation substrate pKar2 in these kinase mutants in pulse-assays and none of the kinase mutants had defects in pKar2 translocation (Figure

3.46), suggesting that the observed effect with the reporter was specific to the Mns1 SP. Both post-translational import of wildtype pp α F (Figure 3.47) and co-translational import of pDPAPB (Figure 3.48) was functional in these kinase mutants and I did not see any precursor accumulation, suggesting the kinase mutations do not cause general translocation defects. When I investigated whether the proline-directed kinase mutants affected the levels of endogenous Gls1 in the ER, I found that in contrast to the *sbh1 S3A/T5A* mutation which reduces Gls1 to around 50% of wildtype levels (Figure 3.10), none of the kinase mutants identified in my screen significantly affected Gls1 levels in the ER of the mutants (Figure 3.50). In addition, when I investigated Gls1 translocation in these cells with a reporter that had glutathione-S-transferase fused to the N-terminus of the Gls1 SP (Figure 3.51) to generate a protein with a more pronounced size difference between cytosolic precursor and signal-cleaved ER-form (Shibuya *et al.*, 2015), I found that while *sbh1S3A/T5A* cells accumulated significant amounts of GSTpGls1 in the cytosol (Figure 3.52), none of the proline-directed kinase mutants did (Figure 3.53). My results suggest that despite their defect in Mns1 Δ gp α F translocation Δ *kns1*, Δ *mck1*, and *cdc28-1* cells were competent for Gls1 import into the ER and hence none of these kinases is likely responsible for N-terminal Sbh1 phosphorylation.

There are a number of possible reasons for my inability to identify the Sbh1 S3/T5 kinase. One possibility is the adaptation of the mutant strain to the absence of the kinase. Adaptation has been observed in yeast strains deficient in SRP function (Ogg *et al.*, 1992). Ogg *et al.* showed that even if this adaptation process cannot restore cell physiology to a wild-type state, cells that are grown for a prolonged time in the absence of SRP or SRP receptor no longer show pronounced protein translocation defects (Ogg *et al.*, 1992). They also showed that this adaptation is a physiological process and is not due to the accumulation of a suppressor mutation (Ogg *et al.*, 1992).

Another possible explanation is kinase redundancy, which is very common in yeast. Kinase redundancy means that paralogous kinases can have the potential to replace a deleted kinase in some or many of its functions and moderate like that the effects of this individual kinase deletion (Lepore *et al.*, 2016). An example of kinase redundancy that has been reported is the case of Fus3 and Kss1 in the Cell Cycle (Elion *et al.*, 1991). Fus3 is

functionally redundant with Kss1 for a step in signal transduction between the β subunit of the G protein and the Ste12 transcriptional activator, showing that a single step in a cellular regulatory process can be successfully executed by more than one kinase (*Elion et al., 1991*). Something that could have happened is that one of the Proline-directed kinases tested in my screens was in fact the responsible for the S3/T5-Sbh1 phosphorylation, however another kinase might have partially or totally replaced its function in the kinase deletion strain. A partial rescue of Sbh1 phosphorylation by a paralogous kinase would explain why I was able to observe a partial Mns1 Δ gp α F precursor accumulation, when compared to the *sbh1S3A/T5A* mutant strain, in Δ kns1, Δ mck1, and *cdc28-1* at the restrictive temperature (Figure 3.44).

In addition to that, most of the kinase deletion mutants that I used in my screens were from the Euroscarf collection (*Giaever et al., 2002*). About 15% of the strains from the Euroscarf collection are not real deletions, because often the deletion cassette is integrated into the correct locus but the strains are aneuploid and there is a wildtype copy of the gene in another chromosome. Unfortunately, I did not know about this at the moment I designed and performed my experiments, so I did not check the knockout strains by PCR. Hence, there is a high probability that some of the kinase deletions are not actual deletions, which means that a verification of the knockouts needs to be done. This could also be a possible reason for my inability to identify the Sbh1 S3/T5 kinase.

A possible explanation of why I was able to see a partial defect in Mns1 Δ gp α F translocation in Δ kns1, Δ mck1, and *cdc28-1* cells, even when they were competent for Glc1 import into the ER could be that the observed effects are indirect effects (*Ubersax and Ferrel, 2007*). Non-systematic and biochemical studies suggest that kinases vary greatly in the number of sites that they phosphorylate (*Ubersax and Ferrel, 2007*). Also, systematic in vitro proteomic studies in *Saccharomyces cerevisiae* support this proposal: e.g., cyclin-dependent kinase-1 (Cdk1) from yeast phosphorylated hundreds of substrates (*Ptacek et al., 2005*). Since kinases can phosphorylate different substrates, it could be the case that the observed effects in Mns1 Δ gp α F translocation are in fact indirect effects (*Ubersax and Ferrel, 2007*). For example, the kinase activity of Cdc28 is required for efficient transcription, and

for mRNA capping of several genes, including housekeeping genes important for cell-wall integrity, energy supply, translation, and chromatin architecture. In addition, other study reported a kinase-independent role for Cdc28 in regulation of transcription (*Morris et al., 2003*). The partial defect in Mns1 Δ gp α F translocation, and the decreased levels of total Sbh1 observed previously (*Hahn, BSc Thesis, 2020*) in the cdc28-1, could be an indirect consequence of the effect of absent Cdc28 on Sbh1 transcription (*Chymkowitch et al., 2012*). And perhaps this effect on Sbh1 transcription is not strong enough to generate a detectable Gls1 ER import defect. For the case of Kns1 and Mck1, they are both part of the TOR regulation of RNA polymerase III transcription machinery, where in response to nutrient limitation and other types of cellular stress, they repress ribosome and tRNA synthesis (*Lee et al., 2012*). Perhaps, this impossibility of transcription regulation, generated by the absence of these kinases would generate an additional stress in the cell that would somehow lead to the indirect observed effects in Mns1 Δ gp α F translocation.

Other different approach I tried for the identification of the kinase responsible for the S3/T5-Sbh1 phosphorylation was electrophoresis on 18% polyacrylamide, 4M urea SDS gels (*Rais et al., 2004; Swank et al., 1971*) (Figure 3.36 and 3.37). I decided to change the technique, because I did not succeed in my attempts to use Tom22 (phosphorylated by CK1 and dephosphorylated by alkaline phosphatase (AK)) as a proper phosphorylation / dephosphorylation control. I additionally tried Phos-tag SDS-PAGE, which is an electrophoresis technique capable of separating phosphorylated and non-phosphorylated forms of a protein based on phosphorylation levels due to the interaction of the phosphate groups from the phosphorylated proteins with a divalent metal ion that binds to the Phos-tag molecules of the gel (*Nagy et al., 2018*). Unfortunately, because of the nature of this technique, it was extremally difficult to optimize for this particular phosphorylated protein (not shown), so again I decided to change the system used for the screening.

4.5 Phosphorylation-dependent proline isomerase Ess1 contributes to Sbh1 regulation

Both S3 and T5 in Sbh1 are proline-flanked (Figure 1.14A). The conserved enzyme Ess1 (PIN1 in mammals) isomerizes proline residues that are preceded by phosphorylated serine or threonine (Figure 1.14B), so the phosphorylated N-terminus of Sbh1 is a potential Ess1

target (Hanes *et al.*, 2014). An active site mutant, *ess1H164R*, is synthetically lethal with *ssh1* indicating a contribution of Ess1 to ER protein translocation (Gemmill *et al.*, 2005; Atencio *et al.*, 2014). In membrane fraction experiments this lab previously found that about 30% of both wildtype and mutant Ess1 was associated with a crude yeast microsomal fraction, suggesting that Ess1 has membrane-bound targets. In addition, previous students investigated whether the *ess1H164R* mutant had any ER translocation defects by using reporter constructs in which the SP of post-translationally translocated CPY or co-translationally translocated Pho8 were fused to the URA3 gene (Ng *et al.*, 2007). They saw that when these are expressed in *ura3* auxotrophs, the cells can only survive in the absence of uracil if the reporter fails to translocate into the ER or does so more slowly (Ng *et al.*, 2007). Using this assay, they found that *ess1H164R* does not cause general translocation defects. In contrast, it was found that translocation of Gls1 into the ER of *ess1H164R* cells was reduced to about 50% of the wildtype, comparable to the reduction seen in the *sbh1S3A/T5A* strain. This indicates that transport of Gls1 into the ER is dependent not only on the phosphorylation at S3 and T5 of Sbh1, but also on the isomerization by Ess1.

I looked at pKar2 translocation by pulse-labelling in *ess1H164R* and *sec61-32* mutant strains. As expected, I saw a clear translocation defect in the control, the *sec61-32* mutant, but no translocation defect was seen in the wildtype or the *ess1H164R* mutant strain (Figure 3.54). These results show that the *ess1H164R* mutant had no effects on pKar2 import into the ER in a pulse experiment, consistent with previous data showing no general translocation defect for this mutant. In addition, I found that temperature-sensitivity of the *ess1H164R* mutant at 35°C was suppressed in the presence of sorbitol (Figure 3.55) confirming prior results by Gemmill *et al.* (2005) and suggesting that a cell wall defect, similar to the one found in the $\Delta sbh1\Delta sbh2$ mutant strain (Figure 3.30), makes the *ess1H164R* mutant temperature-sensitive. Next, to investigate whether Ess1 and Sbh1 S3/T5 phosphorylation control the same step in ER translocation, I tested whether the effect on Gls1 translocation in *sbh1S3A/T5A* and *ess1H164R* was additive. I measured the amount of Gls1 in $\Delta sbh1\Delta sbh2$, *ess1H164R*, a triple mutant containing $\Delta sbh1\Delta sbh2$ and *ess1H164R*, and their respective wildtype strains by Western blotting. I found that the amount of Gls1 in the ER of all mutant cells was similarly reduced compared to wildtype (Figure 3.57), suggesting that Ess1 and Sbh1 operate at the same stage of translocation.

Computational analyses show that about 10-20% of full-length eukaryotic proteins are intrinsically disordered proteins, and around 35% of all protein residues are classified as intrinsically disordered protein regions (*Ward et al., 2004*). In addition, using a combination of limited proteolysis and mass spectrometry, it has been demonstrated that about 50% of intrinsically disordered regions of soluble proteins are structured, presumably due to interactions with partner proteins (*Leuenberger et al., 2017*). There are many examples showing the several specific mechanisms by which proline regulates the structure and function of intrinsically disordered protein regions, due to their unique chemical properties that determine not only its role as a modulator of secondary structural elements, but also its tendency to promote specific structural motifs (*Theillet et al., 2013*). Due to their inherent differences in stereochemistry, proline cis/trans isomers and proline cis/trans isomerization reactions play important roles in defining different functional states of a protein (*Andreotti, 2003*). Therefore, enzymes that specifically enhance proline cis/trans isomerization are essential for this function. As mentioned before, the conserved enzyme Ess1 isomerizes proline residues that are preceded by phosphorylated serine or threonine, so the phosphorylated N-terminus of Sbh1 is a potential Ess1 target. Taking together, the data generated in this section (Section 4.5) suggest that Ess1 plays an important role in protein transport through the Sec61 channel, and its most likely targets are the proline-flanked phosphorylation sites in Sbh1. These results further support the idea that differential phosphorylation of Sbh1 cytosolic intrinsically disordered domain, followed by isomerization by Ess1, could therefore control its differential association with specific interaction partners under specific physiological circumstances and could regulate the transport of specific proteins into the ER.

4.6 Model for Sbh1 function during ER protein translocation and its regulation by S3/T5 phosphorylation

The results of this study, together with previous results from other students of this laboratory, helped us to generate the following model for ER protein translocation regulation by Sbh1 N-terminal phosphorylation and Ess1 isomerization: When a ribosome-nascent chain complex with a suboptimal targeting sequence arrives at the Sec61 channel,

failure to insert into the lateral gate leads to contact of the targeting sequence with the Sbh1 cytosolic domain in the Sec61 channel vestibule (Figure 4.3, centre). Interaction with Sbh1 allows the targeting sequence to acquire the appropriate conformation, orientation or both for insertion into the lateral gate (Figure 4.3, centre). For proteins whose concentration in the ER needs to be tightly controlled, phosphorylation of S3/T5 and isomerization by Ess1 enhance Sbh1-promoted ER import under specific physiological circumstances (Figure 4.3, right). During active growth, for example, ER import of Mns1 and Gls1 precursors would be maximal to cope with the required higher production of cell wall components whose biosynthesis depends on these enzymes (*Simons et al., 1998*). Also, during induction of the unfolded protein response (UPR), these proteins are essential for degradation of misfolded proteins (*Jakob et al., 1998*). On the contrary, when the cell is going through stationary growth phase or during recovery from the UPR their ER import might be limited to prevent excessive glycan-processing in the ER which would lead to disturbed ER proteostasis. Also, when cells are exposed to an increased environmental osmolarity, ER import would be maximal for osmosensors and for proteins that are involved in the high osmolarity response (HOG) pathway, contributing to hyperosmotic stress tolerance, like Vph1 (*Banerjee et al., 2019*) and Msb2 (*O'Rourke and Herskowitz, 2002*), which are two other phospho-Sbh1 dependent substrates found on the automated microscopic screen (Table 3.3). In addition, the significant expression of the cell wall integrity pathway (CWI) responsive genes is also activated by external hyperosmolarity, suggesting that the adaptative changes in the cell wall architecture are critical for protecting yeast cells against not only the cell wall stress but also the osmotic stress (*Udom et al., 2019*). This means that the HOG pathway cooperates with the CWI pathway to control the expression of cell wall-remodelling genes in order to build the adaptative strength of the cell wall (*Udom et al., 2019*), and this adaptative response may be also regulated by the maximized ER import of crucial substrates in response to cell wall stress and/or osmotic stress done by the phosphorylation of S3/T5-Sbh1 and subsequent isomerization by Ess1.

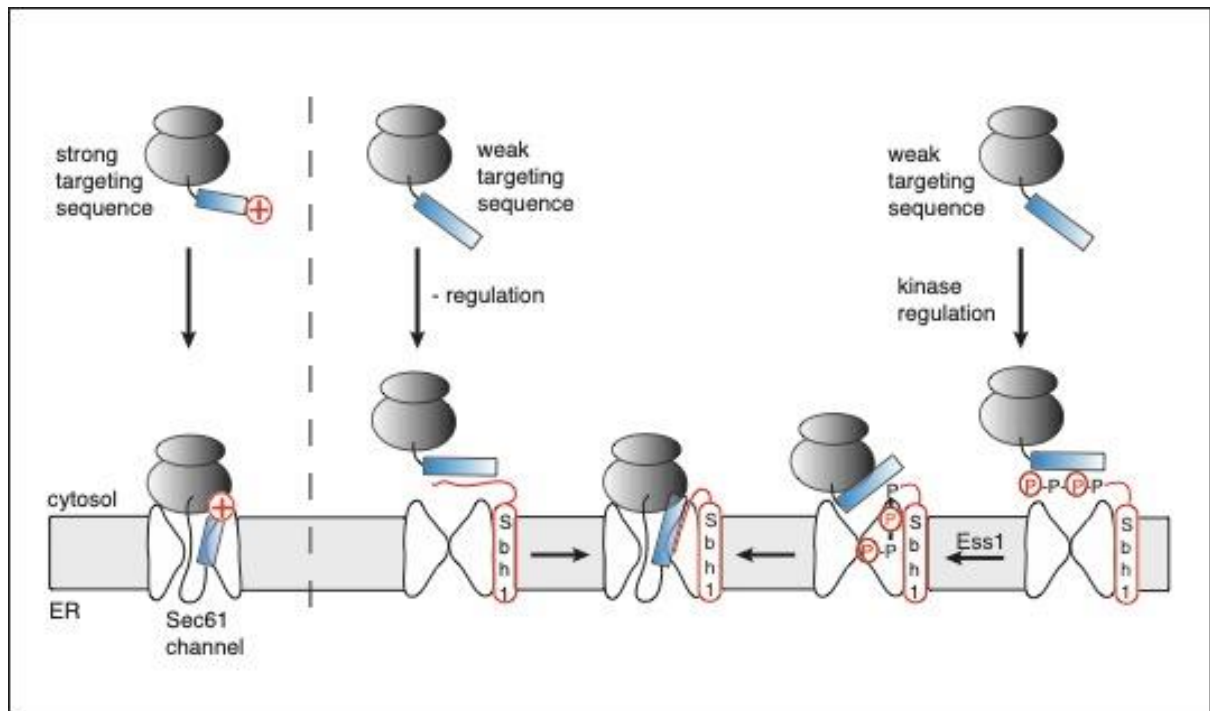


Figure 4.3: Model for Sbh1 function during ER protein translocation and its regulation by S3/T5 phosphorylation. When a ribosome-nascent chain complex with a suboptimal targeting sequence arrives at the Sec61 channel, failure to insert into the lateral gate leads to contact of the targeting sequence with the Sbh1 cytosolic domain in the Sec61 channel vestibule (centre). Interaction with Sbh1 allows the targeting sequence to acquire the appropriate conformation, orientation or both for insertion into the lateral gate (centre). For proteins whose concentration in the ER needs to be tightly controlled, phosphorylation of S3/T5 and isomerization by Ess1 enhance Sbh1-promoted ER import under specific physiological circumstances (right).

As shown for other intrinsically disordered regions, phosphorylation of the N-terminus of Sbh1 may affect protein conformational dynamics or liquid-liquid phase separation (*Bah and Forman-Kay, 2016*), thus regulating interaction with specific ER targeting sequences. The results shown in the current work indicate that access to the ER of these substrates is further controlled by Ess1-dependent isomerization.

Overall, this study shows that ER protein import is not a constitutive or deterministic process, but rather can be control in response to modifications in cellular conditions. As mentioned before, in the context of ER stress, cell wall stress, osmotic stress, or active growth, changes in translocation efficiency are substrate specific, reversible, and physiologically important. And the selectivity of this ER translocation is determined by signal sequences, whose great diversity in terms of hydrophobicity, length, charge bias and amino acid composition gives them differential functionality during ER translocation. The mechanisms by which differences between signal sequences allow substrate-specific and stress-dependent regulation of ER translocation remains to be studied. Interestingly, the interactions between the diverse signal sequences and the translocon after the targeting

process is highly dynamic and also differentially influenced not only by properties of both the signal sequence and the mature region, but also by trans-acting factors that modulate the translocation efficiency (*Hegde and Kang, 2008*).

Understanding the regulatory mechanism of ER protein translocation would contribute to our knowledge about protein secretion in yeast and could also provide potential answers to different pathologies related to protein secretion. For example, Sec61 β is essential for efficient infection of human and insect cells by flaviviruses (*Zhang et al., 2016*). Flavivirus infections constitute substantial human and non-human primate morbidity and mortality worldwide, and among the most important flaviviruses that affects humans worldwide are Zika, Dengue, West Nile and Yellow fever (*Blahove and Carter, 2021*). Dengue Virus alone causes around 400 million infections and 22.000 deaths per year worldwide (*Roy and Bhattacharjee, 2021*). There is no specific treatment for such infections and the only vaccine available is against Yellow Fever. The ER is a focal site in the flavivirus lifecycle because it supports translation, polyprotein processing, replication, and virion morphogenesis, therefore the identification of host gene targets that are selectively required for virus replication, but not host cell survival, provides new targets for pharmacological inhibition (*Zhang et al., 2016*). In another example, it has been proven that the absence of the gene coding for Sec61 β in patients with Polycystic Liver Disease, prevents the biogenesis of the transmembrane protein polycystin-1 (PC1), which leads to cyst formation in the liver, but does not affect ER general translocation, supporting the idea of Sec61 β being required for translocation of specific proteins (*Besse et al., 2017*). In addition, the beta subunit of Sec61 is involved in fungal development and pathogenesis of *M. Oryzae*, the responsible for rice blast, which is one of the most devastating diseases on rice, and the most important agricultural pathogen (*Wei et al., 2020; Xu et al., 2019*).

In summary, In the present work I was able to characterize the *sbh1* mutant strains and identify targeting signals that were generally Sbh1-dependent, dependent on Sbh1 phosphorylation, or dependent on Ess1 isomerization. I was also able to find commonalities in signal sequences that lead to the conclusion that Sbh1-dependent proteins had suboptimal ER targeting sequences. In addition, I developed and optimized different screens for finding the kinase or kinases responsible for S3/T5-Sbh1 phosphorylation. Collectively,

my data suggest a model for ER protein translocation regulation by Sbh1 N-terminal phosphorylation and conformational change induced by Ess1, in which Sbh1 promotes ER import of substrates with suboptimal targeting sequences and in which its activity can be regulated by a conformational change induced by N-terminal phosphorylation. More generally, my results demonstrate how intricate the ER protein translocation system is, enabling the tight regulation and tailoring of translocation according to cellular needs.

References

- Abd-Rabbo D, Michnick SW (2017). Delineating functional principles of the bow tie structure of a kinase-phosphatase network in the budding yeast. *BMC Syst Biol.* 2017 Mar 16;11(1):38.
- Aguilera-Romero A, Sabido-Bozo S, Lopez S, Cortes-Gomez A, Rodriguez-Gallardo S, Perez-Linero AM, Riezman I, Riezman H, Muñiz M (2021). Determination of the lipid composition of the GPI anchor. *PLoS One.* 2021 Aug 13;16(8):e0256184.
- Allen WJ, Collinson I, Römisch K (2019) Post-Translational Protein Transport by the Sec Complex. *Trends Biochem Sci.* 2019 Jun;44(6):481-483
- Amoutzias GD, He Y, Lilley KS, Van de Peer Y, Oliver SG (2012). Evaluation and properties of the budding yeast phosphoproteome. *Mol Cell Proteomics.* 2012 Jun;11(6):M111.009555.
- Ampofo E, Welker S, Jung M, Müller L, Greiner M, Zimmermann R, Montenarh M (2013). CK2 phosphorylation of human Sec63 regulates its interaction with Sec62. *Biochim Biophys Acta.* 2013 Apr;1830(4):2938-45.
- Andreotti AH (2003). Native state proline isomerization: an intrinsic molecular switch. *Biochemistry.* 2003 Aug 19;42(32):9515-24.
- Ast T, Cohen G, Schuldiner M (2013). A network of cytosolic factors targets SRP-independent proteins to the endoplasmic reticulum. *Cell.* 2013 Feb 28;152(5):1134-45.
- Ast T, Aviram N, Chuartzman SG, Schuldiner M (2014). A cytosolic degradation pathway, prERAD, monitors pre-inserted secretory pathway proteins. *J Cell Sci.* 2014 Jul 15;127(Pt 14):3017-23.
- Atencio D, Barnes C, Duncan TM, Willis IM, Hanes SD (2014). The yeast Ess1 prolyl isomerase controls Swi6 and Whi5 nuclear localization. *G3 (Bethesda).* 2014 Mar 20;4(3):523-37.
- Bah A, Vernon RM, Siddiqui Z, Krzeminski M, Muhandiram R, Zhao C, Sonenberg N, Kay LE, Forman-Kay JD (2015). Folding of an intrinsically disordered protein by phosphorylation as a regulatory switch. *Nature.* 2015 Mar 5;519(7541):106-9.
- Bah A, Forman-Kay JD. (2016) Modulation of Intrinsically Disordered Protein Function by Post-translational Modifications. *J Biol Chem.* 2016 Mar 25;291(13):6696-705
- Banerjee S, Clapp K, Tarsio M, Kane PM (2019). Interaction of the late endo-lysosomal lipid PI(3,5)P2 with the Vph1 isoform of yeast V-ATPase increases its activity and cellular stress tolerance. *J Biol Chem.* 2019 Jun 7;294(23):9161-9171.

Barlowe C, Orci L, Yeung T, Hosobuchi M, Hamamoto S, Salama N, Rexach MF, Ravazzola M, Amherdt M, Schekman R (1994). COPII: a membrane coat formed by Sec proteins that drive vesicle budding from the endoplasmic reticulum. *Cell*. 1994 Jun 17;77(6):895-907.

Barlowe CK, Miller EA (2013). Secretory protein biogenesis and traffic in the early secretory pathway. *Genetics*. 2013 Feb;193(2):383-410.

Becker T, Bhushan S, Jarasch A, Armache JP, Funes S, Jossinet F, Gumbart J, Mielke T, Berninghausen O, Schulten K, Westhof E, Gilmore R, Mandon EC, Beckmann R (2009). Structure of monomeric yeast and mammalian Sec61 complexes interacting with the translating ribosome. *Science*. 2009 Dec 4;326(5958):1369-73.

Beckmann R, Bubeck D, Grassucci R, Penczek P, Verschoor A, Blobel G, Frank J (1997). Alignment of conduits for the nascent polypeptide chain in the ribosome-Sec61 complex. *Science*. 1997 Dec 19;278(5346):2123-6.

Bernales S, Papa FR, Walter P (2006). Intracellular signaling by the unfolded protein response. *Annu Rev Cell Dev Biol*. 2006;22:487-508.

Besemer J, Harant H, Wang S, Oberhauser B, Marquardt K, Foster CA, Schreiner EP, de Vries JE, Dascher-Nadel C, Lindley IJ (2005). Selective inhibition of cotranslational translocation of vascular cell adhesion molecule 1. *Nature*. 2005 Jul 14;436(7048):290-3.

Besse W, Dong K, Choi J, Punia S, Fedeles SV, Choi M, Gallagher AR, Huang EB, Gulati A, Knight J, Mane S, Tahvanainen E, Tahvanainen P, Sanna-Cherchi S, Lifton RP, Watnick T, Pei YP, Torres VE, Somlo S (2017). Isolated polycystic liver disease genes define effectors of polycystin-1 function. *J Clin Invest*. 2017 May 1;127(5):1772-1785.

Beuret N, Rutishauser J, Bider MD, Spiess M (1999). Mechanism of endoplasmic reticulum retention of mutant vasopressin precursor caused by a signal peptide truncation associated with diabetes insipidus. *J Biol Chem*. 1999 Jul 2;274(27):18965-72.

Bhadra P, Yadhanapudi L, Römisch K, Helms (2021) How does Sec63 affect the conformation of Sec61 in yeast? *PLoS Comput Biol*. 2021 Mar 29;17(3):e1008855

Bhandari D, Zhang J, Menon S, Lord C, Chen S, Helm JR, Thorsen K, Corbett KD, Hay JC, Ferro-Novick S (2010). Sit4p/PP6 regulates ER-to-Golgi traffic by controlling the dephosphorylation of COPII coat subunits. *Mol Biol Cell*. 2013 Sep;24(17):2727-38.

Biederer T, Volkwein C, Sommer T (1996). Degradation of subunits of the Sec61p complex, an integral component of the ER membrane, by the ubiquitin-proteasome pathway. *EMBO J*. 1996 May 1;15(9):2069-76.

Blahove MR, Carter JR (2021). Flavivirus Persistence in Wildlife Populations. *Viruses*. 2021 Oct 18;13(10):2099.

Blobel G, Dobberstein B (1975). Transfer of proteins across membranes. II. Reconstitution of functional rough microsomes from heterologous components. *J Cell Biol.* 1975 Dec;67(3):852-62.

Bonifacino JS, Glick BS (2004). The mechanisms of vesicle budding and fusion. *Cell.* 2004 Jan 23;116(2):153-66.

Borgese N, Coy-Vergara J, Colombo SF, Schwappach B (2019). The Ways of Tails: the GET Pathway and more. *Protein J.* 2019 Jun;38(3):289-305.

Brachmann CB, Davies A, Cost GJ, Caputo E, Li J, Hieter P, Boeke JD (1998) Designer deletion strains derived from *Saccharomyces cerevisiae* S288C: a useful set of strains and plasmids for PCR-mediated gene disruption and other applications. *Yeast.* 1998 Jan 30;14(2):115-32

Bradley D, Beltrao P (2019). Evolution of protein kinase substrate recognition at the active site. *PLoS Biol.* 2019 Jun 24;17(6):e3000341.

Breker M, Gymrek M, Moldavski O, Schuldiner M (2014). LoQAtE--Localization and Quantitation ATlas of the yeast proteome. A new tool for multiparametric dissection of single-protein behavior in response to biological perturbations in yeast. *Nucleic Acids Res.* 2014 Jan;42(Database issue):D726-30.

Breitkreutz A, Choi H, Sharom JR, Boucher L, Neduva V, Larsen B, Lin ZY, Breitkreutz BJ, Stark C, Liu G, Ahn J, Dewar-Darch D, Reguly T, Tang X, Almeida R, Qin ZS, Pawson T, Gingras AC, Nesvizhskii AI, Tyers M. A global protein kinase and phosphatase interaction network in yeast. *Science.* 2010 May 21;328(5981):1043-6.

Briggs MS, Cornell DG, Dluhy RA, Gierasch LM (1986). Conformations of signal peptides induced by lipids suggest initial steps in protein export. *Science.* 1986 Jul 11;233(4760):206-8.

Brodsky JL, Schekman R (1993). A Sec63p-BiP complex from yeast is required for protein translocation in a reconstituted proteoliposome. *J Cell Biol.* 1993 Dec;123(6 Pt 1):1355-63.

Brodsky JL, Goeckeler J, Schekman R (1995). BiP and Sec63p are required for both co- and posttranslational protein translocation into the yeast endoplasmic reticulum. *Proc Natl Acad Sci U S A.* 1995 Oct 10;92(21):9643-6.

Cai H, Yu S, Menon S, Cai Y, Lazarova D, Fu C, Reinisch K, Hay JC, Ferro-Novick S (2007). TRAPPI tethers COPII vesicles by binding the coat subunit Sec23. *Nature.* 2007 Feb 22;445(7130):941-4.

Cao X, Barlowe C (2000). Asymmetric requirements for a Rab GTPase and SNARE proteins in fusion of COPII vesicles with acceptor membranes. *J Cell Biol.* 2000 Apr 3;149(1):55-66.

- Carmody SR, Tran EJ, Apponi LH, Corbett AH, Wente SR (2010). The mitogen-activated protein kinase Slt2 regulates nuclear retention of non-heat shock mRNAs during heat shock-induced stress. *Mol Cell Biol.* 2010 Nov;30(21):5168-79.
- Castillon GA, Watanabe R, Taylor M, Schwabe TM, Riezman H (2009). Concentration of GPI-anchored proteins upon ER exit in yeast. *Traffic.* 2009 Feb;10(2):186-200.
- Chawla A, Chakrabarti S, Ghosh G, Niwa M (2011). Attenuation of yeast UPR is essential for survival and is mediated by IRE1 kinase. *J Cell Biol.* 2011 Apr 4;193(1):41-50.
- Chen X, VanValkenburgh C, Liang H, Fang H, Green N (2001). Signal peptidase and oligosaccharyltransferase interact in a sequential and dependent manner within the endoplasmic reticulum. *J Biol Chem.* 2001 Jan 26;276(4):2411-6.
- Chen Y, Feldman DE, Deng C, Brown JA, De Giacomo AF, Gaw AF, Shi G, Le QT, Brown JM, Koong AC (2005). Identification of mitogen-activated protein kinase signaling pathways that confer resistance to endoplasmic reticulum stress in *Saccharomyces cerevisiae*. *Mol Cancer Res.* 2005 Dec;3(12):669-77.
- Chen Y, Nielsen J (2016). Flux control through protein phosphorylation in yeast. *FEMS Yeast Res.* 2016 Dec 1;16(8).
- Cheng Z, Jiang Y, Mandon EC, Gilmore R (2005). Identification of cytoplasmic residues of Sec61p involved in ribosome binding and cotranslational translocation. *J Cell Biol.* 2005 Jan 3;168(1):67-77.
- Chen-Wu JL, Padmanabha R, Glover CV (1988). Isolation, sequencing, and disruption of the CKA1 gene encoding the alpha subunit of yeast casein kinase II. *Mol Cell Biol.* 1988 Nov;8(11):4981-90.
- Chester N, Yu IJ, Marshak DR (1995). Identification and characterization of protein kinase CKII isoforms in HeLa cells. Isoform-specific differences in rates of assembly from catalytic and regulatory subunits. *J Biol Chem.* 1995 Mar 31;270(13):7501-14.
- Chymkowitch P, Eldholm V, Lorenz S, Zimmermann C, Lindvall JM, Bjørås M, Meza-Zepeda LA, Enserink JM (2012). Cdc28 kinase activity regulates the basal transcription machinery at a subset of genes. *Proc Natl Acad Sci U S A.* 2012 Jun 26;109(26):10450-5.
- Clapham DE (2007). Calcium signaling. *Cell.* 2007 Dec 14;131(6):1047-58.
- Cohen P (2002). Protein kinases--the major drug targets of the twenty-first century? *Nat Rev Drug Discov.* 2002 Apr;1(4):309-15.
- Cohen Y, Schuldiner M (2011) Advanced methods for high-throughput microscopy screening of genetically modified yeast libraries. *Methods Mol Biol.* 2011;781:127-59

Corsi AK, Schekman R (1996). Mechanism of polypeptide translocation into the endoplasmic reticulum. *J Biol Chem.* 1996 Nov 29;271(48):30299-302.

Costanzo et al. (2016) A global genetic interaction network maps a wiring diagram of cellular function. *Science.* 2016 Sep 23;353(6306):aaf1420

Cox JS, Shamu CE, Walter P (1993). Transcriptional induction of genes encoding endoplasmic reticulum resident proteins requires a transmembrane protein kinase. *Cell.* 1993 Jun 18;73(6):1197-206.

Cox JS, Walter P (1996). A novel mechanism for regulating activity of a transcription factor that controls the unfolded protein response. *Cell.* 1996 Nov 1;87(3):391-404.

Cross BC, Sinning I, Luirink J, High S (2009). Delivering proteins for export from the cytosol. *Nat Rev Mol Cell Biol.* 2009 Apr;10(4):255-64.

De Craene JO, Coleman J, Estrada de Martin P, Pypaert M, Anderson S, Yates JR 3rd, Ferro-Novick S, Novick P (2006). Rtn1p is involved in structuring the cortical endoplasmic reticulum. *Mol Biol Cell.* 2006 Jul;17(7):3009-20.

Delic M, Valli M, Graf AB, Pfeffer M, Mattanovich D, Gasser B (2013). The secretory pathway: exploring yeast diversity. *FEMS Microbiol Rev.* 2013 Nov;37(6):872-914.

Deshaies RJ, Schekman R (1987). A yeast mutant defective at an early stage in import of secretory protein precursors into the endoplasmic reticulum. *J Cell Biol.* 1987 Aug;105(2):633-45.

Devi L, Prabhu BM, Galati DF, Avadhani NG, Anandatheerthavarada HK. Accumulation of amyloid precursor protein in the mitochondrial import channels of human Alzheimer's disease brain is associated with mitochondrial dysfunction. *J Neurosci.* 2006 Aug 30;26(35):9057-68.

Dobson CM (2001). The structural basis of protein folding and its links with human disease. *Philos Trans R Soc Lond B Biol Sci.* 2001 Feb 28;356(1406):133-45.

Driver JA, Zhou XZ, Lu KP (2006). Pin1 dysregulation helps to explain the inverse association between cancer and Alzheimer's disease. *Biochim Biophys Acta.* 2015 Oct;1850(10):2069-76.

Du Y, Ferro-Novick S, Novick P (2004). Dynamics and inheritance of the endoplasmic reticulum. *J Cell Sci.* 2004 Jun 15;117(Pt 14):2871-8.

Dudek J, Pfeffer S, Lee PH, Jung M, Cavalié A, Helms V, Förster F, Zimmermann R (2015). Protein transport into the human endoplasmic reticulum. *J Mol Biol.* 2015 Mar 27;427(6 Pt A):1159-75.

Duden R (2003). ER-to-Golgi transport: COP I and COP II function (Review). *Mol Membr Biol.* 2003 Jul-Sep;20(3):197-207.

Egea PF, Stroud RM (2010). Lateral opening of a translocon upon entry of protein suggests the mechanism of insertion into membranes. *Proc Natl Acad Sci U S A.* 2010 Oct 5;107(40):17182-7.

Elia F, Yadhanapudi L, Tretter T, Römisch K (2019). The N-terminus of Sec61p plays key roles in ER protein import and ERAD. *PLoS One.* 2019 Apr 24;14(4):e0215950.

Elion EA, Brill JA, Fink GR (1991). Functional redundancy in the yeast cell cycle: FUS3 and KSS1 have both overlapping and unique functions. *Cold Spring Harb Symp Quant Biol.* 1991;56:41-9.

Emr S, Glick BS, Linstedt AD, Lippincott-Schwartz J, Luini A, Malhotra V, Marsh BJ, Nakano A, Pfeffer SR, Rabouille C, Rothman JE, Warren G, Wieland FT (2009). Journeys through the Golgi--taking stock in a new era. *J Cell Biol.* 2009 Nov 16;187(4):449-53.

Fagone P, Jackowski S (2009). Membrane phospholipid synthesis and endoplasmic reticulum function. *J Lipid Res.* 2009 Apr;50 Suppl(Suppl):S311-6

Fehrenbacher KL, Davis D, Wu M, Boldogh I, Pon LA (2002). Endoplasmic reticulum dynamics, inheritance, and cytoskeletal interactions in budding yeast. *Mol Biol Cell.* 2002 Mar;13(3):854-65. doi: 10.1091/mbc.01-04-0184. PMID: 11907267; PMCID: PMC99604.

Feldheim D, Rothblatt J, Schekman R (1992). Topology and functional domains of Sec63p, an endoplasmic reticulum membrane protein required for secretory protein translocation. *Mol Cell Biol.* 1992 Jul;12(7):3288-96.

Feng D, Zhao X, Soromani C, Toikkanen J, Römisch K, Vembar SS, Brodsky JL, Keränen S, Jääntti J (2007). The transmembrane domain is sufficient for Sbh1p function, its association with the Sec61 complex, and interaction with Rtn1p. *J Biol Chem.* 2007 Oct 19;282(42):30618-28.

Ferro-Novick S, Brose N (2013). Nobel 2013 Physiology or medicine: Traffic control system within cells. *Nature.* 2013 Dec 5;504(7478):98.

Finke K, Plath K, Panzner S, Prehn S, Rapoport TA, Hartmann E, Sommer T (1996). A second trimeric complex containing homologs of the Sec61p complex functions in protein transport across the ER membrane of *S. cerevisiae*. *EMBO J.* 1996 Apr 1;15(7):1482-94.

Fumagalli F, Noack J, Bergmann TJ, Cebollero E, Pisoni GB, Fasana E, Fregno I, Galli C, Loi M, Soldà T, D'Antuono R, Raimondi A, Jung M, Melnyk A, Schorr S, Schreiber A, Simonelli L, Varani L, Wilson-Zbinden C, Zerbe O, Hofmann K, Peter M, Quadroni M, Zimmermann R, Molinari M (2016). Translocon component Sec62 acts in endoplasmic reticulum turnover during stress recovery. *Nat Cell Biol.* 2016 Nov;18(11):1173-1184.

Galluzzi L, Kepp O, Kroemer G (2012). Mitochondria: master regulators of danger signalling. *Nat Rev Mol Cell Biol.* 2012 Dec;13(12):780-8.

Gardner BM, Pincus D, Gotthardt K, Gallagher CM, Walter P (2013). Endoplasmic reticulum stress sensing in the unfolded protein response. *Cold Spring Harb Perspect Biol.* 2013 Mar 1;5(3):a013169.

Garrison JL, Kunkel EJ, Hegde RS, Taunton J (2005). A substrate-specific inhibitor of protein translocation into the endoplasmic reticulum. *Nature.* 2005 Jul 14;436(7048):285-9.

Gemmill TR, Wu X, Hanes SD (2005). Vanishingly low levels of Ess1 prolyl-isomerase activity are sufficient for growth in *Saccharomyces cerevisiae*. *J Biol Chem.* 2005 Apr 22;280(16):15510-7.

Gerbeth C, Schmidt O, Rao S, Harbauer AB, Mikropoulou D, Opalińska M, Guiard B, Pfanner N, Meisinger C (2013). Glucose-induced regulation of protein import receptor Tom22 by cytosolic and mitochondria-bound kinases. *Cell Metab.* 2013 Oct 1;18(4):578-87.

Geva Y, Crissman J, Arakel EC, Gómez-Navarro N, Chuartzman SG, Stahmer KR, Schwappach B, Miller EA, Schuldiner M (2017). Two novel effectors of trafficking and maturation of the yeast plasma membrane H⁺-ATPase. *Traffic.* 2017 Oct;18(10):672-682.

Giaever et al., (2002) Functional profiling of the *Saccharomyces cerevisiae* genome. *Nature.* 2002 Jul 25;418(6896):387-91

Gierasch LM (1989). Signal sequences. *Biochemistry.* 1989 Feb 7;28(3):923-30.

Gillece P, Luz JM, Lennarz WJ, de La Cruz FJ, Römisch K (1999). Export of a cysteine-free misfolded secretory protein from the endoplasmic reticulum for degradation requires interaction with protein disulfide isomerase. *J Cell Biol.* 1999 Dec 27;147(7):1443-56.

Gilmore R, Walter P, Blobel G (1982). Protein translocation across the endoplasmic reticulum. II. Isolation and characterization of the signal recognition particle receptor. *J Cell Biol.* 1982 Nov;95(2 Pt 1):470-7.

Gilmore R, Blobel G (1983). Transient involvement of signal recognition particle and its receptor in the microsomal membrane prior to protein translocation. *Cell.* 1983 Dec;35(3 Pt 2):677-85.

Gnad F, de Godoy LM, Cox J, Neuhauser N, Ren S, Olsen JV, Mann M (2009). High-accuracy identification and bioinformatic analysis of in vivo protein phosphorylation sites in yeast. *Proteomics.* 2009 Oct;9(20):4642-52.

Goder V, Bieri C, Spiess M (1999). Glycosylation can influence topogenesis of membrane proteins and reveals dynamic reorientation of nascent polypeptides within the translocon. *J Cell Biol.* 1999 Oct 18;147(2):257-66.

Goder V, Junne T, Spiess M (2004). Sec61p contributes to signal sequence orientation according to the positive-inside rule. *Mol Biol Cell*. 2004 Mar;15(3):1470-8.

Gogala M, Becker T, Beatrix B, Armache JP, Barrio-Garcia C, Berninghausen O, Beckmann R (2014). Structures of the Sec61 complex engaged in nascent peptide translocation or membrane insertion. *Nature*. 2014 Feb 6;506(7486):107-10.

Gomez-Navarro N, Miller E (2016). Protein sorting at the ER-Golgi interface. *J Cell Biol*. 2016 Dec 19;215(6):769-778.

Goto M (2007). Protein O-glycosylation in fungi: diverse structures and multiple functions. *Biosci Biotechnol Biochem*. 2007 Jun;71(6):1415-27.

Görllich D, Hartmann E, Prehn S, Rapoport TA (1992). A protein of the endoplasmic reticulum involved early in polypeptide translocation. *Nature*. 1992 May 7;357(6373):47-52.

Görllich D, Rapoport TA (1993). Protein translocation into proteoliposomes reconstituted from purified components of the endoplasmic reticulum membrane. *Cell*. 1993 Nov 19;75(4):615-30.

Griesemer M, Young C, Robinson AS, Petzold L (2014). BiP clustering facilitates protein folding in the endoplasmic reticulum. *PLoS Comput Biol*. 2014 Jul 3;10(7):e1003675.

Gruss OJ, Feick P, Frank R, Dobberstein B (1999). Phosphorylation of components of the ER translocation site. *Eur J Biochem*. 1999 Mar;260(3):785-93.

Guo W, Novick P (2004). The exocyst meets the translocon: a regulatory circuit for secretion and protein synthesis? *Trends Cell Biol*. 2004 Feb;14(2):61-3.

Guo Q, Meng N, Fan G, Sun D, Meng Y, Luo G, Liu Y (2021). The role of the exocytic pathway in cell wall assembly in yeast. *Yeast*. 2021 Oct;38(10):566-578.

Halic M, Beckmann R (2005). The signal recognition particle and its interactions during protein targeting. *Curr Opin Struct Biol*. 2005 Feb;15(1):116-25.

Halic M, Gartmann M, Schlenker O, Mielke T, Pool MR, Sinning I, Beckmann R (2006). Signal recognition particle receptor exposes the ribosomal translocon binding site. *Science*. 2006 May 5;312(5774):745-7.

Hamman BD, Hendershot LM, Johnson AE (1998). BiP maintains the permeability barrier of the ER membrane by sealing the luminal end of the translocon pore before and early in translocation. *Cell*. 1998 Mar 20;92(6):747-58.

Hammer SK, Avalos JL(2017). Harnessing yeast organelles for metabolic engineering. *Nat Chem Biol*. 2017 Aug;13(8):823-832.

- Hanahan D (1983). Studies on transformation of *Escherichia coli* with plasmids. *J Mol Biol.* 1983 Jun 5;166(4):557-80.
- Hanes SD (2014). The Ess1 prolyl isomerase: traffic cop of the RNA polymerase II transcription cycle. *Biochim Biophys Acta.* 2014;1839(4):316-33.
- Hanna DE, Rethinaswamy A, Glover CV (1995). Casein kinase II is required for cell cycle progression during G1 and G2/M in *Saccharomyces cerevisiae*. *J Biol Chem.* 1995 Oct 27;270(43):25905-14.
- Hara-Kuge S, Kuge O, Orci L, Amherdt M, Ravazzola M, Wieland FT, Rothman JE (1994). En bloc incorporation of coatamer subunits during the assembly of COP-coated vesicles. *J Cell Biol.* 1994 Mar;124(6):883-92.
- Hartmann E, Sommer T, Prehn S, Görlich D, Jentsch S, Rapoport TA (1994). Evolutionary conservation of components of the protein translocation complex. *Nature.* 1994 Feb 17;367(6464):654-7.
- Hatahet F, Ruddock LW (2009). Modulating proteostasis: peptidomimetic inhibitors and activators of protein folding. *Curr Pharm Des.* 2009;15(21):2488-507.
- Haßdenteufel S, Johnson N, Paton AW, Paton JC, High S, Zimmermann R (2018). Chaperone-Mediated Sec61 Channel Gating during ER Import of Small Precursor Proteins Overcomes Sec61 Inhibitor-Reinforced Energy Barrier. *Cell Rep.* 2018 May 1;23(5):1373-1386.
- Hegde RS, Bernstein HD (2006). The surprising complexity of signal sequences. *Trends Biochem Sci.* 2006 Oct;31(10):563-71.
- Hegde RS, Kang SW (2008). The concept of translocational regulation. *J Cell Biol.* 2008 Jul 28;182(2):225-32.
- Heinrich SU, Mothes W, Brunner J, Rapoport TA (2000). The Sec61p complex mediates the integration of a membrane protein by allowing lipid partitioning of the transmembrane domain. *Cell.* 2000 Jul 21;102(2):233-44.
- Helmers J, Schmidt D, Glavy JS, Blobel G, Schwartz T (2003). The beta-subunit of the protein-conducting channel of the endoplasmic reticulum functions as the guanine nucleotide exchange factor for the beta-subunit of the signal recognition particle receptor. *J Biol Chem.* 2003 Jun 27;278(26):23686-90.
- Hitt R, Wolf DH (2004). DER7, encoding alpha-glucosidase I is essential for degradation of malformed glycoproteins of the endoplasmic reticulum. *FEMS Yeast Res.* 2004 Sep;4(8):815-20.
- Hizlan D, Robson A, Whitehouse S, Gold VA, Vonck J, Mills D, Kühlbrandt W, Collinson I (2012). Structure of the SecY complex unlocked by a preprotein mimic. *Cell Rep.* 2012 Jan 26;1(1):21-8.

Holthuis JC, van Riel MC, Martens GJ (1995). Translocon-associated protein TRAP delta and a novel TRAP-like protein are coordinately expressed with pro-opiomelanocortin in *Xenopus* intermediate pituitary. *Biochem J.* 1995 Nov 15;312 (Pt 1)(Pt 1):205-13.

Horvath A, Sütterlin C, Manning-Krieg U, Movva NR, Riezman H (1994). Ceramide synthesis enhances transport of GPI-anchored proteins to the Golgi apparatus in yeast. *EMBO J.* 1994 Aug 15;13(16):3687-95.

Hosokawa N, Tremblay LO, You Z, Herscovics A, Wada I, Nagata K (2003). Enhancement of endoplasmic reticulum (ER) degradation of misfolded Null Hong Kong alpha1-antitrypsin by human ER mannosidase I. *J Biol Chem.* 2003 Jul 11;278(28):26287-94.

Hu JH, Malloy C, Tabor GT, Gutzmann JJ, Liu Y, Abebe D, Karlsson RM, Durell S, Cameron HA, Hoffman DA (2020). Activity-dependent isomerization of Kv4.2 by Pin1 regulates cognitive flexibility. *Nat Commun.* 2020 Mar 26;11(1):1567.

Hughes H, Stephens DJ (2008). Assembly, organization, and function of the COPII coat. *Histochem Cell Biol.* 2008 Feb;129(2):129-51.

Huh WK, Falvo JV, Gerke LC, Carroll AS, Howson RW, Weissman JS, O'Shea EK (2003). Global analysis of protein localization in budding yeast. *Nature.* 2003 Oct 16;425(6959):686-91.

Jahn R, Scheller RH (2006). SNAREs--engines for membrane fusion. *Nat Rev Mol Cell Biol.* 2006 Sep;7(9):631-43.

Jakob CA, Burda P, Roth J, Aebi M (1998). Degradation of misfolded endoplasmic reticulum glycoproteins in *Saccharomyces cerevisiae* is determined by a specific oligosaccharide structure. *J Cell Biol.* 1998 Sep 7;142(5):1223-33.

Jan CH, Williams CC, Weissman JS (2014). Principles of ER cotranslational translocation revealed by proximity-specific ribosome profiling. *Science.* 2014 Nov 7;346(6210):1257521.

Jiang Y, Cheng Z, Mandon EC, Gilmore R (2008). An interaction between the SRP receptor and the translocon is critical during cotranslational protein translocation. *J Cell Biol.* 2008 Mar 24;180(6):1149-61.

Jonikas et al. (2009) Comprehensive characterization of genes required for protein folding in the endoplasmic reticulum. *Science.* 2009 Mar 27;323(5922):1693-7

Jung SJ, Jung Y, Kim H (2019). Proper insertion and topogenesis of membrane proteins in the ER depend on Sec63. *Biochim Biophys Acta Gen Subj.* 2019 Sep;1863(9):1371-1380.

Jung SJ, Kim H (2021). Emerging View on the Molecular Functions of Sec62 and Sec63 in Protein Translocation. *Int J Mol Sci.* 2021 Nov 25;22(23):12757.

- Jørgensen MU, Bruun MB, Didion T, Kielland-Brandt MC (1998). Mutations in five loci affecting GAP1-independent uptake of neutral amino acids in yeast. *Yeast*. 1998 Jan 30;14(2):103-14.
- Kabani M, Kelley SS, Morrow MW, Montgomery DL, Sivendran R, Rose MD, Gierasch LM, Brodsky JL (2003). Dependence of endoplasmic reticulum-associated degradation on the peptide binding domain and concentration of BiP. *Mol Biol Cell*. 2003 Aug;14(8):3437-48.
- Kalies KU, Rapoport TA, Hartmann E (1998). The beta subunit of the Sec61 complex facilitates cotranslational protein transport and interacts with the signal peptidase during translocation. *J Cell Biol*. 1998 May 18;141(4):887-94.
- Kalies KU, Allan S, Sergeyenko T, Kröger H, Römisch K (2005). The protein translocation channel binds proteasomes to the endoplasmic reticulum membrane. *EMBO J*. 2005 Jul 6;24(13):2284-93.
- Kang SW, Rane NS, Kim SJ, Garrison JL, Taunton J, Hegde RS (2006). Substrate-specific translocational attenuation during ER stress defines a pre-emptive quality control pathway. *Cell*. 2006 Dec 1;127(5):999-1013.
- Kanshin E, Giguère S, Jing C, Tyers M, Thibault P (2017). Machine Learning of Global Phosphoproteomic Profiles Enables Discrimination of Direct versus Indirect Kinase Substrates. *Mol Cell Proteomics*. 2017 May;16(5):786-798.
- Kawahara T, Yanagi H, Yura T, Mori K (1997). Endoplasmic reticulum stress-induced mRNA splicing permits synthesis of transcription factor Hac1p/Ern4p that activates the unfolded protein response. *Mol Biol Cell*. 1997 Oct;8(10):1845-62.
- Käll L, Krogh A, Sonnhammer EL (2004). A combined transmembrane topology and signal peptide prediction method. *J Mol Biol*. 2004 May 14;338(5):1027-36.
- Keenan RJ, Freymann DM, Walter P, Stroud RM (1998). Crystal structure of the signal sequence binding subunit of the signal recognition particle. *Cell*. 1998 Jul 24;94(2):181-91.
- Kim SJ, Hegde RS (2002). Cotranslational partitioning of nascent prion protein into multiple populations at the translocation channel. *Mol Biol Cell*. 2002 Nov;13(11):3775-86.
- Kim JH, Zhao Y, Pan X, He X, Gilbert HF (2009). The unfolded protein response is necessary but not sufficient to compensate for defects in disulfide isomerization. *J Biol Chem*. 2009;284(16):10400-10408.
- Kinch LN, Saier MH Jr, Grishin NV (2002) Sec61beta--a component of the archaeal protein secretory system. *Trends Biochem Sci*. 2002 Apr;27(4):170-1
- Klis FM, Mol P, Hellingwerf K, Brul S (2002). Dynamics of cell wall structure in *Saccharomyces cerevisiae*. *FEMS Microbiol Rev*. 2002 Aug;26(3):239-56.

- Kos-Braun IC, Jung I, Koš M (2017). Tor1 and CK2 kinases control a switch between alternative ribosome biogenesis pathways in a growth-dependent manner. *PLoS Biol.* 2017 Mar 10;15(3):e2000245.
- Kuehn MJ, Herrmann JM, Schekman R (1998). COPII-cargo interactions direct protein sorting into ER-derived transport vesicles. *Nature.* 1998 Jan 8;391(6663):187-90.
- Laird V, High S (1997) Discrete cross-linking products identified during membrane protein biosynthesis. *J Biol Chem.* 1997 Jan 17;272(3):1983-9
- Lakkaraju AK, Thankappan R, Mary C, Garrison JL, Taunton J, Strub K (2012). Efficient secretion of small proteins in mammalian cells relies on Sec62-dependent posttranslational translocation. *Mol Biol Cell.* 2012 Jul;23(14):2712-22.
- Lang S, Benedix J, Fedeles SV, Schorr S, Schirra C, Schäuble N, Jalal C, Greiner M, Hassdenteufel S, Tatzelt J, Kreutzer B, Edelmann L, Krause E, Rettig J, Somlo S, Zimmermann R, Dudek J (2012). Different effects of Sec61 α , Sec62 and Sec63 depletion on transport of polypeptides into the endoplasmic reticulum of mammalian cells. *J Cell Sci.* 2012 Apr 15;125(Pt 8):1958-69.
- Lee J, Moir RD, McIntosh KB, Willis IM (2012). TOR signaling regulates ribosome and tRNA synthesis via LAMMER/Clk and GSK-3 family kinases. *Mol Cell.* 2012 Mar 30;45(6):836-43.
- Lepore D, Spassibojko O, Pinto G, Collins RN (2016). Cell cycle-dependent phosphorylation of Sec4p controls membrane deposition during cytokinesis. *J Cell Biol.* 2016 Sep 12;214(6):691-703.
- Leuenberger P, Ganschä S, Kahraman A, Cappelletti V, Boersema PJ, von Mering C, Claassen M, Picotti P (2017). Cell-wide analysis of protein thermal unfolding reveals determinants of thermostability. *Science.* 2017 Feb 24;355(6327):eaai7825.
- Levy R, Wiedmann M, Kreibich G (2001). In vitro binding of ribosomes to the beta subunit of the Sec61p protein translocation complex. *J Biol Chem.* 2001 Jan 26;276(4):2340-6.
- Lewis MJ, Pelham HR (1996). SNARE-mediated retrograde traffic from the Golgi complex to the endoplasmic reticulum. *Cell.* 1996 Apr 19;85(2):205-15.
- Li et al., (2011) Systematic exploration of essential yeast gene function with temperature-sensitive mutants. *Nat Biotechnol.* 2011 Apr;29(4):361-7
- Lin R, Allis CD, Elledge SJ (1996). PAT1, an evolutionarily conserved acetyltransferase homologue, is required for multiple steps in the cell cycle. *Genes Cells.* 1996 Oct;1(10):923-42.
- Liou YC, Zhou XZ, Lu KP (2011). Prolyl isomerase Pin1 as a molecular switch to determine the fate of phosphoproteins. *Trends Biochem Sci.* 2011 Oct;36(10):501-14.

Lipschutz JH, Lingappa VR, Mostov KE (2003). The exocyst affects protein synthesis by acting on the translocation machinery of the endoplasmic reticulum. *J Biol Chem*. 2003 Jun 6;278(23):20954-60.

Liu M, Lara-Lemus R, Shan SO, Wright J, Haataja L, Barbetti F, Guo H, Larkin D, Arvan P (2012). Impaired cleavage of preproinsulin signal peptide linked to autosomal-dominant diabetes. *Diabetes*. 2012 Apr;61(4):828-37.

Liu SK, Smith CA, Arnold R, Kiefer F, McGlade CJ (2000). The adaptor protein Gads (Grb2-related adaptor downstream of Shc) is implicated in coupling hemopoietic progenitor kinase-1 to the activated TCR. *J Immunol*. 2000 Aug 1;165(3):1417-26.

Lizák B, Csala M, Benedetti A, Bánhegyi G (2008). The translocon and the non-specific transport of small molecules in the endoplasmic reticulum (Review). *Mol Membr Biol*. 2008 Feb;25(2):95-101.

Lommel M, Bagnat M, Strahl S (2004). Aberrant processing of the WSC family and Mid2p cell surface sensors results in cell death of *Saccharomyces cerevisiae* O-mannosylation mutants. *Mol Cell Biol*. 2004 Jan;24(1):46-57.

Lopez S, Rodriguez-Gallardo S, Sabido-Bozo S, Muñiz M (2019). Endoplasmic Reticulum Export of GPI-Anchored Proteins. *Int J Mol Sci*. 2019 Jul 17;20(14):3506.

Lowe M (2010). Structural organization of the Golgi apparatus. *Curr Opin Cell Biol*. 2011 Feb;23(1):85-93. doi: 10.1016/j.ceb.2010.10.004. Epub 2010 Nov 9. PMID: 21071196.

Lyko F, Martoglio B, Jungnickel B, Rapoport TA, Dobberstein B (1995). Signal sequence processing in rough microsomes. *J Biol Chem*. 1995 Aug 25;270(34):19873-8.

Ma J, Wollmann R, Lindquist S (2002). Neurotoxicity and neurodegeneration when PrP accumulates in the cytosol. *Science*. 2002 Nov 29;298(5599):1781-5.

Ma Z, Atencio D, Barnes C, DeFiglio H, Hanes SD (2012). Multiple roles for the Ess1 prolyl isomerase in the RNA polymerase II transcription cycle. *Mol Cell Biol*. 2012 Sep;32(17):3594-607.

Mackinnon AL, Paavilainen VO, Sharma A, Hegde RS, Taunton J (2014) An allosteric Sec61 inhibitor traps nascent transmembrane helices at the lateral gate. *Elife*. 2014;3:e01483

Mandon EC, Trueman SF, Gilmore R (2013). Protein translocation across the rough endoplasmic reticulum. *Cold Spring Harb Perspect Biol*. 2013 Feb 1;5(2):a013342.

Martin W (2010). Evolutionary origins of metabolic compartmentalization in eukaryotes. *Philos Trans R Soc Lond B Biol Sci*. 2010 Mar 12;365(1541):847-55.

Martins A, Ring A, Omnus DJ, Heessen S, Pfirrmann T, Ljungdahl PO (2019) Spatial and temporal regulation of the endoproteolytic activity of the SPS-sensor-controlled Ssy5 signaling protease. *Mol Biol Cell*. 2019 Oct 1;30(21):2709-2720

Mandon EC, Trueman SF, Gilmore R (2013). Protein translocation across the rough endoplasmic reticulum. *Cold Spring Harb Perspect Biol*. 2013 Feb 1;5(2):a013342.

Marsolier J, Perichon M, DeBarry JD, Villoutreix BO, Chluba J, Lopez T, Garrido C, Zhou XZ, Lu KP, Fritsch L, Ait-Si-Ali S, Mhadhbi M, Medjkane S, Weitzman JB (2015). Theileria parasites secrete a prolyl isomerase to maintain host leukocyte transformation. *Nature*. 2015 Apr 16;520(7547):378-82.

Matlack KE, Misselwitz B, Plath K, Rapoport TA (1999). BiP acts as a molecular ratchet during posttranslational transport of prepro-alpha factor across the ER membrane. *Cell*. 1999 May 28;97(5):553-64.

McBride HM, Neuspiel M, Wasiak S (2006). Mitochondria: more than just a powerhouse. *Curr Biol*. 2006 Jul 25;16(14):R551-60.

McKnight CJ, Stradley SJ, Jones JD, Gierasch LM (1991). Conformational and membrane-binding properties of a signal sequence are largely unaltered by its adjacent mature region. *Proc Natl Acad Sci U S A*. 1991 Jul 1;88(13):5799-803.

Mesbah K, Camus A, Babinet C, Barra J (2006). Mutation in the Trapalpha/Ssr1 gene, encoding translocon-associated protein alpha, results in outflow tract morphogenetic defects. *Mol Cell Biol*. 2006 Oct;26(20):7760-71.

Meyer DI, Krause E, Dobberstein B (1982). Secretory protein translocation across membranes-the role of the 'docking protein'. *Nature*. 1982 Jun 24;297(5868):647-50.

Meyer HA, Grau H, Kraft R, Kostka S, Prehn S, Kalies KU, Hartmann E (2000). Mammalian Sec61 is associated with Sec62 and Sec63. *J Biol Chem*. 2000 May 12;275(19):14550-7.

Michalak M, Corbett EF, Mesaeli N, Nakamura K, Opas M (1999). Calreticulin: one protein, one gene, many functions. *Biochem J*. 1999 Dec 1;344 Pt 2(Pt 2):281-92.

Milstein C, Brownlee GG, Harrison TM, Mathews MB (1972). A possible precursor of immunoglobulin light chains. *Nat New Biol*. 1972 Sep 27;239(91):117-20.

Misselwitz B, Staack O, Matlack KE, Rapoport TA (1999). Interaction of BiP with the J-domain of the Sec63p component of the endoplasmic reticulum protein translocation complex. *J Biol Chem*. 1999 Jul 16;274(29):20110-5.

Mok J, Zhu X, Snyder M (2011). Dissecting phosphorylation networks: lessons learned from yeast. *Expert Rev Proteomics*. 2011 Dec;8(6):775-86.

- Morris MC, Kaiser P, Rudyak S, Baskerville C, Watson MH, Reed SI (2003). Cks1-dependent proteasome recruitment and activation of CDC20 transcription in budding yeast. *Nature*. 2003 Jun 26;423(6943):1009-13.
- Mumberg D, Müller R, Funk M (1994). Regulatable promoters of *Saccharomyces cerevisiae*: comparison of transcriptional activity and their use for heterologous expression. *Nucleic Acids Res*. 1994 Dec 25;22(25):5767-8.
- Nagy Z, Comer S, Smolenski A (2018). Analysis of Protein Phosphorylation Using Phos-Tag Gels. *Curr Protoc Protein Sci*. 2018 Aug;93(1):e64.
- Nakatsu F, Ohno H (2003). Adaptor protein complexes as the key regulators of protein sorting in the post-Golgi network. *Cell Struct Funct*. 2003 Oct;28(5):419-29.
- Nakatsu Y, Mori K, Matsunaga Y, Yamamotoya T, Ueda K, Inoue Y, Mitsuzaki-Miyoshi K, Sakoda H, Fujishiro M, Yamaguchi S, Kushiya A, Ono H, Ishihara H, Asano T (2017). The prolyl isomerase Pin1 increases β -cell proliferation and enhances insulin secretion. *J Biol Chem*. 2017 Jul 14;292(28):11886-11895.
- Ng DT, Brown JD, Walter P (1996). Signal sequences specify the targeting route to the endoplasmic reticulum membrane. *J Cell Biol*. 1996 Jul;134(2):269-78.
- Ng W, Sergeyenko T, Zeng N, Brown JD, Römisch K (2007). Characterization of the proteasome interaction with the Sec61 channel in the endoplasmic reticulum. *J Cell Sci*. 2007 Feb 15;120(Pt 4):682-91.
- Nguyen D, Stutz R, Schorr S, Lang S, Pfeffer S, Freeze HH, Förster F, Helms V, Dudek J, Zimmermann R (2018). Proteomics reveals signal peptide features determining the client specificity in human TRAP-dependent ER protein import. *Nat Commun*. 2018 Sep 14;9(1):3765.
- Nobel H, Ruiz C, Martin H, Morris W, Brul S, Molina M, Klis FM (2000). Cell wall perturbation in yeast results in dual phosphorylation of the Slr2/Mpk1 MAP kinase and in an Slr2-mediated increase in FKS2-lacZ expression, glucanase resistance and thermotolerance. *Microbiology (Reading)*. 2000 Sep;146 (Pt 9):2121-2132.
- Novick P, Schekman R (1983). Export of major cell surface proteins is blocked in yeast secretory mutants. *J Cell Biol*. 1983 Feb;96(2):541-7.
- Nuoffer C, Horvath A, Riezman H (1993). Analysis of the sequence requirements for glycosylphosphatidylinositol anchoring of *Saccharomyces cerevisiae* Gas1 protein. *J Biol Chem*. 1993 May 15;268(14):10558-63.
- Nyathi Y, Wilkinson BM, Pool MR (2013). Co-translational targeting and translocation of proteins to the endoplasmic reticulum. *Biochim Biophys Acta*. 2013 Nov;1833(11):2392-402.

Ogg SC, Poritz MA, Walter P (1992). Signal recognition particle receptor is important for cell growth and protein secretion in *Saccharomyces cerevisiae*. *Mol Biol Cell*. 1992 Aug;3(8):895-911.

O'Keefe S, High S (2020). Membrane translocation at the ER: with a little help from my friends. *FEBS J*. 2020 Nov;287(21):4607-4611.

Opalińska M, Meisinger C (2014). Mitochondrial protein import under kinase surveillance. *Microb Cell*. 2014 Jan 29;1(2):51-57.

Orlean P (2012). Architecture and biosynthesis of the *Saccharomyces cerevisiae* cell wall. *Genetics*. 2012 Nov;192(3):775-818.

O'Rourke SM, Herskowitz I (2002). A third osmosensing branch in *Saccharomyces cerevisiae* requires the Msb2 protein and functions in parallel with the Sho1 branch. *Mol Cell Biol*. 2002 Jul;22(13):4739-49.

Osborne AR, Rapoport TA, van den Berg B (2005). Protein translocation by the Sec61/SecY channel. *Annu Rev Cell Dev Biol*. 2005;21:529-50.

Ott CM, Lingappa VR (2004). Signal sequences influence membrane integration of the prion protein. *Biochemistry*. 2004 Sep 28;43(38):11973-82.

Paccaud JP, Reith W, Carpentier JL, Ravazzola M, Amherdt M, Schekman R, Orci L (1996) Cloning and functional characterization of mammalian homologues of the COPII component Sec23. *Mol Biol Cell*. 1996 Oct;7(10):1535-46

Panzner S, Dreier L, Hartmann E, Kostka S, Rapoport TA (1995). Posttranslational protein transport in yeast reconstituted with a purified complex of Sec proteins and Kar2p. *Cell*. 1995 May 19;81(4):561-70.

Panzner S, Dreier L, Hartmann E, Kostka S, Rapoport TA (1995). Posttranslational protein transport into the endoplasmic reticulum. *Cold Spring Harb Symp Quant Biol*. 1995;60:31-40.

Park E, Rapoport TA (2011). Preserving the membrane barrier for small molecules during bacterial protein translocation. *Nature*. 2011 May 12;473(7346):239-42.

Park E, Rapoport TA (2012). Mechanisms of Sec61/SecY-mediated protein translocation across membranes. *Annu Rev Biophys*. 2012;41:21-40.

Park E, Ménétret JF, Gumbart JC, Ludtke SJ, Li W, Whynot A, Rapoport TA, Akey CW (2014). Structure of the SecY channel during initiation of protein translocation. *Nature*. 2014 Feb 6;506(7486):102-6.

Pelham HR, Munro S (1993). Sorting of membrane proteins in the secretory pathway. *Cell*. 1993 Nov 19;75(4):603-5.

Pereira F, Rettel M, Stein F, Savitski MM, Collinson I, Römisch K (2019). Effect of Sec61 interaction with Mpd1 on endoplasmic reticulum-associated degradation. *PLoS One*. 2019 Jan 25;14(1):e0211180.

Petersen TN, Brunak S, von Heijne G, Nielsen H (2011). SignalP 4.0: discriminating signal peptides from transmembrane regions. *Nat Methods*. 2011 Sep 29;8(10):785-6.

Pilon M, Römisch K, Quach D, Schekman R (1998) Sec61p serves multiple roles in secretory precursor binding and translocation into the endoplasmic reticulum membrane. *Mol Biol Cell*. 1998 Dec;9(12):3455-73

Piña FJ, Fleming T, Pogliano K, Niwa M (2016). Reticulons Regulate the ER Inheritance Block during ER Stress. *Dev Cell*. 2016 May 9;37(3):279-88.

Plath K, Mothes W, Wilkinson BM, Stirling CJ, Rapoport TA (1998). Signal sequence recognition in posttranslational protein transport across the yeast ER membrane. *Cell*. 1998 Sep 18;94(6):795-807.

Pool MR (2022). Targeting of Proteins for Translocation at the Endoplasmic Reticulum. *Int J Mol Sci*. 2022 Mar 29;23(7):3773.

Powell KS, Latterich M (2000). The making and breaking of the endoplasmic reticulum. *Traffic*. 2000 Sep;1(9):689-94.

Prehn S, Herz J, Hartmann E, Kurzchalia TV, Frank R, Roemisch K, Dobberstein B, Rapoport TA (1990). Structure and biosynthesis of the signal-sequence receptor. *Eur J Biochem*. 1990 Mar 10;188(2):439-45.

Preuss D, Mulholland J, Kaiser CA, Orlean P, Albright C, Rose MD, Robbins PW, Botstein D (1991). Structure of the yeast endoplasmic reticulum: localization of ER proteins using immunofluorescence and immunoelectron microscopy. *Yeast*. 1991 Dec;7(9):891-911.

Preuss D, Mulholland J, Franzusoff A, Segev N, Botstein D (1992). Characterization of the *Saccharomyces* Golgi complex through the cell cycle by immunoelectron microscopy. *Mol Biol Cell*. 1992 Jul;3(7):789-803.

Prinz WA, Grzyb L, Veenhuis M, Kahana JA, Silver PA, Rapoport TA (2000). Mutants affecting the structure of the cortical endoplasmic reticulum in *Saccharomyces cerevisiae*. *J Cell Biol*. 2000 Aug 7;150(3):461-74.

Ptacek J, Devgan G, Michaud G, Zhu H, Zhu X, Fasolo J, Guo H, Jona G, Breitkreutz A, Sopko R, McCartney RR, Schmidt MC, Rachidi N, Lee SJ, Mah AS, Meng L, Stark MJ, Stern DF, De Virgilio C, Tyers M, Andrews B, Gerstein M, Schweitzer B, Predki PF, Snyder M (2005). Global analysis of protein phosphorylation in yeast. *Nature*. 2005 Dec 1;438(7068):679-84.

Radzicka A, Pedersen L, Wolfenden R (1988). Influences of solvent water on protein folding: free energies of solvation of cis and trans peptides are nearly identical. *Biochemistry*. 1988 Jun 14;27(12):4538-41.

Rais I, Karas M, Schagger H (2004). Two-dimensional electrophoresis for the isolation of integral membrane proteins and mass spectrometric identification. *Proteomics*. 2004 Sep;4(9):2567-71.

Ramírez MP, Rivera M, Quiroga-Roger D, Bustamante A, Vega M, Baez M, Puchner EM, Wilson CAM (2017). Single molecule force spectroscopy reveals the effect of BiP chaperone on protein folding. *Protein Sci*. 2017 Jul;26(7):1404-1412.

Rane NS, Yonkovich JL, Hegde RS (2004). Protection from cytosolic prion protein toxicity by modulation of protein translocation. *EMBO J*. 2004 Nov 24;23(23):4550-9.

Rapoport TA (2007). Protein translocation across the eukaryotic endoplasmic reticulum and bacterial plasma membranes. *Nature*. 2007 Nov 29;450(7170):663-9.

Rapoport TA, Li L, Park E (2017). Structural and Mechanistic Insights into Protein Translocation. *Annu Rev Cell Dev Biol*. 2017 Oct 6;33:369-390.

Reithinger JH, Yim C, Kim S, Lee H, Kim H (2014). Structural and functional profiling of the lateral gate of the Sec61 translocon. *J Biol Chem*. 2014 May 30;289(22):15845-55.

Rethinaswamy A, Birnbaum MJ, Glover CV (1998). Temperature-sensitive mutations of the CKA1 gene reveal a role for casein kinase II in maintenance of cell polarity in *Saccharomyces cerevisiae*. *J Biol Chem*. 1998 Mar 6;273(10):5869-77.

Roberts CJ, Pohlig G, Rothman JH, Stevens TH (1989). Structure, biosynthesis, and localization of dipeptidyl aminopeptidase B, an integral membrane glycoprotein of the yeast vacuole. *J Cell Biol*. 1989 Apr;108(4):1363-73.

Rossanese OW, Soderholm J, Bevis BJ, Sears IB, O'Connor J, Williamson EK, Glick BS (1999). Golgi structure correlates with transitional endoplasmic reticulum organization in *Pichia pastoris* and *Saccharomyces cerevisiae*. *J Cell Biol*. 1999 Apr 5;145(1):69-81.

Rossanese OW, Reinke CA, Bevis BJ, Hammond AT, Sears IB, O'Connor J, Glick BS (2001). A role for actin, Cdc1p, and Myo2p in the inheritance of late Golgi elements in *Saccharomyces cerevisiae*. *J Cell Biol*. 2001 Apr 2;153(1):47-62.

Rothblatt JA, Deshaies RJ, Sanders SL, Daum G, Schekman R (1989). Multiple genes are required for proper insertion of secretory proteins into the endoplasmic reticulum in yeast. *J Cell Biol*. 1989 Dec;109(6 Pt 1):2641-52.

Roy SK, Bhattacharjee S (2021). Dengue virus: epidemiology, biology, and disease aetiology. *Can J Microbiol*. 2021 Oct;67(10):687-702.

- Römisch K (2005). Endoplasmic reticulum-associated degradation. *Annu Rev Cell Dev Biol.* 2005;21:435-56.
- Ruggiano A, Foresti O, Carvalho P (2014). Quality control: ER-associated degradation: protein quality control and beyond. *J Cell Biol.* 2014 Mar 17;204(6):869-79.
- Rutkowski DT, Ott CM, Polansky JR, Lingappa VR (2003). Signal sequences initiate the pathway of maturation in the endoplasmic reticulum lumen. *J Biol Chem.* 2003 Aug 8;278(32):30365-72.
- Sacher M, Jiang Y, Barrowman J, Scarpa A, Burston J, Zhang L, Schieltz D, Yates JR 3rd, Abeliovich H, Ferro-Novick S (1998). TRAPP, a highly conserved novel complex on the cis-Golgi that mediates vesicle docking and fusion. *EMBO J.* 1998 May 1;17(9):2494-503.
- Sacristán-Reviriego A, Madrid M, Cansado J, Martín H, Molina M (2014). A conserved non-canonical docking mechanism regulates the binding of dual specificity phosphatases to cell integrity mitogen-activated protein kinases (MAPKs) in budding and fission yeasts. *PLoS One.* 2014 Jan 22;9(1):e85390.
- Schägger H (2006). Tricine-SDS-PAGE. *Nat Protoc.* 2006;1(1):16-22.
- Schibich D, Gloge F, Pöhner I, Björkholm P, Wade RC, von Heijne G, Bukau B, Kramer G (2016). Global profiling of SRP interaction with nascent polypeptides. *Nature.* 2016 Aug 11;536(7615):219-23.
- Schmidt O, Harbauer AB, Rao S, Eyrich B, Zahedi RP, Stojanovski D, Schönfisch B, Guiard B, Sickmann A, Pfanner N, Meisinger C (2011). Regulation of mitochondrial protein import by cytosolic kinases. *Cell.* 2011 Jan 21;144(2):227-39.
- Schneider CC, Ampofo E, Montenarh M (2012). CK2 regulates ATF4 and CHOP transcription within the cellular stress response signalling pathway. *Cell Signal.* 2012 Sep;24(9):1797-802.
- Schröder M (2008). Endoplasmic reticulum stress responses. *Cell Mol Life Sci.* 2008 Mar;65(6):862-94.
- Schuldiner et al. (2005) Exploration of the function and organization of the yeast early secretory pathway through an epistatic miniarray profile. *Cell.* 2005 Nov 4;123(3):507-19
- Schwartz T, Blobel G (2003). Structural basis for the function of the beta subunit of the eukaryotic signal recognition particle receptor. *Cell.* 2003 Mar 21;112(6):793-803.
- Schwarz DS, Blower MD (2016). The endoplasmic reticulum: structure, function and response to cellular signaling. *Cell Mol Life Sci.* 2016 Jan;73(1):79-94.
- Servas C, Römisch K. The Sec63p J-domain is required for ERAD of soluble proteins in yeast (2013). *PLoS One.* 2013 Dec 4;8(12):e82058.

- Shaffer KL, Sharma A, Snapp EL, Hegde RS (2005). Regulation of protein compartmentalization expands the diversity of protein function. *Dev Cell*. 2005 Oct;9(4):545-54.
- Shan SO, Walter P (2005). Co-translational protein targeting by the signal recognition particle. *FEBS Lett*. 2005 Feb 7;579(4):921-6.
- Shao S, Hegde RS (2011). Membrane protein insertion at the endoplasmic reticulum. *Annu Rev Cell Dev Biol*. 2011;27:25-56.
- Sharifpoor S, van Dyk D, Costanzo M, Baryshnikova A, Friesen H, Douglas AC, Youn JY, VanderSluis B, Myers CL, Papp B, Boone C, Andrews BJ (2012). Functional wiring of the yeast kinome revealed by global analysis of genetic network motifs. *Genome Res*. 2012 Apr;22(4):791-801.
- Sharp PM, Li WH (1987). The codon Adaptation Index--a measure of directional synonymous codon usage bias, and its potential applications. *Nucleic Acids Res*. 1987 Feb 11;15(3):1281-95.
- Shaw AS, Rottier PJ, Rose JK (1988). Evidence for the loop model of signal-sequence insertion into the endoplasmic reticulum. *Proc Natl Acad Sci U S A*. 1988 Oct;85(20):7592-6.
- Shen SH, Chrétien P, Bastien L, Slilaty SN (1991). Primary sequence of the glucanase gene from *Oerskovia xanthineolytica*. Expression and purification of the enzyme from *Escherichia coli*. *J Biol Chem*. 1991 Jan 15;266(2):1058-63.
- Shibuya A, Margulis N, Christiano R, Walther TC, Barlowe C (2015). The Erv41-Erv46 complex serves as a retrograde receptor to retrieve escaped ER proteins. *J Cell Biol*. 2015 Jan 19;208(2):197-209.
- Shindiapina P, Barlowe C (2010). Requirements for transitional endoplasmic reticulum site structure and function in *Saccharomyces cerevisiae*. *Mol Biol Cell*. 2010 May 1;21(9):1530-45.
- Shorter J, Warren G (2002). Golgi architecture and inheritance. *Annu Rev Cell Dev Biol*. 2002;18:379-420.
- Sidrauski C, Walter P (1997). The transmembrane kinase Ire1p is a site-specific endonuclease that initiates mRNA splicing in the unfolded protein response. *Cell*. 1997 Sep 19;90(6):1031-9.
- Siepe D, Jentsch S. Prolyl isomerase Pin1 acts as a switch to control the degree of substrate ubiquitylation (2009). *Nat Cell Biol*. 2009 Aug;11(8):967-72.
- Sikorski RS, Hieter P (1989). A system of shuttle vectors and yeast host strains designed for efficient manipulation of DNA in *Saccharomyces cerevisiae*. *Genetics*. 1989 May;122(1):19-27.

Simons JF, Ebersold M, Helenius A (1998). Cell wall 1,6-beta-glucan synthesis in *Saccharomyces cerevisiae* depends on ER glucosidases I and II, and the molecular chaperone BiP/Kar2p. *EMBO J.* 1998 Jan 15;17(2):396-405.

Simon SM, Blobel G (1992). Signal peptides open protein-conducting channels in *E. coli*. *Cell.* 1992 May 15;69(4):677-84.

Skowronek MH, Rotter M, Haas IG (1999). Molecular characterization of a novel mammalian DnaJ-like Sec63p homolog. *Biol Chem.* 1999 Sep;380(9):1133-8.

Song W, Raden D, Mandon EC, Gilmore R (2000). Role of Sec61alpha in the regulated transfer of the ribosome-nascent chain complex from the signal recognition particle to the translocation channel. *Cell.* 2000 Feb 4;100(3):333-43.

Sopko R, Huang D, Preston N, Chua G, Papp B, Kafadar K, Snyder M, Oliver SG, Cyert M, Hughes TR, Boone C, Andrews B (2006). Mapping pathways and phenotypes by systematic gene overexpression. *Mol Cell.* 2006 Feb 3;21(3):319-30.

Soromani C, Zeng N, Hollemeyer K, Heinzle E, Klein MC, Tretter T, Seaman MN, Römisch K (2012) N-acetylation and phosphorylation of Sec complex subunits in the ER membrane. *BMC Cell Biol.* 2012 Dec 13;13:34

Soufi B, Kelstrup CD, Stoehr G, Fröhlich F, Walther TC, Olsen JV (2009). Global analysis of the yeast osmotic stress response by quantitative proteomics. *Mol Biosyst.* 2009 Nov;5(11):1337-46.

Spiess M, Junne T, Janoschke M (2019). Membrane Protein Integration and Topogenesis at the ER. *Protein J.* 2019 Jun;38(3):306-316.

Stagg SM, Gürkan C, Fowler DM, LaPointe P, Foss TR, Potter CS, Carragher B, Balch WE (2006). Structure of the Sec13/31 COPII coat cage. *Nature.* 2006 Jan 12;439(7073):234-8.

Stirling CJ, Rothblatt J, Hosobuchi M, Deshaies R, Schekman R (1992) Protein translocation mutants defective in the insertion of integral membrane proteins into the endoplasmic reticulum. *Mol Biol Cell.* 1992 Feb;3(2):129-42

Swaney DL, Beltrao P, Starita L, Guo A, Rush J, Fields S, Krogan NJ, Villén J (2013). Global analysis of phosphorylation and ubiquitylation cross-talk in protein degradation. *Nat Methods.* 2013 Jul;10(7):676-82.

Swank RT, Munkres KD (1971). Molecular weight analysis of oligopeptides by electrophoresis in polyacrylamide gel with sodium dodecyl sulfate. *Anal Biochem.* 1971 Feb;39(2):462-77.

Theillet FX, Kalmar L, Tompa P, Han KH, Selenko P, Dunker AK, Daughdrill GW, Uversky VN (2013). The alphabet of intrinsic disorder: I. Act like a Pro: On the abundance and roles of

proline residues in intrinsically disordered proteins. *Intrinsically Disord Proteins*. 2013 Apr 1;1(1):e24360.

Theillet FX, Binolfi A, Frembgen-Kesner T, Hingorani K, Sarkar M, Kyne C, Li C, Crowley PB, Gierasch L, Pielak GJ, Elcock AH, Gershenson A, Selenko P (2014). Physicochemical properties of cells and their effects on intrinsically disordered proteins (IDPs). *Chem Rev*. 2014 Jul 9;114(13):6661-714.

Toikkanen J, Gatti E, Takei K, Saloheimo M, Olkkonen VM, Söderlund H, De Camilli P, Keränen S (1996). Yeast protein translocation complex: isolation of two genes SEB1 and SEB2 encoding proteins homologous to the Sec61 beta subunit. *Yeast*. 1996 Apr;12(5):425-38.

Toikkanen JH, Miller KJ, Söderlund H, Jäntti J, Keränen S. (2003) The beta subunit of the Sec61p endoplasmic reticulum translocon interacts with the exocyst complex in *Saccharomyces cerevisiae*. *J Biol Chem*. 2003 Jun 6;278(23):20946-53

Tong AH, Evangelista M, Parsons AB, Xu H, Bader GD, Pagé N, Robinson M, Raghibizadeh S, Hogue CW, Bussey H, Andrews B, Tyers M, Boone C (2001). Systematic genetic analysis with ordered arrays of yeast deletion mutants. *Science*. 2001 Dec 14;294(5550):2364-8.

Tooze SA, Martens GJ, Huttner WB (2001). Secretory granule biogenesis: rafting to the SNARE. *Trends Cell Biol*. 2001 Mar;11(3):116-22.

Touati SA, Hofbauer L, Jones AW, Snijders AP, Kelly G, Uhlmann F (2019). Cdc14 and PP2A Phosphatases Cooperate to Shape Phosphoproteome Dynamics during Mitotic Exit. *Cell Rep*. 2019 Nov 12;29(7):2105-2119.e4.

Tran JR, Tomsic LR, Brodsky JL. A Cdc48p-associated factor modulates endoplasmic reticulum-associated degradation, cell stress, and ubiquitinated protein homeostasis (2011). *J Biol Chem*. 2011 Feb 18;286(7):5744-55.

Travers KJ, Patil CK, Wodicka L, Lockhart DJ, Weissman JS, Walter P (2000). Functional and genomic analyses reveal an essential coordination between the unfolded protein response and ER-associated degradation. *Cell*. 2000 Apr 28;101(3):249-58.

Tripathi A, Mandon EC, Gilmore R, Rapoport TA (2017). Two alternative binding mechanisms connect the protein translocation Sec71-Sec72 complex with heat shock proteins. *J Biol Chem*. 2017 May 12;292(19):8007-8018.

Tsukazaki T, Mori H, Fukai S, Ishitani R, Mori T, Dohmae N, Perederina A, Sugita Y, Vassilyev DG, Ito K, Nureki O (2008). Conformational transition of Sec machinery inferred from bacterial SecYE structures. *Nature*. 2008 Oct 16;455(7215):988-91.

Ubersax JA, Ferrell JE Jr (2007). Mechanisms of specificity in protein phosphorylation. *Nat Rev Mol Cell Biol*. 2007 Jul;8(7):530-41.

- Udom N, Chansongkrow P, Charoensawan V, Auesukaree C (2019). Coordination of the Cell Wall Integrity and High-Osmolarity Glycerol Pathways in Response to Ethanol Stress in *Saccharomyces cerevisiae*. *Appl Environ Microbiol*. 2019 Jul 18;85(15):e00551-19.
- Valk E, Venta R, Ord M, Faustova I, Kõivomägi M, Loog M (2014) Multistep phosphorylation systems: tunable components of biological signaling circuits. *Mol Biol Cell*. 2014 Nov 5;25(22):3456-60
- Van den Berg B, Clemons WM Jr, Collinson I, Modis Y, Hartmann E, Harrison SC, Rapoport TA (2004). X-ray structure of a protein-conducting channel. *Nature*. 2004 Jan 1;427(6969):36-44.
- Viotti C (2016). ER to Golgi-Dependent Protein Secretion: The Conventional Pathway. *Methods Mol Biol*. 2016;1459:3-29.
- Voeltz GK, Prinz WA, Shibata Y, Rist JM, Rapoport TA (2006). A class of membrane proteins shaping the tubular endoplasmic reticulum. *Cell*. 2006 Feb 10;124(3):573-86.
- von Heijne G (1984). How signal sequences maintain cleavage specificity. *J Mol Biol*. 1984 Feb 25;173(2):243-51.
- von Heijne G (1985). Signal sequences. The limits of variation. *J Mol Biol*. 1985 Jul 5;184(1):99-105.
- von Heijne G (1986). Towards a comparative anatomy of N-terminal topogenic protein sequences. *J Mol Biol*. 1986 May 5;189(1):239-42.
- von Heijne G, Gavel Y (1988). Topogenic signals in integral membrane proteins. *Eur J Biochem*. 1988 Jul 1;174(4):671-8.
- von Heijne G (1990). The signal peptide. *J Membr Biol*. 1990 May;115(3):195-201.
- Voorhees RM, Fernández IS, Scheres SH, Hegde RS (2014). Structure of the mammalian ribosome-Sec61 complex to 3.4 Å resolution. *Cell*. 2014 Jun 19;157(7):1632-43.
- Voorhees RM, Hegde RS (2016). Structure of the Sec61 channel opened by a signal sequence. *Science*. 2016 Jan 1;351(6268):88-91.
- Voorhees RM, Hegde RS (2016). Toward a structural understanding of co-translational protein translocation. *Curr Opin Cell Biol*. 2016 Aug;41:91-9.
- Walter P, Blobel G (1981). Translocation of proteins across the endoplasmic reticulum. II. Signal recognition protein (SRP) mediates the selective binding to microsomal membranes of in-vitro-assembled polysomes synthesizing secretory protein. *J Cell Biol*. 1981 Nov;91(2 Pt 1):551-6.

- Wang J, Sevier CS (2016). Formation and Reversibility of BiP Protein Cysteine Oxidation Facilitate Cell Survival during and post Oxidative Stress. *J Biol Chem.* 2016 Apr 1;291(14):7541-57.
- Wang X, Johnsson N (2005). Protein kinase CK2 phosphorylates Sec63p to stimulate the assembly of the endoplasmic reticulum protein translocation apparatus. *J Cell Sci.* 2005 Feb 15;118(Pt 4):723-32.
- Ward JJ, Sodhi JS, McGuffin LJ, Buxton BF, Jones DT (2004). Prediction and functional analysis of native disorder in proteins from the three kingdoms of life. *J Mol Biol.* 2004 Mar 26;337(3):635-45.
- Waters MG, Evans EA, Blobel G (1988). Prepro-alpha-factor has a cleavable signal sequence. *J Biol Chem.* 1988 May 5;263(13):6209-14.
- Wei YY, Liang S, Zhang YR, Lu JP, Lin FC, Liu XH (2020). MoSec61 β , the beta subunit of Sec61, is involved in fungal development and pathogenicity, plant immunity, and ER-phagy in *Magnaporthe oryzae*. *Virulence.* 2020 Dec;11(1):1685-1700.
- Weill, Uri et al. (2018) Genome-wide SWAp-Tag yeast libraries for proteome exploration. *Nature methods* vol. 15,8 (2018): 617-622
- West M, Zurek N, Hoenger A, Voeltz GK (2011). A 3D analysis of yeast ER structure reveals how ER domains are organized by membrane curvature. *J Cell Biol.* 2011 Apr 18;193(2):333-46.
- Wild K, Halic M, Sinning I, Beckmann R (2004). SRP meets the ribosome. *Nat Struct Mol Biol.* 2004 Nov;11(11):1049-53.
- Wilkinson BM, Esnault Y, Craven RA, Skiba F, Fieschi J, K'epès F, Stirling CJ (1997). Molecular architecture of the ER translocase probed by chemical crosslinking of Sss1p to complementary fragments of Sec61p. *EMBO J.* 1997 Aug 1;16(15):4549-59.
- Wittke S, Dünwald M, Albertsen M, Johnsson N (2002). Recognition of a subset of signal sequences by Ssh1p, a Sec61p-related protein in the membrane of endoplasmic reticulum of yeast *Saccharomyces cerevisiae*. *Mol Biol Cell.* 2002 Jul;13(7):2223-32.
- Wolin SL, Walter P (1989). Signal recognition particle mediates a transient elongation arrest of preprolactin in reticulocyte lysate. *J Cell Biol.* 1989 Dec;109(6 Pt 1):2617-22.
- Wright PE, Dyson HJ (2015). Intrinsically disordered proteins in cellular signalling and regulation. *Nat Rev Mol Cell Biol.* 2015 Jan;16(1):18-29.
- Wu X, Wilcox CB, Devasahayam G, Hackett RL, Arévalo-Rodríguez M, Cardenas ME, Heitman J, Hanes SD (2000) The Ess1 prolyl isomerase is linked to chromatin remodeling complexes and the general transcription machinery. *EMBO J.* 2000 Jul 17;19(14):3727-38

- Wu X, Cabanos C, Rapoport TA (2019). Structure of the post-translational protein translocation machinery of the ER membrane. *Nature*. 2019 Feb;566(7742):136-139.
- Xu S, Wang B, Li L, Zhou Q, Tian M, Zhao X, Peng J, Liu F, Chen Y, Xu Y, Feng X (2020). Effects of camptothecin on the rice blast fungus *Magnaporthe oryzae*. *Pestic Biochem Physiol*. 2020 Feb;163:108-116.
- Yachie N, Saito R, Sugiyama N, Tomita M, Ishihama Y (2011). Integrative features of the yeast phosphoproteome and protein-protein interaction map. *PLoS Comput Biol*. 2011 Jan 27;7(1):e1001064.
- Yim C, Jung SJ, Kim JEH, Jung Y, Jeong SD, Kim H (2018). Profiling of signal sequence characteristics and requirement of different translocation components. *Biochim Biophys Acta Mol Cell Res*. 2018 Nov;1865(11 Pt A):1640-1648.
- Zhang L, Winkler S, Schlottmann FP, Kohlbacher O, Elias JE, Skotheim JM, Ewald JC (2019). Multiple Layers of Phospho-Regulation Coordinate Metabolism and the Cell Cycle in Budding Yeast. *Front Cell Dev Biol*. 2019 Dec 17;7:338.
- Zhang R, Miner JJ, Gorman MJ, Rausch K, Ramage H, White JP, Zuiani A, Zhang P, Fernandez E, Zhang Q, Dowd KA, Pierson TC, Cherry S, Diamond MS (2016). A CRISPR screen defines a signal peptide processing pathway required by flaviviruses. *Nature*. 2016 Jul 7;535(7610):164-8.
- Zhao X, Jääntti J (2009). Functional characterization of the trans-membrane domain interactions of the Sec61 protein translocation complex beta-subunit. *BMC Cell Biol*. 2009 Oct 26;10:76.
- Zhou XZ, Lu KP (2016). The isomerase PIN1 controls numerous cancer-driving pathways and is a unique drug target. *Nat Rev Cancer*. 2016 Jul;16(7):463-78. doi: 10.1038/nrc.2016.49. Epub 2016 Jun 3. PMID: 27256007.
- Zhu G, Fujii K, Belkina N, Liu Y, James M, Herrero J, Shaw S (2005). Exceptional disfavor for proline at the P + 1 position among AGC and CAMK kinases establishes reciprocal specificity between them and the proline-directed kinases. *J Biol Chem*. 2005 Mar 18;280(11):10743-8.
- Zimmermann R, Eyrisch S, Ahmad M, Helms V (2011). Protein translocation across the ER membrane. *Biochim Biophys Acta*. 2011 Mar;1808(3):912-24.

Acknowledgements

First of all, I would like express my sincere gratitude to my PhD supervisor Prof. Dr. Karin Römisch for the continuous support of my PhD study and research, for her patience, motivation, and immense knowledge. Prof. Römisch gave me the opportunity to work in her lab, allowing me to grow as a scientist and giving me the tools and the guidance for becoming more independent in the lab. I am truly thankful for all your support, and specially for your patience.

I would also like to thank my second PhD supervisor Prof. Dr. Martin Van der Laan, for his interest in my work and the very important suggestions and input he gave me on our meetings.

I would like to thank Prof. Dr. Maya Schuldiner and her group from Weizmann Institute of science for their contribution to this work and their help with the high content microscopic screening. Thanks for allowing me to spend those weeks in your lab, it was truly a great experience.

I would also like to thank Duy Nguyen and Volkhard Helms from the Center for Bioinformatics at Saarland University, for their contribution to this work, for the statistical analysis of the screen results and for providing me with their valuable suggestions regarding to data analysis.

I thank Tom Stevens for his contribution with the anti-DPAPB antibody; Howard Riezman for his contribution with the anti-Gas1 antibody; and Charles Barlowe for his contribution with the anti-Gls1 antiserum and the full-length GST-GLS1 expression construct.

I would also like to thank Prof. Dr. Schmitt's group, who kindly shared equipment, reagents and strains with us whenever needed. Really good and friendly people up there.

I thank also Fabio Pereira and Lalitha Yadhanapudi for sharing this adventure with me, many good and stressful moments have been shared, even a Pandemic! Thank you both for been always there! Good friends this lab gave me.

I thank Prof. Dr. Gert-Wieland Kohring for his support and help on my first years in the lab, your advices always helped me whenever I had a technical or theoretical question.

I also thank Mark Lommel for all his help and support in the past two years. Many things in the lab got much easier because of your fresh impute and new approaches, so thank you for that.

Many thanks to Carmen Clemens, who with her great energy and humour made my days in this lab feel always like a better journey. Thanks for all the help over the years, and thank for becoming also a good friend. My stay in Germany would not have been the same without your presence.

I also thank Birgit Hasper for the great help she gave me when we worked together in the lab or in the practicums. It was great to share also those first years of my PhD with you.

I thank also Juncal Z. González, for helping me with all the administrative issues and paperwork from the very beginning. It is hard to be in a country where you cannot speak the language, but everything became enormously easier with your help, even when it was not part of your work responsibilities. In addition, we share the same language so I felt like being a bit at home.

I must also thank all the students I supervised during these 5 years in the lab while they were doing their internships, who put some fresh ideas and fun into the lab. Specially to Aline Leguede, who after her master stayed here for a bit longer and helped me with a lot of technical stuff and also became a good friend.

I would also like to thank my friends both in Argentina and in Germany, which are also a fundamental part of my life and without whom none of this would have been possible. Thanks for always being there.

Finally, I would like to thank my family in Argentina, without whom this thesis would never have been possible. Thanks to my parents and brothers, you are fiscally far away but very close spiritually. My parents always taught me and my brothers that success is not having a great degree or a lot of money; success is just being happy, so simple, so obvious (viejos sabios). All I am today at a personal level I owe to you guys.